www.icens.eu

ICENS

11TH INTERNATIONAL CONFERENCE ON ENGINEERING AND NATURAL SCIENCES

BOOK OF PROCEEDINGS

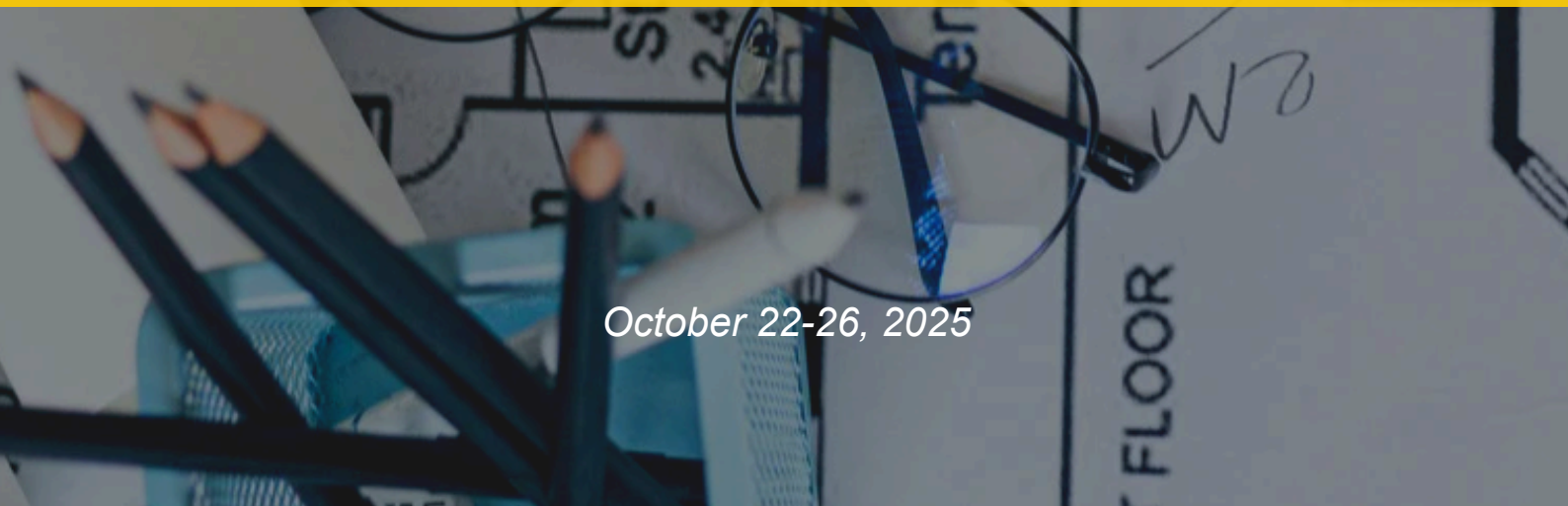

October 22-26, 2025

Organized by

CSUN

University of CINCINNATI

Partners

CNR GROUP

11th INTERNATIONAL CONFERENCE ON ENGINEERING AND NATURAL SCIENCES (ICENS)

ISBN 978-605-81426-1-9
ISSN 2687-2447

PROCEEDINGS OF THE 11th INTERNATIONAL CONFERENCE ON ENGINEERING AND NATURAL SCIENCES (ICENS) OCTOBER 22 TO 26, 2025 IN SARAJEVO, BOSNIA AND HERZEGOVINA

Edited by

Prof. Dr. Özer Çınar

Published by:

info@icens.eu
www.icens.eu
www.cnrgroup.eu

CNR Group Laboratuvar ve Arge Hizmetleri Sanayi Ticaret Limited Şirketi Çifte Havuzlar Mah., Eski Londra Asfaltı Cad., Kuluçka Mrk., A1 Blok, 151/1C, Iç Kapı No:1 B-20, Esenler / Istanbul, 34220

ISBN 978-605-81426-1-9

ISSN 2687-2447

SCIENTIFIC COMMITTEE

1. Prof. Dr. Adisa Parić - University of Sarajevo - Bosnia and Herzegovina
2. Prof. Dr. Aleksandar Dimitrov - Ss. Cyril and Methodius University - North Macedonia
3. Prof. Dr. Alexander Golub - National University of Kyiv-Mohyla Academy - Ukraine
4. Prof. Dr. Alexander Litvinenko - National University of Food Technologies (Kyiv) - Ukraine
5. Prof. Dr. Alit Ibraimi - University of Tetova - North Macedonia
6. Prof. Dr. Anita Grozdanov - Ss. Cyril and Methodius University - North Macedonia
7. Prof. Dr. Asif Šabanović – International University of Sarajevo - Bosnia and Herzegovina
8. Prof. Dr. Bekir Erol Ak - Harran University - Turkey
9. Prof. Dr. Cem Şensöğüt - Dumlupınar University - Turkey
10. Prof. Dr. Christos Douligeris - University of Erlangen-Nurnberg - Germany
11. Prof. Dr. Dragutin T. Mihailović - University of Novi Sad - Serbia
12. Prof. Dr. Evgeniy Shtefan - National University of Food Technologies (Kyiv) - Ukraine
13. Prof. Dr. Falko Dressler - University of Paderborn - Germany
14. Prof. Dr. Houssam Toutanji – Western Michigan University - USA
15. Prof. Dr. Ian F. Akyıldız – Georgia Institute of Technology - USA
16. Prof. Dr. İsmail Usta - Marmara University - Turkey
17. Prof. Dr. Kateryna Derevska - National University of Kyiv-Mohyla Academy - Ukraine
18. Prof. Dr. Liljana Gavrilovska - Ss Cyril and Methodius University - Macedonia
19. Prof. Dr. Lukman Thalib - Qatar University - Qatar
20. Prof. Dr. M. Asghar Fazel – University of Environment - Iran
21. Prof. Dr. Mikhailov Volodymyr - Taras Shevchenko National University of Kyiv - Ukraine
22. Prof. Dr. Mykola Glybovets - National University of Kyiv-Mohyla Academy - Ukraine
23. Prof. Dr. Muammer Koç - Hamad bin Khalifa University - Qatar
24. Prof. Dr. Nadia Bilko - National University of Kyiv-Mohyla Academy - Ukraine
25. Prof. Dr. Özer Çınar – Yıldız Technical University - Turkey
26. Prof. Dr. Perica Paunovik - Ss. Cyril and Methodius University - Macedonia
27. Prof. Dr. Rifat Škrijelj – University of Sarajevo - Bosnia and Herzegovina
28. Prof. Dr. Samir Đug - University of Sarajevo - Bosnia and Herzegovina
29. Prof. Dr. Tanju Karanfil – Clemson University - USA
30. Prof. Dr. Ümit Alver – Karadeniz Technical University - Turkey
31. Prof. Dr. Wolfgang Gerstacker - University of Erlangen-Nurnberg - Germany
32. Prof. Dr. Vladyslav Sukhenko - National University of Life and Environmental Sciences of Ukraine (Kyiv) - Ukraine
33. Prof. Dr. Vullnet Ameti - University of Tetova - North Macedonia
34. Prof. Dr. Yılmaz Yıldırım - Bülent Ecevit University - Turkey
35. Prof. Dr. Yousef Haik - Hamad bin Khalifa University - Qatar
36. Assist. Prof. Dr. Abdelwahab Tahsin - Eqyptian Russian University - Egypt
37. Assist. Prof. Dr. Agon Memeti - University of Tetova - North Macedonia
38. Assoc. Prof. Dr. Alaa Al Hawari - Qatar University - Qatar
39. Assist. Prof. Dr. Arianit Reka - University of Tetova - North Macedonia
40. Assoc. Prof. Dr. Fatih Ungan - Cumhuriyet University - Turkey
41. Assoc. Prof. Dr. Izudin Dzafic - International University of Sarajevo - Bosnia and Herzegovina
42. Assoc. Prof. Dr. Kateryna Syera - National University of Life and Environmental Sciences of Ukraine (Kyiv) - Ukraine
43. Assist. Prof. Dr. Muhamed Hadziabdic - International University of Sarajevo - Bosnia and Herzegovina
44. Assoc. Prof. Dr. Nusret Drešković - University of Sarajevo - Bosnia and Herzegovina
45. Assoc. Prof. Dr. Polina Vakuliuk - National University of Kyiv-Mohyla Academy - Ukraine
46. Assoc. Prof. Dr. Senija Tahirovic - International University of Sarajevo - Bosnia and Herzegovina
47. Assoc. Prof. Dr. Victor Karamushka - National University of Kyiv-Mohyla Academy - Ukraine
48. Assoc. Prof. Dr. Victoria Konovalova - National University of Kyiv-Mohyla Academy - Ukraine
49. Assoc. Prof. Dr. Yuriy Kravchenko - National University of Life and Environmental Sciences of Ukraine (Kyiv) - Ukraine
50. Assist. Prof. Dr. Fatih Taktak - Uşak University - Turkey
51. Assist. Prof. Dr. Fouzi Tabet - German Biomass Research Center - Germany
52. Assist. Prof. Dr. Haris Gavranovic - International University of Sarajevo - Bosnia and Herzegovina
53. Assist. Prof. Dr. Hüseyin Pehlivan - Gebze Technical University - Turkey
54. Assist. Prof. Dr. Sasan Rabieh - Shahid Beheshti University - Iran
55. Assist. Prof. Dr. Ševkija Okerić - University of Sarajevo - Bosnia and Herzegovina
56. Assist. Prof. Dr. J. Amudhavel - VIT Bhopal University - India
57. Dr. Zsolt Hetesi - National University of Public Service, Budapest - Hungary
58. Dr. Zsolt T. Németh - National University of Public Service, Budapest - Hungary

ORGANIZATION COMMITTEE

Chairman of the Conference

Prof. Dr. Özer Çınar – Yıldız Technical University

Members of the Committee

Prof. Dr. Ümit Alver (Co-Chairman) - Karadeniz Technical University - Turkey
Assist. Prof. Dr. Sasan Rabieh - Shahid Beheshti University - Iran
Alma Ligata - Zenith Group - Bosnia and Herzegovina
Ismet Uzun - Zenith Group - Bosnia and Herzegovina
Musa Kose - Zenith Group - Bosnia and Herzegovina

WELCOME TO ICENS 2025

On behalf of the organizing committee, we are pleased to announce that the ***11th*** *International Conference on Engineering and Natural Sciences* ***(ICENS 2025)*** *held from* ***October 22 to 26, 2025 in Sarajevo, Bosnia and Herzegovina****. ICENS provides an ideal academic platform for researchers to present the latest research findings and describe emerging technologies, and directions in Engineering and Natural Sciences issues. The conference seeks to contribute to presenting novel research results in all aspects of Engineering and Natural Sciences. The conference aims to bring together leading academic scientists, researchers and research scholars to exchange and share their experiences and research results about all aspects of Engineering and Natural Sciences. It also provides the premier interdisciplinary forum for scientists, engineers, and practitioners to present their latest research results, ideas, developments, and applications in all areas of Engineering and Natural Sciences. The conference will bring together leading academic scientists, researchers and scholars in the domain of interest from around the world. The scientific program will focus on current advances in the research, production and use of Engineering and Natural Sciences with particular focus on their role in maintaining academic level in Engineering and Applied Sciences and elevating the science level. The conference's goal will to provide a scientific forum for all international prestige scholars around the world and enable the interactive exchange of state-of-the-art knowledge. The conference will focus on evidence-based benefits proven in clinical trials and scientific experiments.*

Best regards,
Prof. Dr.Özer ÇINAR

ICENS 11TH INTERNATIONAL CONFERENCE ON ENGINEERING AND NATURAL SCIENCE October 22-26 2025 Sarajevo

Batch Rectification of Multicomponent Mixtures in Closed Mode of Operation

Adnan Hadzihasanovic[1*], *Muhamed Bijedić*[2]

[1]Plamingo doo
[2]Tehnološki Fakultet Tuzla

*adnan.h2012@gmail.com

Abstract:

Two working regimes are considered – with constant and with variable liquid holdups in vessels. Two subvariants of regime with variable liquid holdups are considered too – with arbitrary initial distribution of charge among vessels and when majority of charge is distributed into still pot. Separation of mixture with four components is simulated, with equimolar composition and where the least volatile component dominates. Process simulation is conducted by performing rigorous integration, using BDF method. The working regimes are compared with respect to quantity and purity of products obtained, for specified time of process duration.

Keywords: Batch Rectification, Multicomponent Mixtures, Closed Mode Of Operation, Total Reflux Operation

ICENS 11TH INTERNATIONAL CONFERENCE ON ENGINEERING AND NATURAL SCIENCE October 22-26 2025 Sarajevo

Mathematical Modeling And Experimental Validation of a Non-Catalytic Ethylene Oxide Hydrolysis Reactor System

Marwan Batiha[1*]

[1]**Al-Hussein Bin Talal University**

*mmbatiha@ahu.edu.jo

Abstract:

This study presents a comprehensive dynamic model for the non-catalytic hydrolysis of ethylene oxide (EO) to produce monoethylene glycol (MEG), diethylene glycol (DEG), and triethylene glycol (TEG). The process model includes a stirred mixing tank, a heat exchanger, and a tubular plug-flow reactor. Each unit operation is mathematically modeled and linearized to obtain transfer functions for control system analysis. A block-flow diagram is developed, and the model's validity is verified using experimental data from an industrial-scale heat exchanger. The results show strong agreement between model predictions and measured data, supporting the model's use for process optimization and control system synthesis.

Keywords: Dynamic Modeling, Ethylene Oxide, Hydrolysis, Process Control, Reactor Dynamics, Heat Exchanger

ICENS 11TH INTERNATIONAL CONFERENCE ON ENGINEERING AND NATURAL SCIENCE October 22-26 2025 Sarajevo

Energy Performance Assessment of Low-Gwp R32/R1234yf Blends For Heat Pump Applications

Vedat Oruç[1], Atilla G. Devecioğlu[1]*

[1]Dicle University

*voruc@dicle.edu.tr

Abstract:

This study presents a theoretical analysis of low-global warming potential (GWP) refrigerant blends based on R32 and R1234yf for use in single-stage heat pump systems. Six alternative refrigerant mixtures, including commercial blends (R454A, R454B, R454C), a pre-commercial formulation (DR5), and two novel proposed mixtures (Mix1 and Mix2), were evaluated. The analysis was conducted by a comparative energetic performance assessment at an evaporator (+5 C) and two condenser temperature (40 and 50 C) cases. The parameters such as compressor power consumption, volumetric cooling capacity, heating capacity, and coefficient of performance for a heat pump (COPh) were calculated and compared. Among the blends, R454B demonstrated the highest heating capacity and compressor power consumption, whereas Mix1 showed the lowest values for both parameters. DR5 yielded the highest VCC. Despite slight variations, the COPh values were generally similar across all mixtures. The results suggest that carefully optimized R32/R1234yf mixtures with GWP<500 can offer feasible, efficient, and environmentally favourable alternative refrigerants for future heat pump applications.

Keywords: Low-GWP Refrigerants, R32/R1234yf Mixtures, Heat Pump Performance, Heating Capacity

ICENS 11TH INTERNATIONAL CONFERENCE ON ENGINEERING AND NATURAL SCIENCE October 22-26 2025 Sarajevo

Numerical Investigation of Submerged Vanes on Discharge Distribution at Open-Channel Bifurcations

Firat Gumgum[1*]

[1]Dicle University

*firat.gumgum@dicle.edu.tr

Abstract:

Submerged vanes are hydraulic structures widely used for purposes such as protecting riverbanks from erosion, redirecting sediment fluxes, facilitating desilting at water intakes, etc. These structures are typically installed with a specified skew angle relative to the flow direction and exert a notable influence on flow characteristics by generating tip vortices. The vortices induced by the vanes are anticipated to increase the amount of water diverted into lateral intakes. The present study aims to numerically examine the effects of submerged vanes on discharge distribution at open-channel bifurcations. Numerical simulations were performed using the FLOW-3D HYDRO software. The model consisted of a T-shaped rectangular channel system, in which the main channel was 5.2 m long and the diversion channel was 3.6 m long. Both channels had a width of 0.30 m, and bed sills with a height of 0.025 m were positioned at the channel outlets. Two simulation scenarios were considered. In the first case, the bifurcation system was modeled without submerged vanes to establish the reference condition. In the second case, a submerged vane field was introduced at the bifurcation zone. This vane field consisted of six arrays; each comprised of two rows of vanes. The vane height was set to 0.3 times the approaching flow depth, and the skew angle of the vanes was specified as 30°. The flow was resolved using the Large Eddy Simulation (LES) turbulence closure, with the Smagorinsky coefficient set to 0.5 to account for subgrid-scale turbulence effects. The numerical results demonstrated that the presence of the submerged vane field substantially influenced the discharge distribution, leading to a 13.9% increase in the diverted discharge compared to the case without vanes.

Keywords: Submerged Vanes, Flow Division, Discharge Distribution

Sustainable Soil Strength Improvement Using Agricultural Waste in Geotechnical Applications

Huseyin Kursat Celik[1], Tolga Tikit[1], Isinay E. Yuzay[2], Pelin Aklik[1]*

[1]Department of Civil Enginering, Faculty of Enginering, Izmir University of Economics
[2]Department of Genetics And Bioenginering, Faculty of Enginering, Izmir University of Economics

*pelin.aklik@ieu.edu.tr

Abstract:

With the growing population and advancing technologies, there is an increasing need to recycle materials to reduce waste generation globally. The agro-food industry, in particular, produces large quantities of waste and by-products, which pose both financial and environmental challenges. For example, 3.214.522 tonnes of almonds are produced worldwide annually, and Turkey ranks as the 5th largest almond producer, generating around 150,000 tonnes each year, of which approximately 40% is waste (mainly almond shells).

This study explored the potential use of agricultural waste, specifically almond shell powder and the biochars derived from them, in order to improve the soil strength in geotechnical engineering applications. In the experimental phase, almond shell powder and biochars were first mixed at a 1:1 ratio. These mixtures were then combined with dry loose sandy soil at varying weight ratios (10%, 20%, and 30% w/w). The soil mixtures were subjected to direct shear testing using a shear box apparatus with dimensions of 60 × 60 × 30 mm. Normal stresses of 60, 120, and 180 kPa were used. The inclusion of almond shell powder and biochars were found to improve both the internal friction angle and cohesion, thereby enhancing the overall shear strength of the soil.

The utilization of almond shell powder and biochars represent a promising approach not only for waste valorization in the agro-food sector but also for advancing sustainable practices in geotechnical engineering by expanding the application of bio-based soil improvement materials.

Keywords: Soil Improvement, Shear Strength, Biochar, Almond Shell Powder

ICENS 11TH INTERNATIONAL CONFERENCE ON ENGINEERING AND NATURAL SCIENCE
October 22-26 2025 Sarajevo

Evaluating User Experience And Dataspace Integration in a Virtual Reality Cultural Heritage Applications

Selma Rizvic[1], Irfan Prazina[1], Bojan Mijatovic[2], Dusanka Boskovic[1], Štefan Kohek[3],Domen Mongus[3]*

[1]University of Sarajevo - Faculty of Electrical Engineering
[2]Sarajevo School of Science And Technology
[3]University of Maribor

*selma.rizvic@etf.unsa.ba

Abstract:

Cultural heritage is crucial for preserving our identity and history, while Virtual Reality (VR) is becoming a powerful tool for showcasing it. To explore the value of VR in this field, we developed a VR application specifically for presenting cultural heritage. Our application allows a convincing presentation of WWI events in Central Europe through interactive digital storytelling about a mosque at a battlefield in Slovenia. In this paper, we outline the application's structure and analyze its impact on cultural heritage perception. We also propose an architecture of Dataspaces integration within the VR-based application and experimentally justify the integration of dataspaces to use cultural heritage data within the application. We evaluated the application through a qualitative User eXperience evaluation study with 10 anonymous users, assessing both its functionality and the requirements for the dataspace integration. Our findings show that the VR experience is highly immersive, demonstrating the value of using this technology. The results also highlight the necessity of integrating dataspaces to further enhance the application's capabilities.

Keywords: Digital Heritage, Interactive Digital Storytelling, Virtual Reality, Dataspaces

ICENS 11TH INTERNATIONAL CONFERENCE ON ENGINEERING AND NATURAL SCIENCE October 22-26 2025 Sarajevo

Mixed Convection Heat Transfer Investigation in a Vertical Duct Having Heated Trapezoidal Obstacles Employing Nanofluid of Cuo-Water

***Koray Karabulut*[1*], *Yeliz Alnak*[1]**

[1]Sivas Cumhuriyet University

*koray.karabulut@hotmail.com

Abstract:

In this study, mixed convection heat transfer and flow structures around obstacles in a channel containing three trapezoidal geometry constant heat flux barrier elements, two at the top and bottom on the left side and one at the right side of parallel vertical plates, were numerically investigated employing CuO-water nanofluid and in comparison with water. The numerical investigation was carried out by solving the continuity, momentum and energy equations in a steady, laminar and two-dimensional using the Ansys-Fluent computer program. In order to direct the flow to the heated obstacle elements within the channel, flow direction fins were placed on the upper inlet surfaces of the channel at 45o and 60o angles. Except for the obstruction elements, all surfaces of the channel and the flow directors are adiabatic. CuO-water nanofluid and water at 293 K inlet temperature were used as working fluids in the duct. While the Reynolds number (Re) values in the study were 50, 100, 150 and 200, the modified Richardson number (Ri*) values were taken as 100 and 150 and the Flow Crossing Distance (FCD) ratio in the channel was taken as a constant of 2. The results of the study were found to be in good agreement with the experimental and numerical results in the literature. It was determined that for Re = 200 and Ri* = 150, the Num number of the heated obstacle element located on the upper left side of the channel with 60o angled fins is 24.09% higher than the water fluid when CuO-water nanofluid is used. In addition, it was found that for Re = 100 and Ri* = 100, in the case of 60o angle and nanofluid use, the PEC value decreased by 2.1%, while in the 45o angle case, this value increased by 0.97%.

ACKNOWLEDGEMENT

This study was supported by Sivas Cumhuriyet University Scientific Research Projects (CÜBAP) unit with project number STBMYO-2024-005.

Keywords: Mixed Convection; Trapezoidal Obstacle; Cuo-Water Nanofluid; Fin

[*]This study was supported by Sivas Cumhuriyet University Scientific Research Projects (CÜBAP) unit with project STBMYO-2024-005

ICENS 11TH INTERNATIONAL CONFERENCE ON ENGINEERING AND NATURAL SCIENCE
October 22-26 2025 Sarajevo

Enhancing Water Quality Monitoring For Early Detection of Harmful Algal Blooms

Fatma Özge Özkök[1*]

[1]Erciyes University

*fozgeozkok@erciyes.edu.tr

Abstract:

Harmful algal blooms (HABs) pose a growing threat to river ecosystems, water quality, and human health. Early detection and accurate prediction of algal growth are essential for effective water management and sustainable monitoring practices. Traditional chemical and biological analyses are often labor-intensive, costly, and slow, limiting their practical use for real-time monitoring.

In this study, we propose a data-driven approach to forecast the abundance of seven harmful algal species in rivers based on environmental and chemical parameters, including water temperature, pH, dissolved oxygen, and nutrient concentrations, alongside river-specific factors such as flow rate and size. Using a Multilayer Perceptron (MLP) model, we capture complex non-linear relationships between these features and algal frequencies, enabling multi-output prediction from aggregated water sample data.

Experimental results demonstrate that the MLP model provides accurate predictions across all algal species, outperforming conventional machine learning approaches in mean absolute error and robustness. The model's predictive capability supports the development of early warning systems and automated monitoring tools, offering a cost-effective solution for real-time water quality management.

This work highlights the potential of deep learning-based methods to bridge scientific knowledge and practical water management, contributing to sustainable strategies for preventing and controlling harmful algal blooms.

Keywords: Harmful Algal Blooms, Water Security, Early Warning Systems, Deep Learning, Data-Driven Prediction

[*]This study is supported by the COST Action CA23160 Effective Lake Management: Reducing Cyanobacteria by Actions in the Catchment

ICENS 11TH INTERNATIONAL CONFERENCE ON ENGINEERING AND NATURAL SCIENCE
October 22-26 2025 Sarajevo

Therapeutic Promise of Skimmin Isolated From Matricaria Chamomilla L. in Pulmonary Arterial Hypertension Via Tgf-B Pathway Modulation

Sila Ozlem Sener[1], Talat Nasim[2]*

[1]University Of Health Scieneces, Türkiye
[2]University Of Bradford, Bradford, Uk

silaozlem.sener@sbu.edu.tr

Abstract:

Introduction: Pulmonary arterial hypertension (PAH) is a progressive cardiovascular disorder that frequently leads to right ventricular failure and premature death [1]. Among the therapeutic targets under investigation, the transforming growth factor-β (TGF-β) receptor family-particularly TGFBR2-and their downstream signaling cascades are considered critical [2]. In recent years, natural compounds have attracted growing attention as promising therapeutic candidates for PAH, owing to their diverse bioactivities and potential to modulate key molecular pathways [3].

The aim of the study: In this study, we examined the therapeutic potential of skimmin, a coumarin derivative isolated from Matricaria chamomilla L., in the regulation of TGF-β signaling within the context of PAH.

Research methods: A series of experimental approaches, including isolation and identification studies, reporter assays, RT-PCR/qPCR analyses, and cell proliferation studies, were employed to elucidate its biological effects.

Results: Data from reporter activity and gene expression profiling revealed that skimmin attenuates TGF-β pathway activation by suppressing SMAD3 phosphorylation and reducing pai-1 transcript levels. Moreover, skimmin significantly inhibited the abnormal proliferative response of pulmonary artery smooth muscle cells (PASMCs) harboring the bmpr2 R899X+/− mutation upon TGF-β1 stimulation, while exerting no detectable cytotoxic effects on wild-type PASMCs.

Conclusion: Taken together, this work provides the first comprehensive evidence of skimmin as a natural modulator of TGF-β signaling in PAH, underscoring not only the growing role of plant-derived bioactive compounds in PAH therapy but also the potential translational applications of skimmin in PAH and other TGF-β–related disorders.

Acknowledgment

We would like to acknowledge the Turkish Scientific and Technical Research Council (TUBITAK) for supporting the study with the 2219 TUBITAK International Post Doctoral Research Fellowship Programme.

Keywords: Keywords: Matricaria Chamomilla L., PAH, Skimmin, TGF-B, TGFBR2

**This study is supported by the Turkish Scientific and Technical Research Council (TUBITAK).*

ICENS 11TH INTERNATIONAL CONFERENCE ON ENGINEERING AND NATURAL SCIENCE
October 22-26 2025 Sarajevo

Mechanical And Thermal Properties of Polypropylene-Based Composites Reinforced With Plane Tree Seed Fibers And Organoclay

Lemiye Atabek Savaş[1], Recep Tayyip Yiğci[2], Ceren Loğoğlu[2], Yunus Emre Gündoğar[2]

[1]Erciyes University
[2]Erciyes University, Department of Aerospace Engineering Engineering

atabekl@erciyes.edu.tr

Abstract:

In this study, polypropylene (PP) based composites were prepared by using the melt blending method by reinforcing plane tree seed fiber (PTF) at different ratios (10, 20, and 30wt.%) and adding various amounts of organoclay (1-5wt.%) to each fiber ratio. Mechanical performance was assessed through tensile and flexural tests, while thermal stability was investigated using thermogravimetric analysis (TGA).

Tensile test results revealed that the addition of PTF decreased the tensile strength and elongation rate compared to pure PP; however, an improvement in tensile strength was achieved with increasing fiber content. However, the elastic modulus of the composites containing 20 wt.% and 30 wt.% PTF increased compared to pure PP, and the highest value (998 MPa) was observed in the composite containing 30 wt.% PTF. In terms of tensile strength, the addition of varying amounts (1-5 wt.%) of organoclay to composites containing 10%, 20%, and 30% PTF did not result in a significant difference compared to their counterparts containing only PTF; all groups exhibited similar tensile strength values. The modulus of elasticity increased depending on the fiber content, especially with adding 3-5% organoclay. Flexural tests revealed a similar trend. The highest flexural strength and modulus were observed in the composite containing 30 wt.% PTF (55.8 MPa, 2401 MPa), while organoclay addition led to slight reductions or moderate improvements depending on the combination. TGA results revealed that the incorporation of PTF reduced the thermal stability of the composites, evidenced by a lower temperature corresponding to 5% weight loss (T5%). The Tmax values, indicating the temperature at which the material undergoes the most rapid mass loss during thermal decomposition, were generally comparable to neat PP for both the PTF-only and PTF/organoclay composites, with some formulations exhibiting slightly higher values. These findings highlight the potential of PTF and organoclay to tailor the properties of PP-based composites.

Keywords: Polypropylene, Plane Tree Seed Fibers, Organoclay, Composites.

[*]This study was supported by TÜBİTAK under the 2209-A University Students Research Projects Support Program.

ICENS 11TH INTERNATIONAL CONFERENCE ON ENGINEERING AND NATURAL SCIENCE October 22-26 2025 Sarajevo

2-D Sedimentary Thickness Modeling of The Sinanpaşa Basin Using Gravity Data Inversion

Fatma Figen Altinoğlu[1*]

[1]**Department of Geological Engineering, Faculty of Engineering, Pamukkale University**

*faltinoglu@pau.edu.tr

Abstract:

The Sinanpaşa Basin, located on the eastern margin of the Western Anatolian extensional province, is a Neogene sedimentary basin formed under the Aegean extensional tectonic regime. Determining sedimentary thickness within the basin is essential for reconstructing its tectonic and geological evolution and for evaluating its potential in terms of mineral resources, hydrocarbons, geothermal energy, and groundwater reserves. Situated among several basins with known mineralization and geothermal activity, the Sinanpaşa Basin holds considerable significance for both geological and resource-oriented studies. In this study, Bouguer gravity data were utilized to develop two-dimensional models of sedimentary thickness through a Particle Swarm Optimization (PSO)-based inversion approach. Eight north–south oriented profiles, perpendicular to the basin's structural trend, were analyzed to characterize subsurface geometry. The inversion results demonstrate notable variations in sedimentary thickness, with the western section—between Düzağaç and Tokuşlar villages—exhibiting the greatest thickness, reaching approximately 490 m in one profile. It should be emphasized that this value corresponds to a single profile, and deeper sections may exist elsewhere in the basin.

The analysis further indicates a gradual decrease in sedimentary thickness from west to east, consistent with the structural and depositional trends of the basin. These findings corroborate previous regional studies while providing refined insights into the basin's subsurface architecture. The integration of gravity inversion and PSO modeling proves to be an effective methodology for delineating sedimentary frameworks in complex extensional settings. Overall, this study advances the understanding of the Sinanpaşa Basin's sedimentary configuration, offering a foundation for future geophysical, geological, and resource exploration efforts in Western Anatolia, and emphasizing the importance of precise subsurface characterization in tectonically active basins.

Keywords: Sinanpaşa Basin, Sedimentary Thickness, Gravity Inversion, Particle Swarm Optimization

ICENS 11TH INTERNATIONAL CONFERENCE ON ENGINEERING AND NATURAL SCIENCE October 22-26 2025 Sarajevo

Quantitative Estimation of Source Depth in Self-Potential Anomalies of Simple Geometric Bodies

Erdinç Öksüm[1*]

[1]DEPARTMENT OF GEOPHYSICAL ENGINEERING, FACULTY OF ENGINEERING AND NATURAL SCIENCES, SÜLEYMAN DEMIREL UNIVERSITY

*erdincoksum@sdu.edu.tr

Abstract:

Self-potential (SP) methods are commonly used in geophysical studies to detect sulfide ore bodies such as copper, lead, and zinc by measuring naturally occurring electrical potentials in the subsurface. Despite their practical significance, quantitative interpretation, particularly the estimation of source depth and structural index, remains challenging due to the inherent non-uniqueness of potential field problems. This study introduces a new approach for the interpretation of isolated SP anomalies, which establishes a direct relation between the horizontal derivative of the anomaly and the source depth and shape factor. By using two successive points from a transformed anomaly, the method enables simultaneous estimation of depth and model index, and subsequently allows calculation of the polarization angle and electric dipole moment. The technique is simple, avoids complex inversion procedures, and can be applied efficiently to geometrical models. Its performance was tested on noise-free synthetic datasets representing an infinite vertical cylinder, a horizontal cylinder, and a sphere, and in all cases, the estimated parameters accurately reproduced the true model values, confirming the method's reliability. While the present work is limited to synthetic examples, future studies will explore its robustness under noisy conditions, real field applications, and the impact of uncertainties in anomaly origin selection. Overall, the results highlight the promise of the proposed approach while stressing the importance of further validation under realistic conditions.

Keywords: Self-Potential Anomaly, Depth Estimation, Simple Geometric Bodies, Quantitative Interpretation

ICENS 11TH INTERNATIONAL CONFERENCE ON ENGINEERING AND NATURAL SCIENCE October 22-26 2025 Sarajevo

Numerical Investigation of Flow Characteristics in River Bridges With Different Designs

Pinar Ozenci[1], Omer Faruk Dursun[1], Mahmut Aydogdu[2]*

[1]Inonu University
[2]Malatya Turgut Ozal University

*ofdursun@gmail.com

Abstract:

Bridges, crucial infrastructure facilities in modern human life, are constructed to provide uninterrupted transportation on roads and railways. River bridges are subject to significantly greater risks of abrasion, erosion, and failure than other bridges. The flow characteristics created and modified by river flow at and around the foundations of bridge piers during floods can cause bridge collapses. These failures lead to loss of life, property, and transportation disruptions.

In this study, river bridges with different plan designs were numerically analyzed. Geometric characteristics such as whether the bridges are perpendicular to the river axis or angled, despite similar abutment spans and abutment heights, abutment widths, whether they are straight, curved, or split in plan, and the bending angle of broken-shaped bridges were investigated. For this purpose, Ansys/Fluent, a software capable of performing calculations using the Computational Fluid Dynamics (CFD) method, was used. Flow characteristics such as flow velocity, pressures, turbulence, wall stresses, and flow directions, as well as their effects on the bridge piers, were determined and discussed. All results were compared with each other and with the literature and interpreted.

Keywords: Flood, Hydraulic Design Of Bridges, River Hydraulics, Bridge Failure, Cfd

A Meshfree Approach to Beam And Plate Structures: Element-Free Galerkin Implementation With Gauss Quadrature

Yakup Hakan Aydin[1*], Muhsin Gokhan Gunay[1]

[1]Isparta University of Applied Sciences

aydinyakup@isparta.edu.tr

Abstract:

This study investigates the mechanical behavior of beam and plate structures using the Element-Free Galerkin (EFG) method, a meshfree approach that eliminates the need for predefined connectivity among nodes. Unlike the finite element method (FEM), which requires complex meshing and suffers from mesh dependency, EFG employs moving least squares (MLS) shape functions combined with weight functions to construct the approximation. The formulation was implemented in Python within the Spyder environment, and numerical integration was carried out using Gauss quadrature.

To enhance solution quality, systematic variations in the number of nodes and Gauss integration points were performed. The results indicate that increasing node density improves accuracy but also raises computational cost, while optimal selections of Gauss points significantly reduce integration errors without excessive overhead. The bending and buckling responses of beams and plates under different boundary conditions were analyzed, and the outcomes were compared against FEM solutions. The EFG method consistently demonstrated higher accuracy in capturing displacement and stress fields, especially in regions with steep gradients, while also showing improved stability against mesh distortion problems typical of FEM.

Overall, the findings reveal that meshfree methods, and in particular EFG, provide flexible, accurate, and computationally efficient alternatives for structural mechanics problems. This work not only validates the practicality of implementing EFG through Python-based tools but also emphasizes its potential to advance the modeling of complex engineering systems requiring precision and adaptability.

Keywords: Element-Free Galerkin, Meshfree Methods, Beam, Plate, Gauss Quadrature, Python

ICENS 11TH INTERNATIONAL CONFERENCE ON ENGINEERING AND NATURAL SCIENCE October 22-26 2025 Sarajevo

Simulation-Based Comparative Analysis of Non-Isolated Dc–Dc Converters For Photovoltaic Systems

Mehmet Can Sekanli[1], Mert Öpöz[1], Samet Yalçin[1], Okan Bingöl[1]*

[1]Isparta University of Applied Sciences

*mehmetsekanli@isparta.edu.tr

Abstract:

The rapid growth of photovoltaic (PV) applications has intensified the need for high-efficiency power-conversion stages capable of adapting to variable irradiance and load conditions. Non-isolated DC–DC converters play a critical role in extracting and regulating energy from PV arrays, yet selecting the most suitable topology remains challenging due to trade-offs among efficiency, voltage gain, ripple characteristics, and component stress.

This study presents an analytical and simulation-based comparison of five widely used non-isolated DC–DC converters - boost, buck-boost, SEPIC, Ćuk, and Zeta - operating in a PV environment. Average state-space modeling is employed to derive closed-form expressions for voltage conversion ratio, current ripple, and conduction and switching losses, providing a unified analytical framework for evaluation. Each topology is implemented and tested in the LTspice environment under identical PV source conditions.

Simulation results reveal that the boost converter achieves the highest voltage gain but suffers from increased current ripple. The SEPIC and Zeta converters exhibit excellent input–output decoupling and low output ripple at the expense of greater component count. The Ćuk converter delivers continuous input current and robust dynamic response, though with moderate efficiency due to higher conduction losses. Analytical predictions and LTspice simulations show strong agreement, confirming the validity of the modeling approach.

The comparative findings highlight the distinct advantages and limitations of each topology, offering practical guidance for engineers and researchers when selecting non-isolated converters for PV systems where galvanic isolation is not required. This work provides a comprehensive reference for optimizing PV power-conversion stages with respect to efficiency, voltage regulation, and overall system performance.

Keywords: Photovoltaic (PV) Systems, Non-Isolated DC–DC Converters, Ltspice Simulation

ICENS 11TH INTERNATIONAL CONFERENCE ON ENGINEERING AND NATURAL SCIENCE October 22-26 2025 Sarajevo

Emi Analysis of Ćuk Converters Used in Photovoltaic Systems

Mehmet Can Sekanli[1], Mert Öpöz[1], Samet Yalçin[1], Okan Bingöl[1]*

[1]Isparta University of Applied Sciences

*mehmetsekanli@isparta.edu.tr

Abstract:

Electromagnetic interference (EMI) has become a major concern in photovoltaic (PV) power conversion systems, particularly in DC–DC converters where high-frequency switching operations generate conducted and radiated disturbances. Among various non-isolated topologies, the Ćuk converter is widely employed in PV applications due to its continuous input current and wide voltage conversion capability. However, the inherent switching transitions can introduce significant EMI issues, potentially affecting compliance with international standards and the reliable operation of surrounding electronic equipment.

This study presents a comprehensive EMI analysis of a Ćuk converter operating in a PV environment, carried out through LTSpice-based simulations. A Line Impedance Stabilization Network (LISN) is integrated into the test setup to accurately capture conducted EMI spectra over the relevant frequency range. The analysis focuses on quantifying differential-mode and common-mode noise components, as well as identifying the influence of switching frequency, duty cycle, and passive component selection on EMI behavior.

Preliminary simulation results reveal distinct conducted EMI profiles under varying operating conditions, highlighting the trade-offs between efficiency and electromagnetic compatibility. The findings provide valuable insights into the EMI characteristics of Ćuk converters in PV systems and establish a foundation for developing effective mitigation strategies, such as optimized filter design and improved switching techniques.

Keywords: Photovoltaic (PV) Systems, Electromagnetic Interference (EMI), Line Impedance Stabilization Network (LISN)

ICENS 11TH INTERNATIONAL CONFERENCE ON ENGINEERING AND NATURAL SCIENCE October 22-26 2025 Sarajevo

L-Type DGS Decoupling Mechanism Design For 5G Mimo Antenna Systems

Tuğberk Akpinar[1], Elif Merve Küçüköner[1]*

[1]Suleyman Demirel University

*elifkucukoner@sdu.edu.tr

Abstract:

In this study, a decoupling mechanism was designed for 5G multiple-input multiple-output (MIMO) antennas under the 6 GHz frequency. A microstrip patch antenna was selected as the MIMO antenna structure, and a metal strip was placed between the antennas on the top layer as the decoupling mechanism for this two-element structure, and a defected ground structure was created on the ground plane. The design was performed using CST Studio Suite. A Rogers RT-Duroid 5880 with a dielectric constant of 2.2 and a loss tangent of 0.0009 was used as the substrate. A time domain solver was used as the analyzer. The dgs was generated by etching 8 of two complementary L-shaped structures rotated by 90 degrees. A decoupling mechanism in the form of a flat metal strip was placed between the two antennas on the top plane, thus improving both isolation and gain. The distance between the antennas was reduced to 0.175 λ. The antenna operates at a frequency of 3.48 GHz, where isolation is −21.6 dB and the antenna provides a gain of 6.523 dBi. These results demonstrate that the designed antenna is suitable for 5G applications due to its efficient performance and compact size.

Keywords: Antenna, Decoupling, DGS, Mimo

ICENS 11TH INTERNATIONAL CONFERENCE ON ENGINEERING AND NATURAL SCIENCE October 22-26 2025 Sarajevo

A Review on Conventional And Twin-Tail Configurations in Fighter Aircraft: Comparative Aerodynamic Performance

Orhan Keklikcioglu[1*], Doguhan Aydin[1]

[1]Erciyes University

*keklikcioglu@erciyes.edu.tr

Abstract:

The aerodynamic design of fighter aircraft plays a decisive role in flight performance, maneuverability, fuel efficiency, and overall operational effectiveness. Among the key design elements, tail configurations are critical for ensuring stability, controllability, and stealth performance. This paper presents a literature-based review focusing on the comparative evaluation of conventional and twin-tail configurations in terms of their aerodynamic characteristics.The conventional tail configuration offers advantages of reduced drag and lower structural weight, yet it may encounter control limitations at high speeds and aggressive flight conditions. In contrast, the twin-tail configuration enhances aircraft stability, particularly at high angles of attack and during dynamic maneuvers, providing superior handling qualities. However, this design may increase radar cross-section (RCS) and structural weight, which must be considered in modern stealth-oriented designs. Review of experimental and CFD-based studies indicates that these tail configurations exhibit significant differences in lift, drag, and moment coefficients under varying flow conditions.

This review further synthesizes findings on the impact of tail designs on aerodynamic efficiency, maneuvering capability, buffeting resistance, and vortex generation. Particular attention is given to stealth technologies, highlighting that the influence of tail configurations on radar signature has been relatively underexplored and remains a promising research gap. In conclusion, this review provides a systematic evaluation of the aerodynamic trade-offs between conventional and twin-tail fighter aircraft designs. By consolidating existing knowledge, it aims to guide future investigations and contribute to the development of more efficient, agile, and stealth-capable combat aircraft.

Keywords: Aerodynamics, Fighter Aircraft, Tail Design, Cfd, Stealth Technology

[*]ERU BAP FYL-2025-14678

ICENS 11TH INTERNATIONAL CONFERENCE ON ENGINEERING AND NATURAL SCIENCE
October 22-26 2025 Sarajevo

Assessing The Impact of Prosopis Juliflora on Tick Oviposition And Survival

Nada Ahmad Assaad[1], Fatima Alkhayat[1], Mohammed Abu-Dieyeh[1], Iman Saleh[1]*

[1]**Qatar University, Department of Biological And Environmental Sciences**

*nada_assaad995@hotmail.com

Abstract:

The widespread use of synthetic acaricides has led to environmental problems and the development of resistance, making ticks significant vectors of diseases that impair both humans and animals, and have serious negative effects on the economy and human health. For long-term tick management and control, Prosopis juliflora and other plant-based extracts provide a practical and eco-friendly alternative. Between February 2024 and January 2025, tick samples were taken from camels at various livestock farms spread around Qatar in various municipalities. These samples were then identified at the species level both morphologically and molecularly. To determine the oviposition inhibition (%) and mortality rates, female Hyalomma dromedarii ticks, both engorged and unfed, were subjected to varying concentrations of Prosopis juliflora extract using the adult immersion test (AIT). R software and the GLM model were used to statistically analyze the plant extract's efficacy and impact on tick survival. The acaricidal activity of P. juliflora against H. dromedarii was evaluated at each of the tested dosages (0.05 mg/mL to 0.5 mg/mL). An effective dosage of 0.05 mg/ml was sufficient to kill 50% of the ticks, according to the dose-response study, and the untreated ticks' chances of surviving were 1.72 times higher than those of the treated groups. Future studies should examine different dosages, pinpoint important bioactive components, and evaluate P. juliflora's effects at every stage of the tick life cycle.

Keywords: Prosopis Juliflora, Qatar, Tick, Vector-Borne Diseases, Ecology, Oviposition, Survival Rate

ICENS 11TH INTERNATIONAL CONFERENCE ON ENGINEERING AND NATURAL SCIENCE
October 22-26 2025 Sarajevo

Clustering European Islands Based on Renewable Energy And Environmental Features

***Mustafa Ozan Özkök*[1*]**

[1]Sakarya University

*mustafaozanozkok.34@gmail.com

Abstract:

European islands exhibit significant diversity in renewable energy potential and environmental characteristics. In this study, key features such as island area, surrounding water fraction, solar and wind energy potential, and geographic location were used to perform an unsupervised clustering analysis. The K-Means algorithm was applied to group islands based on their energy and environmental profiles, allowing the identification of clusters with similar characteristics. The resulting clusters were analyzed to highlight differences in energy potential and environmental attributes, providing insights into which islands are suitable for renewable energy development and which require careful environmental management. This clustering approach offers a visual and analytical tool for comparative assessment of islands, supporting sustainable energy planning and ecosystem conservation. The study demonstrates how machine learning techniques can efficiently synthesize geographic and environmental data to inform strategic decisions for small and medium-sized islands.

Keywords: European Islands, Renewable Energy, Environmental Features, Clustering, Machine Learning

[*]*This study is supported by the CA21158 COST Action (SMILES).*

Microplastics in Insects: A Review on Uptake, Impacts, And Environmental Implications

Nada Ahmad Assaad[1], Fatima Alkhayat[2], Veerasingam Subramanian[3], Sankaran Rajendran[3], Talaat Ahmed[3]*

[1]Qatar University
[2]Qatar University, Department Of Biological And Environmental Sciences
[3]Environmental Science Center, Qatar University, Doha, Qatar

*nada_assaad995@hotmail.com

Abstract:

Plastic particles ranging in size from 1 µm to 5 mm are known as microplastics (MPs), and have become ubiquitous contaminants across air, water, sediment, food, biota, and even within humans. Recent studies reveal that insects, one of the most diverse and ecologically significant groups of organisms, are increasingly exposed to MPs. This review summarizes current knowledge on MP contamination in insects, including the types and sources of MPs, exposure pathways such as ingestion, inhalation, and dermal contact, as well as the analytical techniques used for their detection and quantification. It also, examines the physiological and biological effects of MPs on insects, including behavioral changes affecting feeding, locomotion, and navigation, along with disruptions in development, reproduction, and cellular integrity.

The review also highlights the potential for MPs to bioaccumulate and transfer tropically through food webs. Despite growing research interest, significant knowledge gaps remain, particularly regarding species diversity, long-term impacts, ecological consequences, and the need for standardized detection techniques. Addressing these gaps is crucial for understanding the full extent of MP impacts on insect populations and for developing strategies to mitigate associated environmental risks, thereby safeguarding biodiversity and ecosystem functionality.

Keywords: Microplastics, Insects, Terrestrial Ecosystems, Biodiversity Impacts, Trophic Transfer, Bioaccumulation, Freshwater Systems

**This work was supported by the Qatar University funded grant: QUHI-CAS-25_26-808*

FULL-TEXT ARTICLES

ICENS 11TH INTERNATIONAL CONFERENCE ON ENGINEERING AND NATURAL SCIENCE October 22-26 2025 Sarajevo

Investigation of the Risks of Neglecting Vertical Earthquake Effects in Masonry Buildings within the Scope of TBEC-2018

Kamran Samadi[1], Mehmet Firat Karapinar[2], Baris Sayin[3]

Abstract

Despite the studies available in the literature on the effect of the vertical earthquake component in recent years, codes have lagged in this area. Traditional masonry structures are already considered a high-risk building category, but they are also particularly vulnerable to the vertical component of an earthquake being neglected. The aim of this study is to reveal the risks that may arise from not considering the vertical earthquake effect in the seismic assessment of traditional masonry buildings in the TBEC-2018 earthquake code. For this purpose, a two-storey prototype model was subjected to nonlinear time history analysis for two different scenarios: The first scenario considered only the horizontal effects (H), while the second scenario considered both the horizontal and vertical effects (H+V) of the earthquake. Near fault records were used to see the effect of the vertical component more clearly. When considering the vertical component of the earthquake, increases of 270% and 338% in floor acceleration values and increases of 198% and 212% in vertical displacement values were observed for the second and first floors, respectively. In addition, the vertical elastic design spectrum defined in TBEC-2018 has remained below the average spectrum obtained from actual earthquake records. Therefore, it has been proven that accounting for vertical earthquake effects is inevitable in the seismic performance assessment of traditional masonry buildings. Otherwise, any assessment and strengthening application in these structures would not be reliable or realistic. Thus, TBEC-2018 and other similar earthquake codes must establish clear and explicit rules in this context.

Keywords: Masonry Structure, Near Fault Earthquake, Seismic Performance Assessment, TBEC-2018, Vertical Earthquake Component.

1. INTRODUCTION

Earthquake ground motion is inherently a three-dimensional phenomenon. This allows for the recording of ground acceleration in three orthogonal components using an accelerometer. As a result, structures under seismic action exhibit a tri-directional response [1].

The fundamental difficulty in seismic structural design arises from the horizontal components of ground motion. Structures possess considerably less lateral capacity compared to their capacity to resist gravity loads. Lateral seismic acceleration results in inertial forces, which in turn lead to significant shear forces and overturning moments. Consequently, the focus of earthquake engineering in structural design has predominantly been on the horizontal seismic components. This approach is reflected in TBEC-2018 [2], in line with other prevalent and contemporary codes.

Conventional unreinforced masonry (URM) structures are inherently brittle systems, demonstrating significant structural deficiencies when subjected to seismic events. The low tensile and shear capacity of their base materials (e.g., brick, stone) renders them incapable of resisting lateral earthquake-induced loads. This vulnerability is exacerbated by the lack of ductile behavior in the load-bearing system, an inability to preserve structural integrity due to inadequate connections between structural elements, and the magnification of inertial forces owing to their heavy mass [3]. The fact that they have not received engineering services makes these structures even more risky. The most obvious evidence of this is the collapse of masonry structures and the resulting loss of life in the 2023 Kahramanmaraş earthquake.

Accordingly, it is clear that for masonry structures, neglecting the vertical component of an earthquake can pose significant risks, beyond consideration of their overall structural performance. This is because, in near-fault earthquakes, vertical ground accelerations can reach critical levels and intensify structural damage.

[1] Institute of Graduate Sciences, Istanbul University-Cerrahpasa, İstanbul, Türkiye, kamran.samadi@gmail.com
[2] Structural Engineer (PhD) mehmetfiratkarapinar@gmail.com
[3] Corresponding author: Istanbul University-Cerrahpasa, Department of Civil Engineering, Structural Engineering Division, 34320, Istanbul, Türkiye, barsayin@iuc.edu.tr

The literature on this topic can be classified into two primary categories of research. The first category focuses specifically on the influence of the vertical component of earthquakes on masonry structures, whereas the second investigates the general performance of these buildings under near fault ground motions. For instance, Di Michele et al. [4] investigated the effect of the vertical seismic component on masonry buildings during near-fault earthquakes, aiming to highlight the deficiencies of seismic codes like Eurocode 8 in this regard. The investigators conducted nonlinear dynamic time-history analyses on a two-storey prototype stone masonry model representing typical Italian constructions. The results revealed significant fluctuations in axial forces at the upper floor levels. Moreover, they underscored that due to the short fundamental periods of masonry buildings (0.05-0.15s), their susceptibility to resonance with the high-frequency vertical ground motion component is elevated, potentially leading to an amplified response. Liberatore et al. [5] addressed a stone masonry model using the Finite-Discrete Element Method approach, in addition to utilizing data from remote sensing systems, to investigate the effect of the vertical earthquake component on masonry buildings. The analysis results revealed that in masonry structures with low cohesion (weak mortar), the vertical acceleration component leads to an average 9% increase in base shear, resulting in a significant increase in structural damage. Bilgin and Hysenlliu [6] comparatively investigated the seismic behavior of low- and mid-rise masonry buildings under near-fault and far-fault earthquake records. For this purpose, they designed three prototype models representing the buildings in the study region and subjected them to Nonlinear Pushover Analysis. According to the analysis results, the models exceeded the Collapse Prevention limit in 35% of the far-fault scenarios, whereas this rate increased to 41% in the near-fault scenarios. Consequently, it was demonstrated that near-fault earthquakes have a more destructive effect on masonry buildings. Chieffo et al. [7] investigated the effect of the vertical ground motion component in near-fault earthquakes on a historical masonry structure. The model was subjected to nonlinear dynamic time-history analysis under two scenarios: horizontal components only (H) and a combination of horizontal and vertical components (H+V). According to the analysis results, it was observed that the axial forces were much higher in the scenario including the vertical component, thus negatively affecting the bearing and shear capacity of the walls. Consequently, it was determined that the H+V scenario increased the probability of damage and collapse by approximately 13% compared to the H-only scenario. Bayraktar et al. [8] investigated the effect of the vertical earthquake component on the damage mechanisms of masonry domes. For this purpose, they modeled a masonry dome and performed a nonlinear dynamic time-history analysis. According to the analysis results, the combined action of horizontal and vertical components, in comparison with the purely horizontal earthquake effect, caused an increase of 41.4% and 35.9% in the relative horizontal and vertical displacements, respectively. In another study, Bilgin [9] subjected three model groups, representing 19 different masonry building typologies, to Nonlinear Pushover Analysis to investigate their behavior under near-fault and far-fault scenarios. The results indicated that near-fault earthquake records induced greater structural damage, and higher displacement demands compared to far-fault records. Najafgholipour et al. [10] investigated the seismic behavior of historical masonry towers under far-fault and near-fault earthquakes. For this purpose, three different historical masonry towers were modeled and subjected to nonlinear dynamic time-history analysis. The results showed that the towers sustained greater damage during near-fault earthquakes, particularly in the presence of the fling-step effect. Gani et al. [11] investigated various seismic phenomena by analyzing the 2023 Kahramanmaraş earthquake records. The evaluation of the available records revealed that under near-fault effects, the recorded spectra exceeded even the DD-1 level of TBEC-2018 (The largest earthquake corresponding to the MCE earthquake level). Consequently, it was concluded that the design spectra of TBEC-2018 is inadequate.

Traditional masonry buildings, prevalent in the rural areas of developing countries, require strengthening as they are typically constructed using traditional methods and without engineering services. Furthermore, it is anticipated that when these types of buildings collapse due to earthquakes or other causes, they are likely to be replaced with new masonry structures. However, strengthening or reconstruction efforts for traditional masonry buildings will be unsafe without accounting for the effect of the vertical earthquake component. Despite this urgent need, TBEC-2018 [2] does not directly and explicitly address the vertical earthquake effect in the design and assessment of masonry buildings. To address this gap, nonlinear time-history analyses were performed on a prototype masonry building model. In these analyses, structural responses were numerically compared for cases with and without the inclusion of the vertical earthquake component, and the potential risks to structural safety posed by neglecting vertical effects under TBEC-2018 [2] were evaluated.

2. MODEL AND ANALYSIS METHOD

In this study, a two-storey prototype was designed as representative of traditional unreinforced brick masonry (URM) structures found in Turkey. The exterior walls are thickness of 45 cm, while the interior walls are 40 cm thick. All floor systems are composed of 15 cm thick solid slabs. Each storey height is defined as 3 m Figure 1 illustrates the structural plans and a 3D rendering of the model.

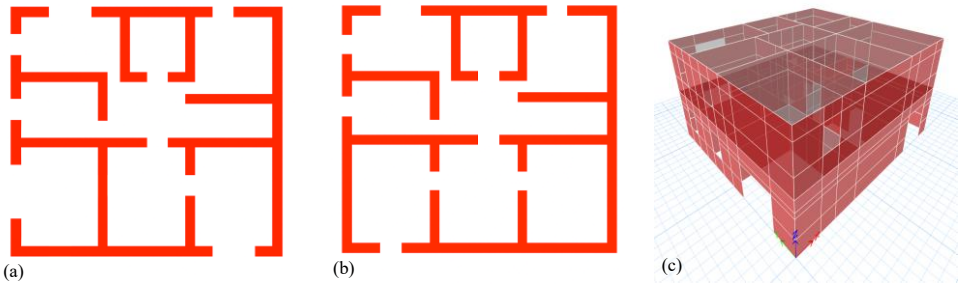

Figure 1. Masonry model; (a): ground floor plan; (b): 1 normal floor; (c): three-dimensional view.

2.1. Material Characteristics

The properties for the bricks were adopted from the work of Akcay et al. [12] and Bozkurt et al. [13], which was conducted on an identical structure. Accordingly, the material properties are listed in Table 1.

Table 1. Material characteristics

Material	Compressive strength (MPa)	Elasticity modulus (MPa)	Poisson ratio
Brick	11.3	8475	0.25
Concrete	25.0	31000	0.20

2.2. Load Definitions

The static loads for the structural model were determined based on the provisions of TS498 [14] and are summarized in Table 2.

Table 2. Load definitions

Load Type	Value
Dead (weight density)	25.5 kN/m^3 for brick / 25 kN/m^3 for concrete
Live	2 kN/m^2
Cladding	2 kN/m^2
Roof	1 kN/m^2
Snow	0.75 kN/m^2

The spectral acceleration parameters required for obtained of the horizontal and vertical elastic response spectra were derived from the Turkey Earthquake Hazard Map [15]. These parameters are provided in Table 3.

Table 3. Elastic spectra parameters

Parameter	Value
S_{DS}	1.347
S_{D1}	0.705
Site class	ZD
Damping	0.05

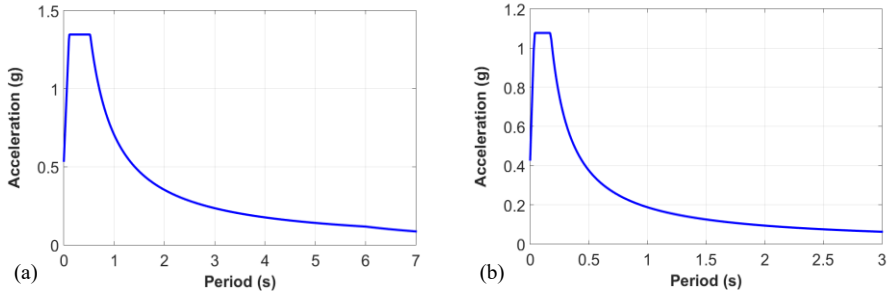

Figure 2. Elastic spectrum; (a): horizontal; (b): vertical.

2.3. Time History Analysis Method

The time-history analysis method is an advanced procedure that enables the most accurate prediction of structural response and is applicable to all structures. Therefore, nonlinear time-history analysis was employed to investigate the behavior of the modeled masonry structure. In accordance with TBEC-2018 [2], the initial phase involves selecting a suite of ground motion records consistent with parameters such as site conditions, distance to the fault, and fault mechanism. The subsequent phase is the scaling of the selected ground motions. As per the code, scaling of earthquake records is conducted using two approaches: simple amplitude scaling or spectral matching. This study, however, utilizes the simple scaling method.

The simple scaling procedure involves first calculating the resultant of the two horizontal components for each ground motion. The mean resultant spectrum is then obtained by averaging these resultants. A period range, spanning from 0.2 to 1.5 times the structure's fundamental period, is established for comparison. Within this range, the scale factor is determined to ensure that the mean resultant spectrum does not fall below 1.3 times the horizontal elastic design spectrum at any point. Regarding the vertical component, its scaling requires calculating the average spectrum of the vertical records. For the comparison, a period range is utilized with a lower bound of 0.1 s and an upper bound identical to that of the horizontal scaling. The scale factor for the vertical component is then selected to ensure that the average vertical spectrum is greater than or equal to the vertical elastic design spectrum throughout this specified range.

Within the scope of this study, 7 near-fault accelerograms, selected using the PEER database [16] and the ground-motion selection recommendations of FEMA P-695 [17], are presented in Table 4. These records were scaled by a simple amplitude-scaling procedure using a MATLAB [18] code developed by the authors [19].

Table 4. Ground-motion records

No	RSN no	Event	Fault type	Year	Magnitude	*R_{jb} (km)	**R_{rup} (km)	***Vs_{30} (m/s)	Pulse like
1	4458	Montenegro	Reverse	1979	7.1	3.97	5.76	318.74	√
2	181	Imperial Valley-06	Strike Slip	1979	6.53	0	1.35	203	√
3	1063	Northrigde-01	Reverse	1994	6.69	0	6.5	282.25	√
4	8119	Christchurch, NZ	R.Oblique	2011	6.2	1.92	1.98	206	√
5	6962	Darfield, New Zealand	Strike Slip	2010	7	0	1.54	295.74	√
6	1114	Kobe, Japan	Strike Slip	1995	6.9	3.31	3.31	198	√
7	319	West Morland	Strike Slip	1981	5.9	6.18	6.5	193.67	×

* R_{jb}: Joyner boore distance, ** R_{rup}: Rupture distance, *** $V_{S,30}$: Time-averaged shear wave velocity to 30 m depth.

Figure 3 presents the unscaled and scaled horizontal components of the selected earthquake acceleration time histories. Additionally, the vertical components of the earthquake records are provided. Since the average value of the vertical components exceeded the vertical elastic spectrum values within the specified period range, no scaling coefficient was applied.

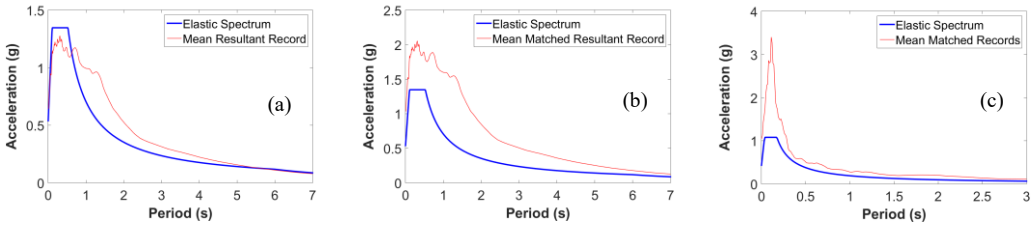

Figure 3. Horizontal elastic spectrum and mean record; (a): unscaled; (b): scaled; (c): vertical elastic spectrum and mean record.

3. ANALYSIS RESULTS

Nonlinear time-history analyses were performed first using only the horizontal components (H) of the earthquake acceleration records and then using all components (H+V). Subsequently, the axes of the horizontal earthquake components were rotated by 90°, and the analyses were repeated. The absolute maximum values of the obtained results were selected, and their averages were calculated. For both scenarios, storey accelerations, storey drifts, base overturning moments, wall stresses, wall internal forces and moments, storey shear forces, and vertical displacements were examined.

3.1. Storey Accelerations

According to the analysis results, significant increases were observed in the Z-direction for the (H+V) scenario. The maximum storey acceleration values of the model for the (H) and (H+V) scenarios are presented on a storey-by-storey basis in Table 5.

Table 5. Accelerations in the Z-direction

Storey	Z axis acceleration						
	Excluding vertical component (H)			Including vertical component (H+V)			Rate of increase
	+ [g]	- [g]	V/H ratio	+ [g]	- [g]	V/H ratio	(%)
2	0.391	0.403	0.29	1.447	1.139	1.06	270.07
1	0.304	0.311	0.31	1.331	1.002	1.35	337.82

3.2. Overturning Moment

Significant increases have been identified in the base overturning moment values in the X and Y directions because of vertical earthquake loads. The increase in ratios obtained are presented in Table 6.

Table 6. Overturning moments

X direction (%)	Y direction (%)
98.47	110.40

3.3. Wall Stresses

Significant increases in vertical compression stresses were observed in the vertical (pier) and horizontal (spandrel) load-bearing members due to the vertical seismic excitation. Table 7 presents the average variation ratios of the vertical compression stresses occurring in the structural members. Figure 4 illustrates the average vertical compression stress obtained for cases excluding and including the vertical earthquake acceleration.

Table 7. Wall stresses

Structural Member	Rate of increase (%)
Pier	9.70
Spandrel	4.91

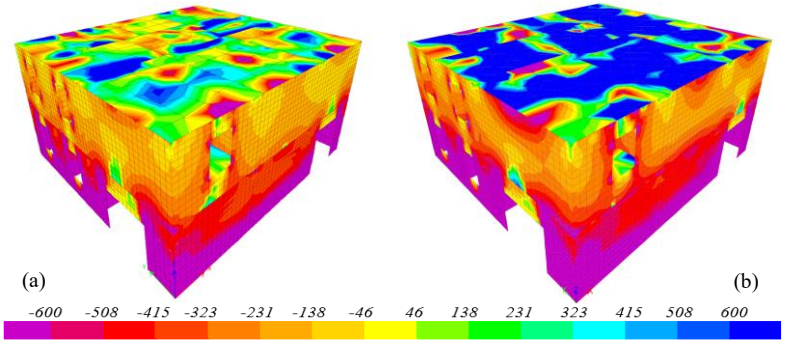

Figure 4. Average wall stresses; (a): excluding vertical component; (b): including vertical component; (kN/m²).

3.4. Wall Forces and Moments

Significant increases were observed in the pier elements, defined as the vertical components of the masonry walls, including in-plane shear forces, axial forces, out-of-plane bending moments, and torsional moments. No notable variations were detected in the out-of-plane shear forces or in-plane bending moments. Conversely, no significant changes were identified in the force and moment values of the spandrel elements, which were defined as the horizontal components of the masonry walls. The relevant average variation ratios are provided in Table 8, and the average axial tension force results are presented in Figure 5.

Table 8. Wall forces and moments

Structural Member	Rate of increase (%)				
	Shear force (Thickness direction)	Axial force (Vertical direction) C*	Axial force (Vertical direction) T**	Bending moment (Length direction)	Torsional moment (Vertical direction)
Pier	18.19	29.57	241.41	19.49	11.92

* Compressive force, ** Tension force

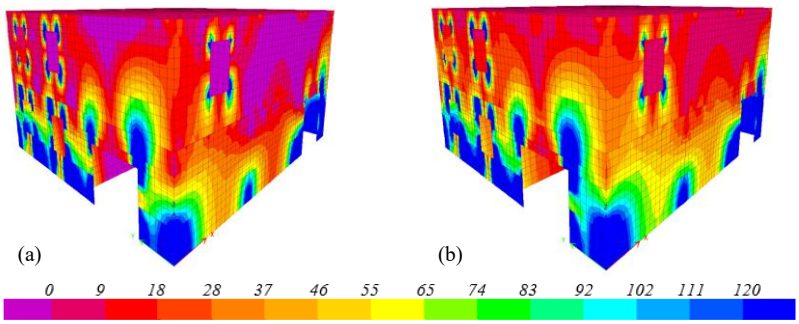

Figure 5. Average axial tension forces; (a): excluding vertical component; (b): including vertical component; (kN/m).

3.5. Vertical Displacements

The vertical displacement values at the upper ends of both stories were examined. Significant increases in vertical displacements were observed, and the average increase ratios are presented in Table 9. Although the absolute vertical displacement values obtained for the H+V scenario remained small, the influence of the vertical earthquake component becomes evident when evaluated in percentage terms.

Table 9. Vertical displacements

Storey	Rate of Increase (%)
2	197.6
1	211.8

4. CONCLUSIONS

This study aims to highlight the risks associated with the fact that the effects of vertical seismic actions are not directly addressed by TBEC-2018 [2] for traditional masonry buildings. Within this scope, a prototype model representing the existing traditional masonry building stock in Türkiye was developed. To better observe the effects of the vertical seismic component, seven near-fault earthquake records were selected and scaled. Nonlinear time-history analyses were carried out for two scenarios: one considering only the horizontal components (H) of the ground motion records, and the other considering both the horizontal and vertical components (H+V). Based on the analysis results, the influence of including the vertical component of the earthquake was evaluated as follows:

- No significant changes were observed in the horizontal storey accelerations, storey drifts, or storey shear forces.
- Vertical storey accelerations increased by 270% on the second storey and 338% on the first storey.
- The base overturning moments increased by an average of 99% in the X-direction and 110% in the Y-direction.
- The vertical compression stresses in the vertical (pier) and horizontal (spandrel) load-bearing members increased by an average of 10% and 5%, respectively.
- In the vertical load-bearing members (piers), the in-plane shear forces and axial forces increased by an average of 18% and 29% (in compression) and 241% (in tension), respectively. Additionally, the out-of-plane bending moments and torsional moments increased by an average of 20% and 12%, respectively.
- The vertical displacement values at the upper ends of both stories increased by 198% on the second storey and 212% on the first storey.
- Compared to the symmetric prototype model examined in this study, structures with lower material strength or geometric irregularities are expected to be more vulnerable to the effects of vertical seismic actions.

- It is recommended that the consideration of vertical seismic effects be mandated, particularly in regions with high seismic hazard and at near-fault distances.
- The average vertical spectrum values obtained from the earthquake records exceeded the vertical elastic design spectrum values recommended by TBEC-2018 [2] across all periods. Therefore, if the vertical elastic design spectrum defined in TBEC-2018 [2] is used in design or assessment procedures, there is a risk of underestimating the structural responses.

In conclusion, this study adopted an approach different from the TBEC-2018 [2] code by considering the effect of vertical seismic action on a traditional masonry model. The analysis results numerically demonstrated that the vertical earthquake component significantly amplifies structural responses. In this context, it is believed that the present study contributes to literature and can serve as a reference for future updates of seismic design codes.

REFERENCES

[1] A.K. Chopra, Dynamics of Structures: Theory and Applications to Earthquake Engineering, 4th edition, Prentice Hall, Boston, United States of America, 2012.
[2] TBEC-2018: Turkey Building Seismic Code: Rules for design of buildings under earthquake effect, Official Gazzette, 18.03.2018, 30364 (in Turkish).
[3] V. Koç, "Examined to the Behavior of Earthquake Exposed Masonry and Rural Buildings with Construction Rules to be Considered in Masonry Structures", Journal of Graduate School of Natural and Applied Sciences, 2016.
[4] F. Di Michele, C. Cantagallo and E. Spacone, "Effects of the vertical seismic component on seismic performance of an unreinforced masonry structures", Bulletin of Earthquake Engineering, 2020.
[5] D. Liberatore, C. Doglioni, O. AlShawa, S. Atzori and L. Sorrentino, "Effects of coseismic ground vertical motion on masonry constructions damage during the 2016 Amatrice-Norcia (Central Italy) earthquakes", Soil Dynamics and Earthquake Engineering, 2019.
[6] H. Bilgin and M. Hysenlliu, "Comparison of near and far-fault ground motion effects on low and mid-rise masonry buildings", Journal of Building Engineering, 2020.
[7] N. Chieffo, M. Mosoarca, A. Formisano, P. B. Lourenço and G. Milani, "The effect of ground motion vertical component on the seismic response of historical masonry buildings: The case study of the Banloc Castle in Romania", Engineering Structures, 2021.
A. Bayraktar, E. Hökelekli, F. Şermet and A. S. Mosallam, "A FRCM technique for strengthening of masonry domes against near-fault pulse-like vertical excitations", Engineering Failure Analysis, 2024.
[8] H. Bilgin, "Effects of near-fault and far-fault ground motions on nonlinear dynamic response and seismic damage of masonry structures", Engineering Structures, 2024.
[9] M. A. Najafgholipour, Z. Hamidian, H. Darvishi and P. Gardoni, "The failure assessment of historical masonry towers subjected to near-field and far-field ground motions", Engineering Failure Analysis, 2025.
[10] E. Gani, S. Öztürk, A. Sarı, "Examination of the severe impact of the February 6, 2023 earthquakes on Antakya district considering pulse-like ground motions, supershear rupture, and basin effects", Soil Dynamics and Earthquake Engineering, 2025.
[11] C. Akcay, T.S. Bozkurt, B. Sayin and B. Yildizlar, "Seismic retrofitting of the historical masonry structures using the numerical approach", Construction and Building Materials, 2016.
[12] T.S. Bozkurt, B. Sayin, C. Akcay, B. Yildizlar and N. Karacay, "Restoration of the historical masonry structures based on laboratory experiments", Journal of Building Engineering, 2016.
[13] TS 498, "Design load values for dimensioning of structural elements", 2021.
[14] Afad, "Türkiye earthquake hazard map", 2025.
[15] Peer, "Pacific earthquake engineering research center", 2025.
[16] Fema P695, "Quantification of building seismic performance factors", 2009.
[17] Matlab, "Analyze data-develop algorithmes and create models", 2024.
[18] M.F. Karapınar, B. Gunes, and B. Sayin, "Nonlinear time history analysis of a low-storey RC building: Comparison of the existing and retrofitted states", Journal of Structural Engineering & Applied Mechanics, 2023.

BIOGRAPHY

PhD candidate Kamran Samadi is currently engaged in the pursuit of his doctoral thesis, which focuses on the seismic progressive collapse of reinforced concrete buildings. This research is being conducted at Istanbul University-Cerrahpasa. Concurrently, he is engaged in the study of historical masonry buildings and the execution of various earthquake performance evaluation analyses.

Dr. Mehmet Firat Karapinar is a graduate of Istanbul University-Cerrahpasa. He is currently engaged in scientific research on structural analysis, with a particular focus on the vertical component effect of earthquakes and buildings equipped with seismic isolators.

Dr. Sayin currently employed by Department of Civil Engineering at Istanbul University-Cerrahpaşa as a Professor. Dr. Sayin graduated from Istanbul University with BS, MS and PhD in Civil Engineering. During the graduate education, he worked as a Research Assistant in the Department of Civil Engineering at the University. Between 2009 to 2015, Dr. Sayin worked as a structural engineer in the Department of Construction and Technical Affairs of the University. His research areas are historical masonry structures, RC buildings, fiber composites and industrial waste. He has published over 170 articles regarding civil engineering and architecture areas.

ICENS 11TH INTERNATIONAL CONFERENCE ON ENGINEERING AND NATURAL SCIENCE October 22-26 2025 Sarajevo

Comparative Performance of Shear Wall Addition and Base Isolation for the Seismic Retrofitting of Mid-Rise RC Buildings

Mehmet Firat Karapinar[1], Kamran Samadi[2], Baris Sayin[3]

Abstract

Mid-rise reinforced concrete buildings constitute a significant portion of the existing building stock. As these structures were designed according to more lenient code requirements of their time and have experienced material degradation, they now require strengthening. This study compares the effectiveness of adding shear walls and implementing a base isolation system for the seismic retrofitting techniques of such buildings. For this purpose, two conventional fixed-base models (with and without shear walls) and one base-isolated model were designed and subjected to nonlinear time history analysis. To more distinctly compare the structural responses, near-fault ground motion records were selected. The application of base isolation resulted in average reductions of 49.16% and 49.12% in storey accelerations along the X and Y directions, respectively; an average decrease of 77.34% in storey drifts in X and Y directions and an average decrease of 60.83% in storey shear forces in X and Y directions were recorded. These findings indicate that utilizing a base isolation system is more effective in improving the seismic performance of mid-rise reinforced concrete buildings. Notably, while adding shear walls, particularly in upper stories, increased storey accelerations, the reduction of these accelerations in the base-isolated model underscores the reliability of base isolation in also protecting non-structural elements. Consequently, this comparison provides a practical framework for decision-makers in the retrofitting processes of mid-rise reinforced concrete buildings.

Keywords: Base Isolation, Near Fault Earthquake, RC Buildings, Seismic Retrofitting Techniques, Shear Wall.

1. INTRODUCTION

Ensuring structural safety in seismically vulnerable regions constitutes the most critical objective of modern earthquake engineering. To achieve this goal, reinforced concrete structures, as the most widely used structural system globally, hold a central position both as a potential risk factor and a focus of solutions. Despite their extensive use, a significant portion of the existing reinforced concrete building stock is highly vulnerable to earthquakes due to factors such as non-compliance with current seismic code requirements, variability in construction quality, and material degradation from environmental effects [1]. This situation results in the seismic performance of these structures falling below acceptable safety levels, creating unacceptable risks for life safety [2]. Consequently, the development and implementation of effective and economical retrofitting techniques to improve the seismic behavior and earthquake resistance of these vulnerable structures emerges as an urgent engineering challenge [3].

The shear wall addition method, applied to improve the seismic performance of existing reinforced concrete buildings, creates significant positive effects on structural behavior while also introducing various practical challenges. The most notable structural advantage of this method is that it substantially enhances the building's lateral stiffness [4]. The increased stiffness leads to a shortening of the structure's natural vibration period and consequently a reduction in inter-storey drift demands under seismic effects; this plays a critical role in limiting damage to both structural and non-structural elements [5]. However, this method also has significant drawbacks, namely architectural constraints, technical difficulties, and the necessity for building vacancy during implementation.

Emerging as an alternative to conventional retrofitting techniques, seismic base isolation is an advanced engineering practice that aims to significantly mitigate seismic effects by decoupling the structure from ground motion at the foundation level. The fundamental principle of this technique is to elongate the natural vibration period of the structure, shifting it beyond the dominant period range of the earthquake ground motion [6]. This increase in period substantially reduces the spectral accelerations acting on the structure and, consequently, the storey shear forces, thereby minimizing the seismic demand on the existing structural members [7]. Furthermore, while displacements are largely concentrated within the isolation layer,

[1] Structural Engineer (PhD), mehmetfiratkarapinar@gmail.com
[2] Institute of Graduate Sciences, Istanbul University-Cerrahpasa, İstanbul, Türkiye, kamran.samadi@gmail.com
[3] Corresponding author: Istanbul University-Cerrahpasa, Department of Civil Engineering, Structural Engineering Division, 34320, Istanbul, Türkiye, barsayin@iuc.edu.tr

keeping inter-storey drifts under control, the reduction in storey accelerations in the superstructure protects both non-structural components and valuable equipment inside the building. Although the effectiveness of the method depends on the stiffness and mass characteristics of the structure, it has been observed to yield optimum results particularly for retrofitting mid-rise reinforced concrete buildings (approximately 5-15 stories); indeed, the shear force reduction achieved through period elongation is more pronounced in such structures compared to both very rigid low-rise buildings and already flexible high-rise buildings [8].

There is no direct and definitive storey range definition for mid-rise buildings in the literature on reinforced concrete structures. Based on indirect references from some reliable sources, buildings with 5 to 10 stories can be considered as mid-rise [9-11]. However, it is more realistic to classify mid-rise buildings based on their seismic behavior. This is because mid-rise buildings exhibit a response under seismic loads where both shear and bending deformations interact significantly. This complex dynamic behavior distinctly separates mid-rise buildings from both low-rise and high-rise structures, necessitating their treatment as a separate category within seismic performance assessments.

Comparative studies on the effectiveness of adding shear walls versus using base isolators for retrofitting mid-rise reinforced concrete buildings are limited in the current literature. For instance, De Angelis and Cancellara [12] investigated the effectiveness of adding shear walls and an isolation system for retrofitting a 5-storey RC building with torsional irregularity. Base isolation reduced shear forces by an average of 70%, yielding up to 70% reinforcement savings in the lower-storey columns and 40% in the beams. Despite the addition of shear walls in the fixed-based model, torsional behavior could not be fully controlled. The researchers emphasized that the isolation method was not only successful in improving structural behavior but also a cost-effective alternative. Fares [13] modeled a 10-storey regular-plan RC building without shear walls with fixed-base and base-isolated conditions on different soil classes and subjected them to nonlinear time history analysis. Base isolation reduced spectral acceleration values by approximately 50% for each soil type, proving significantly effective in improving structural performance, even on soft soils. Asghshahr and Rafiei [14] compared the behavior of 10 and 15-storey fixed-base and base-isolated RC models with shear walls under near-fault earthquakes using nonlinear time history analysis. Results for the isolated models showed reductions of up to 71% in inter-storey drifts, 60% in storey accelerations, and 60% in base shear forces. Ozer et al. [15] examined the effectiveness of different isolator types in reducing seismic demands on 3, 5, 7, and 9-storey RC frame models using nonlinear time history analysis. Comparative analysis results revealed that base isolation (particularly with LRB-type isolators) significantly improved the seismic performance of the RC frame systems. Fu et al. [16] compared the seismic behavior of a 14-storey RC model in fixed-base and base-isolated conditions. Additionally, they performed a shake table test using a 3-storey physical model. While base isolation reduced storey accelerations and relative storey drifts, it was less effective in reducing storey velocities. Absolute storey displacement values could double compare to the fixed-base building, especially under pulse-like earthquakes, thus revealing the limitations of base isolation in protecting non-structural components.

In the current literature, comparative studies on fixed-base and base isolated reinforced concrete buildings have generally focused on four model typologies: (a) fixed-base frame without shear wall, (b) fixed-base frame with shear wall, (c) base isolated frame without shear wall and (d) base isolated frame with shear wall. However, existing studies have typically focused on only two or three of these model types within a limited perspective. In this study, a 7-storey reinforced concrete model, categorized as mid-rise, was designed with a fixed-base frame without shear wall as the control model. Comparative versions of this model—namely, a fixed-base with shear wall frame and a base isolated frame without shear wall—were also developed for performance analysis. To more distinctly capture changes in acceleration values, particularly in upper stories, near-fault ground motion records were selected and scaled, distinguishing between forward directivity and fling-step effects. Finally, the effectiveness of adding shear walls and implementing base isolation in improving the seismic performance of mid-rise reinforced concrete buildings was compared by interpreting numerical data obtained from nonlinear time history analysis. The results demonstrate that the base-isolated system is more effective in reducing structural responses and enhancing overall performance. Future studies plan to expand the scope of this research by incorporating a fourth numerical model and conducting a cost-effectiveness analysis, including a payback period calculation. This aims to provide a practical perspective for decision-makers in the field of seismic retrofitting and contribute to the identification of cost-effective strategies.

2. MODEL AND ANALYSIS METHOD

Within the scope of the study, conventional building models with and without reinforced concrete shear walls, as well as a base-isolated building model without shear walls, were developed. All models consist of 7 stories, with the storey height specified as 3.5 m for the first storey and 3.0 m for the remaining stories. With a bay spacing of 5 m, the total plan length is 20 m in both horizontal directions. In the conventional building models, the column cross-sections were defined as 60×60 cm and the beam cross-sections as 60×60 cm. In the base-isolated building model, the column cross-sections were selected as 60×60 cm and the beam cross-sections as 60×60 cm in the typical stories. In the isolation storey, the column cross-sections were defined as 120×120 cm and the beam cross-sections as 70×60 cm. In all models, the slab thickness was selected as 15 cm, while the reinforced concrete shear wall thickness was specified as 40 cm. The structural plans are presented in Figure 1.

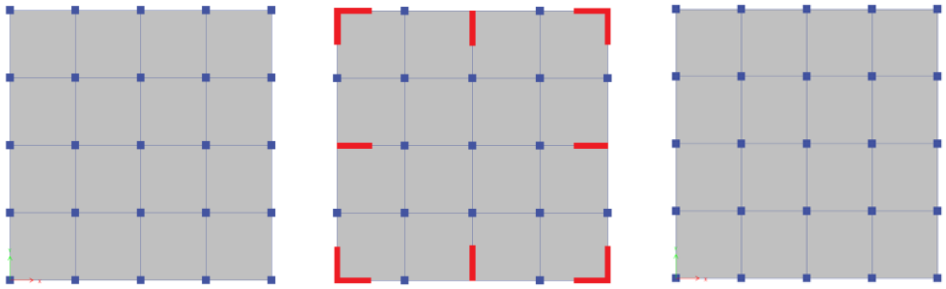

Figure 1. Typical floor plan of the RC structure; (a): without shear walls; (b): with shear walls; (c): base-isolated

2.1. Material Characteristics

The material properties were defined as presented in Table 1.

Table 1. Material characteristics

Material	Compressive strength (MPa)	Elastisicity modulus (MPa)
Concrete	40 for the below isolation system 35 for the above isolation system and other models	34000 33000
Rebar	420	$2x10^5$

2.2. Load Definitions

In the structural model, the static loads were defined as presented in Table 2, based on TS-498 [17].

Table 2. Load definitions

Load Type	Value
Dead *	25 kN/m^3
Live	2 kN/m^2
Cladding	2 kN/m^2
Wall	6.5 kN/m for main walls, 1 kN/m^2 for partition walls
Roof	1.5 kN/m^2
Snow	0.75 kN/m^2
Temperature	20° has been assumed
* weight density of concrete	

2.3. Elastic Spectra

Using the Turkey Earthquake Hazard Map [18], the relevant spectral parameters were determined. The horizontal and vertical elastic spectra were then generated. Table 3 presents the spectral parameters, and Figure 2 illustrates the horizontal and vertical spectra for the DD-2 seismic level.

Table 3. Elastic spectra parameters

Parameter	Value (DD-1)	Value (DD-2)
S_{DS}	2.348	1.347
S_{D1}	1.115	0.705
Site class	ZD	
Damping	0.05	

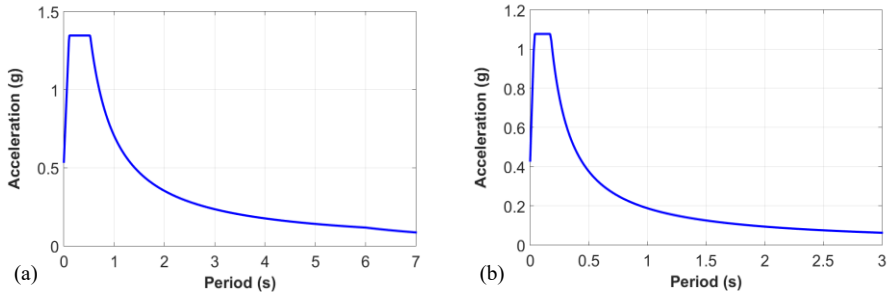

Figure 2. Elastic spectrum at DD-2 earthquake level; (a): horizontal; (b): vertical.

2.4. Isolator Properties

In the base-isolated structural model, lead-rubber bearings (LRBs) were employed to resist potential tensile effects that may occur under near-fault conditions. Using the data obtained from the analyses, the safety checks in TBEC-2018 [2] and the stability checks in Eurocode 1337-3 [19] were performed. The properties of the isolators are presented in Table 4.

Table 4. Isolator properties

Parameter	Value
Isolator diameter	950 mm
Lead diameter	230 mm
Shear modulus	0.55 MPa
Yield stress of lead	10 MPa
Total elastomer thickness	350 mm

2.5. Time History Analysis Method

A nonlinear time history analysis was performed to compare the seismic retrofitting of mid-rise reinforced concrete buildings through the implementation of shear walls and base isolation systems, in accordance with established methodologies in the literature. This analysis method is capable of capturing the realistic response of the structural model through the use of actual earthquake acceleration records. In other words, by applying an earthquake acceleration record representing a real seismic event to the model, both the local and global behavior of the structure can be predicted. Therefore, it ranks among the most reliable methods for a rational comparison of retrofitting techniques.

In the initial stage, seven earthquake acceleration records were selected (Table 5) in accordance with parameters such as site conditions, distance to the fault, and source mechanism, by utilizing the PEER [20] and AFAD [21] databases as well as the recommendations of FEMA-P695 [22]. To capture the structural responses more distinctly during the analysis, all acceleration records were selected as near-fault events, considering the Forward Directivity / Fling Step characteristics. These records were scaled using a simple scaling method [24] through a code developed by the authors in MATLAB [23].

Table 5. Time history records

No	RSN no	Event	Fault type	Year	Magnitude	*R_{JB} (km)	**R_{rup} (km)	***$V_{S,30}$ (m/s)	Pulse like
1	1084	Northridge-01	Reverse	1994	6.69	0	5.4	251.0	Forward directively
2	1063	Northridge-01	Reverse	1994	6.69	0	6.5	282.3	Forward directively
3	1114	Kobe, Japan	Strike Slip	1995	6.9	3.3	3.3	198.0	Forward directively
4	184	Imperial Valley-06	Strike Slip	1979	6.53	5.1	5.1	202.3	Forward directively
5	1491	Taiwan Chi Chi	Reverse Oblique	1999	7.62	7.6	7.6	350.0	Fling step
6	TK-8101	Düzce	Strike Slip	1999	7.1	0	9.7	282.0	Fling step
7	1176	Kocaeli	Strike Slip	1999	7.51	1.4	4.8	297.0	Fling step

*Rjb: Joyner Boore distance, **Rrup:Rupture distance, *** $V_{S,30}$:Time-averaged shear wave velocity to 30 m depth.

Subsequently, the conventional structures were analyzed under the DD-2 (Design Basis Earthquake: DBE) earthquake level. In the base-isolated structure, the portion below the isolation system (substructure) was analyzed under the DD-1 (Maximum Considered Earthquake: MCE) earthquake level, while the portion above the isolation system (superstructure) was analyzed under the DD-2 (Design Basis Earthquake: DBE) earthquake level. Figure 3 presents the unscaled and scaled response spectra for the shear wall–free model under the DD-2 earthquake level.

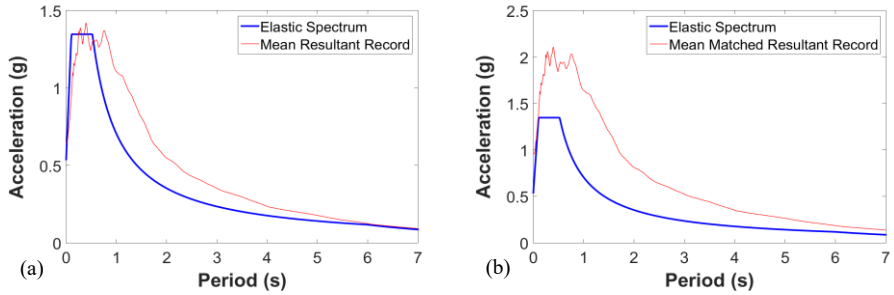

Figure 3. Horizontal elastic spectrum and mean record at DD-2 earthquake level; (a): unscaled; (b): scaled.

3. ANALYSIS RESULTS

Nonlinear time history analyses were initially conducted without altering the orientations of the earthquake acceleration records. Subsequently, the analyses were repeated after rotating the axes of the horizontal earthquake components by 90°. The largest absolute values from the obtained results were selected, and their averages were calculated. For all models, the storey accelerations, inter-storey drifts, and storey shear forces were examined.

3.1. Storey Accelerations

The storey accelerations occurring in both horizontal directions were examined, and the maximum values are presented in Table 6.

Table 6. Maximum storey accelerations

Storey	Acceleration (g)					
	Fixed Base				Base isolated	
	Exclude shear wall		Include shear wall			
	X direction	Y direction	X direction	Y direction	X direction	Y direction
7	1.896	1.897	2.360	2.359	0.807	0.806
6	1.708	1.705	1.938	1.940	0.653	0.654
5	1.563	1.563	1.605	1.601	0.575	0.577
4	1.359	1.360	1.471	1.467	0.485	0.485
3	1.204	1.204	1.267	1.263	0.553	0.554
2	0.999	0.998	1.025	1.022	0.602	0.602
1	0.741	0.741	0.848	0.849	0.714	0.714

In the scenario where reinforced concrete shear walls were added to the reference model (shear wall–free fixed-base model), the storey accelerations increased on average by 10.16% in the X direction and 10.04% in the Y direction. As a result of applying base isolation, the storey accelerations decreased on average by 49.16% in the X direction and 49.12% in the Y direction. The storey acceleration graphs are presented in Figure 4.

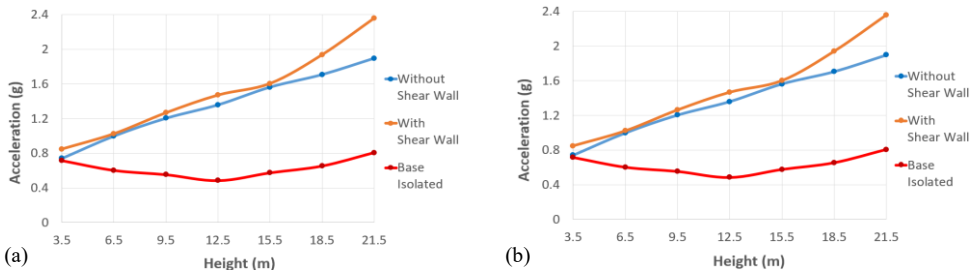

Figure 4. Storey accelerations; (a): X direction; (b): Y direction.

3.2. Inter-Storey Drifts

The inter-storey drifts occurring in both horizontal directions were examined, and the maximum values are presented in Table 7. In the base-isolated structure, the first-floor slab was not considered for inter-storey drifts, as it is located immediately above the isolators. Because there is no slab beneath the considered floor that belongs to the superstructure for comparison, the corresponding values are not presented in Table 7.

Table 7. Maximum inter-storey drifts

Storey	Drifts					
	Fixed Base				Base isolated	
	Exclude shear wall		Include shear wall			
	X direction	Y direction	X direction	Y direction	X direction	Y direction
7	0.0073	0.0073	0.0100	0.0100	0.0019	0.0019
6	0.0121	0.0121	0.0114	0.0114	0.0030	0.0030
5	0.0169	0.0169	0.0123	0.0123	0.0039	0.0039
4	0.0210	0.0210	0.0127	0.0127	0.0045	0.0045
3	0.0238	0.0238	0.0122	0.0122	0.0050	0.0050
2	0.0245	0.0245	0.0103	0.0103	0.0048	0.0048
1	0.0172	0.0172	0.0054	0.0054	-	-

In the scenario where reinforced concrete shear walls were added to the reference model (shear wall–free fixed-base model), the inter-storey drifts increased on average by 30.12% in both the X and Y directions. In the case of applying base isolation, the inter-storey drifts decreased on average by 77.34% in both the X and Y directions. The inter-storey drift graphs are presented in Figure 5.

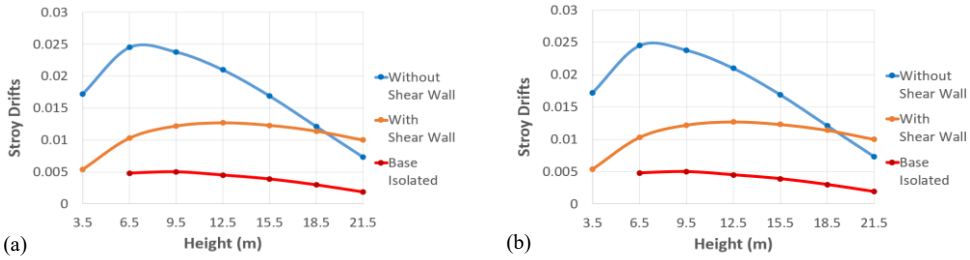

Figure 5. Inter-storey drifts; (a): X direction; (b): Y direction.

3.3. Storey Forces

The storey shear forces occurring in both horizontal directions were examined, and the maximum values are presented in Table 8. In the scenario where reinforced concrete shear walls were added to the reference model (shear wall–free fixed-base model), the storey shear forces increased on average by 13.53% in the X direction and 13.66% in the Y direction. In the case of applying base isolation, the storey shear forces decreased on average by 60.83% in both the X and Y directions.

Table 8. Maximum storey forces

Storey	Shear forces (kN)					
	Fixed Base				Base isolated	
	Exclude shear wall		Include shear wall			
	X direction	Y direction	X direction	Y direction	X direction	Y direction
7	10744	10739	13198	13219	6291	6290
6	9097	9096	10791	10752	4218	4219
5	8074	8086	8324	8330	3253	3255
4	6554	6550	6819	6820	2317	2321
3	5094	5096	5323	5382	1553	1551
2	3933	3930	4468	4472	1161	1162
1	2486	2491	3184	3184	835	835

4. CONCLUSIONS

In this study, the effectiveness of adding shear walls and implementing base isolation for improving the seismic performance of mid-rise reinforced concrete buildings has been compared. In this context, a structural model without reinforced concrete shear wall elements was designed as a reference model for control purposes. The configurations of the model including shear walls and base isolation were also developed, and these models were examined comparatively within the scope of structural performance analysis. Data obtained from nonlinear time history analysis was evaluated as follows:

- When the structure was strengthened through the addition of reinforced concrete shear walls, the inter-storey drifts exhibited a significant reduction. However, due to the increase in structural stiffness, increases in storey accelerations and storey shear forces were observed.
- With the implementation of base isolation, the floor accelerations decreased by an average of 49.16% in the X direction and 49.12% in the Y direction. Inter-storey drifts were reduced by an average of 77.34% in both directions, while the storey shear forces experienced an average reduction of 60.83% in both X and Y directions. These findings provide evidence that base-isolated systems constitute a far more reliable method for protecting non-structural elements and critical equipment commonly present in buildings such as hospitals.
- The conventional models meet the targeted controlled damage performance level. The base-isolated structural model meets the immediate occupancy performance objective by remaining below the limited damage performance level. This implies that, whereas conventional structures may experience structural damage after the earthquake, base-isolated structures are not expected to sustain any structural damage.

Consequently, this study has demonstrated that, in the seismic retrofitting of mid-rise reinforced concrete buildings, the use of base-isolated systems is more effective compared to the addition of reinforced concrete shear walls. All structural parameters presented within the scope of this study support this finding. In future studies, the interaction between shear walls and base isolation systems will also be examined, and these retrofitting methods will be compared from a cost perspective within a broader research framework. Our aim is to provide a practical and realistic framework for the seismic retrofitting of existing mid-rise reinforced concrete buildings in literature.

REFERENCES

[1] H. Sezen, A.S. Whittaker, K.J. Elwood and K.M. Mosalam, “Performance of reinforced concrete buildings during the August 17, 1999 Kocaeli, Turkey earthquake, and seismic design and construction practise in Turkey”, Engineering Structures, 2003.

[2] TBEC-2018: Turkey Building Seismic Code: Rules for design of buildings under earthquake effect, Official Gazzette, 18.03.2018, 30364 (in Turkish).

[3] M.N. Fardis, Seismic Design, Assessment and Retrofitting of Concrete Buildings, Springer, 2009.

[4] FEMA 356, Prestandard and Commentary for The Seismic Rehabilitation of Buildings, American Society of Civil Engineers, Reston, Virginia, 2000.

[5] U. Ersoy, G. Özcebe, Reinforced Concrete (Volume I), 7th Edition, Evrim Publishing, 2017 (in Turkish).

[6] A.K. Chopra, Dynamics of Structures: Theory and Applications to Earthquake Engineering, 4th edition, Prentice Hall, Boston, United States of America, 2012.

[7] F. Naeim, J.M. Kelly, Design of Seismic Isolated Structures, John Wiley & Sons, INC., 1999.

A. Martelli, M. Forni, G. Panza, “Features, recent application and conditions for the correct use of seismic isolation systems”, Earthquake Resistant Engineering Structures VIII, September 2011.

[8] FEMA P-58-1, Seismic Performance Assessment of Buildings, Applied Technology Council, Redwood City, California, 2018.

[9] J. Moehle, Seismic Design of Reinforced Concrete Buildings, McGraw-Hill Education, 2015.

[10] M. J. N. Priestley, G. M. Calvi, and M. J. Kowalsky, Displacement-Based seismic design of structures, IUSS Press, Pavia, Italy, 2008.

[11] F. De Angelis and D. Cancellara, “Dynamic analysis and vulnerability reduction of asymmetric structures: Fixed base vs base isolated system, Composite Structures” Composite Structures, 2019.

A. M. Fares, “Comparison between fixed base and isolated base in seismic response of high-rise buildings: a case study”, Challenge Journal of Structural Mechanics, 2020.

[12] M. R. S. Asghshahr and S. Rafiei, “Seismic Response of Base-isolated Dual-system Reinforced Concrete Buildings at a Near-fault Site”, Amirkabir Journal of Civil Engineering, 2022 (in Persian).

[13] E. Ozer, M. Inel and B. T. Cayci, “Seismic Performance Comparison of Fixed and Base-Isolated Models”, Iranian Journal of Science and Technology, Transactions of Civil Engineering, 2023.

[14] H. Fu, Y. Cao and Z. Qu, “Substructural shake table testing for nonstructural elements of various damage sensitivity in a fixed-base and a base-isolated building”, Engineering Structures, 2024.

[15] TS 498, “Design load values for dimensioning of structural elements”, 2021.

[16] Afad, “Türkiye earthquake hazard map”, 2025.

[17] EN 1337-3, “Structural bearings-part 3: elastomeric bearings”, 2005.

[18] Peer, “Pacific earthquake engineering research center”, 2025.

[19] Afad, “Türkiye ground motion database and analysis system”, 2025.

[20] FEMA P695, “Quantification of building seismic performance factors”, 2009.

[21] Matlab, “Analyze data-develop algorithmes and create models”, 2024.

[22] M.F. Karapınar, B. Gunes, and B. Sayin, “Nonlinear time history analysis of a low-storey RC building: Comparison of the existing and retrofitted states”, Journal of Structural Engineering & Applied Mechanics, 2023.

BIOGRAPHY

Dr. Mehmet Firat Karapinar is a graduate of Istanbul University-Cerrahpasa. He is currently engaged in scientific research on structural analysis, with a particular focus on the vertical component effect of earthquakes and buildings equipped with seismic isolators.

Kamran Samadi is currently engaged in the pursuit of his doctoral thesis, which focuses on the seismic progressive collapse of reinforced concrete buildings. This research is being conducted at Istanbul University-Cerrahpasa. Concurrently, he is engaged in the study of historical masonry buildings and the execution of various earthquake performance evaluation analyses.

Dr. Sayin currently employed by Department of Civil Engineering at Istanbul University-Cerrahpaşa as a Professor. Dr. Sayin graduated from Istanbul University with BS, MS and PhD in Civil Engineering. During the graduate education, he worked as a Research Assistant in the Department of Civil Engineering at the University. Between 2009 to 2015, Dr. Sayin worked as a structural engineer in the Department of Construction and Technical Affairs of the University. His research areas are historical masonry structures, RC buildings, fiber composites and industrial waste. He has published over 170 articles regarding civil engineering and architecture areas.

ICENS 11TH INTERNATIONAL CONFERENCE ON ENGINEERING AND NATURAL SCIENCE
October 22-26 2025 Sarajevo

Enhancing Discharge Distribution in Open-Channel Bifurcations Using Submerged Vanes: A Numerical Study

Fırat Gümgüm[1]

Abstract

This study numerically investigates the influence of submerged vanes on discharge distribution at an open-channel bifurcation using Flow-3D HYDRO. Two simulations were performed under identical boundary conditions: one representing an uncontrolled diversion and another incorporating a submerged vane-field for flow control. In the vane-field configuration, six arrays of vanes with a height equal to 0.3 times the approach flow depth and a skew angle of 30° were installed. The simulations employed a Large Eddy Simulation (LES) turbulence model with the Smagorinsky subgrid-scale closure. Results revealed that vane-induced vortices altered the near-bed and near-surface velocity structures by deflecting the near-surface flow toward the DC and the near-bed flow toward the MC outer wall. This flow reorganization enhanced the diverted discharge by 13.9% relative to the uncontrolled case.

Keywords: submerged vanes, flow division, open channel bifurcation

1. INTRODUCTION

Diversion channels are constructed along the sides of rivers or canals to convey a portion of the approaching flow into irrigation, hydropower, or water supply systems. The diverted discharge may be either regulated by control gates or governed passively by the local flow hydraulics and sediment dynamics near the intake entrance. In the latter case, when sediment effects are disregarded, the controlling mechanism is the flow division phenomenon, a complex three-dimensional process whose dynamics determine how the discharge is distributed between the main channel and the diversion channel [1]. Considering the vertical velocity distribution, the higher momentum of the near-surface flow makes it more resistant to turn into the diversion channel, whereas the near-bed flow, having lower momentum, is more easily diverted [2], [3]. Consequently, a greater proportion of near-bed water enters the diversion channel, reducing the overall diverted discharge relative to the total approach flow. This disproportion is thought be moderated through the use of submerged vanes.

Submerged vanes are hydraulic structures typically installed on river-beds for various purposes, including the protection of riverbanks, regulation of sediment deposition, desilting of diversion channels, stabilization of riverbeds, etc. A submerged vane, being placed with a small skew angle, creates a pressure difference between its upstream and downstream faces which leads to the generation of a tip [4]. This tip vortex directs the near-bed flow towards the low-pressure (lee) side of the vane, while the near-surface flow toward the high-pressure (leading) side of the vane. Therefore, the deflection of the near-surface flow towards the intake, while the near-bed flow away from intake, can increase the amount of the diverted discharge.

In this numerical study, the objective is to investigate the influence of submerged vanes on discharge distribution under such conditions. Two simulations were conducted: one representing an uncontrolled diversion and another incorporating a submerged vane-field for flow control.

2. THE MODEL

The simulations were conducted in Flow-3D HYDRO software. The main channel (hereafter, MC) and the diversion channel (hereafter, DC) were 5.2 m and 3.6 m long, respectively. Both channels were 0.3 m wide, and the DC was connected to the MC 2 m from the upstream end. 2.5 cm high bed sills were placed at the end of the channels. The approach flow discharge was 6 L/s. In the first (reference) simulation, the bifurcation was left uncontrolled to obtain the reference conditions. In the second simulation, a submerged vane-field was installed to the system. This vane-field consisted of six arrays; each comprised of two rows of vanes. The vane height was set to 0.3 times the approaching flow depth, and the skew angle of the vanes was specified as 30°. The outlook of the model and the layout of the vane-field are given in Figure 1.

[1] Corresponding author: Dicle University, Department of Civil Engineering, 21280, Sur/Diyarbakir, Turkey.
firat.gumgum@dicle.edu.tr

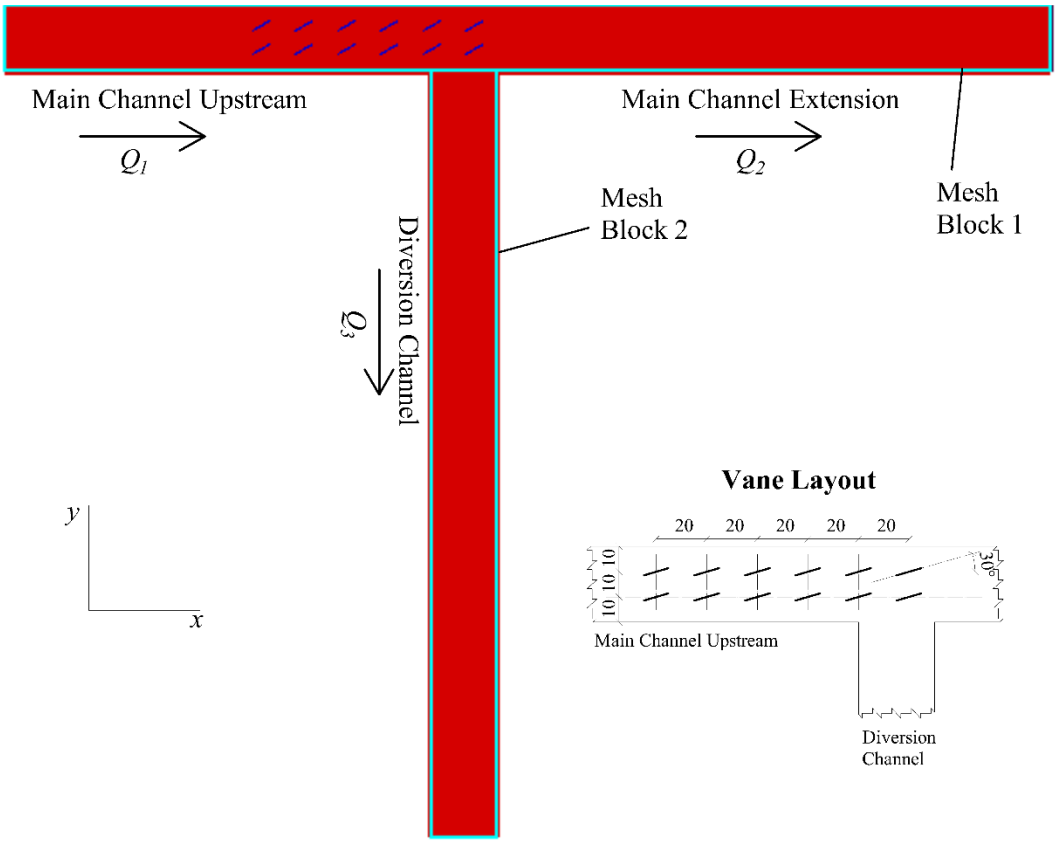

Figure 1. The outlook of the model and the layout of the vane-field

Large Eddy Simulation (LES) model with the Smagorinsky subgrid-scale was preferred for the turbulence closure scheme. Smagorinsky coefficient was set to C_S = 0.05 for the computation of eddy viscosity. The momentum equations were discretized using a second-order numerical scheme. A similar model, developed for a different incoming discharge, was validated in a previous study by the author [5], and the same modelling strategy was adopted in the present work.

3. RESULTS AND DISCUSSION

Time-averaged velocity fields near the bed, at z = 1 cm, and near the surface, at z = 4.5 cm, for the reference simulation are presented in Figure 2a and 2b, respectively. (u, v) velocity vectors are initially oriented along the MC. As the flow approaches the bifurcation zone, these vectors gradually deflect toward the inner wall of the MC and entrance of the DC, with a more pronounced deflection at z = 1 cm. Downstream of the bifurcation, the flow in the MC expands toward its inner wall. A stagnation zone forms at the downstream corner of the DC, where the associated high pressure induces a downward motion along the adjoining walls, as indicated by the negative values of the vertical velocity component, w. In the MC downstream, the flow exhibits a slight deflection toward the outer wall at z = 1 cm, while it remains nearly aligned with the channel axis at z = 4.5 cm. The velocity magnitudes are initially higher along the inner wall of the MC downstream before becoming more uniform farther downstream. Within the DC, (u, v) field exhibits smaller magnitudes at z = 4 cm along 3b/4 from the DC inner wall, compared to those at z = 1 cm.

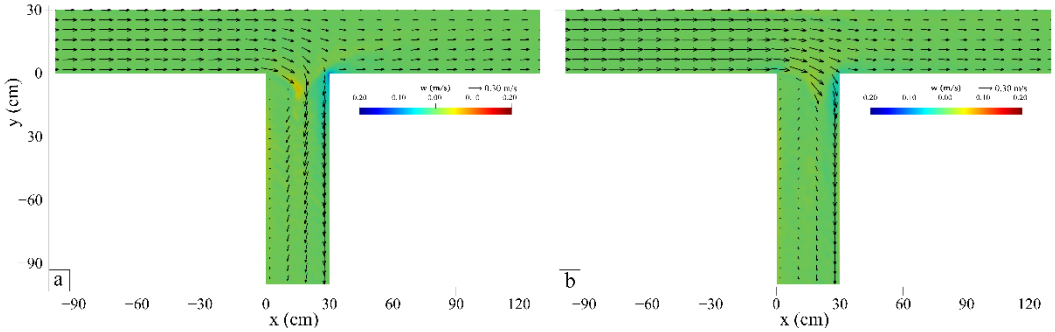

Figure 2. Time-averaged velocity field of the reference simulation at (a) z = 1 cm, (b) z = 4.5cm.

Time-averaged velocity fields near the bed, at z = 1 cm, and near the surface, at z = 4.5 cm, for the vane-field simulation are given in Figure 3a and 3b, respectively. The vane-induced vortices deflect the (u, v) vectors toward the outer wall of the MC at z = 1 cm, and toward the inner wall of the MC at z = 4.5. cm. Compared to Figure 2b, a larger portion of the near-surface flow is directed towards the DC entrance, resulting in a 13.9% increase in the diverted discharge. However, the limited flow deflection near the MC inner wall suggests that the present vane-field configuration is not optimal, and that further improvement could enhance the diverted discharge.

The flow patterns downstream of the MC remain broadly similar to those in the reference simulation. In Figure 3a, the upward and downward motions associated with the vane tip vortex are evident from the relatively higher positive and negative values of the vertical velocity component, w. Strong downflow persists around the downstream corner at both depths, however, the greater flow deflection at z = 4.5 cm intensifies the impact at this corner, producing positive values of w.

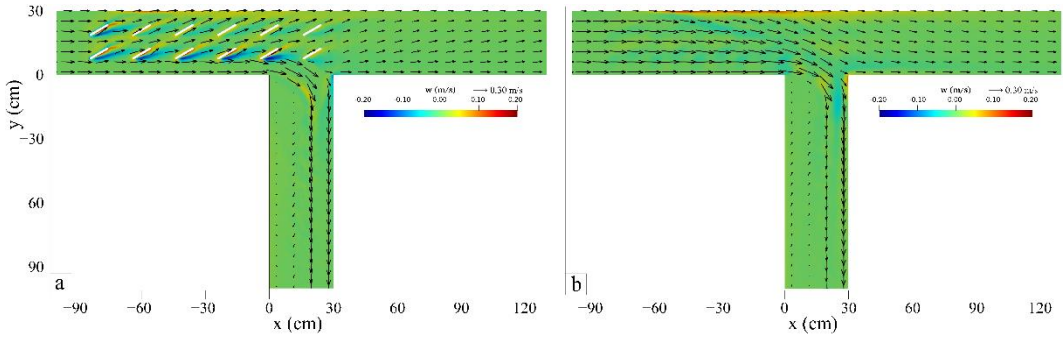

Figure 2. Time-averaged velocity field of the vane-field simulation at (a) z = 1 cm, (b) z = 4.5cm.

4. CONCLUSION

In this numerical study, it was aimed to investigate the influence of submerged vanes on discharge distribution under the given flow conditions. Two simulations were conducted: one representing an uncontrolled diversion and another incorporating a submerged vane-field for flow control. The results showed that the vane-induced vortices modified the near-bed and near-surface velocity fields, deflecting the near-surface flow toward the diversion channel and increasing the diverted discharge by 13.9% compared to the uncontrolled case.

REFERENCES

[1] F. Gumgum, "Division of flow at open channel bifurcations," *Physics of Fluids*, vol. 37, no. 2, 2025.

[2] N. L. Rao, K. Sridharan, and M. Y. A. Baig, "Experimental study of the division of flow in an open channel," in *Proceedings of the Conference on Hydraulic and Fluid Mechanics*, 1968, pp. 139–142.

[3] V. S. Neary and A. J. Odgaard, "Three-dimensional flow structure at open-channel diversions," *Journal of Hydraulic Engineering*, vol. 119, no. 11, pp. 1223–1230, 1993.

A. J. Odgaard and Y. Wang, "Sediment management with submerged vanes. I: Theory," *Journal of Hydraulic Engineering*, vol. 117, no. 3, pp. 267–267, 1991.

[4] F. Gumgum, " Effect of the Diversion Angle at Lateral Diversions: A Numerical Study," in *Proceedings of 10th International Conference of Engineering and Natural Science*, 2024, pp. 41–46.

ICENS 11TH INTERNATIONAL CONFERENCE ON ENGINEERING AND NATURAL SCIENCE October 22-26 2025 Sarajevo

Method for Near-Wellbore Control Region Delineation in Tight Gas Reservoirs Based on Neural ODE Surrogate Modeling

Wenbo Jiang [1], Guoqing Han [1], Jin Shu [1], Zhenduo Yue [1], Xingyuan Liang [1], Guangzu Wang [1], Yabo Li [1]*

Abstract

Tight sandstone gas reservoirs are characterized by low porosity, low permeability, and low gas saturation, and generally require hydraulic fracturing for effective development. After fracturing, the reservoir exhibits strong heterogeneity and multi-scale flow behavior, forming a radial composite flow system composed of the stimulated and unstimulated zones, with the stimulated region commonly regarded as the primary drainage area of gas wells. During production, significant interactions occur between the reservoir and the wellbore; however, the slow evolution of reservoir seepage and the rapid fluctuations of wellbore dynamics lead to a pronounced mismatch in time scales. Conventional numerical simulation methods struggle to balance high temporal resolution with computational efficiency.

To address this issue, this study employs neural ordinary differential equations (neural ODEs) as a training framework to construct surrogate models. The training data are obtained from reservoir simulations with conventional time steps. By leveraging the adaptive time-stepping capability of neural ODEs, the trained surrogate model is able to generate predictions with higher temporal resolution than the original simulations, thereby achieving time-scale matching between reservoir seepage and wellbore dynamics and enabling real-time analysis of reservoir responses to transient wellbore operations. Furthermore, the surrogate model is applied to investigate the impact range of wellbore production fluctuations over different time scales, leading to the proposal of a delineation criterion for the near-wellbore control region. This provides methodological support for the scientific determination of grid refinement ranges in numerical simulations. The findings not only enhance computational efficiency and predictive accuracy, but also contribute to the establishment of more reliable reservoir simulation frameworks and provide engineering guidance for production strategy optimization and efficient development of tight gas reservoirs..

Keywords: Tight sandstone gas reservoir, Reservoir–wellbore coupling, Neural ODE, Near-wellbore control region, Surrogate model

1. INTRODUCTION

Tight sandstone gas reservoirs are important unconventional natural gas resources, characterized by low porosity, low permeability, and low gas saturation. Due to their extremely limited intrinsic flow capacity, tight gas reservoirs typically require hydraulic fracturing to achieve effective development. Following fracturing, a high-conductivity stimulation zone forms around the wellbore (Xu et al., 2024), imparting a distinct radial composite flow pattern to the reservoir (Ren et al., 2024). The stimulated zone differs significantly from the native reservoir in terms of petrophysical properties and pressure dynamics, making the near-wellbore region a critical area that controls well productivity. A deep understanding of the flow behavior in this region is therefore essential for optimizing reservoir stimulation and designing rational production strategies.

[1] College of Petroleum Engineering, China University of Petroleum (Beijing), Beijing, China, 876043221@qq.com

[*] Corresponding author: College of Petroleum Engineering, China University of Petroleum (Beijing), Beijing, China. cup_706ac@163.com

During production, there exists a pronounced disparity in temporal scales between the reservoir and the wellbore. Gas flow within the wellbore is influenced by production, liquid carrying, and operational adjustments, causing flow rate and pressure fluctuations on the order of seconds to minutes. In contrast, reservoir flow evolution is governed by pore structure and permeability, and pressure propagation occurs much more slowly, typically on the scale of hours to days. This mismatch in temporal scales necessitates extremely small time steps in numerical simulations to synchronize wellbore dynamics with reservoir response, resulting in high computational costs and long simulation times. Achieving high temporal resolution while improving simulation efficiency remains a key challenge in the dynamic study of tight gas reservoirs. In recent years, data-driven approaches have been introduced to reservoir flow prediction, offering improved computational efficiency to some extent (Rahmanifard et al., 2024). However, these models are often trained on discrete time series, making it difficult to capture the continuous-time evolution of the system, and they generally lack physical constraints, limiting their generalization ability (Hu et al., 2025). Consequently, developing a surrogate model that adapts to variable time steps and retains physical interpretability has become a crucial step toward efficient reservoir–wellbore coupled simulations.

To address these challenges, this study introduces a neural ordinary differential equation (Neural ODE) framework to construct a surrogate model for tight gas reservoirs, enabling high-temporal-resolution prediction of flow dynamics (Chen et al., 2018). By employing adaptive time integration for continuous system-state modeling, the proposed approach achieves higher temporal resolution than conventional numerical simulations while maintaining computational efficiency. The trained surrogate model allows for analyzing reservoir dynamic responses to wellbore flow fluctuations across different time scales and provides criteria for delineating near-wellbore control regions. This, in turn, supports refined numerical simulation grids and optimized production strategies for tight gas reservoirs.

2. PAGE LAYOUT

After hydraulic fracturing, a radially composite flow system with significant heterogeneity is formed near the wellbore in tight sandstone gas reservoirs. According to the degree of stimulation and seepage characteristics, the near-wellbore zone can be divided into three parts: the hydraulic fracture zone (HFZ), the stimulated reservoir volume (SRV), and the unstimulated matrix zone (UMZ). These regions differ significantly in pore structure, permeability, pressure transmission rate, and temporal response, which together determine the range of wellbore pressure disturbance responses over different time scales. Among them, the HFZ and SRV jointly constitute the main flow-conducting system.

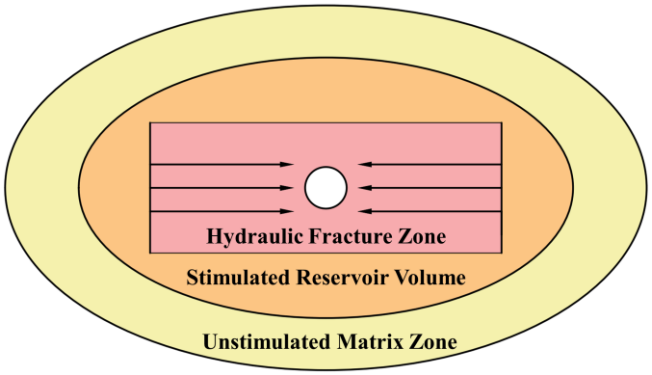

Figure 2.Division of horizontal flow regions in a hydraulically fractured well

2.1. Hydraulic Fracture Zone（HFZ）

The HFZ corresponds to the main fracture channels created by hydraulic fracturing. The fracture width typically ranges from 0.1 to 5 mm, with permeability reaching 0.1–100 mD and relatively high porosity. Gas flow in this zone exhibits linear flow behavior, dominated by high-velocity non-Darcy effects and stress sensitivity of the fractures. The HFZ directly connects to the wellbore, acting as the primary zone responding to wellbore pressure dynamics. Its governing equation is expressed as:

$$\frac{?p_f}{?t} = \frac{k_f}{\mu_g c_t ?_f}\frac{?^2 p_f}{?x^2} \quad (1)$$

where p_f is the fracture pressure, k_f is the fracture permeability, μ_g is the gas viscosity, c_t is the total compressibility, ϕ_f is the fracture porosity.

2.2. Stimulated Reservoir Volume（SRV）

The SRV consists of secondary fractures and the stimulated matrix surrounding the main fractures, forming a dual-porosity medium system. The permeability of secondary fractures typically ranges from 10^{-3} to 1 mD, while the matrix permeability increases by 1–2 orders of magnitude compared with the original reservoir. Gas flow in this region is controlled by the coupled effect of fracture conduction and matrix gas supply, and can be mathematically represented as:

$$\frac{\partial p_{mf}}{\partial t} = \frac{k_f}{\mu_g c_t \phi_f} \nabla^2 p_{mf} + \alpha\left(p_m - p_{mf}\right) \quad (2)$$

$$\frac{\partial p_m}{\partial t} = \frac{k_m}{\mu_g c_t \phi_m} \nabla^2 p_m - \alpha\left(p_m - p_{mf}\right) \quad (3)$$

where p_{mf} is the pressures in the SRV fractures, p_m is the pressures in the SRV matrix, αis the fracture–matrix interaction coefficient

In the SRV, gas first flows from the stimulated matrix into secondary fractures, then converges through the fracture network toward the main fracture, and finally enters the wellbore. Owing to the long lateral extension of the main fracture, the convergence process in the SRV exhibits a typical elliptical flow pattern, with isobars distributed elliptically and the strongest pressure gradients located near the two wings of the main fracture.

2.3. Unstimulated Matrix Zone（UMZ）

The UMZ lies at the outer boundary of the reservoir, far from the production well, and retains the original pore–throat structure of the tight sandstone. Its permeability is extremely low (10^{-5}–10^{-3} mD), and gas flow is significantly affected by non-Darcy effects and slippage flow. Gas in the matrix flows toward the SRV boundary, also forming an elliptical flow pattern. The gas seepage equation in this zone is expressed as:

$$\nabla \cdot \left(\frac{k(p)}{\mu_g} \nabla p\right) = c_t \frac{\partial p}{\partial t} \quad (4)$$

where the permeability varies with pressure following the Klinkenberg correction model (Klinkenberg et al., 1941; Yang et al., 2021):

$$k(p) = k_0 \left(1 + \frac{b}{p}\right) \quad (5)$$

Where k_0 is the intrinsic permeability, b is the slippage factor.

2.4. Time-Scale Coupling and Near-Wellbore Control Range

According to Equation (1), the characteristic time scale of the HFZ can be defined as:

$$T_f = \frac{L_f^2 \mu_g c_t \phi_f}{k_f} \quad (6)$$

where L_f is the fracture half-length. Due to the large k_f, $T_f$is very small, indicating that the fracture zone can respond almost instantaneously to transient wellbore pressure variations, showing a typical fast dynamic response.

Equations (2) and (3) correspond to two typical time scales (Equation (7) and (8)), usually satisfying $T_{f,SRV} \ll T_{m,SRV}$, implying that the SRV fracture system responds rapidly, whereas the matrix exhibits a delayed supply effect. As the SRV simultaneously provides storage and flow-conducting functions, it responds to wellbore dynamic disturbances at intermediate frequencies.

$$T_{f.SRV} = \frac{L_{f.SRV}^2 \mu_g c_t \phi_f}{k_f} \quad (7)$$

$$T_{m,SRF} = \frac{L_{m,SRF}^2 \mu_g c_t \phi_m}{k_m} \quad (8)$$

From Equation (5), the characteristic time scale of the UMZ can be expressed as:

$$T_{UMZ} = \frac{L_{UMZ}^2 \mu_g c_t \phi_m}{k(p)} \quad (9)$$

Since $k(p)$ is very small, T_{UMZ} is generally much larger than the period of wellbore pressure oscillations, indicating that this region contributes mainly to long-term pressure support.

If the characteristic period of wellbore pressure fluctuation is denoted as T_w, the three regions satisfy:

$$\tau_f < T_w < \tau_{f,SRV} < \tau_{m,SRV} < \tau_{UMZ} \quad (10)$$

When $T_i < T_w$, region i can effectively respond to wellbore dynamic disturbances; when $T_i > T_w$, it primarily acts as a buffer or gas storage region. Accordingly, the analytical criterion for determining the control radius of the near-wellbore zone can be derived as:

$$r_c = \sqrt{\frac{k_i T_w}{\mu_g c_t \phi_i}} \quad (11)$$

3. CONSTRUCTION OF THE NEURAL DIFFERENTIAL EQUATION SURROGATE MODEL

To characterize the nonlinear evolutionary behavior of the tight-gas reservoir–wellbore system under complex dynamic operating conditions and achieve high-accuracy modeling across multiple time scales, this study develops a surrogate model based on Neural Ordinary Differential Equations (Neural ODEs). By representing the system-state evolution in continuous time and parameterizing the differential operator with a neural network, the model provides an adaptive approximation to the nonlinear reservoir dynamics while maintaining both physical interpretability and computational efficiency

3.1. Model Formulation

The core idea of Neural ODEs is to approximate the temporal evolution of system state variables using a neural-network-based function. Let $h(t)$ denote the hidden state vector and $u(t)$ represent external driving variables (e.g., wellhead pressure or production rate). The system dynamics can be written as:

$$\frac{dh(t)}{dt} = f(h(t), u(t), t, \theta) \tag{12}$$

$$\hat{y}(t) = g(h(t); \phi) \tag{13}$$

Where $f(\cdot)$ is a neural network parameterized by θ, responsible for representing the complex nonlinear dynamic behavior within the reservoir. The function $g(\cdot)$, parameterized by ϕ, serves as the output mapping that transforms the latent system state into observable physical quantities, such as bottomhole flowing pressure, gas production rate, or near-wellbore pressure distribution.

During forward computation, the model uses a numerical ODE solver to integrate the system dynamics (Equation 12), enabling predictions at arbitrary time points and supporting continuous-time dynamic response modeling.

To address the multi-scale flow behavior in tight-gas reservoirs, a normalized characteristic time variable $t^* = {}^{t}/_{T_{ref}}$ is introduced. The characteristic time constants of different flow regions （T_f、$T_{f,SRV}$、$T_{m,SRV}$、T_{UMZ}） are incorporated as auxiliary inputs to enhance the model's ability to distinguish region-dependent flow dynamics and improve fitting accuracy and generalization across time scales.

3.2. Model Training and Implementation

The model is trained using the Adam optimization algorithm to achieve efficient parameter updates (Reyad et al., 2022). Adam combines the advantages of momentum and adaptive learning rates, offering good convergence and stability in deep-learning applications. The training objective is defined by a composite loss function that includes both a Mean Squared Error (MSE) term and an L2 regularization term, balancing predictive accuracy and model complexity. The loss function is expressed as:

$$L = \frac{1}{N}\sum_{i=1}^{N}(s_i - \hat{s}_i)^2 + \lambda \sum_{j=1}^{M} w_j^2 \tag{14}$$

where S_i and $\hat{S}_i$ denote the true and predicted values, $N$is the number of samples, w_j is the j-th model parameter, and λ is the regularization coefficient.

The MSE term quantifies point-wise deviation between predictions and observations, reflecting how well the surrogate model approximates the target dynamics. The L2 regularization term suppresses excessively large parameter weights, reducing the risk of overfitting under limited data.

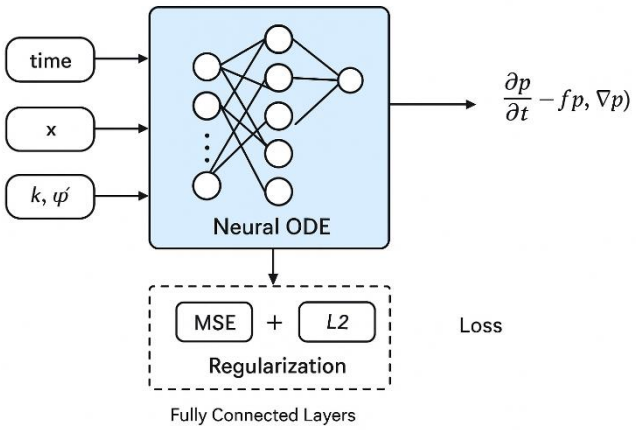

Figure2.Schematic diagram of the surrogate model architecture.

During implementation, the original physical-simulation data are divided into training and validation sets. The Neural ODE model is iteratively optimized using the training set, while the validation set is employed to monitor loss evolution and prevent overfitting. The training process terminates when the loss function converges or the validation error stops decreasing. The resulting surrogate model provides an efficient mapping between complex transient flow behavior and wellbore production responses, enabling rapid simulation of unsteady-state flow in tight-gas reservoirs.

3.3. Model Validation

The Neural ODE framework embeds a neural network within a differential equation solver, enabling end-to-end learning of continuous-time dynamics. Compared with conventional time-series models such as RNNs and LSTMs, Neural ODEs can adaptively track temporal evolution with variable step sizes, thereby avoiding accuracy loss and redundant computation caused by fixed sampling intervals. To assess the effectiveness of the proposed Neural ODE–based surrogate model, this study draws upon recent advances in the modeling of complex physical systems and transient dynamical processes, and evaluates the method from a literature-based comparative perspective with respect to accuracy and computational efficiency.

Rubanova et al. (2019) introduced the Latent ODE model, which integrates ordinary differential equations with variational autoencoders to enable continuous modeling of irregularly sampled time series. Their work demonstrated the capability of Neural ODEs to learn latent evolution patterns in complex dynamical systems. Subsequently, Norcliffe et al. (2021) extended the framework by incorporating second-order dynamics into the Augmented Neural ODE formulation, allowing the model to capture more intricate transient behavior and inertial effects, and thereby improving accuracy and stability in nonlinear physical process modeling. More recently, Celia et al. (2025) compared Neural ODEs with Neural Operators in time-series forecasting tasks and found that the former achieved faster convergence and higher predictive accuracy under the same computational budget.

Taken together, these studies substantiate the advantages of Neural ODEs for dynamic surrogate modeling in tight-gas reservoirs. Neural ODEs offer a favorable balance between physical consistency, temporal resolution, and computational efficiency, providing a solid theoretical and methodological foundation for real-time simulation of coupled wellbore–reservoir processes.

4. METHOD FOR DELINEATING THE NEAR-WELLBORE CONTROL REGION

Building upon the Neural ODE–based surrogate model, this study further develops a dynamic delineation method for the near-wellbore control region in hydraulically fractured tight-gas reservoirs, using the model-predicted pressure field and flow characteristics.

After hydraulic fracturing, the near-wellbore flow system exhibits pronounced heterogeneity and multiscale behavior, and may be conceptualized as comprising three distinct regions: the fracture-dominated region, the stimulated reservoir volume, and the unstimulated matrix region. The flow-control relationship among these regions can be expressed as:

$$\frac{\partial p}{\partial t} = \nabla \cdot (k \nabla p) + T_i(t) \quad (i = f, s, m) \tag{15}$$

where k_i denotes the effective permeability of the fracture, SRV, and matrix regions, and $T_i(t)$ represents the characteristic time response of each structural domain. By comparing the temporal response across regions, a characteristic time scale can be defined as:

$$T_i = \frac{L_i^2}{\alpha_i} \tag{16}$$

where L_i is the representative length of the region and $\alpha_i = {k_i}/{(\phi_i c_{ti} \mu)}$ is the pressure diffusion coefficient.

Using the high-resolution dynamic predictions of the surrogate model, the pressure distribution $p(x,t)$ and pressure gradient ${\partial p}/{\partial x}$ are computed at each time step. A normalized pressure-gradient attenuation factor is then introduced:

$$\beta(x,t) = \frac{1}{p_w(t) - p_e} \left| \frac{\partial p(x,t)}{\partial x} \right| \tag{17}$$

When $\beta(x,t)$ falls below a critical threshold β_c, the corresponding location is defined as the effective boundary of the pressure disturbance. By tracking the temporal evolution of this boundary and integrating its trajectory over time, the stabilized control radius r_c can be determined, thereby enabling a dynamic delineation of the near-wellbore region.

$$r_f < r \le r_{SRV} (\text{SRV}) \tag{18}$$

$$r_{SRV} < r \le r_c (\text{UMZ}) \tag{19}$$

5. RESULTS AND DISCUSSION

This study verifies the effectiveness of the Neural ODE–based surrogate model in characterizing the flow behavior of tight-gas reservoirs. Comparisons with numerical simulation results demonstrate that the surrogate model can accurately reproduce pressure evolution trends and transient variations while significantly reducing computational cost. The computational efficiency is improved by approximately one order of magnitude relative to conventional numerical simulation. Moreover, the model exhibits notable advantages in capturing the nonlinear relationship between rapid wellbore pressure fluctuations and the slow reservoir response. Owing to its adaptive time-stepping mechanism, the Neural ODE model can dynamically allocate computational effort—maintaining high temporal resolution during periods of strong transient behavior and automatically extending step size during quasi-steady stages—thus achieving efficient computation without compromising accuracy.

Based on the proposed method for delineating near-wellbore control regions, this study systematically elucidates the classification framework and the derivation of the corresponding criteria. By integrating insights from numerical simulations and surrogate model predictions, the influence of wellbore pressure perturbations on reservoir flow behavior across multiple time scales is clarified. From a theoretical perspective, this work establishes a method for determining the extent of the near-wellbore control region, offering a new approach to addressing the time-scale mismatch problem commonly encountered in tight-gas reservoir flow simulation.

ACKNOWLEDGMENT

This work were financial support from Science Foundation of China University of Petroleum, Beijing (No.2462023YJRC019).

This work were financial support from National Natural Science Foundation of China (No.52204059).

REFERENCES

[1] Ren, L., Dou, M., Dong, X., Chen, B., Zhang, L., Sun, J., Jing, C., Zhang, W., Zhou, D., & Li, H. (2024). Quantitative characterization of stimulated reservoir volume (SRV) fracturing effects in naturally fractured unconventional hydrocarbon reservoirs. Frontiers in Earth Science, 12, 1419631. https://doi.org/10.3389/feart.2024.1419631

[2] Xu, J., Liu, Y., & Sun, W. (2024). Production simulation of stimulated reservoir volume in gas hydrate formation with three-dimensional embedded discrete fracture model. Sustainability, 16(22), 9803. https://doi.org/10.3390/su16229803

[3] Rahmanifard, H., & Gates, I. (2024). A comprehensive review of data-driven approaches for forecasting production from unconventional reservoirs: Best practices and future directions. Artificial Intelligence Review, 57(8), 213. https://doi.org/10.1007/s10462-024-10865-5

[4] Hu, Y., Xin, X., Yu, G., Deng, W. (2025). Deep insight: An efficient hybrid model for oil well production forecasting using spatio-temporal convolutional networks and Kolmogorov–Arnold networks. Scientific Reports, 15, 8221. https://doi.org/10.1038/s41598-025-91412-2

[5] Chen, R. T. Q., Rubanova, Y., Bettencourt, J., Duvenaud, D. (2018). Neural ordinary differential equations. arXiv Preprint arXiv:1806.07366. https://doi.org/10.48550/arXiv.1806.07366

[6] Klinkenberg, L. J. (1941). The permeability of porous media to liquids and gases. Drilling and Production Practice, American Petroleum Institute, 200–213.

[7] Yang, Y., Zhang, L., & Li, X. (2021). Investigation of gas slippage and adsorption effects on apparent permeability in tight gas reservoirs. Fuel, 283, 119293.

[8] Reyad, M.; Sarhan, A. M.; Arafa, M. (2023). A modified Adam algorithm for deep neural network optimization. Neural Computing and Applications, 35(23), 17095–17112. doi:10.1007/s00521-023-08568-z.

[9] Rubanova, Y., Chen, R. T. Q., Duvenaud, D. (2019). Latent ODEs for irregularly-sampled time series. Advances in Neural Information Processing Systems, 32, 5320–5330.

[10] Norcliffe, A., Bodnar, C., Day, B., Simidjievski, N., Lio, P. (2021). On second order behaviour in augmented neural ODEs. Advances in Neural Information Processing Systems, 34, 7220–7231.

[11] Celia, M., Monaco, S., & Apiletti, D. (2025). A comparative study of neural ordinary differential equations and neural operators for modeling temporal dynamics. Neural Computing & Applications. Advance online publication.

ICENS 11TH INTERNATIONAL CONFERENCE ON ENGINEERING AND NATURAL SCIENCE October 22-26 2025 Sarajevo

Reservoir-Type Gas Storage Production: Fast Prediction Using Integrated Reservoir–Wellbore Surrogate Models

Wenbo Jiang [14], Guoqing Han [15] Jin Shu [16] Zhenduo Yue [17] Xingyuan Liang [18] Guangzu Wang [19] Yabo Li [20]

Abstract

Reservoir-type gas storage, reconstructed from depleted oil reservoirs, offers large storage capacity and high geological security, making it a key infrastructure for ensuring natural gas supply balance and seasonal peak regulation. However, due to multiple cycles of gas injection and liquid withdrawal, the reservoir fluid system evolves from oil–water two-phase to oil–gas–water three-phase flow, forming a strongly nonlinear and multi-scale coupled system. Traditional numerical simulations can characterize reservoir and wellbore dynamics but are computationally expensive and highly parameter-dependent, limiting their applicability for rapid prediction and dynamic optimization.

To address these challenges, this study proposes an integrated reservoir–wellbore surrogate modeling framework for fast prediction of reservoir-type gas storage behavior. The framework employs Neural Ordinary Differential Equations (Neural ODEs) to jointly model reservoir seepage and transient wellbore flow. Leveraging the adaptive time-stepping capability of Neural ODEs, the proposed model achieves temporally consistent and high-resolution dynamic predictions while maintaining strong physical consistency. This approach significantly reduces computational cost, enhances model generalization, and supports broad applications such as injection–production cycle analysis, operation regime optimization, and digital twin system construction for gas storage facilities.

The proposed framework provides a new pathway for intelligent simulation and rapid decision-making in complex underground energy storage systems, offering substantial theoretical and engineering significance for the scientific design and efficient operation of reservoir-type gas storage..

Keywords: reservoir-type gas storage; reservoir–wellbore coupling; surrogate model; neural ordinary differential equation; rapid prediction

1. INTRODUCTION

With the accelerating global transition toward a low-carbon and diversified energy structure, natural gas has become an increasingly important component of the global energy mix, serving as a key buffer and peaking resource. To cope with seasonal fluctuations in natural gas demand and the instability of gas supply, many countries have accelerated the construction of underground gas storage facilities to enhance system flexibility and energy resilience (Demchuk et al., 2025; Osieczko et al., 2019). Among various gas storage types, gas reservoir–type storage converted from depleted gas reservoirs is one of the most widely used forms, featuring a mature geological structure, large storage capacity, and low construction cost.In contrast, oil reservoir–type storage requires multiple rounds of high-pressure gas injection and liquid withdrawal to establish an effective storage space (Figure 1). Its oil–gas–water three-phase flow behavior and strong reservoir heterogeneity result in pronounced nonlinear and multiscale coupling characteristics, leading to generally lower injectivity

[14] College of Petroleum Engineering, China University of Petroleum (Beijing), Beijing, China, 876043221@qq.com

[15] Corresponding author: College of Petroleum Engineering, China University of Petroleum (Beijing), Beijing, China. cup_706ac@163.com

[16] College of Petroleum Engineering, China University of Petroleum (Beijing), Beijing, China, pe_shujin@163.com

[17] College of Petroleum Engineering, China University of Petroleum (Beijing), Beijing, China yuezd1999@163.com

[18]College of Petroleum Engineering, China University of Petroleum (Beijing), Beijing, China, xyliang@cup.edu.cn

[19] College of Petroleum Engineering, China University of Petroleum (Beijing), Beijing, China, w1215109088@163.com

[20] College of Petroleum Engineering, China University of Petroleum (Beijing), Beijing, China, pe_yaboli@163.com

and deliverability. This results in pronounced nonlinearity and multi-scale coupling behavior, leading to strong interactions between reservoir pressure dynamics and transient wellbore flow that pose significant challenges for accurate prediction and operational optimization.

Traditional numerical simulators (e.g., Eclipse, CMG) can capture the coupled behavior between the reservoir and wellbore but remain computationally intensive due to the high dimensionality of the governing three-phase flow equations and the restrictive time-stepping schemes. Analytical models, though computationally efficient, rely on strong simplifications that limit their applicability to complex reservoir–wellbore systems. Therefore, achieving fast, stable, and physically consistent modeling of reservoir–wellbore dynamics remains a critical challenge for both research and engineering applications of reservoir-type gas storage.

Fig. 1—Figure 1. Conceptual illustration of the reservoir-type gas storage cycle, showing the gas injection, soaking, and production stages. The process involves multiple rounds of high-pressure gas injection and liquid withdrawal, leading to the evolution of oil–water two-phase flow into a complex oil–gas–water three-phase system.

In recent years, the rapid advancement of artificial intelligence (AI) has introduced data-driven surrogate modeling as a promising direction in petroleum engineering. Surrogate models can efficiently approximate the dynamic response of complex physical systems based on numerical simulations or field data, enabling fast prediction and parameter optimization. Among these, the Neural Ordinary Differential Equation (Neural ODE)—which embeds continuous-time dynamics into deep neural networks—offers adaptive time-stepping and strong physical consistency, demonstrating great potential for modeling transient multiphase flow in reservoirs and wellbores (Chen et al., 2018).

Building upon these concepts, this study proposes an integrated reservoir–wellbore surrogate modeling framework for fast prediction in reservoir-type gas storage. Centered on the Neural ODE approach, the framework jointly models reservoir seepage and transient wellbore flow through a unified data-driven architecture. This design significantly reduces computational cost while maintaining high accuracy, providing an efficient pathway toward intelligent simulation, digital-twin construction, and real-time optimization of underground gas storage systems.

2. METHODOLOGY

2.1. Integrated Framework Overview

The proposed integrated framework for reservoir-type gas storage aims to unify the dynamic processes of the reservoir and wellbore into a continuous-time coupled dynamical system. Centered on the Neural Ordinary Differential Equation (Neural ODE), the framework learns the temporal derivatives of key state variables, enabling efficient approximation and dynamic prediction of complex physical processes. Unlike traditional discrete-time simulations, the method provides adaptive representation across multiple temporal scales while maintaining physical consistency, thereby capturing the interaction mechanisms between reservoir pressure propagation and transient wellbore flow more accurately.

The training data are obtained from high-fidelity numerical simulators encompassing both reservoir and wellbore processes. Through systematic preprocessing, normalization, and feature construction, the framework establishes a coherent mapping among physical quantities. As illustrated in Figure 2, the overall architecture consists of three primary modules: data generation, surrogate modeling, and predictive inference. This unified structure provides a consistent computational foundation for coupled prediction and intelligent optimization in underground gas storage systems.

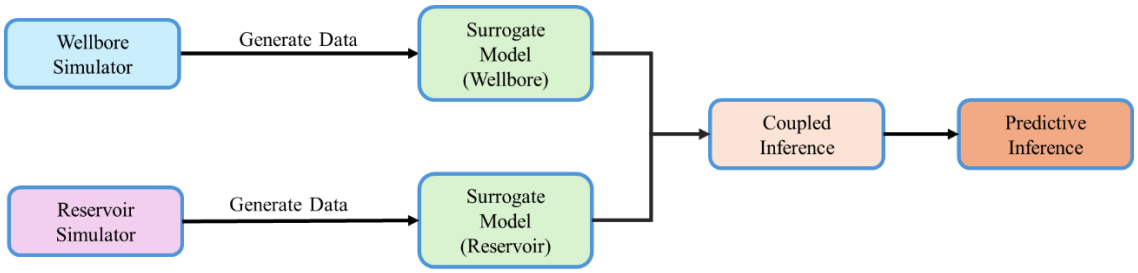

Fig. 2—Overall architecture of the integrated surrogate model framework.

2.2. Neural ODE-Based Surrogate Modeling

In the dynamic modeling of reservoir-type gas storage systems, the coupled reservoir–wellbore processes exhibit strong nonlinearity, unsteadiness, and multi–time-scale characteristics. Traditional analytical or numerical methods often struggle to achieve both accuracy and computational efficiency under such complexity. To address this issue, a data-driven surrogate modeling strategy is introduced, which learns the mapping relationships between control parameters, static physical properties, and system dynamic responses from high-fidelity numerical simulation data. Unlike purely black-box approaches, the proposed surrogate model incorporates physical constraints and conservation relationships into its structure, ensuring both computational efficiency and physical consistency (Forouzanfar et al., 2015).

The Neural Ordinary Differential Equation (Neural ODE) provides a continuous-time framework for learning system dynamics. Its core concept is to approximate the temporal derivatives of system states using a trainable neural network, formulated as:

$$\frac{dt(t)}{dt} = \mathrm{NN}(s(t), t, \theta) \tag{1}$$

Where $s(t)$ represents the system state, $\boldsymbol{t}$ stands for time, and NN is the neural network function that models system dynamics by fitting the laws of dynamic evolution; θ are the parameters of the neural network. By solving this differential equation, the model yields a continuous evolution of the system state over time.

Compared with conventional discrete-time neural architectures such as RNNs or LSTMs (Prater et al., 2024; Hewamalage et al., 2021; Kani, et al., 2019), the Neural ODE offers three main advantages in modeling gas storage systems:

1) Temporal continuity and adaptive time-stepping, naturally accommodating the distinct time scales of the reservoir and wellbore;.
2) Physical consistency, enabling hybrid surrogate modeling through the integration of boundary and conservation constraints;
3) High scalability, allowing seamless coupling with predictive and optimization modules. These characteristics make Neural ODE an efficient and physically coherent approach for dynamic simulation of complex underground gas storage systems.

2.3. Coupled Reservoir–Wellbore Prediction

The dynamic operation of reservoir-type gas storage involves a bidirectional coupling between reservoir seepage and transient wellbore flow, where pressure and flow rate interact in real time (Shu et al., 2025). The proposed Neural ODE-based surrogate framework establishes a unified continuous-time coupling between the reservoir and wellbore domains, fundamentally overcoming the limitations of traditional stepwise simulations in time synchronization and boundary condition handling.

Within this framework, the reservoir surrogate model predicts the dynamic variation of bottom-hole pressure (BHP), while the wellbore surrogate model calculates the corresponding gas production rate based on transient multiphase flow characteristics. The two components exchange information through interface variables: the reservoir model provides pressure boundary conditions for the wellbore model, and the resulting gas rate is fed back to the reservoir system. This physics-informed interaction mechanism, illustrated in Figure 3, enables accurate representation of transient nonlinear responses between the reservoir and wellbore.

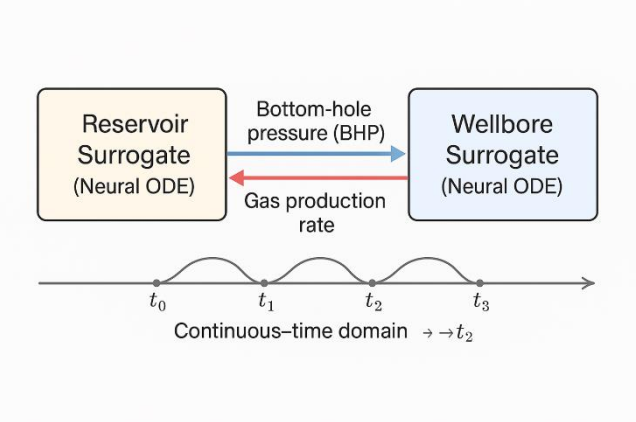

Fig. 3—Coupled prediction mechanism between reservoir and wellbore modules.

Compared with conventional iterative coupling schemes, the proposed framework achieves a significant reduction in computational cost—up to two orders of magnitude—while maintaining strong physical consistency and predictive accuracy. This approach not only enhances computational efficiency and stability but also provides a practical foundation for real-time optimization and digital twin implementation of underground gas storage systems (Ahmed et al., 2022).

2.4. Model Training and Implementation

The training data for the proposed integrated reservoir–wellbore surrogate model were obtained from high-fidelity numerical simulations covering both reservoir seepage and transient multiphase flow in the wellbore. Unified data interfaces and consistent temporal resolution were applied to ensure synchronized mapping and feature alignment across the two domains. All input parameters—including static geological properties, operational control variables, and initial states—were normalized and tensorized to maintain numerical stability across different physical dimensions.

Model training was performed using the Adam optimization algorithm (Reyad et al., 2022), with a composite loss function consisting of a Mean Squared Error (MSE) term and an L2 regularization term to balance predictive accuracy and model complexity. The Mean Squared Error (MSE) measures the pointwise numerical deviation between the model's predictions and the true values, expressed as:

$$L_{mse} = \frac{1}{N}\sum_{i=1}^{N}\|\hat{s}_i - s_i\|^2 \tag{2}$$

where S^_i and S_i represent the predicted and true states of the model at the i- th time step, respectively.

In deep learning model training, to prevent overfitting of the network structure under limited samples, regularization constraints are typically applied to model parameters. In this study, an L2 regularization term was incorporated into the multi-mechanism composite loss function to suppress excessive fluctuations in model parameters, thereby improving training stability and enhancing the model's generalization capability, expressed as:

$$L_{L2} = \sum_j \| \theta_j \|^2 \tag{3}$$

where θ_j denotes all the parameters of the neural network.

The Neural ODE component was solved using an adaptive-step numerical integrator, which ensured computational efficiency and stability during backpropagation (Illarionov et al., 2022). The entire framework was implemented in PyTorch, enabling modularity, flexibility, and scalability for various dynamic simulation tasks.

The proposed approach demonstrates strong extensibility and adaptability, allowing seamless application to different types of gas storage systems and wellbore–reservoir configurations. Its end-to-end design provides an efficient and practical foundation for digital twin construction, operational optimization, and intelligent control of underground gas storage facilities.

3. RESULTS AND DISCUSSION

3.1. Conceptual Demonstration of Dynamic Prediction

To illustrate the dynamic prediction capability of the proposed Neural ODE-based surrogate model in the continuous-time domain, a conceptual simulation analysis was conducted to demonstrate the method's physical rationality and feasibility. The analysis was based on an assumed injection–production cycle of a reservoir system, focusing on the temporal evolution of the pressure field to validate the model's ability to capture continuous dynamics. Unlike traditional discrete-time simulations, the Neural ODE framework adaptively adjusts the integration step size, ensuring computational stability while accurately representing flow behaviors across multiple time scales.

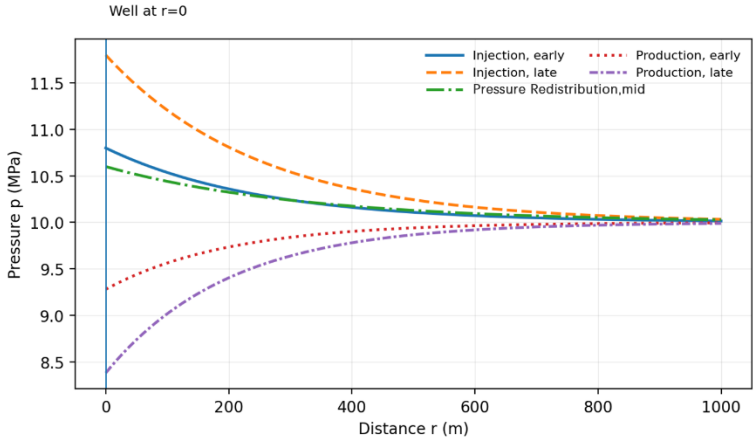

Fig. 4—Conceptual Reservoir Pressure Propagation Over Distance.

Figure 4 presents the dynamic evolution of reservoir pressure along the radial direction. During the injection phase, near-well pressure rises rapidly and propagates outward. After injection stops, pressure redistribution occurs as the pressure field gradually smooths and approaches equilibrium. During the production phase, near-well pressure declines and the pressure front retreats toward the well. The figure qualitatively demonstrates the model's ability to capture the propagation and attenuation of pressure waves within the reservoir, consistent with physical expectations.

Overall, the Neural ODE surrogate model produces smooth and differentiable pressure responses in the continuous-time domain, avoiding the cumulative errors and abrupt transitions often observed in discrete-time neural networks. Its adaptive time-stepping mechanism enables efficient and physically consistent simulation, providing a solid foundation for fast prediction and digital-twin development of reservoir-type gas storage systems.

3.2. Comparative Evaluation with Traditional Simulation.

To evaluate the performance of the proposed Neural ODE-based surrogate model, a conceptual comparison was conducted against conventional numerical simulators in terms of computational efficiency and predictive accuracy. Traditional numerical simulation tools (e.g., Eclipse, CMG) discretize the governing equations using explicit or implicit schemes and integrate them step-by-step to capture multiphase flow behavior. Although they provide high-fidelity physical representations, coupled reservoir–wellbore systems typically require fine temporal resolution and strict convergence criteria, resulting in heavy computational loads and long run times. In contrast, the Neural ODE surrogate model learns the continuous-time evolution of key state variables from simulation data, enabling fast and stable dynamic prediction of system behavior.

Table 1— Illustrative performance comparison.

Model Type	Average Time per Case	Speed-up	R^2	MAPE (%)
Full-physics Simulation	Hours	—	1.000	—
Surrogate Model (N-ODE)	Minutes	$\times 10^2$	≈0.99	<2

Table 1 presents an illustrative performance comparison under representative storage operation conditions. As shown, the proposed surrogate model achieves an order-of-magnitude acceleration in computation while maintaining high consistency with full-physics simulation results, with mean relative errors for pressure and flow rate within a few percent. This demonstrates that the Neural ODE approach can substantially reduce computational cost without compromising predictive fidelity.

Overall, the surrogate model exhibits clear advantages for real-time analysis, parameter optimization, and digital-twin construction of dynamic gas storage systems, providing a practical and efficient alternative for large-scale engineering applications.

3.3. Conclusion and Outlook

This study presents an integrated reservoir–wellbore surrogate modeling framework for fast prediction in reservoir-type gas storage systems. Centered on the Neural Ordinary Differential Equation (Neural ODE), the proposed approach unifies reservoir seepage and transient wellbore flow through a data-driven formulation. The results demonstrate that the model can

achieve high predictive accuracy while significantly reducing computational cost, providing a new and efficient pathway for dynamic simulation and optimization of complex underground gas storage systems.

Compared with conventional numerical simulators, the proposed framework exhibits notable advantages in temporal continuity, adaptive time-stepping, and multi-scale consistency, offering theoretical support for real-time analysis and parameter inference during storage operations. Furthermore, the framework is inherently extensible and can be integrated with various physical constraints, generative networks, or reinforcement learning algorithms to further enhance physical consistency and decision-making capability.

Future research will focus on three directions:

1) Incorporating high-fidelity simulation and field monitoring data to improve model generalization and transferability;.
2) Developing multi-well coupled surrogate systems to enable intelligent optimization and coordinated control at the cluster scale;
3) Integrating digital-twin concepts with cloud–edge collaborative computation to establish a new paradigm for intelligent operation of reservoir-type gas storage.

ACKNOWLEDGMENT

This work were financial support from Science Foundation of China University of Petroleum, Beijing (No.2462023YJRC019).

This work were financial support from National Natural Science Foundation of China (No.52204059).

REFERENCES

[1] Demchuk, Y., Shogenov, K., Shogenova, A., Merson, B., Vincent, C.J. (2025). Geological and Petrophysical Properties of Underground Gas Storage Facilities in Ukraine and Their Potential for Hydrogen and CO2 Storage. SUSTAINABILITY, 17(6). https://doi.org/10.3390/su17062400..
[2] Osieczko, K., Gazda, A., & Duan, M. (2019). Factors determining the construction and location of underground gas storage facilities. Acta Montanistica Slovaca, 24(3), 234-244.
[3] Chen, R. T. Q., Rubanova, Y., Bettencourt, J., Duvenaud, D. (2018). Neural ordinary differential equations. arXiv Preprint arXiv:1806.07366. https://doi.org/10.48550/arXiv.1806.07366
[4] Illarionov, E., Temirchev, P., Voloskov, D., Kostoev, R., Simonov, M., Pissarenko, D., Orlov, D., Koroteev, D. (2022). End-to-end neural network approach to 3D reservoir simulation and adaptation. Journal of Petroleum Science and Engineering, 208(Part A), 109332. https://doi.org/10.1016/j.petrol.2021.109332.
[5] Kani, J.N., Elsheikh, A.H., 2019. Reduced-Order Modeling of Subsurface Multi-phase Flow Models Using Deep Residual Recurrent Neural Networks. Transp. Porous Media 126, 713–741. https://doi.org/10.1007/s11242-018-1170-7.
[6] Prater, R., Hanne, T., Dornberger, R. (2024). Generalized performance of LSTM in time-series forecasting. Applied Artificial Intelligence, 38(1), 1-28. https://doi.org/10.1080/08839514.2024.2377510.
[7] Forouzanfar, F., Pires, A.P., Reynolds, A.C., 2015. Formulation of a Transient Multi-Phase Thermal Compositional Wellbore Model and its Coupling with a Thermal Compositional Reservoir Simulator. Presented at the SPE Annual Technical Conference and Exhibition, OnePetro. https://doi.org/10.2118/174749-MS.
[8] Shu, J., Han, G., Yue, Z., Wang, X., Peng, L., Li, J. (2025). An accurate and efficient surrogate model-based framework for coupled wellbore-reservoir modeling. In Proceedings of the SPE Advances in Integrated Reservoir Modelling and Field Development Conference and Exhibition (SPE-225298-MS). Abu Dhabi, UAE: Society of Petroleum Engineers (SPE). https://doi.org/10.2118/225298-MS.
[9] Ahmed, S.E., San, O., Kara, K., Younis, R., Rasheed, A., 2021. Multifidelity computing for coupling full and reduced order models. PLOS ONE 16, e0246092. https://doi.org/10.1371/journal.pone.0246092.
[10] Reyad, M.; Sarhan, A. M.; Arafa, M. (2023). A modified Adam algorithm for deep neural network optimization. Neural Computing and Applications, 35(23), 17095–17112. doi:10.1007/s00521-023-08568-z.

ICENS 11TH INTERNATIONAL CONFERENCE ON ENGINEERING AND NATURAL SCIENCE
October 22-26 2025 Sarajevo

Sustainable production of maleic anhydride: minimizing by-product formation in industrial fixed-bed tubular reactor

Ervin Karić[1*], Ivan Petric[1], Edina Ibrić[1], Maida Smajlović[1], Marijana Marković[1], Maida Kuduzović[1], Emir Suljaković[1], Ermin Mujkić[2]

Abstract

The synthesis of maleic anhydride from n-butane in an industrial fixed-bed reactor is presented, with emphasis on reducing by-product formation. The modeling and simulation of an industrial fixed-bed reactor are also presented in this paper. The research was conducted using industrial process data collected from a fixed-bed reactor over a defined period, addressing challenges related to conversion, yield, selectivity, and minimization of acrylic acid formation. The numerical software package MATLAB was used for solving the system of mathematical model equations. By decreasing the molar flow of n-butane at the reactor inlet by 15%, the conversion of n-butane and the yield of maleic anhydride increased by 6.89% and 3.13%, respectively, while the amount of acrylic acid formed was reduced by 2.10%. Conversely, increasing the molar flow of oxygen at the reactor inlet by 15% led to a 13.12% increase in the molar percentage of acrylic acid, whereas decreasing the oxygen flow by 15% reduced the molar percentage of acrylic acid by 10.77%. Increasing the pressure of the reaction mixture at the reactor inlet by 15% raised the molar percentage of acrylic acid by 6.93%, while decreasing the pressure by 15% reduced it by 8.04%. The selectivity of acrylic acid increases with higher inlet pressure due to enhanced n-butane conversion. Given that the main objective of the n-butane oxidation process to maleic anhydride is to achieve high n-butane conversion and maleic anhydride yield while minimizing acrylic acid formation, the optimal strategy is to reduce the molar flow of n-butane at the reactor inlet.

Keywords:

1. INTRODUCTION

The partial selective oxidation of n-butane to maleic anhydride with molecular oxygen is commercially well-established and strongly associated with the vanadium phosphorus oxide (VPO) catalyst [1]. Maleic Anhydride (MA) is the anhydride of cis-butenedioic acid (maleic acid); this molecule has a four carbon cyclic structure, containing also one oxygen atom. The molecule is also known with other names: 2,5-Furandione, Dihydro-2,5-dioxofuran, cis- Butanedioic anhydride [2]. Maleic anhydride is an important intermediate in the chemical industry, used in the production of agricultural chemicals and lubricant additives, and it is also a constituent component of several copolymers [3]. Over 50% of the global demand for maleic anhydride is used for the production of unsaturated polyester resins [3]. Initially, maleic anhydride was produced by the partial oxidation of benzene using a vanadium–molybdenum oxide (V_2O_5–MoO_3) catalyst [4]. Following the adoption of n-butane as a feedstock for maleic anhydride production, the number of studies on the synthesis of maleic anhydride via n-butane oxidation increased sharply ([5]-[9]). Reference [10] published one of the most significant early review articles addressing the catalytic properties of VPO catalysts, catalyst preparation mechanisms, and the kinetics of n-butane oxidation to maleic anhydride. The review covered a total of 188 studies. The formation of acrylic acid as a reaction by-product was also considered to assess its impact on the overall process efficiency. The present study focuses on modeling and simulating the formation of acrylic acid as a by-product during the partial oxidation of n-butane to maleic anhydride in an industrial fixed-bed tubular reactor. Using actual plant data, we implemented and numerically solved the mathematical model, based on the reactor model developed by [11] and kinetic data from [12], using MATLAB. Based on model, the variations of reactant and product molar flows along the reactor length were analyzed as a function of catalyst mass. The study specifically examined the influence of key process parameters, including n-butane and oxygen feed flow rates and reaction mixture pressure on acrylic acid formation. The modeling results provide insight into the sensitivity of by-product formation to operating conditions and can guide strategies for minimizing undesired side reactions in industrial operation.

[1] *Corresponding author*: [1]*Department of Chemical Engineering, Faculty of Technology, University of Tuzla, Urfeta Vejzagića 8, 75000 Tuzla, Bosnia and Herzegovina.* ervin.karic@untz.ba

[2] *Koksara d.o.o. Lukavac, Željeznička 1, 75300 Lukavac, Bosnia and Herzegovina*. ermin_mujkic@koksara.ba

2. MATERIALS AND METHODS

2.1. Description of the industrial reactor

For this study, industrial data from a fixed-bed tubular reactor used for maleic anhydride production were employed. The reactor consists of a large number of parallel tubes filled with a vanadium–phosphorus oxide (VPO) catalyst. The catalyst and reactor configuration are representative of typical industrial operation. Specific geometric details, catalyst porosity, and other sensitive operational parameters are omitted to maintain confidentiality.

2.2. Mathematical model

The mathematical model of the reactor, originally developed by [11], was used as the basis for this study and updated with new industrial measurements to reflect current operating conditions and reactor performance.

2.3. Kinetic model

The general scheme of the selective oxidation of *n*-butane to maleic anhydride can be represented by a combination of series and parallel reactions, as proposed by [13]:

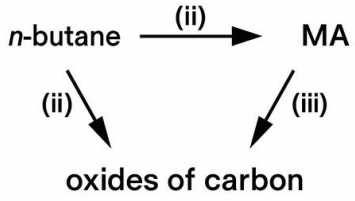

Figure 1. General scheme of the selective oxidation of n-*butane to maleic anhydride [13]*

In addition to the reactions mentioned above, the following equation was also considered for the formation of acrylic acid:

$$n - C_4H_{10} + 3.25O_2 \rightarrow C_3H_4O_2 + 0.5CO + 0.5CO_2 + 5H_2O \quad (4)$$

The kinetic model for the process scheme was taken from [12], where the Eley–Rideal approach was adopted to describe the kinetics of partial oxidation of *n*-butane [14].

$$r_1 = \frac{k_1 \cdot p_{butane} \cdot \sqrt{p_{O_2}}}{1 + b_{H_2O} \cdot p_{H_2O} + b_{butane} \cdot p_{butane}} \quad (5)$$

$$r_2 = \frac{k_2 \cdot p_{butane} \cdot \sqrt{p_{O_2}}}{1 + b_{H_2O} \cdot p_{H_2O} + b_{butane} \cdot p_{butane}} \quad (6)$$

$$r_3 = \frac{k_3 \cdot p_{MA} \cdot \sqrt[4]{p_{O_2}}}{1 + b_{H_2O} \cdot p_{H_2O} + b_{butane} \cdot p_{butane}} \quad (7)$$

where: r_1 - reaction rate of the first reaction (variable), k_1 - is the kinetic parameter of the first reaction (variable), p_{butane} - butane partial pressure (Pa), p_{O_2} - oxygen partial pressure (Pa), b_{H_2O} - kinetic parameter for water (-),p_{H_2O} - water partial pressure (Pa), r_2 - reaction rate of the second reaction (variable), k_2 - kinetic parameter of the second reaction (variable), r_3 - reaction rate of the third reaction (variable) k_3 - kinetic parameter of the third reaction (variable), and p_{MA} - maleic anhydride partial pressure (Pa).

The kinetic model of reaction (4) is presented by the following equation from [15]:

$$r_4 = k_4 \cdot p_{aa}^{0.68} \cdot p_{O_2}^{0.33} \quad (8)$$

where: r_4 - reaction rate of the fourth reaction (variable), k_4 - is the kinetic parameter of the first reaction (mol kg^{-1} s^{-1}), p_{aa} - acrylic acid partial pressure (Pa)

2.4. Model Simulation and Parametric Analysis

The mathematical model equations were numerically solved using the MATLAB software package. The system of ordinary differential equations describing the variation of component molar flows and temperature along the reactor length was solved using the ode45 solver, based on an explicit Runge–Kutta method of fourth and fifth order. The simulation was performed using industrial process data as input parameters. The effects of changes in the n-butane and oxygen feed flow

rates, as well as the inlet temperature and pressure of the reaction mixture, on the formation of acrylic acid were analyzed. These parameters were varied in the range of ±15% relative to the base case to evaluate their influence on acrylic acid generation within the reactor.

3. RESULTS AND DISCUSSION

Figure 2 shows the variation of the molar flow rates of *n*-butane (FA) and oxygen (FB) along the reactor as a function of the catalyst mass (W). The simulation was performed under the operating conditions of maleic anhydride synthesis by the partial oxidation of *n*-butane in a fixed-bed tubular reactor.

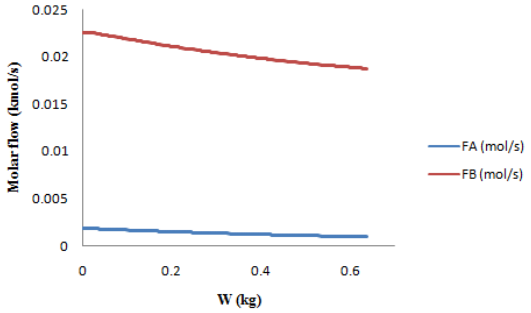

Figure 2.Variation of n-butane and oxygen molar flows along the reactor axial coordinate (as a function of catalyst mass).

Results show that n-butane flow decreases with increasing catalyst mass, as higher conversion consumes n-butane along the reactor, which agrees with the findings of [16] regarding conversion increase along the reactor length. Notably, the reduction in n-butane flow is more pronounced than that of oxygen, which aligns with the stoichiometry of the reaction. Reference [16] reported that n-butane conversion increases along the reactor length. In our study, the n-butane flow decreases with increasing catalyst mass. This is expected, as higher conversion leads to consumption of n-butane, reducing its flow along the reactor. The observed decrease in molar flows along the reactor length corresponds to enhanced reactant conversion, particularly in the initial section of the reactor, where reactant concentrations and temperature gradients are maximal. Moving further along the reactor, the reaction rate diminishes as the concentration of n-butane drops, resulting in a reduced contribution to overall conversion at higher catalyst masses. This pattern suggests that the reaction is mainly kinetically controlled in the early stages of the reactor, while at larger catalyst masses, mass transfer limitations begin to influence the process. Figure 3 shows the variation of the flow rates of carbon monoxide (FC), maleic anhydride (FD), and carbon dioxide (FE) as a function of catalyst mass, illustrating the consumption and formation trends of these species along the reactor.

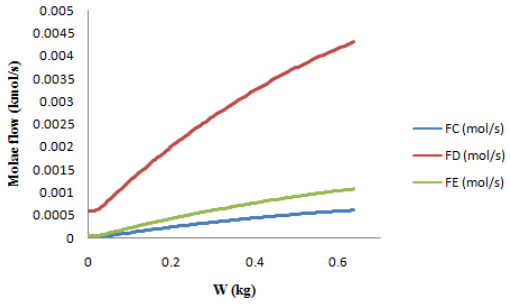

Figure 3.Variation of carbon monoxide (FC), maleic anhydride (FD), and carbon dioxide (FE) molar flows along the reactor axial coordinate (as a function of catalyst mass).

The profiles of carbon monoxide (FC), maleic anhydride (FD), and carbon dioxide (FE) molar flows as a function of catalyst mass (W) show that the formation of the desired product maleic anhydride steadily increases along the reactor, indicating efficient conversion of n-butane. At the same time, the flow rates of carbon monoxide and carbon dioxide also rise gradually, reflecting the generation of minor by-products through side reactions. The increase in carbon monoxide and carbon dioxide is much smaller compared to FD, demonstrating that the reaction remains highly selective toward maleic anhydride. The results obtained in this study are consistent with the findings of [16]. The selectivity of maleic anhydride increased along the length of the reactor, and the selectivity of carbon dioxide also increased. The ratio of carbon monoxide to carbon dioxide initially increased and then decreased in their study, indicating that in the later stages more carbon dioxide was produced than carbon monoxide. In our experiments, the selectivity of maleic anhydride and carbon dioxide similarly increased with increasing catalyst mass, while the flow of carbon monoxide also continuously increased, although at a lower rate than carbon dioxide. This indicates that maleic anhydride and carbon dioxide formation dominate the reaction, but carbon monoxide production continues throughout the reactor, confirming the influence of catalyst mass on the distribution of all

products. These results confirm the effectiveness of the catalyst and the progressive nature of the oxidation process along the reactor length.

Table 1 shows the effect of changes in the n-butane inlet flow (FA_{inlet}), expressed as a percentage, on the molar flow of acrylic acid at the reactor outlet (FG).

Table 1. Effect of n-butane inlet molar flow on the molar flow of acrylic acid at the reactor outlet (FG)

FA_{inlet} (%)	F_G (kmol/s)
-15	0.000774
-10	0.000779
-5	0.000786
0	0.000791
+5	0.000795
+10	0.000802
+15	0.000804

By decreasing the molar flow of n-butane at the reactor inlet by 15%, the conversion of n-butane and the yield of maleic anhydride increased by 6.89% and 3.13%, respectively, while the amount of acrylic acid formed was reduced by $1.7 \cdot 10^{-5}$ (or 2.10%). Reference [17] demonstrated that increasing the percentage of n-butane at the reactor inlet led to a higher yield of maleic anhydride, while the overall conversion of n-butane decreased due to losses in undesired side reactions. The reduction in n-butane conversion caused by these losses explains why increasing the n-butane flow at the reactor inlet results in a higher molar flow of acrylic acid at the reactor outlet. Reference [18] found that increasing the concentration of n-butane at the reactor inlet increases the selectivity toward acrylic acid, which in turn leads to higher acrylic acid production, as also demonstrated in this study.

Table 2 shows the effect of changes in the oxygen inlet flow (FB_{inlet}), expressed as a percentage, on the molar flow of acrylic acid at the reactor outlet.

Table 2. Effect of oxygen inlet molar flow on the molar flow of acrylic acid at the reactor outlet

FB_{inlet} (%)	F_G (kmol/s)
-15	0.0007059
-10	0.000781
-5	0.00075
0	0.000791
+5	0.000795
+10	0.000799
+15	0.000895

Increasing the molar flow of oxygen at the reactor inlet by 15% led to a 13.12% increase in the molar percentage of acrylic acid, whereas decreasing the oxygen flow by 15% reduced the molar percentage of acrylic acid by 10.77%. These results indicates that a higher oxygen availability promotes the oxidation of n-butane and the subsequent formation of intermediate products such as maleic anhydride and acrylic acid. Enhanced oxygen concentration improves the reaction rate by providing sufficient oxidizing species on the catalyst surface, thereby increasing the overall conversion and yield. However, excessive oxygen may also favor complete combustion reactions, leading to undesired formation of CO and CO_2, which can reduce selectivity toward valuable products.

Table 3 shows the effect of the reaction mixture temperature at the reactor inlet, expressed as a percentage, on the molar flow of acrylic acid at the reactor outlet.

Table 3. Effect of the reaction mixture temperature at the reactor on the molar flow of acrylic acid at the reactor outlet

T (%)	F_G (kmol/s)
-15	0.000771
-10	0.000779
-5	0.000785
0	0.000791
+5	0.000797
+10	0.000804
+15	0.000808

Data from Table 3 show that the acrylic acid molar flow (FG) varies slightly with changes in the inlet temperature of the reaction mixture**.** A 15 % decrease in the inlet temperature reduces FG from 0.000791 kmol/s (reference value at 0 %) to 0.000771 kmol/s, corresponding to a decrease of approximately 2.53 %. Conversely, a 15 % increase in inlet temperature

raises FG to 0.000808 kmol/s, representing an increase of 2.15 % relative to the reference value. These results indicate that the acrylic acid flow is moderately sensitive to the inlet temperature: higher temperatures slightly increase the flow, while lower temperatures reduce it. This behavior is consistent with the reaction kinetics of n-butane oxidation, where higher temperatures accelerate the reaction rate, and lower temperatures slow down acrylic acid formation. Reference [19] reported that acrylic acid begins to appear in trace amounts at temperatures above 402 °C. Considering that in this study the reaction mixture temperature at the reactor outlet is 421.34 °C, the observed increase in acrylic acid production with increasing temperature is consistent with these findings. Additionally, increasing the temperature enhanced acrylic acid selectivity [20], which is also observed in this study.

Table 4 shows the effect of the reaction mixture pressure at the reactor inlet, expressed as a percentage, on the molar flow of acrylic acid at the reactor outlet.

Table 4. Effect of the reaction mixture pressure at the reactor on the molar flow of acrylic acid at the reactor outlet

P (%)	F_G (kmol/s)
-15	0.000736
-10	0.000741
-5	0.000765
0	0.000791
+5	0.000801
+10	0.000837
+15	0.000855

Increasing the pressure of the reaction mixture at the reactor inlet by 15% raised the molar percentage of acrylic acid by 6.93%, while decreasing the pressure by 15% reduced it by 8.04%. This indicates that reductions in pressure have a stronger impact on acrylic acid production than equivalent increases, emphasizing the critical role of maintaining optimal reactor inlet pressure. The results also suggest that pressure control can be an effective tool for stabilizing production rates under varying operational conditions. Reference [21] investigated the effect of pressure variation on acrylic acid yield and found that increasing the pressure enhanced the yield up to a certain point, after which a slight decrease was observed at the reactor outlet.

4. CONCLUSION

The results of this study demonstrate that the molar flow of acrylic acid (FG) is sensitive to variations in key reactor operating parameters. Increasing the inlet flows of n-butane and oxygen, as well as the feed temperature and pressure, generally enhances FG, whereas decreasing these parameters reduces it. The flow of acrylic acid shows moderate sensitivity to feed temperature, with a 15 % increase resulting in a 2.15 % rise in FG and a 15 % decrease causing a 2.53 % reduction, consistent with the kinetics of n-butane oxidation. Pressure effects are more pronounced: a 15 % increase in inlet pressure raises FG by 6.93 %, while a 15 % decrease reduces it by 8.04 %, indicating that reductions in pressure have a stronger impact than equivalent increases. Variation of n-butane and oxygen feed rates affects both selectivity and production, with higher n-butane flows increasing the molar flow of acrylic acid but slightly reducing overall n-butane conversion due to side reactions, while higher oxygen flows improve both yield and selectivity toward acrylic acid. Furthermore, the analysis of molar flows along the reactor as a function of catalyst mass shows that n-butane is consumed more rapidly than oxygen in the early section of the reactor, corresponding to higher conversion, and that the formation of acrylic acid, maleic anhydride, and by-products is progressively influenced by catalyst distribution. The kinetic and mathematical models, validated with industrial data, provide reliable predictions of reactor performance and can be used to optimize operating conditions and stabilize acrylic acid production.

ACKNOWLEDGMENT

The authors acknowledge the Ministry of Education and Science of Tuzla Canton for funding the project “Minimizing the release of by-products into the environment from the synthesis of maleic anhydride in an industrial fixed-bed tubular reactor”. The authors also thank Ermin Mujkić, Director of the Maleic Anhydride Plant at Koksara d.d. Lukavac, for his support and assistance during this study.

REFERENCES

[1] N. Stegmann, C. Ochoa-Hernández, K.N. Truong, H. Petersen, C., Weidenthaler, and W. Schmidt, W, “The mechanism and pathway of selective partial oxidation of n-butane to maleic anhydride studied on titanium phosphate catalysts,” *ACS Catalysis*, vol. 20, pp. 15833-15840, 2023.

[2] Caldarelli, “New reactants and improved catalysts for maleic anhydride synthesis, ” Doctoral dissertation, Univ. of Bologna, Bologna, Italy, Department of Industrial Chemistry, 2012.

[3] D. Lesser, “Dynamic Behavior of Industrial Fixed Bed Reactors for the Manufacture of Maleic Anhydride,” Doctoral dissertation, Clausthal Univ. of Technology, Clausthal-Zellerfeld, Germany, Faculty of Mathematics/Computer Science and Mechanical Engineering, 2016.

[4] Y. Ye, "Experimental study on *n*-Butane partial oxidation to maleic anhydride in a solid electrolyte membrane reactor," Doctoral dissertation, Otto-von-Guericke-Univ. of Magdeburg, Magdeburg, Germany, 2006.
[5] R.L. Varma, and D. N. Saraf, "Selective Oxidation of C4 Hydrocarbons to Meleic Anhydride," *Industrial & Engineering Chemistry Product Research and Development*, vol. 18, pp. 7-13, 1979.
[6] M. Brutovský, and Š. Gerej, "Effect of various modifying elements on the catalytic properties of vanadium-phosphorus catalysts in oxidation of butane," *Collection of Czechoslovak Chemical Communications*, vol. 47, pp. 403-408, 1982.
[7] K. Hodnett, and B. Delmon, "Influence of reductive pretreatments on the activity and selectivity of vanadium-phosphorus oxide catalysts for n-butane partial oxidation, "*Industrial & Engineering Chemistry Fundamentals*, vol. 23, pp. 465-470. 1984.
[8] G. Centi, G., Fornasari, and F. Trifiro, F. "*n*-Butane oxidation to maleic anhydide on vanadium-phospohorus oxides: Kinetic analysis with a tubular flow stacked-pellet reactor," *Industrial & Engineering Chemistry Product Research and Development*, vol. 24, pp. 32-37, 1985.
[9] T. P. Moser, and G. L. Schrader, G. L., "Selective oxidation of *n*-butane to maleic anhydride by model V-P-O catalysts.," *Journal of Catalysis*, vol. 92, pp. 216-231, 1985.
[10] G. Centi, F. Trifiro, J. R. Ebner, and V. M. Franchetti, "Mechanistic aspects of maleic anhydride synthesis from C4 hydrocarbons over phosphorus vanadium oxide," *Chemical Reviews*, vol. 88, pp. 55-80, 1988.
[11] Petric, and E. Karić, "Simulation of commercial fixed-bed reactor for maleic anhydride synthesis: application of different kinetic models and industrial process data," *Reaction Kinetics, Mechanisms and Catalysis*, vol. 126, pp. 1027-1054. 2019.
[12] R. Guettel, and T. Turek, "Assessment of micro-structured fixed-bed reactors for highly exothermic gas-phase reactions," *Chemical Engineering Science*, vol. 65, pp. 1644-1654, 2010.
[13] S. K. Bej, and M. S. Rao, "Selective oxidation of n-butane to maleic anhydride. 3. Modeling studies," *Industrial & engineering chemistry research*, vol. 30, pp. 1829-1832, 1991.
[14] Becker, "Katalytische Wandreactorkonzepte für MSA-Synthese und Methanol-Dampfreformierung," Doctoral dissertation, Institut fur Chemische Verfahrenstechnik der Universitat Stuttgart, Stuttgart, Germany, 2002.
[15] Y. Dong, "Modeling chemistry and flow in catalytic fixed-bed reactors with detailed geometry, " Doctoral dissertation, Technische Universität Hamburg, Hamburg, Germany, 2018.
[16] Romano, A. Di Giuliano, K. Gallucci, P .U. Foscolo, C. Cortelli, S. Gori, S., and M. Novelli," Simulation of an industrial turbulent fluidized bed reactor for *n*-butane partial oxidation to maleic anhydride," *Chemical Engineering Research and Design*, vol. 114, pp.79-88, 2016.
[17] S. Roy, M.P. Duduković, and P. L. Mills, P. L., "A two-phase compartments model for the selective oxidation of *n*-butane in a circulating fluidized bed reactor," *Catalysis Today*, vol. 6, pp. 73-85, 2000.
[18] G. S. Patience, and M. J. Lorences," VPO transient oxidation kinetics, " *International Journal of Chemical Reactor Engineering*, vol. 4, pp. 1-16, 2006.
[19] X. F. Huang, C. Y., Li, B. H., Chen, and P. L. Silveston, "Transient kinetics of *n*-Butane oxidation to maleic anhydride over a VPO catalyst," *AIChE Journal*, vol. 48, pp. 846-855, 2002.
[20] M. J. Lorences, G. S., Patience, F. V., Díez, and J. Coca, "Transient n-butane partial oxidation kinetics over VPO," *Applied Catalysis A: General*, vol. 26, pp. 193-202, 2004.
[21] M. Dente, S., Pierucci, E., Tronconi, M., Cecchini, M., and F. Ghelfi, "Selective oxidation of n-butane to maleic anhydride in fluid bed reactors: detailed kinetic investigation and reactor modelling," *Chemical engineering science*, vol. 58, pp. 643-648, 2003.

BIOGRAPHY

Ervin Karić is an Assistant Professor at the University of Tuzla, Faculty of Technology, Department of Chemical Engineering. He enrolled in the Chemical Engineering program at the University of Tuzla in 2008/2009 and completed his Bachelor's studies in 2012 with an average grade of 9.059. He received his Master's degree in Chemical Engineering and Technology in 2016 and his PhD in Chemical Engineering in 2021, both with an average grade of 10.00. Dr. Karić has participated in several national research projects, including the optimization of maleic anhydride synthesis from n-butane in an industrial fixed-bed reactor. He is the author and co-author of numerous scientific publications in chemical engineering. He teaches undergraduate and graduate courses in process and chemical engineering, supervises graduate students, and actively contributes to the academic community through teaching, research, and national and international collaborations.

ICENS 11TH INTERNATIONAL CONFERENCE ON ENGINEERING AND NATURAL SCIENCE
October 22-26 2025 Sarajevo

The Sensitivity of Local Water Springs to Climatic and Tectonic Impacts: The Gündüzbey Spring Example

Ufuk Yükseler[1], Ö. Faruk Dursun[1]*

Abstract

The escalating pressures on natural systems due to global warming-induced climate change are becoming increasingly apparent[1]. Water resources, in particular, are among the components where the most pronounced effects of climate change are observed[2]. Irregularities in precipitation regimes, a persistent increase in temperature, and rising evaporation rates collectively threaten the quantity and sustainability of both surface and groundwater sources[3]. This precarious situation underscores the critical necessity for the protection and sustainable management of local resources that hold strategic importance for drinking and utility water supply[4].

This study focuses on the Gündüzbey water spring in Malatya province, which plays a vital role in the regional drinking water supply[5]. The utilized dataset comprises long-term discharge (flow rate) values of the spring, along with essential climatic parameters (precipitation and temperature) specific to the Malatya region[6]. To investigate the impact of climate change on the spring, the presence of trends in the discharge and climate series was initially assessed using various trend analysis methods[7]. Subsequently, the relationships between discharge and the climatic parameters were explored through correlation and regression analyses to determine the sensitivity of discharge values to climatic variability[8].

Furthermore, the study examined the potential effects of the Kahramanmaraş-centered earthquake that occurred on February 6, 2023, which severely impacted the region, on the Gündüzbey spring[9]. The time series was segmented into pre- and post-earthquake periods, and statistical methods were employed to analyze any sudden changes or structural breaks in the discharge values[10]. The discussion also addresses whether the earthquake induced changes in the permeability characteristics of the aquifers and altered the conditions for water emergence at the surface[11].

Keywords: Trend Analysis, Climate Change, Water Resources, Gündüzbey, KahramanMaraş's Earthquakes.

1. INTRODUCTION

Climate change is defined as persistent alterations in the average values and variability of climate over periods spanning decades to centuries. According to the IPCC, the primary drivers of these shifts include greenhouse gas emissions, modifications in land use, and other anthropogenic factors (Zillman, 2001). Specifically, Global warming is the long-term process of heating the Earth's surface and sea level, caused by the retention of heat in the atmosphere due to greenhouse gases released from human activities such as fossil fuel combustion and deforestation.

Global warming profoundly influences the hydrological cycle, generating significant uncertainties concerning the availability, distribution, quality, and utilization of water resources (Gosling & Arnell, 2016; Ciampittiello et al., 2024). Rising temperatures increase evaporation and evapotranspiration, altering precipitation regimes and surface runoff, which intensifies the risk of regional water scarcity, particularly in basins across South and East Asia (Nasonova et al., 2018; Özdemir et al., 2024). Furthermore, the accelerated melting of snow cover and glaciers disrupts the seasonal distribution of water, consequently heightening the risks of both droughts and floods (Elgendy et al., 2024). Groundwater quality is also negatively affected by climate change-related meteorological processes and land use changes, as shifts in temperature and precipitation patterns influence the transport of contaminants into the groundwater (Dao et al., 2024; Zhu et al., 2015).

The hydrological impacts of climate change have been examined at various scales by numerous researchers. For instance, Abbas et al. (2022) highlighted that changes in climatic parameters such as temperature and precipitation strongly affect evaporation, snowmelt, and surface runoff, leading to alterations in the timing and magnitude of river discharges. Large-scale basin projections employing General Circulation Models (GCM) and Representative Concentration Pathways (RCP) scenarios have revealed considerable uncertainties regarding the impact of different climate scenarios on discharge (Nasonova et al., 2018). Similarly, a global-scale analysis by Gudmundsson et al. (2021) found that observed trends in low, high, and mean river flows at 7250 gauging stations were consistent only with models that incorporated the effects of anthropogenic greenhouse gases.

[1] Inönü University, Department of Civil Engineering, 44280, Battalgazi/Malatya, Turkey.
ufukyukseler12@gmail.com

[*] Corresponding author: Inönü University, Department of Civil Engineering, 44280, Battalgazi/Malatya, Turkey.
ofdursun@gmail.com

Studies on groundwater dynamics also reveal the compound effects of climatic and geological factors. Elkhoury, Brodsky & Agnew (2006) analyzed long-term well data in Southern California, demonstrating that earthquakes can cause transient increases in aquifer permeability. Correspondingly, research by Manga et al. (2012) showed that transient stresses, such as earthquake shaking, can induce both short- and long-term effects on aquifer fractures. A study in the Tuscany region of Italy established strong correlations between the "Standardized Groundwater Index (SGI)," "Standardized Precipitation Index (SPI)," and "Standardized Precipitation Evapotranspiration Index (SPEI)," leading to future groundwater drought projections under RCP 4.5 and RCP 8.5 scenarios (Secci et al., 2021). These findings underscore the crucial role of temperature increases in influencing evapotranspiration and drought processes (Asoka & Mishra, 2019).

In this study, the Gündüzbey spring, which serves as the primary drinking water source for the city center of Malatya, is investigated. The research evaluates the potential impacts of climate change on the spring using trend analysis methods (Burn & Elnur, 2002; Hamed & Rao, 1998; Mann, 1945; Spearman, 1904; Şen, 2012; Yue et al., 2002; Yue & Wang, 2004) and examines the hydrogeological effects of the February 6, 2023, Kahramanmaraş-centered earthquake on the Gündüzbey source. Time series data were analyzed by dividing them into pre- and post-earthquake periods, statistically assessing the existence of sudden changes or structural breaks in discharge values (Çeliker et al., 2021; Zhang et al., 2019; Sönmez & Kale, 2020). Additionally, a detailed discussion is provided on whether the earthquake caused changes in the hydraulic conductivity properties of the aquifers and potential alterations to the conditions under which the water emerges at the surface.

2. STUDY AREA

The Gündüzbey Capture Facility (Kaptaj) is a vital resource for the drinking and utility water supply of Malatya city center, serving as a fundamental water source for the region over many years. The Gündüzbey Capture Facility has been collecting natural spring water filtered through the region's rocks and geological formations and delivering it to the city residents since 1946.

The water collected by the Kaptaj is typically around 11–13 °C and is conveyed to the city network with only chlorination, without undergoing complex treatment. This practice indicates that the source's natural structure is well-preserved, allowing the water to be supplied directly for consumption.

Gündüzbey neighborhood, where the Capture Facility is located, is approximately 7–8 km from the Malatya city center. Its strategic location allows the clear spring water, emerging from the foothills of the Beydağı mountains, to reach the city by gravity. The historical and cultural significance of the water source is also frequently highlighted in local literature. Gündüzbey spring water is associated with historical and cultural narratives among the local populace, and the source and its surroundings are considered important both for urban water supply and as a picnic and recreational area.

The function of the Gündüzbey Kaptaj gained particular prominence after the February 6, 2023, earthquakes. The temporary interruption or turbidity of the water flow from the source following the Kahramanmaraş earthquakes demonstrated its critical role for the city's water network. Furthermore, Gündüzbey's existing capacity and water quality serve as a reference point when planning alternative drinking water sources, with new sources often compared against the Gündüzbey standard.

Given these characteristics, the Gündüzbey spring is an indispensable water supply point for Malatya from geological, hydrogeological, and socio-cultural perspectives. This study will evaluate the Gündüzbey source's water supply process, discharge characteristics, quality status, and, specifically, the hydrogeological changes following the 2023 earthquake. The Gündüzbey Capture Facility, which collects the water naturally flowing from between the rocks, has been continuously meeting the city's water needs since 1946.

3. METHODOLOGY

Climate change significantly impacts the hydrological cycle, consequently affecting the flow regimes of streams. Long-term trends in fundamental climatic variables such as precipitation, temperature, and evaporation play a determining role in the sustainability of water resources and the dynamics of floods and droughts. In this context, trend analyses are utilized to interpret the relationship between climatic variables and stream flows and to statistically ascertain the significance of these changes. Trend analyses are crucial tools for identifying increasing or decreasing trends in time series and are widely applied in climate change studies (Dursun et al., 2021; Şen, 2017).

In this study, the Mann–Kendall (MK) (Mann, 1945; Hamed & Rao, 1998), Spearman's Rho (SR) (Spearman, 1904), and Şen's Innovative Trend Analysis (ITA) (Şen, 2012) methods were employed to determine the trends in the long-term flow data of the studied stream and related meteorological parameters (precipitation, temperature, etc.). These methods were chosen because they can reveal the direction and magnitude of the trend independent of the assumptions regarding the data distribution (Yue et al., 2002; Yue & Wang, 2004).

3.1. Mann-Kendall (MK) Test

The Mann-Kendall test is a non-parametric statistical method widely used to detect the presence of monotonic (linear or non-linear) trends in time series (Kendall, 1975). It does not require the data to be normally distributed and is less sensitive to outliers. The test calculates a test statistic S based on the sign of the difference between every pair of data points in the

series. A positive S statistic indicates an increasing trend, while a negative S statistic indicates a decreasing trend. The significance of the test result is usually evaluated using the Z-statistic based on a normal approximation. The MK test is frequently preferred for trend analysis of climate change and hydrological variables. (Yue & Wang, 2004; Hamed & Rao, 1998).

3.2. Spearman's Rho (SR) Test

The Spearman's Rho test, based on Spearman's rank correlation coefficient, is a non-parametric method that determines the direction and strength of the monotonic relationship between two variables. Similar to the MK test, it does not require the data to be normally distributed. The correlation coefficient ρ is calculated based on the rank differences of the observations after the data have been ordered. A positive or negative value ρ indicates the direction of the increasing or decreasing trend. It is often used in hydrological and meteorological series for validation or comparison alongside the MK test (Yue et al., 2002).

3.3. *Şen's Innovative Trend Analysis (ITA) Method*

The Innovative Trend Analysis (ITA) method, developed by Şen (2012), allows for trend detection without being bound by classical statistical assumptions. This method involves dividing the data series into two equal halves and plotting the first half in ascending order on the x-axis and the second half, also in ascending order, on the y-axis. The distribution of the data points relative to the 1:1 reference line provides visual and quantitative information about the direction and magnitude of the trend (Kisi & Ay, 2014). If the majority of the points lie above the 1:1 line, an increasing trend is present; if they lie below, a decreasing trend is present. The most significant advantage of this method is its independence from assumptions regarding data distribution, autocorrelation, or seasonality. Consequently, it is frequently preferred for climatic and flow data (Şen, 2012; Şen, 2017; Kisi & Ay, 2014).

4. RESULTS AND DISCUSSION

Non-parametric methods, specifically Spearman's Rho, Mann-Kendall, and Seasonal Mann-Kendall tests, were initially applied to the Gündüzbey spring discharge data.

The results of the Spearman's Rho test ρ=0.0136 and p=0.835 indicated no statistically significant trend in the discharge series. Similarly, the Mann-Kendall test yielded Z=-0.476 and p=0.634, suggesting a weak decreasing trend, but one that was not statistically significant. The Seasonal Mann-Kendall test revealed seasonal variability in the trend. Statistically significant decreasing trends were detected particularly in March (Z=-2.21, p=0.027), May (Z=-2.99, p = 0.0028), and December (Z=-2.36, p=0.018). Conversely, a significant increasing trend was found in September (Z=1.97, p=0.049). Trends observed in other months were deemed statistically insignificant.

Table 1. Trend Analysis Results of Flow Discharges According to Nonparametric Methods

Test Method	Z or ρ Value	p-Value	Trend Direction	Significance (α=0.05)
Spearman's rho	ρ = 0.0136	0.835	Increase	Insignificant
Mann-Kendall	Z = –0.476	0.634	Decrease	Insignificant
Seasonal MK (March)	Z = –2.21	0.027	Decrease	Significant
Seasonal MK (May)	Z = –2.99	0.0028	Decrease	Significant
Seasonal MK (December)	Z = –2.36	0.018	Decrease	Significant
Seasonal MK (September)	Z = 1.97	0.049	Increase	Significant
Other Months (General)	–	p > 0.05	–	Insignificant

The Innovative Trend Analysis (ITA) method was also applied to the discharge values of the Malatya drinking water station. The analysis showed that the vast majority of the data points lie above the 1:1 reference line. This implies that the values in the second half of the series are generally higher than those in the first half. The mean difference was calculated as Δmean=+0.794 m³/s indicating a positive (increasing) trend in the discharge values.

Based on the combined results of the Spearman's Rho, Mann-Kendall, and ITA methods, the discharge series for the Gündüzbey source, which supplies Malatya's drinking water, shows no significant overall increasing or decreasing trend. However, the ITA method indicated a slight upward trend, contrasting with the classical tests. This finding suggests that the discharge values are generally stable, with potential changes being weak and primarily seasonal. Furthermore, no sharp change in the spring's discharge values was observed immediately after the February 6 earthquake; however, any partial changes may become clearer with longer-term future data.

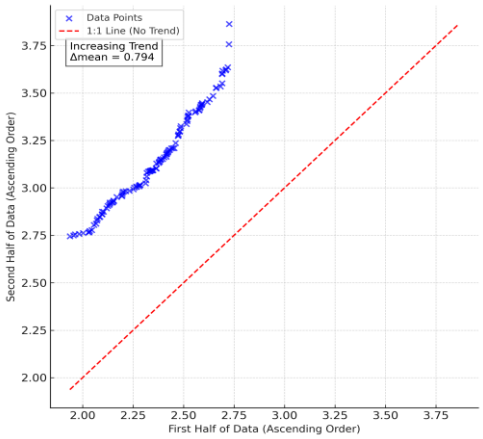

Figure 2. Results of the Şen-ITA Method for Gündüzbey Spring Discharge Values

As a result of the statistical analyses, no significant long-term trend was detected in the annual total precipitation data of the study area. The Spearman Rho test results ($\rho = -0.092$, $p = 0.374$) indicate a weak and statistically insignificant negative relationship between precipitation values and time. The Mann–Kendall test ($Z = -0.27$, $p = 0.79$) similarly does not indicate a significant increasing or decreasing trend. When the seasonal Mann–Kendall test was evaluated on a monthly basis, an increasing trend was observed in the 4th month and a decreasing trend in the 8th month; however, most of these trends were not found to be statistically significant. Finally, the results of Şen's Innovative Trend Analysis (Şen–ITA) indicate a weak decreasing trend because the slope coefficient ($b = 0.894$) is below 1, while the high coefficient of determination ($R^2 = 0.972$) reveals a strong similarity between the periods. When all these results are evaluated together, it can be said that there was no significant and statistically significant change in the rainfall amounts during the study period and that the rainfall regime in the region generally exhibited a stable structure (Table 2).

As a result of the statistical analyses, no significant long-term trend was detected in the annual total precipitation data of the study area. The Spearman Rho test results ($\rho = -0.092$, $p = 0.374$) indicate a weak and statistically insignificant negative relationship between precipitation values and time. The Mann–Kendall test ($Z = -0.27$, $p = 0.79$) similarly does not indicate a significant increasing or decreasing trend. When the seasonal Mann–Kendall test was evaluated on a monthly basis, an increasing trend was observed in the 4th month and a decreasing trend in the 8th month; however, most of these trends were not found to be statistically significant. Finally, the results of Şen's Innovative Trend Analysis (Şen–ITA) indicate a weak decreasing trend because the slope coefficient ($b = 0.894$) is below 1, while the high coefficient of determination ($R^2 = 0.972$) reveals a strong similarity between the periods. When all these results are evaluated together, it can be said that there was no significant and statistically significant change in the rainfall amounts during the study period and that the rainfall regime in the region generally exhibited a stable structure (Table 2).

Table 2. Precipitation Values Trend Analysis Results

Test Type	Parameter(s)	Result / Value	Trend Direction	Significance / Comment
Spearman Rho	$\rho = -0.092$, $p = 0.374$	Weak negative correlation	Decrease	Insignificant ($p>0.05$)
Mann-Kendall	$Z = -0.27$, $p = 0.79$	Very weak trend	Decrease	Insignificant ($p>0.05$)
Seasonal MK (Monthly)	4 increase, 8 decrease montths	General weak decrease trend	-	Mostly insignificant
Şen ITA (Annual)	$b = 0.894$, $R^2 = 0.972$	Strong relationship, slight decrease	Decrease	Weak trend

According to the results of Şen's Innovative Trend Analysis (Şen-ITA), applied to the annual total precipitation series for the period 1929–2024, a weak decreasing trend in long-term precipitation is observed. The regression slope ($b = 0.894$) is less than one, indicating that annual precipitation amounts in the second half of the observation period (1977–2024) were slightly lower than in the first half (1929–1976). The coefficient of determination ($R^2 = 0.972$) was quite high, indicating that the precipitation patterns between the two periods were largely similar and that there was a strong relationship between the data. However, the slope being very close to 1 indicates that this decreasing trend is statistically weak (Figure 3).

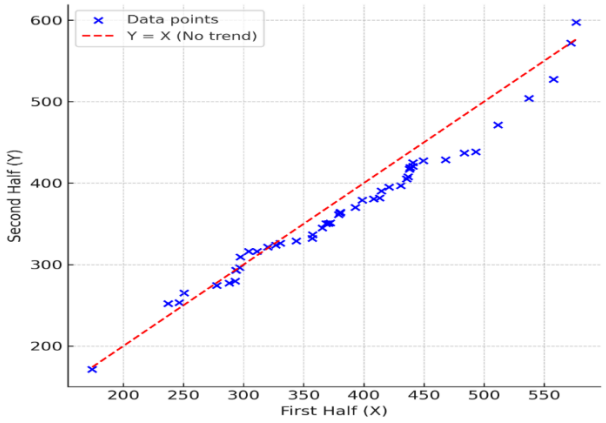

Figure 3. Şen-ITA Method Results of Malatya Province Rainfall Values

Spearman's rho test was applied to the long-term monthly mean temperature series for Malatya province. This test is a nonparametric method that evaluates the sequential relationship between the data and determines whether there is a significant trend toward increase or decrease in the time series. The analysis yielded $\rho = 0.0501$ and $p = 0.0895$. A positive Rho coefficient indicates a weak upward trend in the series. However, a p-value greater than 0.05 indicates that this trend is not statistically significant. Therefore, according to Spearman's rho test, no significant trend was detected in the monthly mean temperature series for the Malatya region; however, the overall trend is slightly upward.

The Mann-Kendall test is a nonparametric method widely used to determine the presence of long-term trends toward increase or decrease in hydrological and meteorological time series. The analysis yielded $Z = 1.719$ and $p = 0.0856$. A positive Z statistic indicates an increasing trend in the series. However, a p-value greater than 0.05 ($p > 0.05$) indicates that this trend is not statistically significant. Accordingly, according to the Mann-Kendall test, although there is no significant increasing or decreasing trend in the temperature series for Malatya province, the general direction of the trend is upward.

The seasonal Mann-Kendall trend test was applied to the monthly average temperature series for Malatya province. This method is a variant of the classical Mann-Kendall test that takes seasonal variability into account and evaluates the direction and significance of the trend for each month separately.

According to the analysis results, statistically significant increasing trends were identified in 8 out of 12 months on a monthly basis ($p < 0.05$). This indicates an increasing trend in temperature values, particularly throughout most of the year. The trends observed in other months, while positive, are not statistically significant due to p-values greater than 0.05.

Overall, there is a significant seasonal upward trend in the monthly average temperature series for Malatya province. This finding suggests that, although the trend appears weak in annual analyses, temperatures have risen significantly, particularly in certain months. This result demonstrates that a seasonal warming trend is influential in the region's climatic conditions (Table 3).

Table 3. Temperature Values Trend Analysis Results

Test Method	Statistic	p-Value	Trend Direction	Significance (α=0.05)	Explanation
Spearman's rho	$\rho = 0.0501$	0.0895	Increase	Insignificant	Weak increasing trend, not statistically significant.
Mann-Kendall	$Z = 1.719$	0.0856	Increase	Insignificant	Positive trend observed but did not reach the significance level.
Seasonal Mann-Kendall	-	$p < 0.05$ (8 ay)	Increase	Significant (Seasonal)	Significant increasing trend detected in 8 out of 12 months.
Innovative Trend Analysis (ITA)	Δmean = +17.184	-	Increase	-	The second half of the series is significantly higher than the first half; the increasing trend is pronounced.

The Innovative Trend Analysis (ITA) method was applied to the long-term monthly average temperature series for Malatya province. This method divides the time series into two equal parts, compares the values of the first half (early period) and the second half (late period), and determines the trend direction using a 1:1 reference line.

As a result of the analysis, the mean of the first half of the series was calculated as ($Mean_1$ = {:.3f}°C), and the mean of the second half as ($Mean_2$ = {:.3f}°C). The difference between these two means is Δmean = +17.184°C, indicating a significant positive increasing trend. The majority of the data points lie above the 1:1 line, indicating a significant increase in temperature values in the second half of the series. Therefore, according to the ITA method, there is a significant upward trend in the long-term temperature series for the Malatya region. This result supports the weak positive trend detected in the classical Mann-Kendall test and shows that the temperature regime in the region has a warming trend over time (Figure 4).

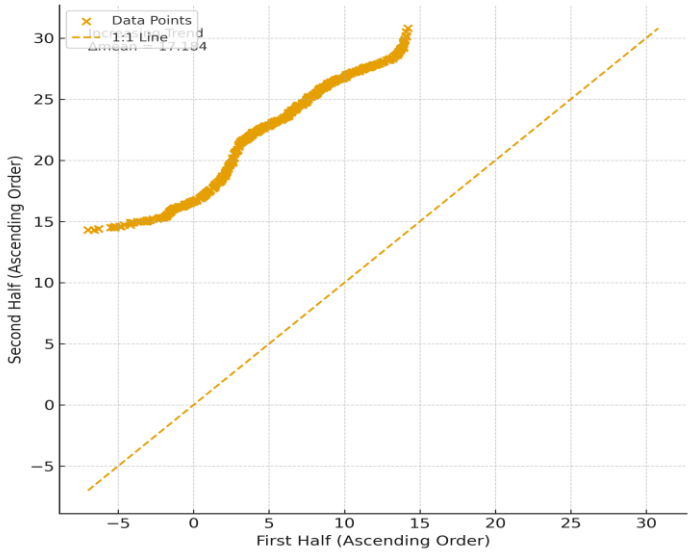

Figure 4. Şen-ITA Method Results of Malatya Province Temperature Values

5. CONCLUSIONS

This study evaluated precipitation, temperature, and Gündüzbey spring discharge data for Malatya province and its surroundings to investigate the effects of climate change and the Kahramanmaraş-centered earthquake of February 6, 2023, on the hydrological system in the region. The nonparametric trend analyses and innovative trend approach applied in the study revealed the region's climatic behavior on a long-term and seasonal scale.

The results reveal a generally stable flow pattern in Gündüzbey spring discharge values, with no significant long-term increase or decrease observed. Seasonal analyses revealed decreasing trends in some months and partial increases in other periods. This suggests that the spring is sensitive to seasonal climatic variability.

The analysis of precipitation data revealed that long-term precipitation amounts in the region are generally stable, with no significant decreasing or increasing trends. This result indicates that the Malatya region is in relative equilibrium in terms of precipitation regime.

The analysis of temperature data revealed a significant warming trend on a regional scale. The observation of upward trends throughout most of the year indicates that temperatures in Malatya province are exhibiting a long-term upward trend and that climatic warming is beginning to take hold on a regional scale.

Post-earthquake analyses indicate that, while no sudden or sharp changes were observed in the Gündüzbey spring's flow rate, small and temporary fluctuations occurred in the spring's flow characteristics. This suggests that the earthquake caused limited hydrodynamic changes in the aquifer structure, but the system generally maintained its geological and hydrological balance. Long-term monitoring studies are crucial for revealing the permanent effects of such seismic events on the spring's flow behavior.

Overall, it has been concluded that precipitation is stable, temperatures are on an increasing trend, and water resources generally follow a balanced course in Malatya province. Furthermore, it is emphasized that the combined effects of climatic changes and earthquakes are critical for monitoring temporary or permanent changes that may occur in groundwater systems

over the long term. These findings provide an important scientific basis for assessing the resilience of the Gündüzbey spring and similar hydrogeological systems to climatic changes and seismic impacts.

REFERENCES

[1] Abbas, M., Zhao, L., & Wang, Y. (2022). Perspective impact on water environment and hydrological regime owing to climate change: A review. Hydrology, 9(11), 203.

[2] Asoka, A., & Mishra, V. (2019). Groundwater pumping to increase food production causes persistent groundwater drought in India. arXiv preprint arXiv:1908.00255.

[3] Burn, D. H., & Elnur, M. A. H. (2002). Detection of hydrologic trends and variability. Journal of Hydrology, 255(1–4), 107–122.

[4] Ciampittiello, M., Marchetto, A., & Boggero, A. (2024). Water resources management under climate change: a review. Sustainability, 16(9), 3590.

[5] Çeliker, M., Yükseler, U., & Dursun, Ö. F. (2021). Trend analyses for discharge-recharge of Tacin karstic spring (Kayseri, Turkey). Journal of African Earth Sciences, 184, 104344.

[6] Dao, P. U., Heuzard, A. G., Le, T. X. H., Zhao, J., Yin, R., Shang, C., & Fan, C. (2024). The impacts of climate change on groundwater quality: A review. Science of the Total Environment, 912, 169241.

[7] Dursun, Ö. F., Yükseler, U., & Alashan, S. (2021). Yağışların Mevsimsel Değişimlerinin Eğilim Analiz Yöntemleri İle Araştırılması: Bingöl İli Örneği. El-Cezeri, 8(1), 45-59.

[8] Elgendy, M., Hassini, S., & Coulibaly, P. (2024). Review of climate change adaptation strategies in water management. Journal of Hydrologic Engineering, 29(1), 03123001.

[9] Elkhoury, J. E., Brodsky, E. E., & Agnew, D. C. (2006). Seismic waves increase permeability. Nature, 441(7097), 1135-1138.

[10] Gosling, S. N., & Arnell, N. W. (2016). A global assessment of the impact of climate change on water scarcity. Climatic Change, 134(3), 371-385.

[11] Gudmundsson, L., Boulange, J., Do, H. X., Gosling, S. N., Grillakis, M. G., Koutroulis, A. G., ... & Zhao, F. (2021). Globally observed trends in mean and extreme river flow attributed to climate change. Science, 371(6534), 1159-1162.

[12] Hamed, K. H., & Rao, A. R. (1998). A modified Mann–Kendall trend test for autocorrelated data. Journal of Hydrology, 204(1–4), 182–196.

[13] Kendall, M. G. (1975). Rank Correlation Methods. Griffin, London.

[14] Kisi, O., & Ay, M. (2014). Comparison of Mann–Kendall and innovative trend method for water quality parameters of the Kizilirmak River, Turkey. Journal of Hydrology, 513, 362–375.

[15] Manga, M., Beresnev, I., Brodsky, E. E., Elkhoury, J. E., Elsworth, D., Ingebritsen, S. E., ... & Wang, C. Y. (2012). Changes in permeability caused by transient stresses: Field observations, experiments, and mechanisms. Reviews of Geophysics, 50(2).

[16] Mann, H. B. (1945). Nonparametric tests against trend. Econometrica, 13(3), 245–259.

[17] Nasonova, O. N., Gusev, Y. M., Kovalev, E. E., & Ayzel, G. V. (2018). Climate change impact on streamflow in large-scale river basins: projections and their uncertainties sourced from GCMs and RCP scenarios. Proceedings of the International Association of Hydrological Sciences, 379, 139-144.

[18] Özdemir, A., Volk, M., Strauch, M., & Witing, F. (2024). The Effects of Climate Change on Streamflow, Nitrogen Loads, and Crop Yields in the Gordes Dam Basin, Turkey. Water, 16(10), 1371.

[19] Secci, D., Tanda, M. G., D'Oria, M., Todaro, V., & Fagandini, C. (2021). Impacts of climate change on groundwater droughts by means of standardized indices and regional climate models. Journal of Hydrology, 603, 127154.

[20] Sönmez, A. Y., & Kale, S. (2020). Climate change effects on annual streamflow of Filyos River (Turkey). Journal of Water and Climate Change, 11(2), 420-433.

[21] Spearman, C. (1904). The proof and measurement of association between two things. The American Journal of Psychology, 15(1), 72–101.

[22] Şen, Z. (2012). Innovative trend analysis methodology. Journal of Hydrologic Engineering, 17(9), 1042–1046.

[23] Şen, Z. (2017). Trend identification simulation and application. Journal of Hydrologic Engineering, 22(5), 04017009.

[24] Yue, S., & Wang, C. Y. (2004). The Mann–Kendall test modified by effective sample size to detect trend in serially correlated hydrological series. Water Resources Management, 18(3), 201–218.

[25] Yue, S., Pilon, P., & Cavadias, G. (2002). Power of the Mann–Kendall and Spearman's Rho tests for detecting monotonic trends in hydrological series. Journal of Hydrology, 259(1–4), 254–271.

[26] Zhang, Q., Xu, C. Y., & Becker, S. (2019). Trends and abrupt changes of precipitation extremes in China during 1960–2010. Hydrological Sciences Journal, 64(3), 257–273.

[27] Zhu, L., Gong, H., Dai, Z., Xu, T., & Su, X. (2015). An integrated assessment of the impact of precipitation and groundwater on vegetation growth in arid and semiarid areas. Environmental earth sciences, 74(6), 5009-5021.

[28] Zillman, J. W. (2001). The IPCC third assessment report on the scientific basis of climate change. Australian Journal of Environmental Management, 8(3), 169-185.

ICENS 11TH INTERNATIONAL CONFERENCE ON ENGINEERING AND NATURAL SCIENCE October 22-26 2025 Sarajevo

Hybrid Model Integrating Data-Driven and Semi-Analytical Approaches: Optimizing Water Control Completion in Bottom-Water Reservoirs with Unconventional Wells

Zhenduo Yue [1], Guoqing Han [1], Jin Shu [1], Yabo Li [1], Wenbo Jiang [1], Xin Wang [1], Junjian Li [1]*

Abstract

This paper presents a hybrid modeling framework that integrates semi-analytical and data-driven approaches to optimize water control completion in bottom-water reservoirs with unconventional wells. The model divides the reservoir vertically into upper and lower sections. The upper section is characterized by a semi-analytical model that accurately describes the pressure distribution along complex well trajectories, while the lower section employs a data-driven neural differential equation model to simulate dynamic changes in pressure and saturation driven by bottom-water movement. Through a coupling strategy, the two models exchange boundary conditions to achieve consistent and efficient simulation of the overall reservoir system. Comparative analysis with commercial numerical simulators demonstrates that the hybrid model maintains high prediction accuracy for both pressure and saturation, with relative errors below 3%, while achieving a computational speed improvement of two to three orders of magnitude. The model is further applied to optimize water control completion configurations, including inflow control valve (ICV) settings and well trajectories, showing its capability to enhance oil production while reducing water cut. This study provides an efficient, accurate, and scalable computational framework for the development and optimization of unconventional wells in bottom-water reservoirs, offering a novel tool for intelligent water control completion design.

Keywords: Bottom-water reservoir; Unconventional well; Semi-analytical model; Data-driven model; Water control completion

1. INTRODUCTION

Bottom-water reservoirs are widely distributed in China and around the world, representing one of the most important types of remaining oil resources[1]. However, during the development of such reservoirs, a strong pressure difference often exists between the oil layer and the underlying aquifer[2]. As production continues, bottom water tends to rise along the lower part of the wellbore, forming a “water cone” or “water tongue.” Once the water breaks through into the wellbore, the water cut increases rapidly, while oil production declines sharply, severely affecting recovery efficiency and economic performance[3]. For unconventional wells—such as horizontal or multilateral wells—the challenges are even greater, as the extended well trajectory and complex completion structure lead to non-uniform flow distributions, making the bottom-water coning behavior more complicated and water control more difficult[4]. Therefore, achieving effective water-control completion design and optimization in bottom-water reservoirs has become a critical direction in current reservoir development research.

Traditional numerical reservoir simulation methods, such as finite difference or finite element approaches, can accurately describe two-phase flow behavior and pressure distribution, serving as fundamental tools in reservoir engineering studies[5]. However, these methods often suffer from high computational cost and long simulation time, particularly in heterogeneous reservoirs with complex geometries[6]. Moreover, to accurately capture near-wellbore flow characteristics, fine grid discretization is required, which further increases the computational burden and limits the applicability of these models in real-time optimization or multi-scenario sensitivity analysis[7].

[1] China University of Petroleum (Beijing), Beijing, China, yuezd1999@163.com

[*] Corresponding author: China University of Petroleum (Beijing), Department of Petroleum Engineering, 102200, Beijing, China. cup_706ac@163.com

In contrast, semi-analytical models approximate the solution of flow equations through analytical expressions, maintaining physical rationality while significantly improving computational efficiency[8]. Such models are well-suited for analyzing wellbore–formation coupling and estimating horizontal well productivity, providing a rapid means of parameter evaluation and screening. Nevertheless, semi-analytical approaches typically rely on idealized assumptions—such as homogeneous formations, single-phase flow, or steady-state conditions—which limit their applicability under complex, heterogeneous, multiphase, and strongly coupled bottom-water reservoir systems. As a result, they often struggle to accurately capture the transient and nonlinear characteristics of water coning dynamics[9].

In recent years, with the rapid advancement of machine learning and deep learning technologies, data-driven models have emerged as a promising direction in reservoir simulation and production forecasting[10]. Neural network–based models can learn nonlinear mappings between inputs and outputs directly from historical production data or numerical simulation results, enabling fast predictions without explicitly solving physical equations[11]. These methods demonstrate strong potential for accelerating reservoir simulation, enhancing history matching, and supporting optimization-based decision-making[12].

To address the aforementioned challenges and demands, this study proposes a hybrid model that integrates semi-analytical and data-driven approaches for optimizing water-control completion in unconventional wells within bottom-water reservoirs. The reservoir is vertically divided into two regions: the upper zone employs a semi-analytical model to accurately calculate pressure distribution and bottom-hole pressure variations around the wellbore, while the lower zone adopts a Neural Ordinary Differential Equation (Neural ODE)–based data-driven model that takes the upper-zone pressure as a boundary condition to dynamically predict the evolution of pressure and water saturation in the bottom-water region. Through this coupled framework, the hybrid model leverages the physical interpretability and geometric precision of semi-analytical methods together with the nonlinear learning and dynamic modeling capabilities of data-driven approaches.

This hybrid model can efficiently and accurately simulate the dynamic process of bottom-water coning, achieving several orders of magnitude acceleration compared to traditional numerical simulation methods. Moreover, it provides detailed characterization of complex well trajectories and completion structures (such as inflow control devices, ICDs/ICVs) without the need for excessive grid refinement, thereby reducing computational costs and enabling rapid evaluation of completion schemes. By utilizing this framework, multiple water-control completion strategies can be simulated and optimized within a short time, offering a powerful tool for real-time decision-making and efficient development of bottom-water reservoirs.

2. METHODOLOGY

2.1. Framework of the Hybrid Model

To address the challenges of multi-scale, strongly nonlinear, and heterogeneous coupling in the water-control optimization of unconventional wells in bottom-water reservoirs, this study proposes a Hybrid Model Framework that integrates a semi-analytical model with a data-driven model. This framework establishes a coordinated modeling system between the physical and data domains, enabling efficient and interpretable modeling of complex wellbore–reservoir systems.

As illustrated in Figure 1, the entire reservoir system is vertically divided into two functional zones:

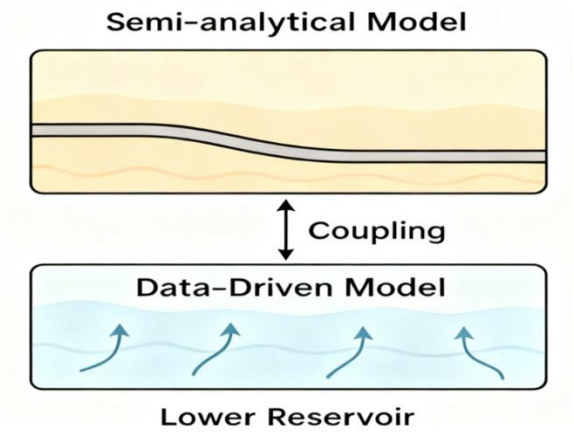

Figure 3. A sample line graph using colors which contrast well both on screen and on a black-and-white hardcopy

Upper Zone (Oil Layer): Centered on the wellbore, the Semi-analytical Model is employed to describe the flow dynamics. Based on Darcy's law, the model derives the bottom-hole pressure distribution through wellbore–formation coupling boundary conditions, while incorporating geometric characteristics such as well trajectory, completion interval length, and permeability anisotropy. This approach allows efficient calculation of pressure variations near the wellbore. The model provides clear physical constraints and strong numerical stability, serving as an accurate boundary condition provider for the lower-zone model.

Lower Zone (Bottom-water Region): A Data-driven Model based on the Neural Ordinary Differential Equation (Neural ODE) is used to simulate the dynamic behavior of the bottom-water region. Taking the lower-boundary pressure distribution from the upper-zone model as input, the Neural ODE dynamically learns the temporal evolution of pressure and water saturation, capturing complex unsteady flow behaviors. By modeling the system in a continuous-time domain, the Neural ODE overcomes the limitations of traditional discrete neural networks in representing dynamic evolution processes.

Figure 2 illustrates the computational workflow of the model: the hybrid framework first employs the semi-analytical model to rapidly compute the pressure distribution in the upper zone and the variation of bottom-hole pressure, which is then passed to the lower-zone model as a boundary condition. The Neural ODE model subsequently predicts the spatiotemporal evolution of pressure and water saturation in the bottom-water region based on this boundary input. Finally, the predicted upper-boundary pressure from the lower model is fed back into the semi-analytical model, achieving dynamic coupling between the two subsystems. This iterative process continues until the system reaches convergence or a specified time step is met, thereby completing the coupling and computation cycle of the hybrid model.

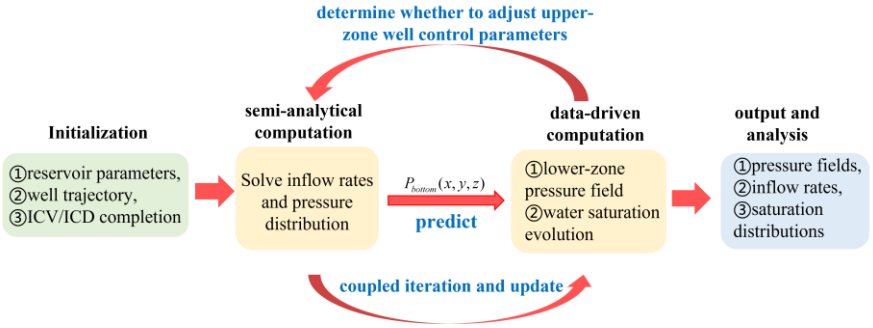

Figure 4. Flowchart of the Hybrid Model Computation Process

2.2. Semi-Analytical Model for the Upper Zone

The upper reservoir represents the main production section controlled by the horizontal well, primarily responsible for oil inflow and wellbore pressure transmission. To accurately characterize the influence of the horizontal well trajectory and completion configuration on productivity while balancing computational efficiency and physical accuracy, this study establishes an integrated semi-analytical model that couples the upper reservoir, completion, and wellbore systems.

The semi-analytical approach serves as a bridge between analytical solutions and numerical discretization, expressing the pressure and flow relationships between the wellbore and the reservoir in an integral or superposition form that can be solved efficiently. This method retains the physical interpretability of the flow mechanism while maintaining high computational efficiency. Compared with fully numerical simulations, the semi-analytical model offers spatial flexibility in describing complex well trajectories (such as horizontal or multilateral wells) and completion structures (such as ICD/ICV segments), making it particularly suitable for fine-scale flow characterization of the wellbore–completion–reservoir system in the upper zone.

The essence of ICD/ICV regulation lies in controlling the inflow rate by adjusting the orifice area. When the fluid passes through the restriction, an additional pressure drop is generated to balance the energy difference between the reservoir and the wellbore. This process can occur in either critical or subcritical flow regimes. For liquid-phase flow, it typically exhibits subcritical characteristics, where the downstream pressure still affects the upstream flow rate.

The pressure drop across the ICD/ICV can be expressed as:

$$\Delta P_{cons} = C_u \frac{\rho q_l^2}{2A_c^2 C_v^2} \quad (1)$$

where C_u is the unit conversion constant, ρ is the mixed-fluid density (kg/m³), A_c is the total orifice cross-sectional area (m²), C_v is the dimensionless valve flow coefficient, and q_l is the fluid flow rate (m³/s).

It can be seen that the pressure drop is governed by both the valve opening and the flow rate—larger flow rates lead to greater pressure drops, while wider valve openings result in smaller pressure losses. Consequently, the pressure drop induced by the ICV introduces a localized energy constraint between the reservoir and wellbore, significantly influencing the inflow distribution across completion segments. To comprehensively characterize the pressure transmission and fluid exchange among the reservoir, wellbore, and completion system, it is necessary to formulate a coupled system of equations under the semi-analytical framework, incorporating both mass conservation and potential difference constraints, enabling the integrated solution of the multi-segment completion system.

- Mass Conservation Equation

$$\sum_{i=1}^{i=n}\sum_{j=1}^{j=m_i+n_i+1} Q_{Di_j} = Q_{Dall} \quad (2)$$

- Potential Difference Equation

$$\varphi_{Dai_{s_js}} = \frac{\varphi_i - \varphi_{ai_{s_js}}}{\varphi_i} = \sum_i^n \sum_j^{m_i+n_i+1} Q_{Di_j}\varphi_{Dai_j}[M(i,j)] \quad (3)$$

- Annular Flow Equation

$$\varphi_{aDi_{s_js}} = \varphi_{aD1_1} - \frac{1}{\varphi_i}\left[\sum_{i=1}^{i_s}\sum_{j=1}^{j_s-i_s} \triangle p_{ai_j} - (i_s-1)\sum_{j=1}^{m_i+n_i+1} \triangle p_{i_j} - \triangle P_{cons_i} + \triangle p_{s_{i+1}}\right] \quad (4)$$

In summary, the model consists of N potential difference equations, N wellbore flow equations, and one overall mass conservation equation. The number of equations equals the number of unknowns, ensuring the system is solvable and the solution is unique.

Through this modeling procedure, the semi-analytical approach efficiently determines the pressure distribution and inflow rate of each completion segment, achieving an integrated flow analysis of the reservoir–completion–wellbore system. This model not only accurately reflects the inflow equalization effects of ICD/ICV control but also provides upper-boundary pressure constraints and boundary conditions for the subsequent data-driven bottom-water model.

2.3. Data-Driven Model for the Lower Zone

In the composite model, the lower reservoir is primarily governed by bottom-water coning and the dynamic evolution of the oil–water interface. The flow behavior in this region exhibits strong nonlinearity, unsteadiness, and highly coupled multiphase flow characteristics. Traditional analytical or semi-analytical methods often struggle to accurately capture these complex dynamic processes. Therefore, this study introduces a Neural Ordinary Differential Equation (Neural ODE)-based dynamic prediction model to simulate the evolution of pressure and water saturation in the lower region.

To ensure the model's physical reliability and data sufficiency, high-fidelity reservoir simulations were first conducted to generate time-series data of pressure and saturation fields under various well-control and reservoir parameter conditions. These simulation datasets capture typical flow features during bottom-water breakthrough—such as water cone formation, oil–water interface deformation, and bottomhole pressure response—providing abundant training samples and physical references for the Neural ODE model.

The Neural ODE framework incorporates a learnable differential operator in continuous time, enabling the network to describe the temporal evolution of the system's states in a continuous form. Unlike traditional time-series neural networks (e.g., RNNs or LSTMs), Neural ODEs do not discretize time explicitly; instead, they represent the system's dynamic process as a parameterized ordinary differential equation (ODE):

$$\frac{d\boldsymbol{y}(t)}{dt} = f_\theta(\boldsymbol{y}(t), t) \quad (5)$$

where $\boldsymbol{y}(t)$ denotes the state vector at time t (including pressure and water saturation), and f_θ is a nonlinear dynamic function parameterized by neural network weights θ. By solving this ODE using numerical integrators (e.g., Runge–Kutta or Adams methods), the model produces a continuous-time evolution of the reservoir state.

In this study, the Neural ODE model receives the bottom pressure distribution $P_{bottom}(x, y, z)$ output from the upper semi-analytical model as a time-dependent boundary condition, while historical simulation data serve as supervision during training. The training objective is defined as:

$$\mathcal{L} = \frac{1}{N}\sum_{N}^{i=1}\left(\left\|P_{pred}^{(i)} - P_{sim}^{(i)}\right\|^2 + \lambda\left\|S_{w,pred}^{(i)} - S_{w,sim}^{(i)}\right\|^2\right) \quad (6)$$

where P_{pred} and $S_{w,pred}$ are the predicted pressure and water saturation, P_{sim} and $S_{w,sim}$ are their corresponding reference results from numerical simulation, and λ are weighting coefficients. Minimizing this loss ensures that the model simultaneously learns the dynamic consistency of pressure and saturation, while capturing the underlying physical mechanisms of bottom-water coning.

3. RESULTS AND DISCUSSION

3.1. Dynamic Water Coning Simulation

The composite model effectively captures the dynamic characteristics of bottom-water coning in unconventional wells within bottom-water reservoirs. According to the model predictions, the upper semi-analytical model provides the pressure distribution around the wellbore and the corresponding bottom boundary pressure, while the lower data-driven model uses this pressure boundary condition to continuously predict the temporal evolution of the pressure field and water saturation in the bottom-water region.

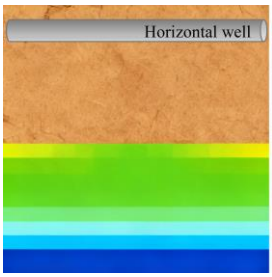

Figure 5. (a) Initial stage with no bottom-water coning in the reservoir

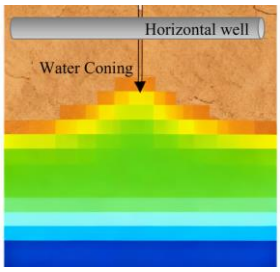

(b) Onset of bottom-water coning in the reservoir

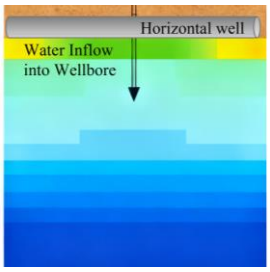

(c) Water breakthrough into the wellbore

For intuitive understanding, Figure 3 presents the water saturation distribution in the reservoir at different times, illustrating three typical stages of bottom-water coning. Figure 3 (a) shows the initial stage with no coning; Figure 3 (b) depicts the onset of coning, where the water cone gradually develops upward; Figure 3 (c) shows water entering the wellbore, leading to increased water production at the wellhead. Figure 3 clearly captures the dynamic evolution of the water cone from formation to wellbore breakthrough, consistent with the actual bottom-water rise observed in reservoirs, demonstrating that the hybrid model effectively reproduces key physical features of bottom-water dynamics.

Moreover, the model's response to different well control conditions, such as ICV/ICD settings, is evident. Lower valve openings can limit water inflow in the early stage, slowing the upward development of the water cone, while higher openings accelerate its growth. The simulation results indicate that the hybrid model not only captures the formation and evolution of the water cone but also provides valuable parameter guidance for water-control completion design.

Overall, the bottom-water rise simulations highlight the potential of the hybrid model in analyzing water coning in unconventional wells: it accurately depicts the dynamic behavior of the water cone and finely resolves the pressure and saturation distribution along the wellbore, providing a reliable numerical basis for subsequent water-control completion optimization.

3.2. Verification of the Hybrid Model

To validate the accuracy and computational efficiency of the hybrid model for unconventional wells in bottom-water reservoirs, its predictions were compared with those from a commercial reservoir simulator (reference model). The primary validation metrics include reservoir pressure error, saturation error, computation time, and speed-up factor. These metrics collectively reflect the hybrid model's performance in terms of physical fidelity and computational efficiency.

Table 2. Comparison between the hybrid model and commercial simulator

Metric	Average Time per Case	Hybrid Model	Relative Error
Average Pressure Error (MPa)	—	—	< 3%
Average Water Saturation Error (%)	—	—	< 3%
Computation Time (hours)	12	0.01	~10^3× faster
Grid Size	100 × 100 × 10	100 × 100 × 10	—

Table 1 presents validation results for a representative horizontal well at several production time points. The hybrid model shows strong agreement with the reference numerical simulator in both pressure and water-saturation predictions, with errors typically below 3%. At the same time, the hybrid model substantially outperforms the commercial simulator in computation time, achieving speed-ups of several orders of magnitude while maintaining comparable accuracy.

The table clearly illustrates that the hybrid model attains a significant improvement in computational efficiency without sacrificing the physical prediction accuracy of the commercial simulator. This indicates that the hybrid approach balances accuracy and speed, making it suitable for predicting pressure and saturation near complex wellbores and for rapid multi-scenario screening and optimization. The validation results further demonstrate that the hybrid model not only accurately captures the dynamics of water-cone development, but also, owing to its fast execution, can support feasibility studies and comparative optimization of alternative completion schemes—thereby providing practical decision support for field development.

3.3. Application in Water-Control Completion Optimization

An important application of the hybrid model lies in supporting water-control completion optimization for unconventional wells in bottom-water reservoirs. By adjusting well control parameters—such as ICV/ICD opening degrees and completion

segment configurations—the model can predict variations in bottom-water rise rate, oil production, and water cut under different control schemes, thereby providing quantitative guidance for optimization design.

During simulation, the model first calculates the bottomhole pressure distribution and inflow profile under different ICV/ICD settings. This information is then fed into the data-driven lower model, which predicts the evolution of pressure and water saturation in the bottom-water zone. Based on the model's predictions, the influence of various completion strategies on water-cone formation and water breakthrough time can be quantitatively evaluated. For instance, appropriately adjusting the ICV/ICD openings can effectively restrict bottom-water influx during the early production stage, delay water-cone development, prolong the high-production period, and reduce water cut.

To intuitively demonstrate the hybrid model's effectiveness in water-control optimization, Table 2 compares oil production, water production, and average water cut under three representative ICV/ICD opening configurations. The results show that optimizing valve openings can significantly reduce water cut at the wellhead while maintaining or even enhancing oil production, providing actionable guidance for completion design.

Table 3. Comparison between the hybrid model and commercial simulator

Control Scheme	Oil Production at Wellhead *Qo* (m^3/d)	Water Production at Wellhead *Qw* (m^3/d)	Average Water Cut *WC* (%)
Scheme A (Low Opening)	115	10	8.0
Scheme B (Medium Opening)	118	12	9.2
Scheme C (High Opening)	120	15	11.1

From the table, it can be observed that a low-opening configuration effectively delays water-cone rise and slows the increase in water cut, though it results in slightly lower oil production; a high-opening configuration achieves higher oil output but leads to faster water-cone formation and earlier water breakthrough; and a medium-opening configuration offers a balanced performance between oil recovery and water control. Such quantitative analysis provides a scientific basis for selecting well-control parameters and optimizing completion schemes, highlighting the hybrid model's strong potential for complex water-control optimization in bottom-water reservoirs.

Overall, the hybrid model not only captures the dynamic evolution of bottom-water rise with high precision but also enables rapid evaluation of various control strategies, offering valuable guidance and decision support for water-control completion design. By applying this model during the design phase, well-control parameters can be pre-optimized to minimize field trial-and-error costs, enhance development efficiency and recovery, and provide a powerful computational tool for managing unconventional wells in bottom-water reservoirs.

CONCLUSION AND OUTLOOK

This study proposes a hybrid model that integrates a semi-analytical method with a data-driven approach for optimizing water-control completions in unconventional wells within bottom-water reservoirs. The model divides the reservoir vertically into two coupled regions: the upper region, represented by a semi-analytical model that accurately characterizes the pressure distribution around the wellbore; and the lower region, modeled using a Neural Ordinary Differential Equation (Neural ODE) framework that dynamically predicts the evolution of pressure and water saturation in the bottom-water zone. Through this coupled structure, the hybrid model enables efficient and physically consistent simulation of complex water-control systems.

Based on dynamic simulations of bottom-water rise, validation against commercial reservoir simulators, and optimization analysis under different control schemes, the main findings are as follows:

- The hybrid model accurately captures the formation and development of the water cone, with pressure and saturation errors remaining within acceptable limits, ensuring strong physical consistency;
- The model demonstrates significant computational advantages over conventional numerical simulators, achieving several orders of magnitude acceleration, thus providing a reliable tool for rapid multi-scenario evaluation and optimization;
- The model effectively evaluates the influence of various ICV/ICD control configurations on oil production, water production, and water cut, offering a quantitative basis for water-control completion design and optimization.

In future work, the model's applicability and functionality can be further extended. This includes incorporating more complex well trajectories and multilateral well geometries to evaluate the model's generalization capability under heterogeneous reservoir conditions; coupling the hybrid model with proxy models or optimization algorithms to achieve automated optimization of water-control completion designs and improve decision-making efficiency; and introducing additional physical constraints, such as reservoir heterogeneity, fluid phase behavior, and thermal effects, to enhance the model's accuracy and reliability in real-field applications.

ACKNOWLEDGMENT

We would like to acknowledge the financial support from the National Natural Science Foundation of China (Project No. 52374055) titled "Fine Numerical Simulation and Optimal Design Method for Water Completion and Multi-Coupling in Horizontal Wells".

REFERENCES

[1] T. Aulie, E. Grødal, H. Asheim, and P. Oudeman, "Experimental Investigation of Cresting and Critical Flow Rate of Horizontal Wells," *SPE Adv. Technol. Ser.*, vol. 3, no. 01, pp. 207–215, Mar. 1995, doi: 10.2118/26639-PA.

[2] W. Wibowo, P. Permadi, P. Mardisewojo, and P. Sukarno, "Behavior of Water Cresting and Production Performance of Horizontal Well in Bottom Water Drive Reservoir: A Scaled Model Study," presented at the SPE Asia Pacific Conference on Integrated Modelling for Asset Management, OnePetro, Mar. 2004. doi: 10.2118/87046-MS.

[3] S. Kalam, S. A. Alnuaim, and M. H. Rammay, "Application of Artificial Intelligence for Water Coning Problem in Hydraulically Fractured Tight Oil Reservoirs," presented at the Offshore Technology Conference Asia, OnePetro, Mar. 2016. doi: 10.4043/26450-MS.

[4] R. F. Yakupov, A. A. Gimazov, V. Sh. Mukhametshin, and R. I. Makaev, "Analytical method for estimating efficiency of oil recovery technology in case of bottom water-drive reservoir, verified on the hydrodynamic model (Russian)," *Neft. Khozyaystvo - Oil Ind.*, vol. 2018, no. 06, pp. 66–69, Jun. 2018, doi: 10.24887/0028-2448-2018-6-66-69.

[5] O. A. Pedrosa Jr. and K. Aziz, "Use of a Hybrid Grid in Reservoir Simulation," *SPE Reserv. Eng.*, vol. 1, no. 06, pp. 611–621, Nov. 1986, doi: 10.2118/13507-PA.

[6] Y. Ding and P. Lemonnier, "Use of Corner Point Geometry in Reservoir Simulation," presented at the International Meeting on Petroleum Engineering, OnePetro, Nov. 1995. doi: 10.2118/29933-MS.

[7] J. Guo, F. Zeng, J. Zhao, and Y. Xu, "A New Model to Predict Fractured Horizontal Well Production," presented at the Canadian International Petroleum Conference, OnePetro, Jun. 2006. doi: 10.2118/2006-076.

[8] S. Wang, Y. Bai, B. Xu, L. Chen, W. Li, and Y. Li, "A Semianalytical Model for Simulating Fluid Flow in Tight Sandstone Reservoirs with a Bottom Aquifer," *Geofluids*, vol. 2021, no. 1, p. 5549411, 2021, doi: 10.1155/2021/5549411.

[9] R. A. Novy, "Pressure Drops in Horizontal Wells: When Can They Be Ignored?," *SPE Reserv. Eng.*, vol. 10, no. 01, pp. 29–35, Feb. 1995, doi: 10.2118/24941-PA.

[10] S. Srinivasan *et al.*, "A machine learning framework for rapid forecasting and history matching in unconventional reservoirs," *Sci. Rep.*, vol. 11, no. 1, p. 21730, Nov. 2021, doi: 10.1038/s41598-021-01023-w.

[11] W. A. Khan, Z. Rui, T. Hu, Y. Liu, F. Zhang, and Y. Zhao, "Application of Machine Learning and Optimization of Oil Recovery Sequestration in the Tight Oil RaensderCvOoir2," *SPE J.*, 2024, doi: 10.2118/219731-PA.

[12] E. Illarionov *et al.*, "End-to-end neural network approach to 3D reservoir simulation and adaptation," *J. Pet. Sci. Eng.*, vol. 208, p. 109332, Jan. 2022, doi: 10.1016/j.petrol.2021.109332.

ICENS 11TH INTERNATIONAL CONFERENCE ON ENGINEERING AND NATURAL SCIENCE October 22-26 2025 Sarajevo

The evaluation of the strengthening methods on the seismic performance of a masonry building with insufficient seismic performance

Barış GÜNEŞ[1], Muhammed AKGÜL[1], Ümit HAFO[1], Barış SAYIN[1]*

Abstract

Globally, particularly in regions with high earthquake risk, determining the seismic performance of existing structures is critical for reducing structural damage in potential earthquakes and retrofitting buildings that fail to meet performance criteria. This study examined the seismic performance of an existing public masonry building in Istanbul based on the Turkish Building Code 2018 (TBEC-2018) and the Guide for Earthquake Risk Management in Historic Buildings (ERMGHB-2017). The structure features a load-bearing system comprising mainly masonry walls supported by reinforced concrete beams and slabs, along with a foundation system constructed from stone elements. The structure was approximately modelled in a three-dimensional finite element model in a computer environment, and linear analyses were performed using the response spectrum analysis method, considering the effects of different modes. The analyses were performed considering the "Performance-Based Design" approach, targeting a "Controlled Damage" performance level for the current DD-2 earthquake level (earth movement with a 10% probability of exceedance in 50 years and a recurrence period of 475 years). The findings revealed that the structure failed to meet the target performance criteria at both the superstructure and foundation levels, indicating that retrofitting was necessary. As part of the retrofitting, reinforced concrete walls and steel beams were added to the structure to increase its load-bearing capacity. The masonry walls were retrofitted with TRM (Textile Reinforced Mortar) and sprayed concrete applications, and the existing foundation was converted to a raft foundation. The structure was re-modelled based on the static retrofitting project and re-evaluated using the same analysis method. It was determined that the retrofitted structure meets the performance target. The study is expected to contribute to the literature by providing guidance for performance-based analyses of masonry structures and assisting in the selection of retrofitting methods.

Keywords: Seismic Performance Assessment, Masonry Structures, Response Spectrum Analysis, Retrofitting Strategies.

1. INTRODUCTION

Masonry walls have played a crucial role as load-bearing or infill components in many structures, from the past to the present. However, their nonlinear behavior under seismic loading is highly complex, making it challenging to predict cracking, separation, and collapse mechanisms. In recent years, experimental and numerical studies have highlighted the significant influence of masonry walls on the overall seismic response of buildings, demonstrating that their performance can be improved through appropriate strengthening techniques.

Recent studies have extensively focused on the seismic behavior and retrofitting of masonry structures through both experimental and analytical approaches. Reference [1] examined an existing masonry school building using the Operational Modal Analysis (OMA) method and observed that the applied strengthening interventions effectively increased the dominant frequency of the structure. Similarly, [2] assessed a historical building damaged during the 2016 El Centro earthquake through response spectrum analysis and reported significant improvements in seismic performance following retrofitting applications. In another experimental investigation, [3] tested unreinforced masonry walls strengthened with Textile Reinforced Mortar (TRM), Glass Fiber Reinforced Polymer (GFRP), and Fiber Reinforced Cementitious Composites (FRCC) under cyclic lateral loading. The results confirmed that the TRM and FRCC methods notably enhanced both strength and deformation capacity. Reference [4] analyzed unreinforced and confined brick masonry school buildings typical in the Himalayan region using response spectrum analysis and proposed a fragility-based approach for assessing reliable performance. Moreover, [5] introduced a multi-component timber-based strengthening system designed to enhance wall-

[1] Istanbul University-Cerrahpasa, Department of Environmental Engineering, 34320, Avcılar/İstanbul, Turkey. bgunes@iuc.edu.tr

[*] Corresponding author: Istanbul University-Cerrahpasa, Department of Environmental Engineering, 34320, Avcılar/İstanbul, Turkey. barsayin@iuc.edu.tr

diaphragm connections and limit in-plane and out-of-plane deformations of masonry walls, as verified through cloud-based nonlinear time-history analyses.

In this study, the seismic performance of an existing masonry building with inadequate structural capacity was evaluated through numerical analyses following the implementation of strengthening techniques. These analyses were conducted in accordance with the procedures outlined in the Turkish Building Earthquake Code (TBEC-2018) and the Guideline for Earthquake Risk Management in Historical Buildings (ERMGHB-2017) [6], [7].

2. MATERIALS AND METHODS

2.1. The Examining Building

The examined structure consists of a basement floor, a ground floor, and three typical upper stories. The existing foundation system consists of continuous stone masonry footings, while the floor system is composed of reinforced concrete slabs. The vertical load-carrying system primarily comprises masonry walls that resist both gravity and lateral loads. As part of the retrofitting works, reinforced concrete shear walls and steel beams were incorporated into the structural system to enhance its overall load-bearing capacity. The reinforced concrete beams and slabs were strengthened using Carbon Fiber Reinforced Polymer (CFRP) fabrics and plates. Additionally, the masonry walls were retrofitted with Textile Reinforced Mortar (TRM) and shotcrete applications. The foundation system was also upgraded, transforming the existing stone masonry footings into a reinforced concrete raft foundation to improve global stability and uniform load transfer.

2.2. Material Examination

Mechanical properties of masonry walls and reinforced concrete elements are given in Tables 1 and 2, respectively.

Table 1. Mechanical Properties of Masonry Walls.

Description	Existing	Retrofited
Type of Masonry Unit	Solid Brick	Solid Brick
Masonry Unit Group	Group I	Group I
Unit Weight, kN/m3	18	18
Characteristic Compressive Strength of Wall, fk MPa	2.8	5.46
Initial Shear Strength of Wall, fvko MPa	0.1	0.2
Tensile Strength of Wall, ft MPa	0.15	0.29
Modulus of Elasticity of Wall, Ewall MPa	2000	3900
Shear Modulus of Wall, Gwall MPa	400	780

Table 2. Mechanical Properties of Reinforced Concrete Elements.

Element	Reinforcement Grade	Concrete Class
Existing Reinforced Concrete Element	S220	C16/20
Strengthening Shotcrete	B500C	C30/37
Strengthening Reinforced Concrete Foundation and Slab	B420C	C30/37

2.3. Soil and Earthquake Parameters

The soil and earthquake parameters of the structure were determined using the “Turkey Earthquake Hazard Maps Interactive Web Application,” prepared by the Turkish Disaster and Emergency Management Presidency (AFAD), and are presented in Table 3 [8].

Table 3. Soil Class and Earthquake Parameters

Parameter	Value / Class
Local soil class	ZC
Earthquake ground motion level	DD-1, DD-2, DD-3
Spectral acceleration coefficients from the Earthquake Hazard Map (g)	DD-1, Ss = 1.484, S1 = 0.415 DD-2, Ss = 0.847, S1 = 0.238 DD-3, Ss = 0.336, S1 = 0.096
Peak ground acceleration (g)	DD-1, PGA = 0.598 DD-2, PGA = 0.349 DD-3, PGA = 0.146
Local site effect coefficients	DD-1, Fs = 1.200, F1 = 1.500 DD-2, Fs = 1.200, F1 = 1.500 DD-3, Fs = 1.300, F1 = 1.500
Spectral Acceleration Coefficients	DD-1, SDS = 1.781, SD1 = 0.623 DD-2, SDS = 1.016, SD1 = 0.357 DD-3, SDS = 0.437, SD1 = 0.144

2.4. Performance Analysis

A numerical model that reliably reflects the existing condition of the building was developed with great attention to detail using the Midas Gen finite element software [9]. The modeling process was conducted with a high degree of precision, supported by a comprehensive review of the available structural documentation and detailed on-site inspections. In the model, reinforced concrete beams were represented as frame elements, whereas masonry walls, shotcrete layers, and foundation components were simulated using plate or wall elements. The three-dimensional static analysis model of the structure is illustrated in Figure 1.

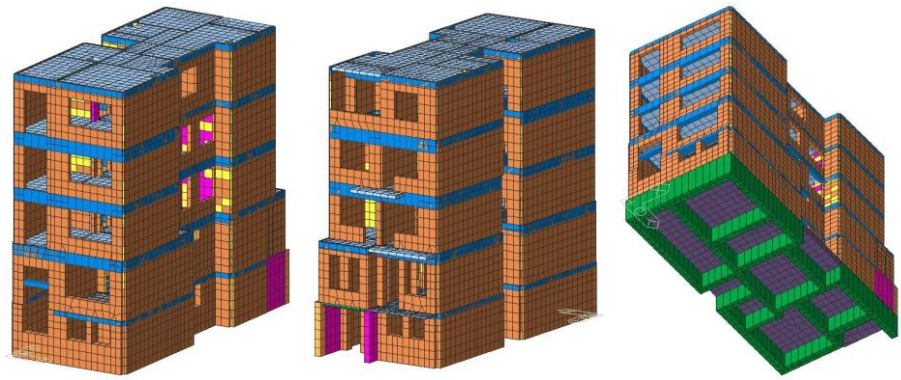

Fig. 1 3D Static Analysis Model of the Buildings

2.5. Performance Assessment Method

The assessment of the building under static and earthquake loads was conducted in accordance with the Turkish Building Earthquake Code (TBEC-2018) [6]. The classification of the structure, target performance levels, required analyses, and design/assessment methods is summarized in Table 4.

Table 4. Performance-Based Analysis and Design Method.

Parameter	Value/Class
Building Use Class, BUC	3
Building Importance Factor, I	1.0
Earthquake Design Class, EDC	1
Building Height Class, BHC	6
Target Structural Performance	Controlled Damage for DD-2
Design/Assessment Method	linear analysis, Strengths-Based Assessment
Response Reduction Factor for Masonry and Reinforced Concrete Assessments	Ra = 3
Structural System Behaviour Factor (R)/ Overstrength Factor (D)	R = 4, D = 2
Building Information Level / Factor	Existing Elements: Limited, 0.75 Retrofitted Elements: Comprehensive, 1.00

2.6. Design Elastic Spectrum

Figure 2 shows the building's response spectrum and spectral acceleration values for the DD-2 earthquake level.

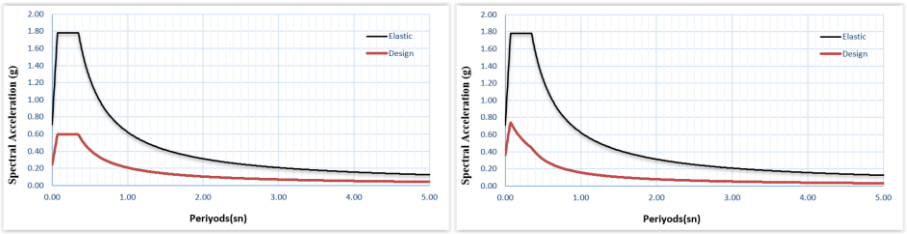

Fig. 2 Response Spectrum and Spectral Acceleration Values for the DD-2 Earthquake Level; Left: Ra=3, D=3; Right: R=4, D=2.

3. RESULTS

3.1. Modal Analysis

The first three mode shapes obtained from the modal analysis are presented in Table 5. As observed, the fundamental mode has a natural vibration period of 0.238 seconds.

Table 5. Results of the modal analysis

Mode	Direction	Period (s)
1	X	0.239
2	Z	0.195
3	Y	0.149

3.2. Statistical Evaluations

The vertical displacements of the structure under dead and live loads, along with the corresponding axial forces, are illustrated in Figures 3 and 4. The compressive stress generated in the masonry infill walls and reinforced concrete members was compared with the allowable stress limits specified for each material type. The results indicated that both the infill walls and the reinforced concrete elements remained within the permissible stress ranges, demonstrating adequate compressive strength under vertical (static) loading conditions.

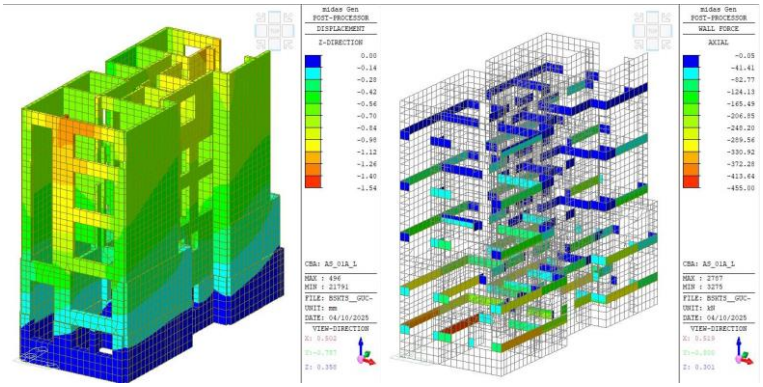

Fig. 3 Displacements Under Vertical Loads and the Axial Forces Generated in the structure.

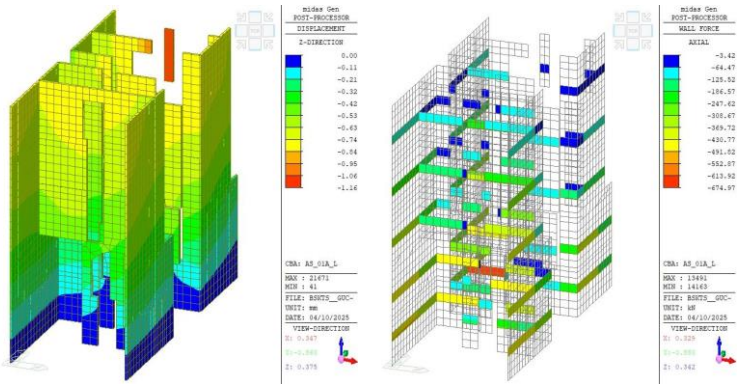

Fig. 4 Displacements Under Vertical Loads and the Axial Forces Generated in the Reinforced Concrete.

3.3. Dynamic Evaluations

Table 6 presents the ratios of total shear forces acting on unqualified masonry and reinforced concrete elements to the story shear forces. Additionally, story drift checks were conducted for the masonry structural system, and Table 7 compares the calculated relative story drifts with the target performance limits.

Table 6. Performance analysis results summary table.

Story	Total Shear of Deficient Vertical Load-Bearing Elements, %			Target Performance Level (CD)
	Masonry	Reinforced Concrete	Total	
basement	4.54	0.00	4.54	√
Ground floor	9.86	0.00	9.86	√
1st floor	4.60	0.00	4.60	√
2nd floor	12.40	0.00	12.40	√
3rd floor	18.36	0.00	18.36	√

Table 7. Verification of Story Drift Ratios.

Story	Displacement, ΔD (mm)		Story Drift Ratio, ΔD/H		Limit Value	Result
	x	y	%	%	%	√ / X
basement	3.52	1.55	0.12	0.05	0.70 (CD)	√
Ground floor	7.11	2.63	0.22	0.08	0.70 (CD)	√
1st floor	8.39	3.01	0.28	0.01	0.70 (CD)	√
2nd floor	7.62	2.93	0.25	0.01	0.70 (CD)	√
3rd floor	6.37	2.65	0.21	0.01	0.70 (CD)	√

3.4. Comparison of Existing and Strengthened Conditions

Table 8 compares the relative story drift ratios for the existing and strengthened conditions of the DD-2 Controlled Damage performance level. The displacements decreased by approximately 45–61% in the X direction and 49–59% in the Y direction. Table 9 presents the shear strength checks for the DD-2 Controlled Damage performance target, showing that the proposed strengthening method in the static retrofit project significantly improved the structural capacity. The proposed retrofit method provided a notable improvement in displacement performance.

Table 8. Comparison of Displacement Values for Vertical Structural Elements Before and After Strengthening

DD2 (CD)	Displacement, ΔD (mm)				Increase Ratio (%)	
	Existing Condition		Strengthened Condition			
	X	Y	X	Y	X	Y
basement	7.72	3.06	3.52	1.55	54.40	49.35
Ground floor	18.34	5.48	7.11	2.63	61.23	52.01
1st floor	18.98	7.49	8.39	3.01	55.80	59.81
2nd floor	15.86	7.02	7.62	2.93	51.95	58.26
3rd floor	11.74	5.90	6.37	2.65	45.74	55.08

Table 9. Comparison of Shear Capacity of Vertical Structural Elements Before and After Strengthening

DD2 (CD)	Total Shear Capacity of Vertical Load-Bearing Elements (%)		Increase Ratio (%)
	Existing Condition	Strengthened Condition	
basement	6.07	95.46	>%100
Ground floor	10.27	90.14	>%100
1st floor	3.36	95.40	>%100
2nd floor	8.78	87.60	>%100
3rd floor	13.12	81.64	>%100

4. CONCLUSION

The structure was modeled to represent the strengthened condition as accurately as possible, based on laboratory test results, geotechnical investigations, the structural retrofitting project prepared by the authors, and detailed on-site observations. Subsequently, performance analyses were carried out in accordance with the criteria specified in the Turkish Building Earthquake Code (TBEC, 2018) and the Guideline for the Seismic Risk Management of Historical Structures (ERMGHB, 2017) [6], [7]. The findings obtained from these analyses form the basis for evaluating the structural behavior and overall seismic performance of the retrofitted building.

- Under vertical loads, the axial forces developed in the masonry vertical load-bearing elements were found to be below their axial load capacities
- Under the combined effects of vertical and seismic loads, the ratio of the total shear force acting on the masonry elements exceeding their shear capacity to the story shear force was below the allowable limit.
- The interstory drift ratio requirements were satisfied under the combined vertical and seismic loading conditions.
- Under vertical loads, the axial forces developed in the reinforced concrete vertical load-bearing elements were found to be below their axial load capacities.
- The foundation demonstrates adequate bearing capacity performance under both vertical loads and the combined effects of vertical and seismic loads.
- The analysis results show that the structure meets the ‘Controlled Damage’ performance target at the DD-2 earthquake level.

REFERENCES

[1] M. Namlı and F. Aras, “Performance evaluation of a seismic strengthening applied on a masonry school building by dynamic analyses,” *Structures*, vol. 62, p. 106200, Apr. 2024.

[2] M. Zucca, E. Reccia, N. Longarini, and A. Cazzani, “Seismic assessment and retrofitting of a historical masonry building damaged during the 2016 Centro Italia seismic event,” *Applied Sciences*, vol. 12, no. 22, p. 11789, 2022.

[3] S. H. Kim, S. H. Park, H. H. Pham, S. J. Lee, N. H. Dinh, and K. K. Choi, “Seismic performance of unreinforced masonry walls with various retrofitting methods,” *International Journal of Architectural Heritage*, vol. 19, no. 9, pp. 1714–1736, 2025.

[4] R. K. Adhikari, A. Parammal Vatteri, and D. D’Ayala, “Seismic performance assessment of low-rise unreinforced and confined brick masonry school buildings using the applied element method,” *Buildings*, vol. 13, no. 1, p. 159, 2023.

[5] N. Damiani, M. Miglietta, G. Guerrini, and F. Graziotti, “Numerical assessment of the seismic performance of a timber retrofit solution for unreinforced masonry buildings,” *International Journal of Architectural Heritage*, vol. 17, no. 1, pp. 114–133, 2023.

[6] *Turkey Building Earthquake Code: Rules for Design of Buildings Under Earthquake Effect (TBEC 2018)*, Official Gazette, no. 30364, Mar. 18, 2018.

[7] *Earthquake Risk Management Guide in Historical Buildings (ERMGHB-2017)*, General Directorate of Foundations, Ankara, Turkey, 2017 (in Turkish).

[8] (2019) AFAD Turkey Earthquake Risk Map Interactive Web Application. [Online]. Available:https://tdth.afad.gov.tr/

[9] *MIDAS Gen: Integrated Solution System for Building and General Structures*, MIDAS Information Technology Co., 2018.

ICENS 11TH INTERNATIONAL CONFERENCE ON ENGINEERING AND NATURAL SCIENCE October 22-26 2025 Sarajevo

Seismic performance assessment of the reinforced-concrete buildings subjected to structural and architectural modifications

Muhammed AKGÜL[1], Barış GÜNEŞ[1], Burak AKALIN[1], Barış SAYIN[1]*

Abstract

Nonlinear performance analyses enable the evaluation of seismic vulnerability and the determination of retrofitting strategies by revealing the behavior of structures under seismic effects. In this context, conducting detailed analyses of structures with irregular geometry and complex structural systems is critically important. This study assesses the seismic performance of a vital transportation facility in Istanbul, whose structural system has developed irregularities due to uncontrolled interventions over time, in accordance with the Turkish Building Code 2018 (TBEC-2018). The structure's three-dimensional finite element model was created in a computer environment, and Nonlinear Time History Analyses were performed. Within this scope, 11 earthquake records compatible with the spectrum were selected and applied to the structure in both directions. The Performance-Based Design and Evaluation (PBD) approach was used in the performance evaluation. The analysis results show that the structure meets the 'Limited Damage' performance target at the DD-3 earthquake level (ground motion with a 50% probability of exceedance in 50 years and a recurrence period of 72 years) and 'Controlled Damage' performance targets at the DD-1 earthquake level (a ground motion with a 2% probability of exceedance in 50 years and a recurrence period of 2475 years). Furthermore, it was concluded that retrofitting does not offer a suitable solution from a static perspective due to existing irregularities and that redesign and reconstruction are more appropriate options. The study is expected to provide a methodological framework for examining the seismic performance of structures with composite structural systems and to contribute to the literature.

Keywords: Nonlinear Time History Analysis, Seismic Performance Assessment, complex structural systems, Retrofitting Strategies

1. INTRODUCTION

A portion of the existing building stock consists of reinforced concrete structural systems. Over time, many of these structures have undergone various structural and architectural modifications. Such modifications may significantly influence the overall integrity and seismic response of the load-bearing system, making accurate performance evaluation essential. In this context, the implementation of appropriate repair and strengthening techniques, when necessary, plays a vital role in mitigating potential human and economic losses that may occur during future earthquakes.

Recent studies have increasingly focused on achieving a more realistic evaluation of the seismic performance of reinforced concrete structures through advanced computational techniques and nonlinear analysis methods. Reference [1] evaluated the behavior of multi-story RC buildings through nonlinear time-history and pushover analyses in ETABS, highlighting the influence of slab configuration and story number on structural response [2]. Similarly, [3] analyzed an irregular historical RC building in SAP2000 to compare nonlinear dynamic and pushover analyses, emphasizing the applicability limits of the latter for irregular geometries [4]. In another study, [5] investigated an existing hospital structure using SeismoStruct and reported that severe damage could occur under strong motions, underscoring the need for retrofitting interventions [6]. From a computational perspective, [7] introduced the Proper Orthogonal Decomposition (POD) technique, achieving a 94% reduction in analysis time while maintaining high accuracy in nonlinear evaluations. Moreover, [8] demonstrated that incorporating structural dynamic characteristics through single-degree-of-freedom (SDOF) oscillator responses significantly improved the correlation between seismic intensity measures (IM) and engineering demand parameters (EDP).

[1] Istanbul University-Cerrahpasa, Department of Environmental Engineering, 34320, Avcılar/İstanbul, Turkey. muhammed.akgul@iüc.edu.tr

[*] Corresponding author: Istanbul University-Cerrahpasa, Department of Environmental Engineering, 34320, Avcılar/İstanbul, Turkey. barsayin@iuc.edu.tr

In this study, the seismic performance of an existing reinforced concrete building that underwent structural and architectural modifications was evaluated using numerical analysis methods. The analyses were conducted in accordance with the procedures outlined in the Turkish Building [9].

2. MATERIAL AND METHODS

2.1. The Examining Building

The building has a generally irregular geometry and consists of ground and attic floors. Several structural interventions have been implemented at various stages during the structure's service life. In certain sections, additional mezzanine floors were subsequently constructed, while in some primary axes, load-bearing walls were removed and replaced with steel members to provide localized strengthening. The foundation system is designed with individual pad footings connected by reinforced concrete tie beams. The floor system consists of timber and steel. The structural system consists of reinforced concrete columns, beams, and load-bearing masonry walls. The roof load-bearing system is composed of steel truss elements. Table 1 presents the principal geometrical properties of the structural members used in the building.

Table 1. Properties of the structural members

Structural Member	Floor	Dimensions (cm)
Foundation	Foundation Level	40 (thickness); Footings connected with 50×40 tie beams
Column	Ground Floor	20×20 (existing); 45×45 (after jacketing)
Beam	Ground Floor	20×15 (existing); 20×50 (after strengthening)
Slab	Ground Floor, Intermediate Floors	15–45 (height); Timber/Steel type

2.2. Material Examination

The unconfined concrete compressive strength was determined as 12.75 MPa for the existing columns and 13.30 MPa for the strengthened columns. Reinforcement tensile tests revealed a yield strength of 220 MPa for the steel.

2.3. Soil and Earthquake Parameters

The soil and earthquake parameters of the structure were determined using the "Turkey Earthquake Hazard Maps Interactive Web Application," prepared by the Turkish Disaster and Emergency Management Presidency, and are presented in Table 2 [10].

Table 2. Soil Class and Earthquake Parameters

Parameter	Value / Class
Local soil class	ZC
Earthquake ground motion level	DD-1, DD-2, DD-3
Spectral acceleration coefficients from the Earthquake Hazard Map (g)	DD-1, Ss = 1.617, S1 = 0.452 DD-2, Ss = 0.929, S1 = 0.257 DD-3, Ss = 0.370, S1 = 0.102
Peak ground acceleration (g)	DD-1, PGA = 0.649 DD-2, PGA = 0.380 DD-3, PGA = 0.161
Local site effect coefficients	DD-1, Fs = 1.200, F1 = 1.500 DD-2, Fs = 1.200, F1 = 1.500 DD-3, Fs = 1.300, F1 = 1.500
Spectral Acceleration Coefficients	DD-1, SDS = 1.940, SD1 = 0.678 DD-2, SDS = 1.115, SD1 = 0.386 DD-3, SDS = 0.481, SD1 = 0.153

2.4. Performance Analysis

A model accurately representing the current condition of the building was prepared using Midas Gen finite element software, based on available documentation and on-site inspections [11]. The model defined reinforced concrete beams and columns as frame elements, while masonry walls were modeled using "plate/wall" elements. The 3D static analysis model of the building is given in Figure 1.

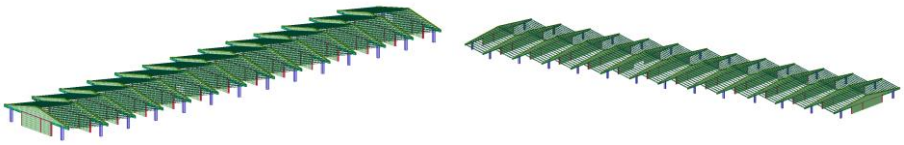

Fig. 1 3D Static Analysis Model of the Buildings

2.5. Performance Assessment Method

The assessment of the building under static and earthquake loads was conducted in accordance with the Turkish Building Earthquake Code (TBEC-2018) [9]. The classification of the structure, target performance levels, required analyses, and design/assessment methods is summarized in Table 3.

Table 3. Performance-Based Analysis and Design Method.

Parameter	Value/Class
Building Use Class, BUC	1
Building Importance Factor, I	1.5
Earthquake Design Class, EDC	1a
Building Height Class, BHC	8
Target Structural Performance	Controlled Damage for DD-1 Limited Damage for DD-3
Design/Assessment Method	Nonlinear analysis, Deformation-Based Assessment and Design
Structural System Behaviour Factor (R)/ Overstrength Factor (D)	R = 1, D = 1
Building Information Level / Factor	Limited, 0.75

2.6. Design Elastic Spectrum

As illustrated in Figure 2, horizontal elastic design spectra were generated for DD-1 and DD-3 earthquake ground motion levels by considering the location and soil parameters of the structure.

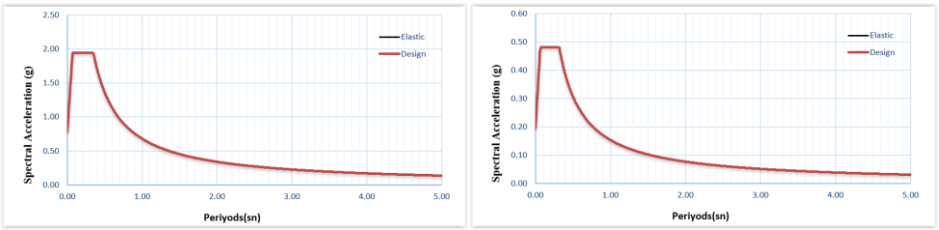

Fig. 2 Response Spectrum and Spectral Acceleration Values for the DD-3 and DD-1 Earthquake Level (R = 1, D = 1)

2.7. Selection and Scaling of Earthquake Records

Figure 3 shows the distance of the structure to the active fault, which is approximately 18.64 km. Eleven earthquake records were selected and scaled. The records were chosen from the PEER Strong Ground Motion Database (2023), considering fault characteristics, site-to-fault distance, and local soil conditions [12]. The summary information of the selected records is presented in Table 4.

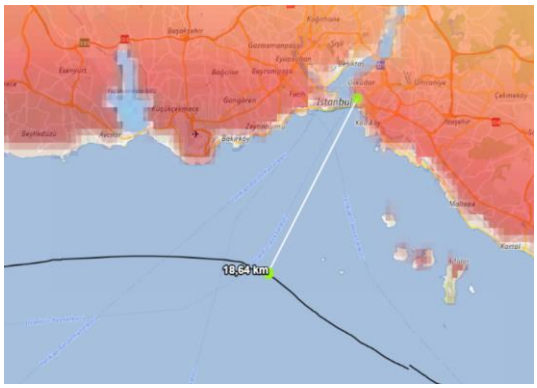

Fig. 3 Distance to active fault.

Table 4. Summary information of selected earthquake records

Record No	Earthquake Year	Earthquake Name	Station	Magnitude	Vs30 (m/s)
01	1999	Kocaeli, Turkey	Duzce	7.51	281.86
02	1979	Coyote Lake	Gilroy Array	5.74	270.84
03	1979	Imperial Valley-06	Brawley Airport	6.53	208.71
04	1990	Manjil, Iran	Abbar	6.95	213.44
05	1979	Imperial Valley-06	Delta	6.53	242.05
06	1999	Hector Mine	Hector	7.13	726.00
07	1961	Hollister-01	Hollister City Hall	5.6	198.77
08	1966	Parkfield	Cholame - Shandon Array	6.19	289.56
09	1940	Imperial Valley-02	El Centro Array	6.95	213.44
10	1989	Loma Prieta	Capitola	6.93	288.62
11	1992	Landers	Coolwater	7.28	352.98

The earthquake records obtained based on the TBEC (2018) acceleration spectrum were scaled using the spectral matching method defined in Section 2.5.3 of the code [9]. The scaling was performed in SeismoMatch software with respect to the DD-1 and DD-3 earthquake ground motion spectra [13]. The comparison between the average acceleration spectra obtained from the scaled records and the target spectra is presented in Figure 4.

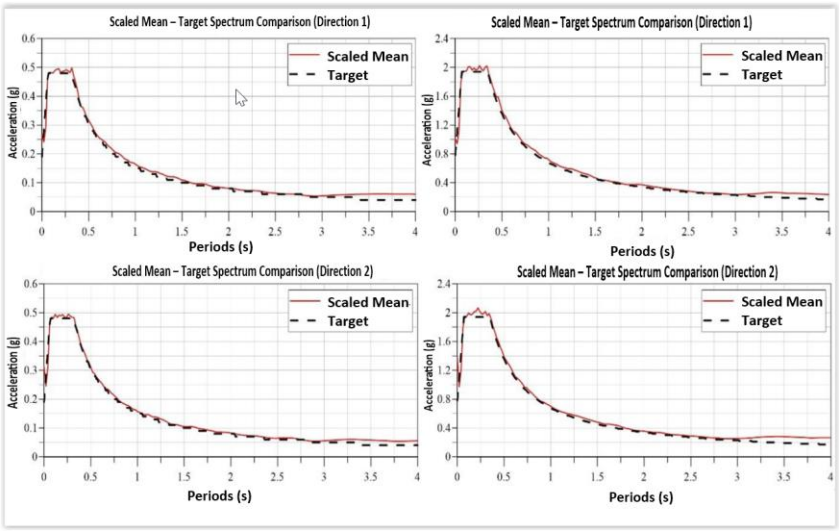

Fig. 4 Average spectrum – target spectrum comparisons for the DD-1 and DD-3 Earthquake Level (Left: DD-1; Right: DD-3).

3. RESULTS

3.1. Modal Analysis

The results of the modal analysis are presented in Table 5. The fundamental vibration period of the structure was determined to be 0.957 seconds. The cumulative mass participation ratios in both principal directions reached approximately 95%, satisfying the requirements specified in the relevant seismic code.

Table 5. Results of the modal analysis

Mode	Direction	Period (s)
1	X	0.957
2	Y	0.934
3	Z	0.842

3.2. Statistical Evaluations

As shown in Figure 5, the displacements under vertical loads and the axial forces generated in the structure are illustrated. The vertical displacements (under dead and live loads) in the structure are shown in Table 6. Analysis results showed that the steel structural elements (roof trusses) did not meet the strength limits under static loads.

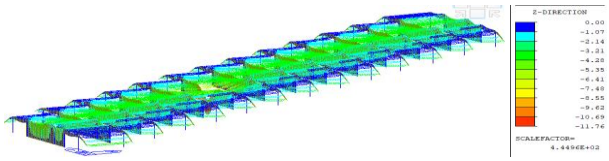

Fig. 5 Displacements Under Vertical Loads and the Axial Forces Generated in the Structure.

Table 6. Structural assessment of steel trusses under static loads

Structural Member	Steel Trusses		Result
	Combined Axial and Bending Strength	Shear Strength	
	X	√	X

3.3. Dynamic Evaluations

As shown in Figures 6 and 7, the deformation and strength checks of the reinforced concrete columns and beams were evaluated under the DD-3 earthquake ground motion. As seen in Table 7, the reinforced concrete columns under seismic effects did not meet the TBEC-2018 deformation requirements; however, the shear strength checks satisfied the required design criteria [9]. As shown in Table 8, the reinforced concrete beams subjected to seismic effects met the TBEC-2018 deformation requirements; however, the shear strength checks did not satisfy the required design criteria [9].

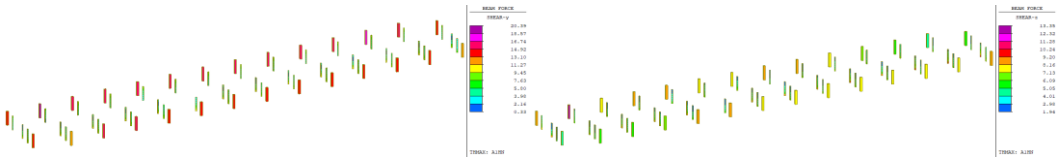

Figure 6. Distribution of shear forces in columns under DD-3 earthquake level.

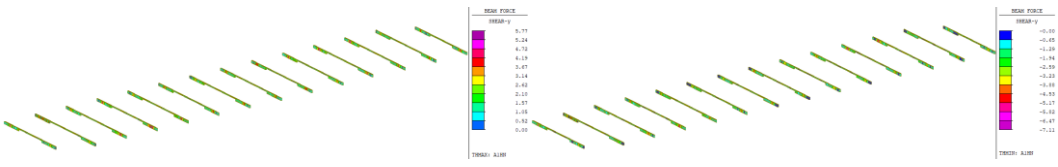

Figure 7. Distribution of shear forces in beams under DD-3 earthquake level.

Table 7. Assessment of columns under DD-3 earthquake ground motion level

Story	Reinforced Concrete Column		Target Performance Level (LD)
	Deformation Check	Shear Check	
basement	X	√	X

Table 8. Assessment of beams under DD-3 earthquake ground motion level

Story	Reinforced Concrete Beam Deformation Check	Shear Check	Target Performance Level (LD)
basement	√	X	X

As shown in Figures 8 and 9, the deformation and strength checks of the reinforced concrete columns and beams were evaluated under the DD-1 earthquake ground motion. As seen in Table 9 and Table 10, the reinforced concrete columns and beam under earthquake effect did not meet the TBEC-2018 deformation requirements, and the shear strength controls did not meet the required design criteria [9].

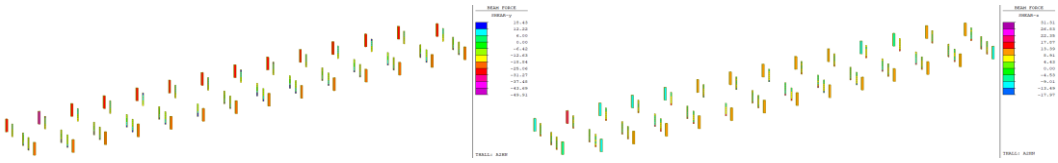

Figure 8. Distribution of shear forces in columns under DD-1 earthquake level.

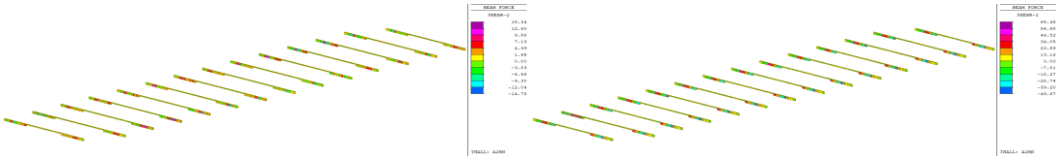

Figure 9. Distribution of shear forces in beams under DD-1 earthquake level.

Table 9. Assessment of columns under DD-1 earthquake ground motion level

Story	Reinforced Concrete Column Deformation Check	Shear Check	Target Performance Level (LD)
basement	X	X	X

Table 10. Assessment of beams under DD-1 earthquake ground motion level

Story	Reinforced Concrete Beam Deformation Check	Shear Check	Target Performance Level (LD)
basement	X	X	X

4. CONCLUSION

Based on the concrete and reinforcement detection reports, structural and damage survey drawings, and on-site inspections, a numerical model was developed to represent the current state of the building. Following this, performance analyses were carried out in accordance with the requirements of the Turkish Building Earthquake Code (TBEC, 2018) [9].

- Based on the analyses performed in accordance with the Turkish Building Earthquake Code (TBEC, 2018), the existing structure was found to be insufficient in meeting the required criteria under static loading conditions [9]. Notably, some members of the steel roof trusses demonstrated inadequate strength, which could lead to potential stability deficiencies.
- The analysis results show that the structure doesn't meet the 'Limited Damage' performance target at the DD-3 earthquake level and 'Controlled Damage' performance targets at the DD-1 earthquake level.
- It was concluded that retrofitting does not offer a suitable solution from a static perspective due to existing irregularities, and that redesign and reconstruction are more appropriate options

REFERENCES

[1] Abd-Elhamed, S. Mahmoud, and K. S. Alotaibi, "Nonlinear analysis of reinforced concrete buildings with different heights and floor systems," *Scientific Reports.*, vol. 13, no. 1, p. 14949, 2023.
[2] *ETABS: Integrated Building Design Software*, Computers and Structures Inc. (CSI), Berkeley, CA, USA, 2022.

[3] Georgiou, S. Kotakis, D. Loukidis, and I. Ioannou, "Case study of seismic assessment of a short irregular historic reinforced concrete structure: time-history vs. pushover nonlinear methods," *Journal of Earthquake Engineering*, vol. 27, no. 16, pp. 4761–4785, 2023
[4] *SAP2000: Integrated Software for Structural Analysis and Design*, Computers and Structures Inc. (CSI), Berkeley, CA, USA, 2022.
[5] K. K. Kuria and O. K. Kegyes-Brassai, "Nonlinear static analysis for seismic evaluation of existing RC hospital building," *Applied Sciences*, vol. 13, no. 21, p. 11626, 2023.
[6] *SeismoStruct – A Computer Program for Static and Dynamic Nonlinear Analysis of Framed Structures*, Seismosoft, Pavia, Italy, 2022.
[7] N. Ayoub, J.-F. Deü, W. Larbi, J. Pais, and L. Rouleau, "Application of the POD method to nonlinear dynamic analysis of reinforced concrete frame structures subjected to earthquakes," *Engineering Structures*, vol. 270, p. 114854, 2022.
[8] L. A. Pinzón, D. A. Hidalgo-Leiva, R. E. Alva, M. A. Mánica, and L. G. Pujades, "Correlation between seismic intensity measures and engineering demand parameters of reinforced concrete frame buildings through nonlinear time history analysis," *Structures*, vol. 57, p. 105276, Nov. 2023.
[9] *Turkey Building Earthquake Code: Rules for Design of Buildings Under Earthquake Effect (TBEC 2018)*, Official Gazette, no. 30364, Mar. 18, 2018.
[10] (2019) AFAD Turkey Earthquake Risk Map Interactive Web Application. [Online]. Available:https://tdth.afad.gov.tr/
[11] *MIDAS Gen: Integrated Solution System for Building and General Structures*, MIDAS Information Technology Co., 2018.
[12] PEER Ground Motion Database. Pacific Earthquake Engineering Research Center (PEER), University of California, Berkeley, CA, USA. [Online]. Available: https://ngawest2.berkeley.edu
[13] SeismoMatch – A Computer Program for Spectrum Matching of Earthquake Records, Seismosoft, Pavia, Italy, 2022

ICENS 11TH INTERNATIONAL CONFERENCE ON ENGINEERING AND NATURAL SCIENCE October 22-26 2025 Sarajevo

Numerical Investigation of Flow Characteristics in River Bridges with Different Designs

Pınar OZENCI[1], O. Faruk DURSUN[1], Mahmut AYDOGDU[2]*

Abstract

Bridges, crucial infrastructure facilities in modern human life, are constructed to provide uninterrupted transportation on roads and railways. River bridges are subject to significantly greater risks of abrasion, erosion, and failure than other bridges. The flow characteristics created and modified by river flow at and around the foundations of bridge piers during floods can cause bridge collapses. These failures lead to loss of life, property, and transportation disruptions.

In this study, river bridges with different plan designs were numerically analyzed. Geometric characteristics such as whether the bridges are perpendicular to the river axis or angled, despite similar abutment spans and abutment heights, abutment widths, whether they are straight, curved, or split in plan, and the bending angle of broken-shaped bridges were investigated. For this purpose, Ansys/Fluent, a software capable of performing calculations using the Computational Fluid Dynamics (CFD) method, was used. Flow characteristics such as flow velocity, pressures, turbulence, wall stresses, and flow directions, as well as their effects on the bridge piers, were determined and discussed. All results were compared with each other and with the literature and interpreted.

Keywords: Flood, Hydraulic design of bridges, River hydraulics, Bridge failure, CFD

INTRODUCTION

River bridges are subject to much greater wear and structural damage than other bridges. The primary reasons for this include excessive loads caused by stream flow and base material movement, scour, changes in the flow direction, and base rise or fall. Ensuring transportation safety is possible by ensuring that river bridges are safe even under the most adverse conditions. Hydrological and hydraulic calculations are performed first when sizing river bridges, followed by structural design. Historical stone bridges built over large rivers often feature arch-type structures with large piers and numerous spans. However, flood-related bridge collapses on river bridges have many causes. Most of these reasons lie outside of direct structural characteristics. Calculation errors, such as inaccurate determination of the river's hydrological and hydraulic flow characteristics, inadequate investigation of substrate movements, and incomplete determination of minimum and maximum flow rates, or artificial factors that alter the natural flow conditions of the river despite all calculations being accurate, compromise bridge safety and lead to collapses. In this thesis, river bridges with different structural designs will be analyzed digitally and their interaction with the river flow will be investigated. Numerous studies on this subject exist in the literature.

This Soydan et al. (2018) conducted numerical simulations using different turbulence closure models (Standard k-ε, Renormalization k-ε, and Realizable k-ε). Experimental studies were conducted at the Çukurova University Hydraulics Laboratory, and the numerical results were compared with the obtained data. As a result of the investigations, the effects of the turbulence models on the flow velocity distribution and water surface profile were evaluated; it was observed that some models did not adequately represent the complex flow structure. Erduran et al. (2023) investigated the effects of different bridge pier types and oblique angles on the water surface profile using both experimental and numerical methods. The experiments were conducted in a test channel located in the Hydraulics Laboratory of Niğde Ömer Halisdemir University. Flow measurements were taken using four different bridge piers (square, circular, rounded, and sharp-edged upstream) and four different oblique angles (0°, 15°, 30°, and 45°). Yanmaz et al. (2007) focused on the hydraulic factors affecting the structural safety of river bridges. They proposed a three-stage evaluation process to ensure the longevity and durability of bridges: examining the geomorphological characteristics of the river, then analyzing the hydrological and hydraulic conditions, and conducting mathematical and physical modeling. In this process, an evaluation system developed by Johnson was used, and streams were scored based on 13 different parameters and their stability was analyzed. Yurtseven (2005) In this thesis, he addressed the scour processes occurring on bridge piers and the key factors affecting these processes. He

[1] Inönü University, Department of Civil Engineering, 44280, Battalgazi/Malatya, Turkey. pozenci.5@gmail.com

[*] Corresponding author: Inönü University, Department of Civil Engineering, 44280, Battalgazi/Malatya, Turkey. ofdursun@gmail.com

[2] Malatya Turgut Özal University, Department of Civil Engineering, 44900, Yeşilyurt/Malatya, Turkey. mahmut.aydogdu@ozal.edu.tr

specifically examined the relationship between scour depth and fluid dynamics, presenting various equations and models within this scope. Equations developed by researchers such as Melville and Sutherland were used as references to analyze the parameters affecting scour depth. Bulut et al. (2018): In this study, they examined scour around the bridge piers of the Ceyhan Viaduct. The study examined the bridge's approximately 29-year service life. The flow conditions to which the bridge was exposed throughout the duration of the project were evaluated, and scour depths were calculated under 25, 50, and 100-year flood flow rates. Mayda (2013) prepared a study as a result of experimental and numerical studies. The primary objective of the study is to better understand the dynamic behavior of local scours occurring around circular-section bridge piers by examining their occurrence. The study utilized both laboratory experiments and numerical modeling, providing a detailed analysis of the scour processes around the bridge piers under moving-base conditions. Particular attention was paid to the depth of scours that develop over time around circular-section piers, their formation mechanisms, and the hydraulic factors affecting these processes. Yılmaz et al. (2020) aimed to assess the flood reliability of river bridges using the HEC-RAS program. In particular, bridges over the Çoruhözü Stream and Batman Stream in Kırıkkale were examined, and their capacity to safely handle different flood flows was analyzed. The evaluations revealed that existing bridges are insufficient to accommodate some flood flows and therefore require reconsideration. Lane et al. (1998) addressed the use of numerical modeling methods to understand flow dynamics in river systems. Particular attention was paid to the comparison of two-dimensional (2D) and three-dimensional (3D) models. It was emphasized that 3D models can more accurately represent complex processes such as flow structures and sediment transport. Ardiclioglu et al. (2022) conducted a study examining the effects of bridge configurations on the hydraulic regime in streams. The primary objective of the study was to better understand the changes bridges exert on the water surface profile and flow velocity. In this study, water surface profiles and flow velocities were analyzed under different bridge spans and flow rates using both experimental and numerical methods. The findings revealed that bridge spans have significant effects on these hydraulic parameters. Chia-Ren et al. (2016) conducted a study examining the interaction between water surface flow and underwater rectangular bridge decks. The study analyzed in detail the effects of Reynolds number, Froude number, blockage ratio, and underwater ratio on the force coefficients (drag and lift) on the bridge decks using the Large Eddy Simulation (LES) method. The role of Reynolds number on these coefficients was particularly emphasized, and the relationship between flow dynamics and the forces acting on the structure was examined. Experimental findings revealed that the blockage rate and Reynolds number, together, significantly impact the hydrodynamic loads experienced by the bridge deck. M. Flint et al. (2017) focused their study on the causes of bridge collapses in the United States. The study specifically addressed five fundamental questions: the magnitude of flood flows, their return times, and how these times vary with the location and conditions of the event. As part of the research, analyses were conducted on 35 different bridges that had experienced collapses, and the relationship between these events and factors such as climate change and land use was evaluated. The findings indicated that the vast majority of bridge collapses occurred during flood events with return periods much shorter than the generally assumed 100-year floods. R. Gautam et al. (2004) conducted a study examining the effects of bridge abutment reinforcement on the Tama River floodplain hydrology in Nagata, Japan. The study was conducted using a combination of long-term hydrogeological observations and artificial neural network (ANN) models. The results revealed that morphological changes in the riverbed and floodplains over the past 120 years have significantly affected both the spatial and temporal distribution of hydraulic parameters in the region. In his research, Johnson (2005) developed a scoring system based on various indicators to assess stream stability. This system considered physical factors such as the soil structure of the river banks, the slope angle, and the condition of the bed material. It also emphasized the need to analyze stream conditions around the bridge through careful observations. This approach stands out as a particularly useful tool for ensuring the safety of bridge foundations, identifying potential erosion risks, and detecting stability problems early. It also contributed to more informed decisions on bridge design, maintenance and repair. Kaya (2010) examined how an artificial neural network (ANN) model can be used to estimate the depth of local erosion (scour) around bridge piers. A dataset consisting of 380 different measurements from the US Federal Highway Administration (FHWA) was used in the study. One of the most striking results of the study is that the model can produce high-accuracy estimates without using excessive data. Even when only four key variables (such as bridge pier shape, flow depth, and flow velocity) were used, the model was able to predict local scour depth quite successfully. Khan et al. (2017) conducted a laboratory study examining the scour depth around bridge piers. In the study, bridge piers of different shapes and sizes were modeled, and erosion depths under various flow conditions were observed. According to the findings, square-shaped piers produced greater erosion depths than circular piers. This demonstrates that the geometry of the bridge pier directly affects its impact on the surrounding streambed. Another important aspect of the research is the comparison of different prediction models. Khosronejad et al. (2012) This study includes experimental and numerical analyses to investigate local erosion (scour) occurring around the bridge piers. Laboratory experiments were conducted on bridge piers with cylindrical, square, and diamond cross-sections, and the results were compared with simulations performed using the URANS model. Zhong (2011) conducted a detailed study of the dynamic response of the Nanjing Dashengguan Yangtze River Bridge to seismic waves. Numerical analyses using the finite element method revealed the effects of seismic waves moving at different speeds on the bridge. The bridge's displacement and internal force responses during an earthquake were calculated, and the variation of these responses with wave speeds was examined. The findings provide important guidance in understanding the seismic resistance of the bridge and have led to improved safety for long-span bridges. Akıntürk et al. (2025), scours occurring in river bridges were investigated under pressure and free-flow conditions. The experiments were conducted at different flow rates and approach flow depths, and scour depths and shapes were evaluated. The results showed that scour hole depths decreased as approach flow depth increased, and scours occurring under full-pressure flow conditions were smaller than those under partial-pressure flow. Yanmaz et al. (2016) focused on assessing the scour risk in river bridge foundations. The study examined adverse scenarios that bridges may encounter throughout their economic life and their effects on the probability of failure. The probability of failure was correlated with the safety factor,

and it was determined that the probability of failure increases with increasing variables in the scour mechanism. Furthermore, sensitivity analyses using different probability density functions (PDF) and coefficients of variation (COV) were found to allow bridge designs to be adapted appropriately to local conditions. Yanmaz et al. (2014) examined riprap coating applications for protecting the piers of river bridges. Riprap has emerged as both a practical and economical option among protection methods using materials such as stone, concrete blocks, or cement-mortar bags. The study also cites an example of a bridge over the Fol Creek, and provides cost details for the riprap coating. Koçyiğit et al. (2016) reviewed research on the safety and hydraulic assessments of river bridges in Turkey. Specifically, they examined the effects of hydraulic factors such as the condition of the riverbeds surrounding the bridges, floods, and erosion on bridge structures. The article emphasized that waste accumulation on bridge piers disrupts flow patterns and increases the risk of erosion. Furthermore, hydraulic assessment methods developed for bridge safety aimed to address the shortcomings of existing systems. Ardiclioglu et al. (2021); describes a study examining the effects of bridge configurations on the hydraulic regime. The primary objective of the research is to observe the changes bridges cause in the water surface profile and flow velocity. Using both experimental and numerical methods, water surface profiles and flow velocities were examined in detail for different flow rates and bridge spans. Berk (2021) reviewed various studies and methods used to estimate local scour depth around bridge piers. These studies focused on developing empirical scour equations by combining experimental data with mathematical models. In particular, the studies of Olsen and Kjellesving (1998) and Nagata et al. (2005) provide good examples of these experimental and mathematical modeling processes. Recently, Artificial Neural Network (ANN) methods have been developed as an alternative to traditional empirical equations. ANNs can flexibly model complex and nonlinear relationships and provide a data-driven approach. Researchers such as Kothyari et al. (1992) and Nazariha (1996) have obtained significant results by examining these temporal changes. Overall, the study emphasizes the importance of scour prediction in bridge engineering using both experimental and modeling methods. Turan (2011); explores an innovative artificial neural network (ANN)-based approach, comparing traditional methods used in bridge design. Nas (2022); aimed in the study to investigate the effects of bridge piers on water surface profiles and swell. The study experimentally investigated the effects of five different bridge piers (square, circular, rounded edges, upstream sharp-edged, and rectangular) on water surface profiles and compared the obtained data with the HEC-RAS numerical model. In addition to experimental studies, the study also incorporated numerical modeling techniques and enabled the acquisition of flow measurements using image processing methods.

In this study, the interaction of certain geometric features of river bridges with stream flow was investigated using Fluent, a software program capable of numerical analysis using the CFD method. We aimed to understand how these geometric features alter flow characteristics and the effects of these changes on bridge piers.

METHOD

Within the scope of this study, numerical studies will be conducted using Ansys/Fluent, a software licensed by the Department of Civil Engineering at İnönü University. These studies will be conducted using powerful computers. Parameters used in the study include the number and geometry of bridge piers, pier spans and heights, bridge plan shape, angle to the flow axis. Numerous study models will be developed and numerically analyzed, and the results will be compared and interpreted with each other and with the literature.

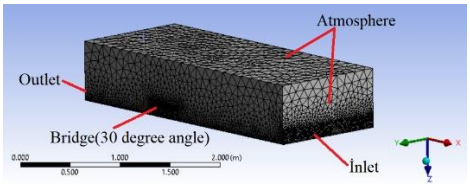

Fig. 1 Mesh structure of the study.

Triangular mesh geometries used in the study. In Table 1, mesh numbers for solutions given below. Volume of Fluid (VOF) model selected and the Standard k-ϵ turbulence model as viscous model in the study. Solutions conducted for 2 phases (air and water).

Table 1. Mesh element numbers used in the studies.

0 Degree	10 Degree	20 Degree	30 Degree
546001	516582	517749	517566

FINDINGS

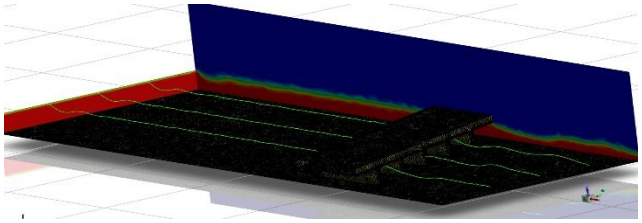

Fig 2. Water surface profiles

In the Fig 2, for 20 degrees, y=0.3, 0.6, 0.9 cm water surface profile, bottom and bridge mesh structure and water surface profile on the left side is shown.

Figure 3 shows the changes in water levels along the channel for bridge angles of 0, 10, 20, and 30 degrees, respectively. As the bridge angles increase, the fluctuations on the water surface increase, and the uniformity of the flow within the channel is disrupted.

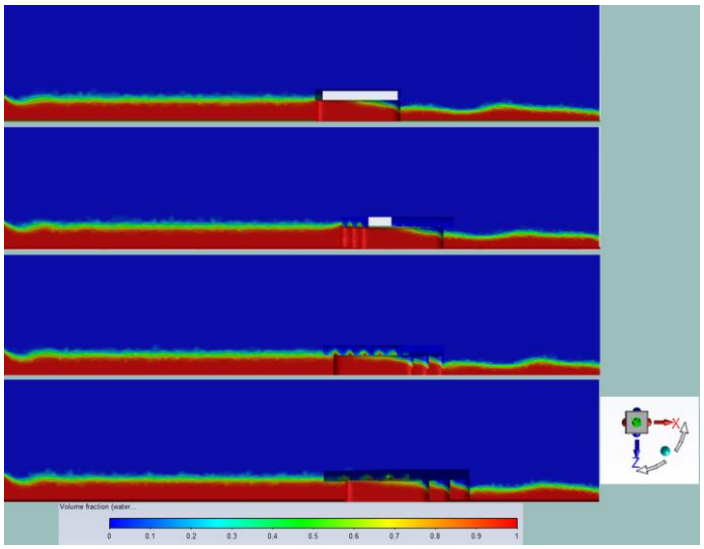

Fig 3. Water level longiditiunal profiles for α=0, 10, 20 and 30 degrees.

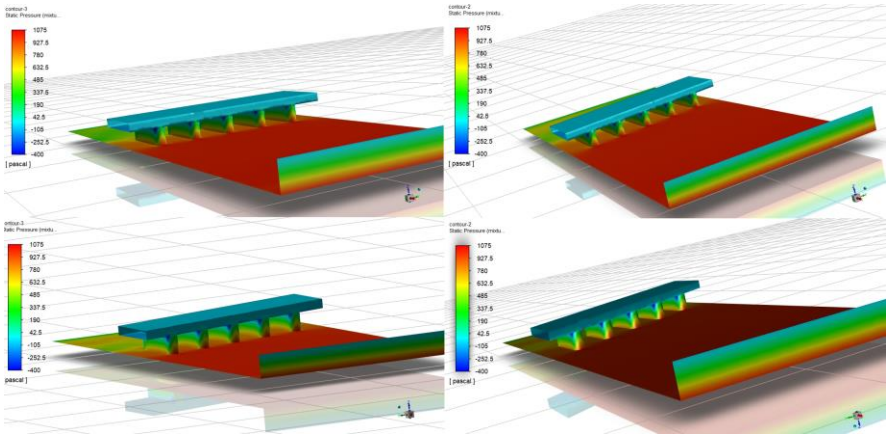

Fig. 4 Static pressures on the bridge surfaces for α=0, 10, 20 and 30 degrees.

When we examine Figure 4, where the static pressures are shown, it is seen that the static pressures on the bridge side surfaces and middle pier walls become irregular as the bridge platform angle increases. Accordingly, the 0 degree angle has the most suitable results.

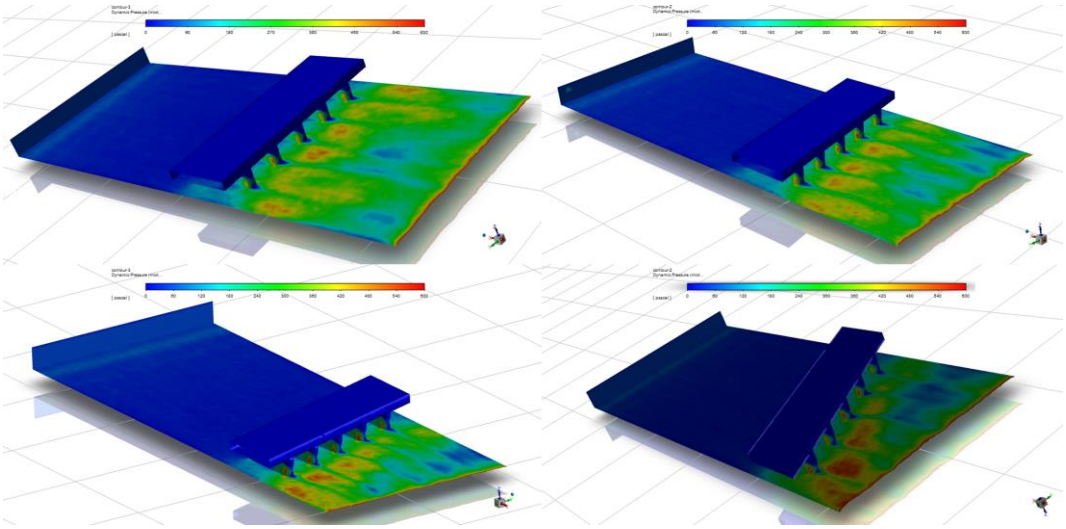

Fig 5. Dynamic pressures on the bridge surfaces for α=0, 10, 20 and 30 degrees.

Figure 5 shows the changes in dynamic pressures at the channel bottom and bridge piers. According to Figure 5, it is seen that there are increasing dynamic pressures especially on the right bank for the bridge angle of 30 degree, and it is also understood that the dynamic pressures on the bridge side surfaces increase with increasing angles.

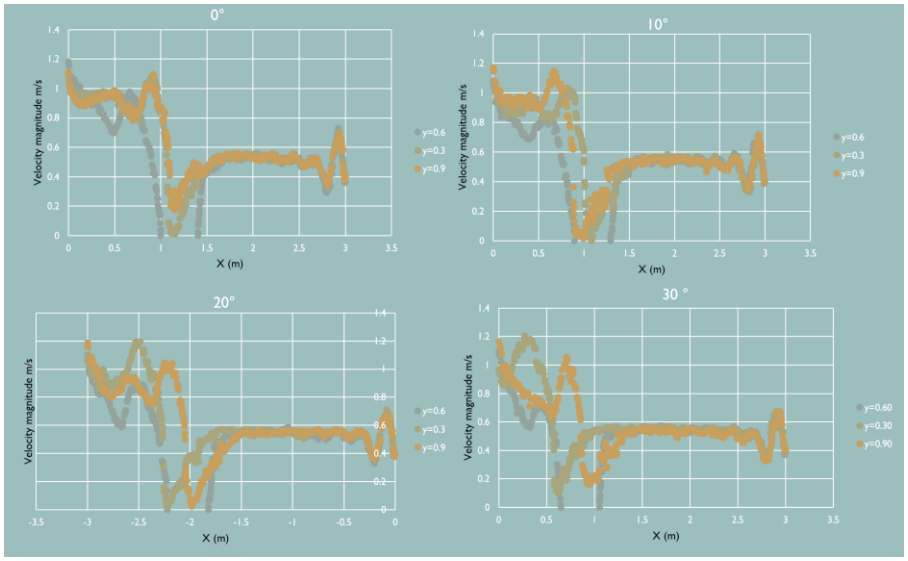

Fig. 6 Velocity magnitudes along the channels for α=0, 10, 20 and 30 degrees.

Figure 6 plots the velocity changes along the channel for widths of 0.3, 0.6, and 0.9 meters as profiles. Accordingly, while the velocity values have similar profiles, they differ for different sections of the channel with increasing angle values. In other words, for the 0-degree test set, the velocity profiles are approximately similar in all sections of the channel. However, for the 30-degree test set, the velocity profiles differ from each other, indicating that lateral, or secondary, currents can also form within the flow.

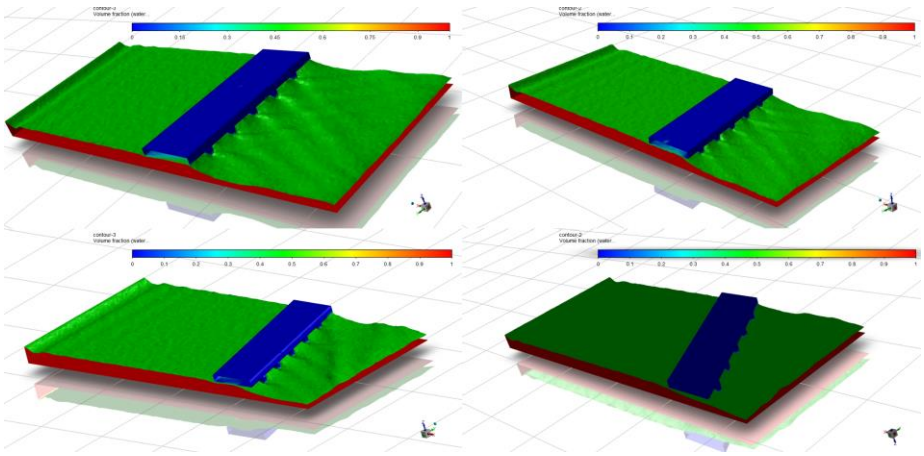

Fig. 7 Free water surface shapes for α=0, 10, 20 and 30 degrees.

Figure 7 shows the shapes of the free water surface. As the angle increases, the vortices that form on the water surface become more differentiated and exhibit a more chaotic appearance. This causes streamlines to collide with each other, creating vortices and dead spots. Consequently, the current swells and the risk of flooding increases.

CONCLUSION

When we examine the velocity profile graphs, we see that the velocity profiles of the model that intersects the channel perpendicularly, that is, at a 0-degree angle, are more homogeneous than those of other models. As this angle increases, the homogeneity deteriorates. In other words, the influence of the side piers on the flow increases, which disrupts the homogeneity of the velocity profiles. The variation of the velocity profiles along the cross-section within the channel flow can cause secondary flows in addition to axial flow, namely, helicoidally flow. This can trigger an irregular scour and accumulation mechanism along the cross-section, as seen in meandering channels.

We can observe the 3D image of the water surface profiles from the phase figures. According to these figures, as the bridge angle increases, the symmetric phase image of the flow is disrupted, and the flow is directed, particularly towards the left bank. Increasing the bridge angle also increased the dynamic pressures asymmetrically.

When examining the static pressures, it is observed that the static pressures on the side surfaces of the bridge piers increase as the bridge angle increases. However, no significant change was observed on the upstream surface of the bridge.

The increase in the bridge angle negatively impacted the upstream water level. Similarly, it caused the downstream water level to fluctuate more.

Acknowledgements: This study supported by Inönü University Scintific Research Projects Units under Grant number of FYL-2025-4273.

REFERENCES

[1] Soydan N. G., Şimşek O. ve Aköz M. S., " Köprü ayağı etrafındaki türbülanslı akımın sayısal ve deneysel analizi", Politeknik Dergisi, (2018).
[2] Erduran K.S , Ünal U. ,Dokuz A.Ş. , Nas M.Ç. "Köprü Ayak Tipi Ve Verevliğinin Su Yüzü Profilleri Üzerindeki Etkisinin Deneysel Ve Sayısal Olarak Araştırılması" Konya Mühendislik Bilimleri Dergisi, (2023).
[3] Yanmaz A.M., Caner A. "Köprülerin Tetkik Ve İzlenmesinde Hidrolik Etkenlerin Değerlendirilmesi" Orta Doğu Teknik Üniv., İnşaat Müh. Böl., Ankara(2007).
[4] Yurtseven M.L. "Köprü Ayakları Arkasında Oluşan Oyulmaların İncelenmesi" İstanbul Teknik Üniversitesi. (2005).
[5] Bulut G., Seçkin N., " Köprü Ayaklarındaki Oyulmalar Üzerine Yöntem Araştırılması " Ç.Ü Fen ve Mühendislik Bilimleri Dergisi Yıl 2018 Cilt: 35-2 (2018).
[6] Mayda O. "Köprü Ayakları Etrafında Oluşanyerel Oyulmaların Hareketli Tabandurumunda Deneysel Ve Nümerikaraştırılması " Dokuz Eylül Üniversitesi, (2013).
[7] N. Yılmaz, H. Bozkurt, Y.Bayazıt"Akarsu Köprülerinin HEC-RAS Programı ile Hidrolik Analizi: Fidanlık Köprüsü Örneği" BŞEÜ Fen Bilimleri Dergisi.(2020).
[8] M. Y. Akıntürk, M.B. Koçyiğit, "Taşkın Durumunda Akarsu Köprülerinde Basınçlı Akım Oyulmasının İncelenmesi" Afet ve Risk Dergisi.(2025).
[9] M. Yanmaz, M. Çalamak "Akarsu Köprü Temellerindeki Oyulma Riskinin Değerlendirilmesi" İmo Teknik Dergi.(2016).
[10] M. Yanmaz, M. Apaydın "Mevcut Akarsu Köprüleri Alt Yapı Elemanlarının Riprapla Korunmasına Yönelik Değerlendirmeler " İnşaat Müh. Bölümü, Orta Doğu Teknik Üniversitesi, (2014).

[11] M. B. Koçyiğit, H. Akay Ve A.M. Yanmaz "Taşkınlar Ve Akarsu Köprülerine Etkıleri" Uluslararası Doğal Afet ve Afet Yönetimi Sempozyumu, (2016).
[12] M. Ardiclioglu , Arzu M. W. Mohamed Hadi, E. Periku, A.Kuriqi "Experimental and Numerical Investigation of Bridge Configuration Effect on Hydraulic Regime " International Journal of Civil Engineering.(2021).
[13] Ö. Berk "Akarsu Köprülerinin Orta Ayaklarında Oluşan Oyulmaların Nedenleri Ve Oyulmaları Önleyici Uygulama Çalışmaları" İstanbul Teknik Üniversitesi.(2021).
[14] K. H.Turan., "Relıabılıty-Based Optımızatıon Of Rıver Brıdges Usıng Artıfıcıal Intellıgence Technıques" A Thesıs Submıtted To The Graduate School Of Natural And Applıed Scıences Of Mıddle East Technıcal Unıversıty. (2011).
[15] M. Ç Nas "Köprü Ayak Tiplerinin Su Yüzü Profillerine Olan Etkilerinin Deneysel Ve Sayısal Olarak İncelenmesi" Niğde Ömer Halisdemir Üniversitesi. (2022) .
[16] S.N. Lane , K.F. Bradbrook , K.S. Richards , P.A. Biron , A.G. Roy"The application of computational fluid dynamics to natural river channels: three-dimensional versus two-dimensional approaches" Geomorphology 29 _1999. 1–20
[17] Mehmet Ardiclioglu, Arzu M. W. Mohamed Hadi, Erion Periku, Alban Kuriqi, "Experimental and Numerical Investigation of Bridge Configuration Effect on Hydraulic Regime" International Journal of Civil Engineering (2022) 20:981–991
[18] Chia-Ren Chu, Ph.D.; Chun-Hsuan Chung; Tso-Ren Wu, Ph.D.; and Chung-Yue Wang, Ph.D. "Numerical Analysis of Free Surface Flow over a Submerged Rectangular Bridge Deck" J. Hydraul. Eng., 04016060.(2016)
[19] Madeleine M. Flint, A.M.ASCE; Oliver Fringer; Sarah L. Billington, M.ASCE;David Freyberg, M.ASCE; and Noah S. Diffenbaugh. "Historical Analysis of Hydraulic Bridge Collapses in the Continental United States" J. Infrastruct. Syst., -1—1.(2017).
[20] Mahesh R. Gautama, Kunio Watanabea,, Hiroyuki Ohnob"Effect of bridge construction on floodplain hydrology—assessment by using monitored data and artificial neural network models" 2004 Elsevier B.V. All rights reserved.
[21] P. A. Johnson "Preliminary Assessment and Rating of Stream Channel Stability near Bridges" J. Hydraul. Eng. 2005.131:845-852.
[22] Abidin Kaya "Artificial neural network study of observed pattern of scour depth around bridge piers" Computers and Geotechnics 37 (2010) 413–418
[23] Khan, Mujahid, Muhammad Tufail, Muhammad Ajmal, Zia Ul Haq, and Tae-Woong Kim. "Experimental analysis of the scour pattern modeling of scour depth around bridge piers." Arabian Journal for Science and Engineering 42, no. 9 (2017): 4111-4130.
[24] Ali Khosronejad, Seokkoo Kang, Fotis Sotiropoulos "Experimental and computational investigation of local scour around bridge piers" Advances in Water Resources 37 (2012) 73–85
[25] Chaoyi Xia and Tieyi Zhong" Numerical analysis of the Nanjing Dashengguan Yangtze River Bridge subjected to non-uniform seismic excitations " C. Xia and T. Zhong / Journal of Mechanical Science and Technology 25 (5) (2011) 1297~1306

ICENS 11TH INTERNATIONAL CONFERENCE ON ENGINEERING AND NATURAL SCIENCE October 22-26 2025 Sarajevo

The evaluation of the effects of repair/strengthening methods on the seismic performance of a reinforced concrete bridge with structural deficiencies

Muhammed AKGÜL[1], Barış GÜNEŞ[1], Necati DOGAN[1], Ali EROL[1], Barış SAYIN[1],*

Abstract

Bridges play strategic roles in security, defence, and post-disaster emergency response processes, and play a critical role in socio-economic recovery. Their direct access to vital facilities such as hospitals, emergency centres, ports, and airports without alternative routes necessitates the examination of the seismic performance of these structures and their retrofitting when necessary. In this study, the seismic behaviour of a bridge with a reinforced concrete structural system on Istanbul's critical transportation networks was evaluated within the framework of the TBSDC 2020 regulation, considering the structure-soil-pile interaction (excluding kinematic interaction). The bridge was analysed in a computer environment using a three-dimensional finite element model, and a nonlinear history analysis was applied. Seven different earthquake records compatible with the structure's spectrum were selected and applied in both directions. In the studies conducted using the design and evaluation approach based on deformation, it was determined that the bridge met the 'Limited Damage' targets for the DD-2a earthquake level (75% exceedance probability in 100 years, 144-year recurrence period) and 'Controlled Damage' for the DD-1 earthquake level (2% probability of exceedance in 50 years, 2475-year recurrence period). The results revealed that the bridge did not meet the performance criteria in its current state and required retrofitting to meet these criteria. Within this scope, the elastomeric bearings were renewed, elastomeric pads were added in front of the seismic dampers, and the middle pier columns and foundations were retrofitted with jacketing. A re-analysis showed that the reinforced bridge achieved the targeted performance levels. The study contributes to the literature by evaluating the seismic performance of bridge-type reinforced concrete structures and developing retrofitting approaches for these structures.

Keywords: Seismic Performance Assessment, Reinforced Concrete Bridges, Nonlinear Time History Analysis, Retrofitting Strategies.

1. INTRODUCTION

Bridges are key components of highway transportation networks, ensuring the continuity of mobility after earthquakes. In seismically active regions such as Türkiye, assessing the seismic performance of these structures is of great importance. Many existing bridges, however, were constructed before performance-based seismic design principles became standard practice. Therefore, evaluating their behavior under earthquake loading is essential for ensuring both structural safety and serviceability. In recent years, several analytical and experimental studies have focused on the seismic performance and retrofitting of existing bridges.

Reference [1] proposed theoretical approaches and strengthening strategies to enhance the seismic resistance and performance of reinforced concrete bridges with low reinforcement ratios. Their proposed method effectively dissipated seismic energy and reduced structural deformations, leading to a significant improvement in the overall seismic resilience of bridges. Reference [2] developed a strengthening approach based on the staged application of Ultra-High-Performance Concrete (UHPC) to mitigate the adverse effects of corrosion in bridge piers. Semi-static laboratory tests were conducted on five pier specimens to measure their load-carrying capacity and deformation performance. Additionally, five finite element models were developed to analyze the interface behavior between corroded and retrofitted sections and to evaluate the nonlinear shear response of the specimens numerically. Reference [3] conducted a comprehensive review of recent

[1] Istanbul University-Cerrahpasa, Department of Environmental Engineering, 34320, Avcılar/İstanbul, Turkey. muhammed.akgul@iüc.edu.tr

[*] Corresponding author: Istanbul University-Cerrahpasa, Department of Environmental Engineering, 34320, Avcılar/İstanbul, Turkey. barsayin@iuc.edu.tr

technologies related to the seismic assessment and retrofitting of existing reinforced concrete bridges. The study evaluated two case studies of existing bridges located in Croatia. The first case focused on the planning and implementation process of the retrofitting method, while the second addressed rapid assessment and temporary strengthening solutions. Reference [4] conducted a comprehensive displacement-based seismic performance assessment of steel truss bridges. In the first phase of the study, simplified analytical formulations were used to estimate the displacement performance of the steel support towers that form the bridge substructure. In the second phase, nonlinear time-history analyses were performed to validate the accuracy of the simplified approach. Reference [5] conducted a comprehensive performance assessment to evaluate the seismic fragility of a multi-span reinforced concrete bridge before and after retrofitting. The seismic response of the bridge was analyzed using Inelastic Pushover Analysis and Incremental Dynamic Analysis (IDA) methods.

In this study, the seismic behavior of a reinforced concrete bridge located on one of Istanbul's critical transportation networks was evaluated in accordance with the Turkish Bridge Earthquake Code (TBSDC-2020) [6].

2. MATERIAL AND METHODS

2.1. The Examining Building

The examined structure is a four-span bridge with spans of varying lengths. The superstructure consists of a prestressed concrete box-girder system that provides the primary load-bearing capacity. Sidewalks are placed along both edges of the bridge deck, which remains continuous over the intermediate supports and includes expansion joints only at the end abutments. The box-girder system is supported by neoprene bearings located on each support. The abutments are composed of wing walls and end walls and are supported by columns and cap beams to ensure structural stability. The technical properties of the bridge are summarized in Table 1.

Table 1. Properties of the structural members

Item	Dimension / Unit	Remarks
Total spans	4	Varying lengths
Longest span	17.18 m	Central span
Span lengths	12.08 / 16.88 / 17.18 / 12.32 m	According to the plan axes
Girder depth	0.95 m	Prestressed concrete box girder
Deck width	12.18–18.03 m	Variable width
Bearing type	Neoprene	At the end and intermediate supports
Sidewalks	1.24–2.43 m	Both edges of the deck
Abutment column	Ø65 cm	Reinforced concrete
Cap beam	125×80 cm	Rectangular section
Wing wall thickness	40 cm	Reinforced concrete
End wall thickness	25 cm	Reinforced concrete

2.2. Strengthening Proposals

The existing supports on the middle legs were removed and replaced with pot supports. The elastomeric bearings at the bridge abutments were replaced with larger-section elastomeric bearings. Conventional enlargement works were carried out in front of the seismic stoppers at the abutments, and elastomeric pads were installed to eliminate gaps between the deck and the abutments. The middle pier columns were strengthened using reinforced concrete jacketing, with longitudinal and transverse reinforcements arranged in the jacket regions. Reinforced concrete infill walls were added between the abutment columns to increase lateral stiffness. The foundations of both the abutments and piers were thickened and extended to enhance their load-bearing capacity. All newly constructed strengthening elements were designed using C35/45 class concrete and B420C grade reinforcing steel.

2.3. Material Examination

Concrete compression tests revealed an average unconfined cylindrical concrete compressive strength of 42.01 MPa and an elastic modulus of 35000 MPa for the bridge's load-bearing elements. Reinforcement tensile tests revealed a yield strength of 420 MPa for the steel.

2.4. Soil and Earthquake Parameters

The soil and seismic hazard parameters for the project site were identified through the Turkey Earthquake Hazard Map Interactive Web Tool provided by AFAD, and the corresponding values are presented in Table 2 [7].

Table 2. Soil Class and Earthquake Parameters

Parameter	Value / Class
Local soil class	ZC
Earthquake ground motion level	DD-1, DD-2, DD-3
Spectral acceleration coefficients from the Earthquake Hazard Map (g)	DD-1, Ss = 2.001, S1 = 0.561 DD-2, Ss = 1.150, S1 = 0.315 DD-3, Ss = 0.433, S1 = 0.115
Peak ground acceleration (g)	DD-1, PGA = 0.788 DD-2, PGA = 0.473 DD-3, PGA = 0.186
Local site effect coefficients	DD-1, Fs = 1.200, F1 = 1.439 DD-2, Fs = 1.200, F1 = 1.500 DD-3, Fs = 1.300, F1 = 1.500
Spectral Acceleration Coefficients	DD-1, SDS = 2.401, SD1 = 0.807 DD-2, SDS = 1.380, SD1 = 0.472 DD-3, SDS = 0.563, SD1 = 0.172

2.5. Performance Analysis

A model that accurately represents the current condition of the building was prepared with utmost precision using the Midas Gen finite element software [8]. The abutment walls, deck, and foundations were modeled using shell finite elements ("plate" elements) that account for both in-plane and out-of-plane degrees of freedom. The bridge pier columns, abutment cap beams, end walls, and abutment columns were modeled using frame elements ("beam/column" elements). The 3D static analysis model of the building is given in Figure 1.

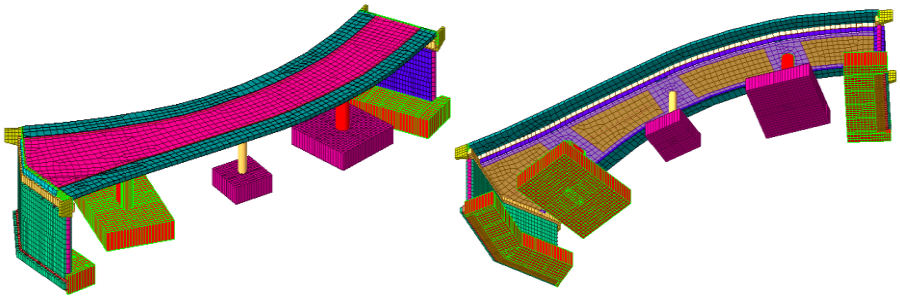

Fig. 1: 3D Static Analysis Model of the Buildings

2.6. Performance Assessment Method

The assessment of the building under static and earthquake loads was conducted in accordance with the Turkish Bridge Seismic Design Code (TBSDC-2020) [6]. The classification of the structure, target performance levels, required analyses, and design/assessment methods is summarized in Table 3.

Table 3. Performance-Based Analysis and Design Method.

Parameter	Value / Class
Bridge Type	Standard Highway Bridge
Bridge Importance Class (BIC)	Important Bridge, BIC = 1
Type of Structural System	Critical
Earthquake Design Class (EDC)	1
Local Soil Class	ZC
Bridge Performance Target	Stage I: Limited Damage for DD-2a Stage II: Controlled Damage for DD-1
Design / Assessment Method	Stage I: Method 2.3, Nonlinear Time History Analysis (NTHA), Evaluation Based on Deformation Stage II: Method 2.3, Nonlinear Time History Analysis (NTHA), Evaluation Based on Deformation

2.7. Design Elastic Spectrum

Figure 2 shows the building's response spectrum and spectral acceleration values for the DD-2a and DD-1 earthquake levels.

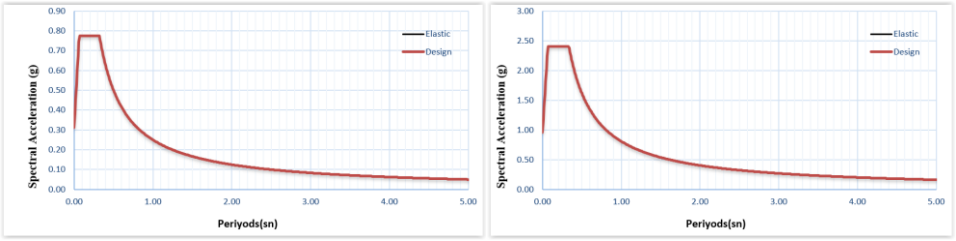

Fig. 2 Response Spectrum and Spectral Acceleration Values for the DD-2a and DD-1 Earthquake Level (R = 1, D = 1).

2.8. Selection and Scaling of Earthquake Records

The structure is situated approximately 13 km from the nearest active fault, as illustrated in Figure 3. Seven ground motion records were selected from the PEER database (2023) based on source mechanism, fault distance, and soil conditions; their summary properties are listed in Table 4 [9].

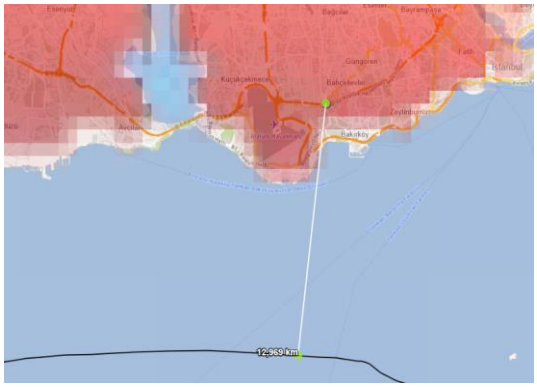

Fig. 3 Distance to active fault.

Table 4. Summary information of selected earthquake records

Record No	Earthquake Year	Earthquake Name	Station	Magnitude	Vs30 (m/s)
01	1990	Manjil, Iran	Abbar	6.95	213.44
02	1999	Hector Mine	Hector	7.13	726.00
03	1979	Imperial Valley-06	El Centro Array	6.53	196.25
04	1999	Kocaeli, Turkey	Duzce	7.51	281.86
05	1994	Northridge-01	Beverly Hills	6.69	545.66
06	1992	Landers	Coolwater	7.28	352.98
07	1999	Duzce, Turkey	Bolu	7.14	293.57

The records were spectrally matched to the (TBSDC-2020) target acceleration spectra using SeismoMatch, and the comparison between the scaled and target spectra is illustrated in Figure 4 [6], [10].

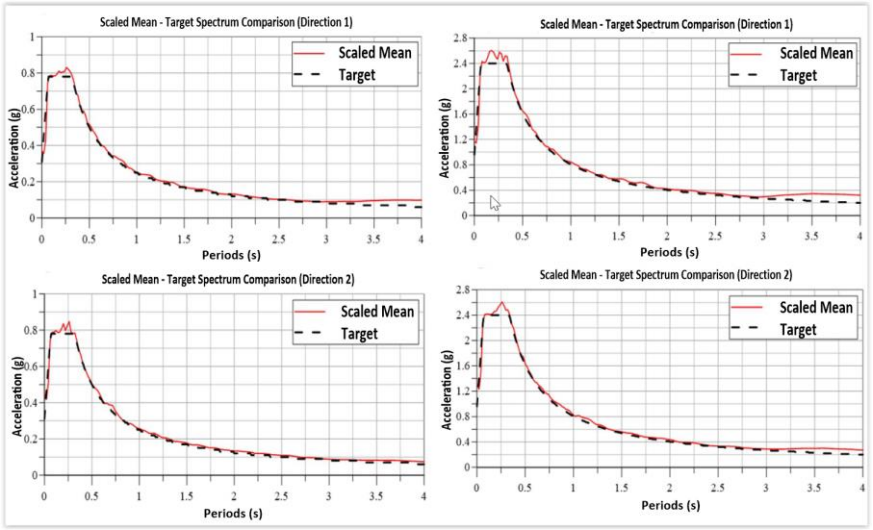

Fig. 4 Average spectrum – target spectrum comparisons for the DD-2a and DD-1 Earthquake Level (Left: DD-2a; Right: DD-1).

3. RESULTS

3.1. Modal Analysis

The outcomes of the modal analysis are summarized in Table 5. The fundamental natural period of the structure was calculated to be 0.435 seconds. In both principal directions, the cumulative mass participation ratios attained approximately 95%, thereby fulfilling the criteria specified in the applicable seismic design code.

Table 5. Results of the modal analysis

Mode	Direction	Period (s)
1	X	0.435
2	Y	0.335
3	Z	0.176

3.2. Nonlinear Dynamic Analysis (Stage 1)

The lateral displacement response of the reinforced concrete bridge corresponding to the DD-2a earthquake ground motion level is illustrated in Figure 5. The maximum horizontal displacement was obtained as approximately 33 mm in the negative Y-direction.

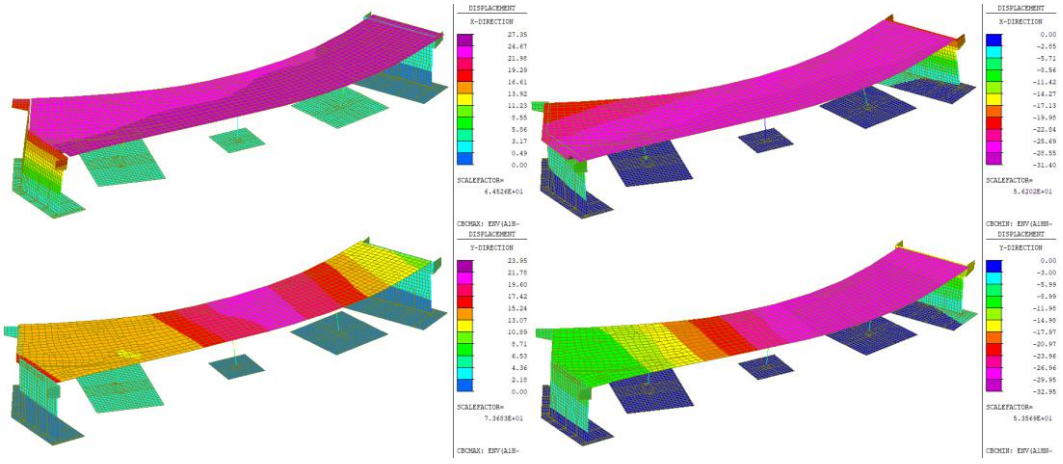

Fig. 5 Displacements in reinforced concrete under the DD-2a earthquake ground motion (Top: X direction; Bottom: Y direction).

Figure 6 presents the shear forces and displacements developed in the middle pier columns under Stage I earthquake effects. As summarized in Table 6, the deformation and shear criteria for the middle pier columns were confidently satisfied under the Stage I earthquake effects.

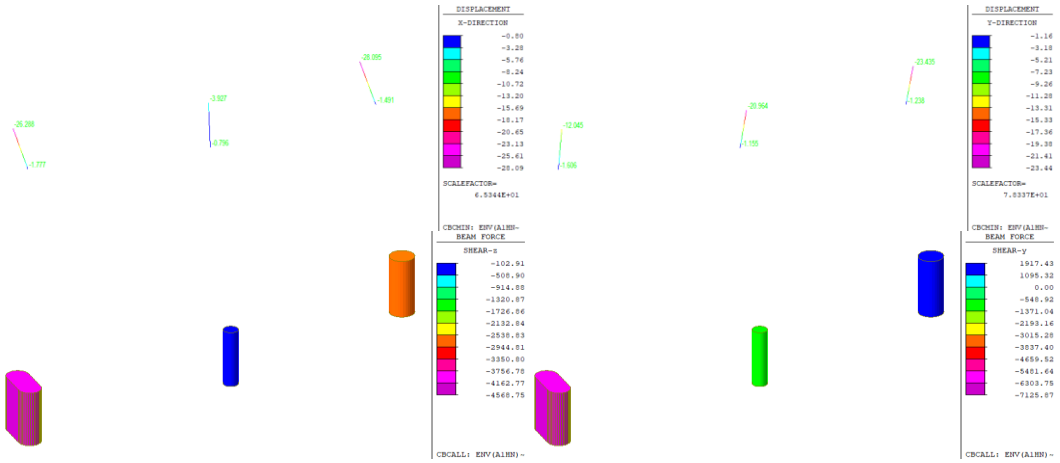

Fig. 6 Shear Forces and Displacements Generated in the middle pier columns Seismic Effects. (DD-2a).

Table 6. The deformation and shear criteria for the middle pier columns. (DD-2a)

Structural Element	Deformation Check	Shear Verification	Result
Pier at Axis 1	√	√	√
Pier at Axis 2	√	√	√
Pier at Axis 3	√	√	√

3.3. Nonlinear Dynamic Analysis (Stage 2)

The lateral displacement response of the reinforced concrete bridge corresponding to the DD-1 earthquake ground motion level is illustrated in Figure 7. The peak lateral displacement reached nearly 74 mm in the negative Y direction.

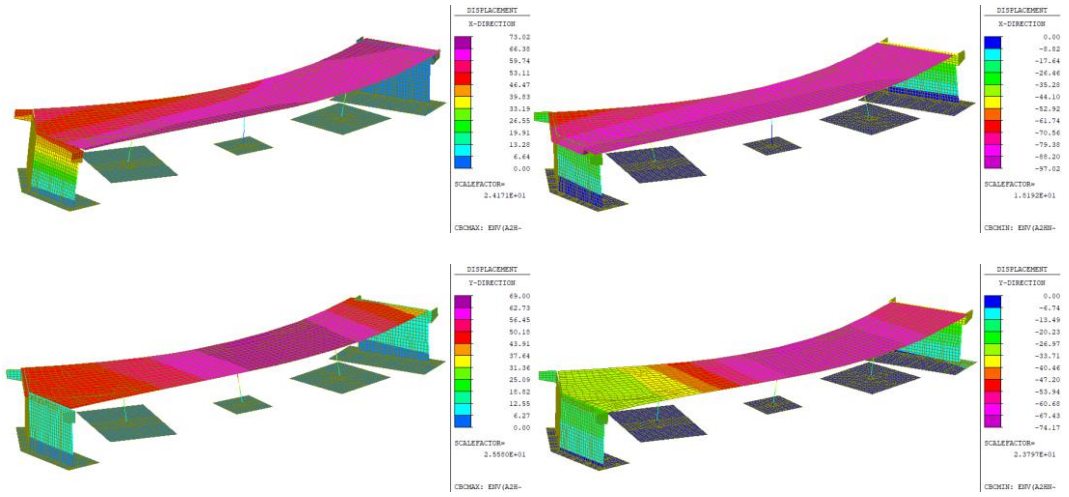

Fig. 7 Displacements in reinforced concrete under the DD-1 earthquake ground motion (Top: X direction; Bottom: Y direction).

Figure 8 illustrates the shear force and displacement responses of the middle pier columns under the Stage II earthquake scenario. As indicated in Table 7, both the deformation and shear capacity requirements of these columns were found to be adequately met with the given seismic demand.

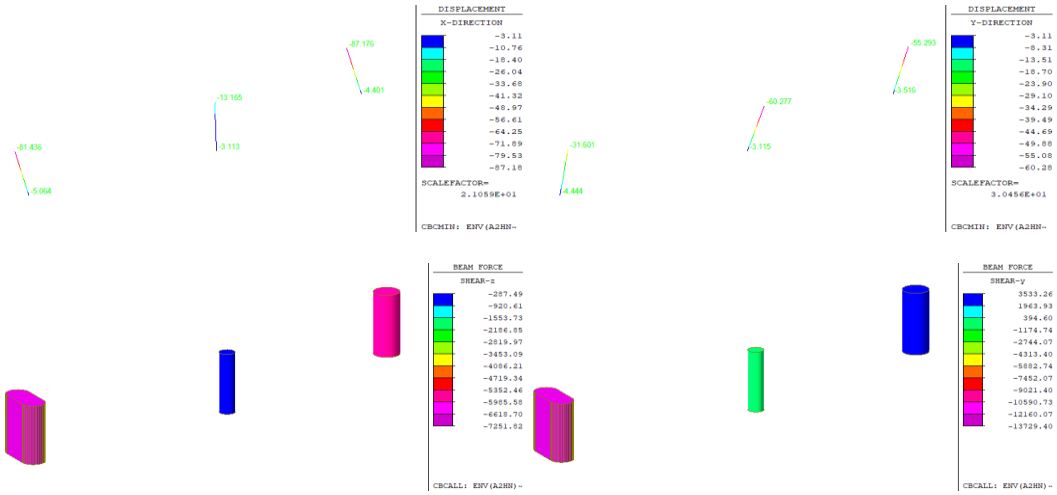

Fig. 8 Shear Forces and Displacements Generated in the middle pier columns Seismic Effects. (DD-1).

Table 7. The deformation and shear criteria for the middle pier columns. (DD-1)

Structural Element	Deformation Check	Shear Verification	Result
Pier at Axis 1	√	√	√
Pier at Axis 2	√	√	√
Pier at Axis 3	√	√	√

4. CONCLUSION

In this study, the structural system characteristics, material properties, and geotechnical conditions of the bridge were examined using available documentation and field data. Subsequently, the seismic performance of the retrofitted bridge was evaluated in accordance with the Turkish Bridge Earthquake Code (TBSDC-2020) [6]. Through the Stage I and Stage II dynamic analyses, it was determined whether the retrofitted structure achieved the intended seismic performance level.

- The analysis results show that the structure meets the 'Limited Damage' performance target at the DD-2a earthquake level.
- According to the analysis results, the retrofitted structure achieved the Controlled Damage performance level when subjected to the DD-1 design earthquake.
- It was concluded that the retrofitted structural elements satisfied the deformation and shear capacity requirements specified by the design code.

REFERENCES

[1] Y. Cheng, Z. Hu, J. Wang, and W. Xie, "Theoretical solutions and retrofitting design methods for enhancing seismic performance and resilience of existing RC multi-column bridge bents with low reinforcement ratios," Structures, vol. 82, p. 110612, Dec. 2025.
[2] J. Su, J. Li, S. Chu, D. Wu, J. Ma, and Z. X. Li, "Assessment of seismic performance for ultra-high performance concrete (UHPC) retrofitted RC bridge piers with height-varying corrosion: A lifetime perspective," Engineering Structures, vol. 339, p. 120693, 2025.
[3] D. Skokandić, A. Vlašić, M. Kušter Marić, M. Srbić, and A. Mandić Ivanković, "Seismic assessment and retrofitting of existing road bridges: State of the art review," Materials, vol. 15, no. 7, p. 2523, 2022.
[4] Nettis, P. Iacovazzo, D. Raffaele, G. Uva, and J. M. Adam, "Displacement-based seismic performance assessment of multi-span steel truss bridges," Engineering Structures, vol. 254, p. 113832, 2022.
[5] H. Ghazal and A. Mwafy, "Seismic fragility assessment of an existing multi-span RC bridge equipped with risk mitigation systems," Buildings, vol. 12, no. 7, p. 982, 2022.
[6] Turkish Bridge Seismic Design Code, Republic of Turkey Ministry of Transport and Infrastructure, Ankara, Turkey, 2020.
[7] (2019) AFAD Turkey Earthquake Risk Map Interactive Web Application. [Online]. Available:https://tdth.afad.gov.tr/
[8] MIDAS Gen: Integrated Solution System for Building and General Structures, MIDAS Information Technology Co., 2018.
[9] PEER Ground Motion Database. Pacific Earthquake Engineering Research Center (PEER), University of California, Berkeley, CA, USA. [Online]. Available: https://ngawest2.berkeley.edu
[10] SeismoMatch – A Computer Program for Spectrum Matching of Earthquake Records, Seismosoft, Pavia, Italy, 2022

ICENS 11TH INTERNATIONAL CONFERENCE ON ENGINEERING AND NATURAL SCIENCE October 22-26 2025 Sarajevo

The seismic performance assessment of reinforced-concrete bridges with pile foundation, using a nonlinear time-history analysis and deformation-based method

Barış GÜNEŞ[1], Muhammed AKGÜL[1], Ali EROL[1], Necati DOGAN[1], Barış SAYIN[1*],

Abstract

Bridges are a fundamental component of transportation networks worldwide. Due to their location, bridges ensure transportation continuity and make significant socio-economic contributions to regional development. The uninterrupted continuation of transportation during emergency response processes following earthquakes and similar disasters further increases the critical importance of bridges. Therefore, it is necessary to examine the behavior of bridges under seismic effects and to address any identified deficiencies with appropriate retrofitting methods. In this study, the seismic performance of a reinforced concrete bridge on Istanbul's major transportation networks was evaluated within the framework of the Principles for the Design of Highway and Railway Bridges and Viaducts Under Earthquake Effects (TBSDC-2020) regulation, considering the structure-ground-pile interaction (excluding kinematic interaction). A three-dimensional analytical model of the structure was created in a computer environment, and nonlinear time history analyses were performed using the finite element method. Seven different earthquake records compatible with the spectrum were selected in this context. The Design and Evaluation Based on Deformation (ŞGDT) method was adopted as the design approach. As a result of the analyses, it was determined that the bridge could not achieve the targeted 'Limited Damage' performance at the DD-2a earthquake level (75% probability of exceedance in 100 years, recurrence period 144 years) and the anticipated 'Controlled Damage' performance at the DD-1 earthquake level (2% probability of exceedance in 50 years, recurrence period 2475 years). This finding reveals that the bridge does not meet the target performance levels in its current state and that appropriate retrofitting measures are required from a static perspective. The study aims to contribute to the literature on modeling bridge structures using the finite element method and performing nonlinear performance analyses that consider the structure-soil-pile interaction (excluding kinematic interaction).

Keywords: Seismic Performance Assessment, Reinforced Concrete Bridges, Nonlinear Time History Analysis, Structure–Soil–Pile Interaction.

1. INTRODUCTION

Accurate assessment of bridge behavior under seismic loading is crucial for predicting potential damage mechanisms and developing appropriate retrofitting strategies. In pile-supported bridges, the complex interaction between the superstructure, piles, and surrounding soil makes it challenging to accurately represent the seismic response of the structure. Consequently, numerous experimental studies, analytical approaches, and advanced numerical models have been proposed in recent years to enhance the understanding of the seismic behavior of pile-supported bridge systems.

Reference [1] developed a simplified analytical model with six degrees of freedom to investigate the seismic behavior of single-pier bridges considering the soil–pile–structure interaction. The nonlinear dynamic response of the model was evaluated through time-history analyses using three different earthquake records. The acceleration responses obtained from the analytical model were compared with the measured accelerations, allowing the authors to assess the model's ability to represent the seismic behavior of the bridge system. Reference [2] investigated the seismic response of a cable-supported bridge with a 1400 m main span under near-fault and far-field ground motions, considering soil–pile–structure interaction

[1] Istanbul University-Cerrahpasa, Department of Environmental Engineering, 34320, Avcılar/İstanbul, Turkey. bgunes@iuc.edu.tr

[*] Corresponding author: Istanbul University-Cerrahpasa, Department of Environmental Engineering, 34320, Avcılar/İstanbul, Turkey. barsayin@iuc.edu.tr

effects. A 1/70-scale physical model of the bridge was tested on a shaking table to determine its dynamic characteristics, and these experimental results were used to develop a three-dimensional analytical model in OpenSees [3]. Based on the analytical and experimental findings, the authors proposed several control strategies aimed at mitigating the adverse effects of near-fault ground motions on the bridge system. Reference [4] employed seismic fragility analysis to investigate the behavior of soil–pile–structure interaction (SPSI) systems subjected to earthquake loading. Nonlinear pushover analyses were performed for various soil conditions and pile properties, and the resulting capacity curves were used to construct corresponding fragility functions. Based on their findings, the authors proposed a practical equation that may assist engineers in evaluating SPSI effects within seismic design frameworks. Reference [5] investigated the dynamic response of a pile-supported bridge pier by considering not only seismic excitation but also wave and current effects. A scaled pier model was tested in the laboratory using the Realistic Water–Structure–Earthquake Interaction Test (RWSEIT), and the experimental observations were validated through comparisons with a three-dimensional finite element model. The study offers valuable insights into the complex fluid–structure–seismic interactions that affect pile-supported coastal bridges.

In this study, the seismic performance of a reinforced concrete bridge located on one of Istanbul's primary transportation corridors was assessed in accordance with the Principles for the Design of Highway and Railway Bridges and Viaducts Under Earthquake Effects (TBSDC-2020) [6]. The evaluation was carried out by explicitly accounting for the interaction between the structure, the supporting piles, and the surrounding ground, while excluding kinematic interaction effects.

2. MATERIAL AND METHODS

2.1. The Examining Building

The bridge has regular geometry and consists of four spans with varying lengths. The superstructure is a prestressed concrete box girder system with a deck width ranging between 12.5 and 12.8 meters, accommodating three traffic lanes. The deck includes expansion joints only at the abutments, while it remains continuous over the intermediate supports. The bridge is supported by pot bearings—larger ones at the piers and smaller ones at the abutments. The abutments include front, wing, and end walls with varying thicknesses. The technical properties of the bridge are summarized in Table 1.

Table 1. Technical Specifications of the Bridge

Item	Dimension / Unit	Remarks
Total spans	4	Regular geometry
Span lengths	26.83 / 34.55 / 34.44 / 27.41 m	Measured along the bottom edge axes
Deck width	12.46–12.80 m	Three traffic lanes
Girder type	Prestressed box girder	Continuous except at end joints
Bearing type	Pot bearings (Ø400 mm ends, Ø1000–1100 mm piers)	Total height 75–150 mm
Abutment walls	Front: 40 cm / Wing: 60 cm / End: 30 cm	Reinforced concrete

2.2. Material Examination

Material testing results indicated that the average unconfined compressive strength of the cylindrical concrete specimens was 34.99 MPa. In comparison, the corresponding elastic modulus was approximately 33,000 MPa for the bridge's primary load-bearing elements. Additionally, reinforcement tensile tests yielded an average steel yield strength of 420 MPa.

2.3. Soil and Earthquake Parameters

The geotechnical and seismic parameters of the project site were determined using the Turkey Earthquake Hazard Map Interactive Web Application developed by the Disaster and Emergency Management Authority (AFAD) [7]. The obtained seismic hazard values are summarized in Table 2.

Table 2. Soil Class and Earthquake Parameters

Parameter	Value / Class
Local soil class	ZC
Earthquake ground motion level	DD-1, DD-2, DD-3
Spectral acceleration coefficients from the Earthquake Hazard Map (g)	DD-1, Ss = 1.711, S1 = 0.480 DD-2, Ss = 0.982, S1 = 0.272 DD-3, Ss = 0.381, S1 = 0.105
Peak ground acceleration (g)	DD-1, PGA = 0.679 DD-2, PGA = 0.403 DD-3, PGA = 0.166

Local site effect coefficients	DD-1, Fs = 1.200, F1 = 1.500 DD-2, Fs = 1.200, F1 = 1.500 DD-3, Fs = 1.300, F1 = 1.500
Spectral Acceleration Coefficients	DD-1, SDS = 2.053, SD1 = 0.720 DD-2, SDS = 1.178, SD1 = 0.408 DD-3, SDS = 0.495, SD1 = 0.157

2.4. Performance Analysis

A numerical model accurately representing the existing condition of the bridge was developed using the Midas Gen finite element software [8]. In this model, the abutment walls, deck slab, and foundation system were discretized with shell (plate-type) finite elements, which capture both in-plane and out-of-plane behaviors. The pier columns, cap beams, end walls, and abutment columns were represented by frame (beam-column) elements to simulate their flexural and axial responses. The three-dimensional static analysis model of the bridge is illustrated in Figure 1.

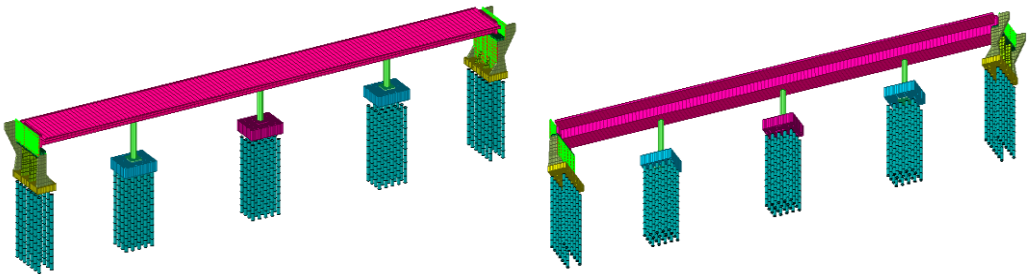

Fig. 1: 3D Static Analysis Model of the Buildings

2.5. Performance Assessment Method

The bridge was analyzed under static and earthquake effects in compliance with the Turkish Bridge Seismic Design Code (TBSDC-2020) [6]. The corresponding structural classification, performance objectives, and analysis and evaluation methodologies defined by the code are outlined in Table 3.

Table 3. Performance-Based Analysis and Design Method.

Parameter	Value / Class
Bridge Type	Standard Highway Bridge
Bridge Importance Class (BIC)	Important Bridge, BIC = 1
Type of Structural System	Non-Critical
Earthquake Design Class (EDC)	1
Local Soil Class	ZC
Bridge Performance Target	Stage I: Limited Damage for DD-2a Stage II: Controlled Damage for DD-1
Design / Assessment Method	Stage I: Method 2.3, Nonlinear Time History Analysis (NTHA), Evaluation Based on Deformation Stage II: Method 2.3, Nonlinear Time History Analysis (NTHA), Evaluation Based on Deformation

2.6. Design Elastic Spectrum

Figure 2 shows the building's response spectrum and spectral acceleration values for the DD-2a and DD-1 earthquake levels.

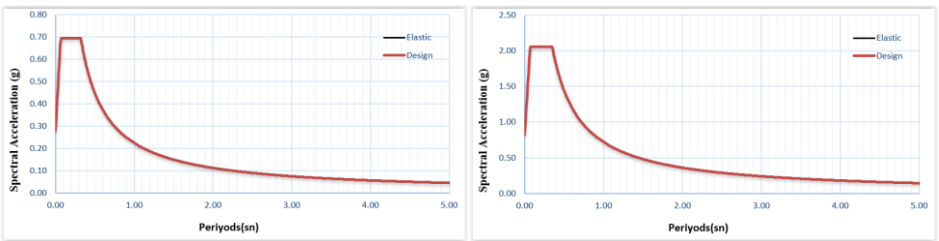

Fig. 2 Response Spectrum and Spectral Acceleration Values for the DD-2a and DD-1 Earthquake Level (R = 1, D = 1).

2.7. Selection and Scaling of Earthquake Records

The site is located nearly 16.4 km from the closest active fault, as presented in Figure 3. To represent potential seismic scenarios, seven earthquake ground motion records were selected from the PEER Ground Motion Database (2023), considering the seismogenic source type, fault distance, and site classification [9]. The summary parameters of these records are provided in Table 4 [9].

Fig. 3 Distance to active fault.

Table 4. Summary information of selected earthquake records

Record No	Earthquake Year	Earthquake Name	Station	Magnitude	Vs30 (m/s)
01	1990	Manjil, Iran	Abbar	6.95	213.44
02	1999	Hector Mine	Hector	7.13	726.00
03	1979	Imperial Valley-06	El Centro Array	6.53	196.25
04	1999	Chi-Chi_ Taiwan	TCU045	7.62	704.64
05	1994	Northridge-01	Beverly Hills	6.69	545.66
06	1992	Landers	Coolwater	7.28	352.98
07	1999	Duzce, Turkey	Bolu	7.14	293.57

The ground motion records were spectrally adjusted to conform to the TBSDC (2020) target acceleration spectrum using SeismoMatch. The correspondence between the scaled spectra and the target spectrum is presented in Figure 4 [6], [10].

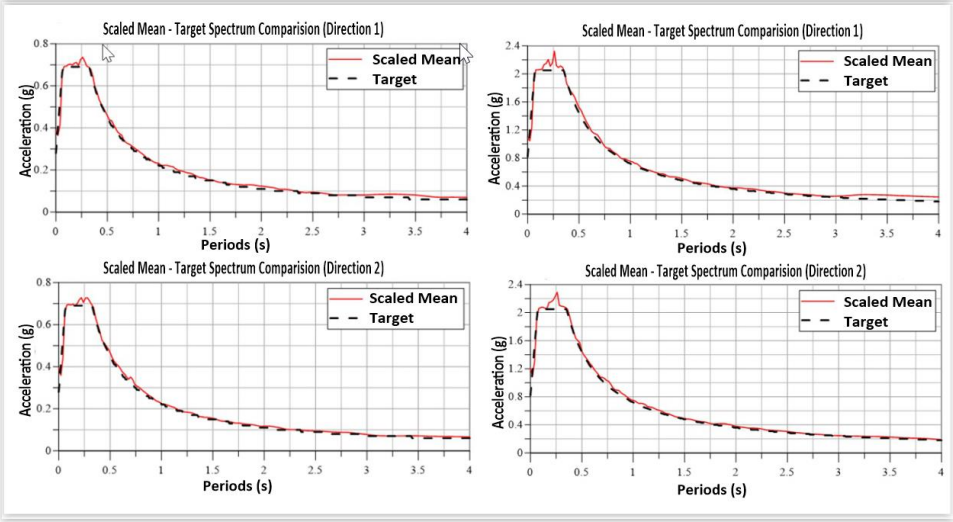

Fig. 4 Average spectrum – target spectrum comparisons for the DD-2a and DD-1 Earthquake Level (Left: DD-2a; Right: DD-1).

3. RESULTS

3.1. Modal Analysis

As summarized in Table 5, the fundamental vibration period of the bridge was determined as 0.639 seconds. The cumulative mass participation ratios in both principal axes exceeded 95%, indicating compliance with the minimum participation criteria defined in the governing seismic code.

Table 5. Results of the modal analysis

Mode	Direction	Period (s)
1	Y	0.639
2	X	0.436
3	Z	0.282

3.2. Nonlinear Dynamic Analysis (Stage 1)

As shown in Figure 5, the reinforced concrete bridge exhibited a maximum lateral displacement of about 40 mm in the negative Y-direction when subjected to the DD-2a earthquake ground motion level.

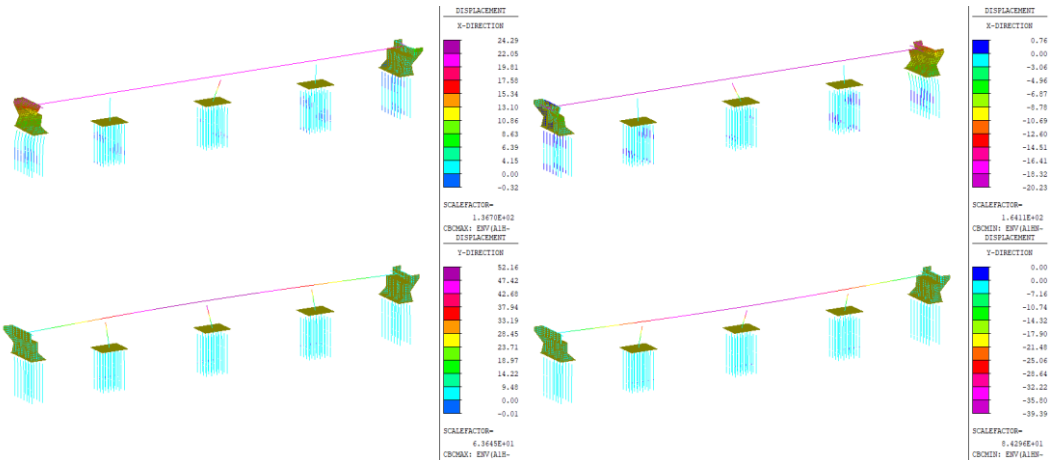

Fig. 5 Displacements in reinforced concrete under the DD-2a earthquake ground motion (Top: X direction; Bottom: Y direction).

As shown in Figure 6, the middle pier columns experienced shear forces and displacement responses associated with the Stage I earthquake effects. The evaluation results, presented in Table 6, confirm that both deformation and shear performance requirements of the columns were met in compliance with the relevant design criteria.

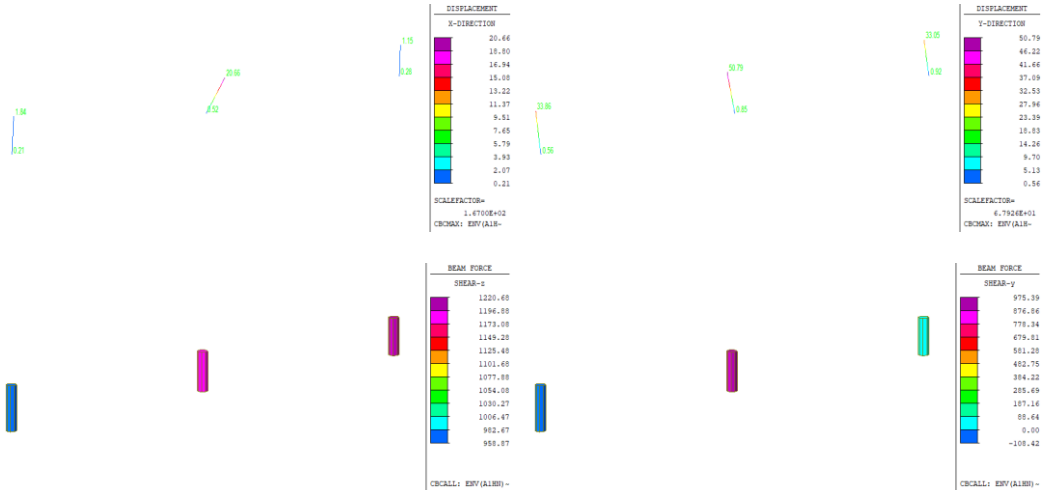

Fig. 6 Shear Forces and Displacements Generated in the middle pier columns Seismic Effects. (DD-2a).

Table 6. The deformation and shear criteria for the middle pier columns. (DD-2a)

Structural Element	Deformation Check	Shear Verification	Result
Pier at Axis 1	√	√	√
Pier at Axis 2	√	√	√
Pier at Axis 3	√	√	√

As seen in Figure 7, the axial forces in the piles under Stage I earthquake effects were examined, and the bearing capacity checks were performed for Soil Profile-1. The final design/internal forces were obtained by averaging the maximum and minimum effects from all earthquake records, as specified in TBSDC-2020 [6]. Under seismic effects, the maximum

compressive and tensile forces in the piles were determined to be 2650 kN and 1100 kN, respectively. The analysis results indicate that the piles possess adequate bearing capacity under the effects of the Stage I earthquake. (DD-2a)

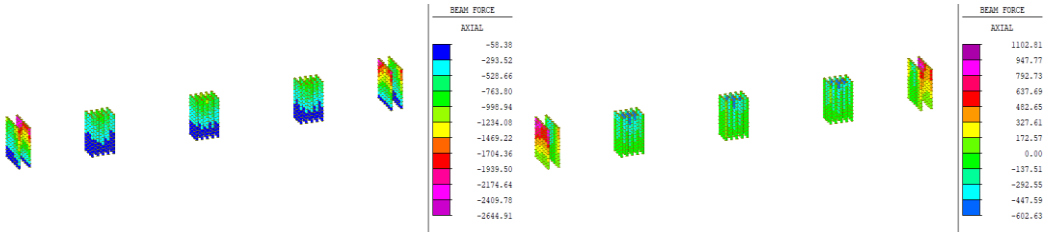

Fig. 7 Axial Forces Generated in the piles Under Seismic Effects (Left: X direction; Right: Y direction),(DD-2a).

3.3. Nonlinear Dynamic Analysis (Stage 2)

As shown in Figure 8, the reinforced concrete bridge exhibited a maximum lateral displacement of about 144 mm in the positive Y-direction when subjected to the DD-1 earthquake ground motion level.

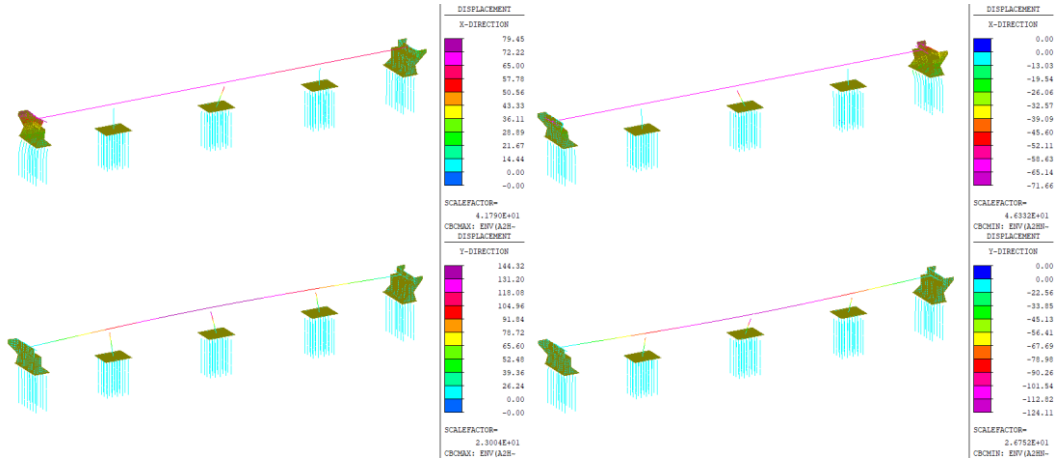

Fig. 8 Displacements in reinforced concrete under the DD-1 earthquake ground motion (Top: X direction; Bottom: Y direction).

Figure 9 presents the shear forces and displacements developed in the middle pier columns under Stage II earthquake effects. As summarized in Table 7, the deformation for the middle pier columns wasn't satisfied, but the shear criteria for the middle pier columns were satisfied under the Stage II earthquake effects.

Fig. 9 Shear Forces and Displacements Generated in the middle pier columns Seismic Effects. (DD-1).

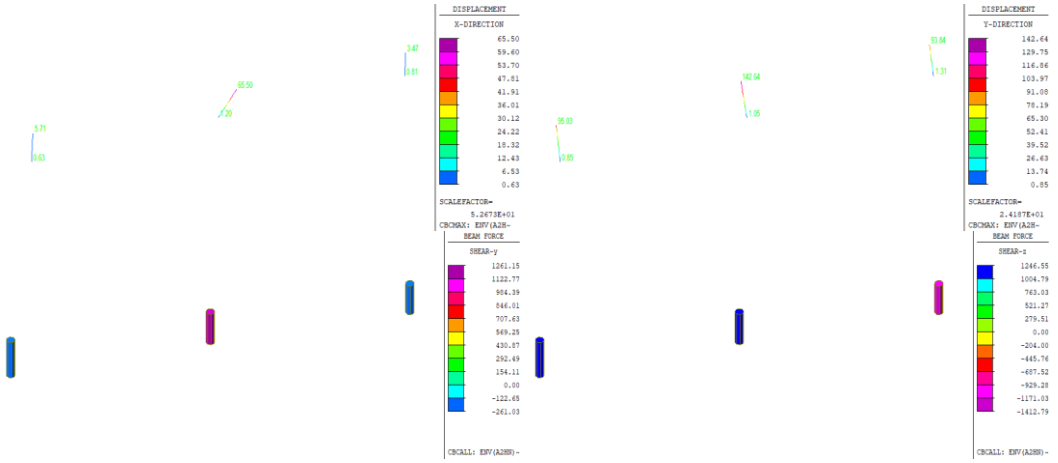

Table 7. The deformation and shear criteria for the middle pier columns. (DD-1)

Structural Element	Deformation Check	Shear Verification	Result
Pier at Axis 1	X	√	X
Pier at Axis 2	X	√	X
Pier at Axis 3	X	√	X

As seen in Figure 10, the axial forces in the piles under Stage II earthquake effects were examined, and the bearing capacity checks were performed for Soil Profile-1. The final design/internal forces were obtained by averaging the maximum and minimum effects from all earthquake records, as specified in TBSDC-2020 [6]. Under seismic effects, the maximum compressive and tensile forces in the piles were determined to be 4200 kN and 2900 kN, respectively. The analysis results indicate that the piles have an inadequate bearing capacity under the effects of the Stage II earthquake. (DD-1)

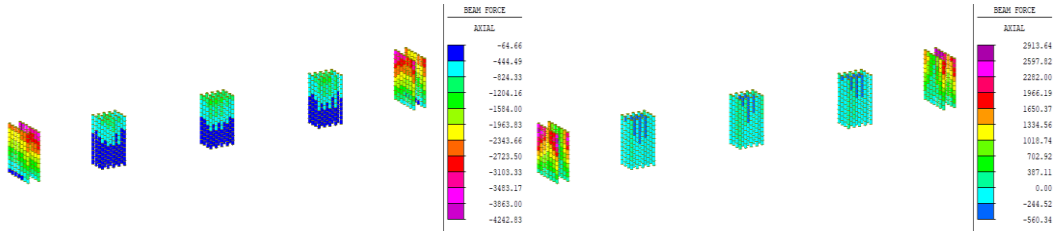

Fig. 10 Axial Forces Generated in the piles Under Seismic Effects (Left: X direction; Right: Y direction),(DD-1).

4. CONCLUSION

The structural configuration, material properties, and geotechnical characteristics of the bridge were analyzed using available records and site investigation data. The seismic performance assessment was performed in compliance with the Turkish Bridge Earthquake Code (TBSDC, 2020) [6]. The outcomes of the Stage I and Stage II dynamic analyses indicated that the structure failed to achieve the desired seismic performance level prescribed by the code.

- It was determined that the bridge could not achieve the targeted 'Limited Damage' performance at the DD-2a earthquake level and the anticipated 'Controlled Damage' performance at the DD-1 earthquake level.

- This finding reveals that the bridge does not meet the target performance levels in its current state and that appropriate retrofitting measures are required from a static perspective.

REFERENCES

[1] V. Shirgir, A. Ghanbari, and A. Massumi, "Analytical model for time history analysis of single pier bridges considering soil–pile structure interaction effects," *Applied Mathematical Modelling*, vol. 93, pp. 257–275, 2021.

[2] W. Xie and L. Sun, "Assessment and mitigation of near-fault earthquake wave effects on seismic responses and pile-soil interactions of the soil-pile-bridge model," *Soil Dynamics and Earthquake Engineering*, vol. 143, p. 106596, 2021.

[3] S. Mazzoni, F. McKenna, M. H. Scott, and G. L. Fenves, *OpenSees: Open System for Earthquake Engineering Simulation – User Command-Language Manual*, Pacific Earthquake Engineering Research Center (PEER), University of California, Berkeley, CA, USA, 2006.

[4] N. Guettafi, D. Yahiaoui, K. Abbeche, and T. Bouzid, "Numerical evaluation of soil-pile-structure interaction effects in nonlinear analysis of seismic fragility curves," *Transportation Infrastructure Geotechnology*, vol. 9, no. 2, pp. 155–172, 2022.
[5] R. Alsultani, I. R. Karim, and S. I. Khassaf, "Dynamic response analysis of coastal piled bridge pier subjected to current, wave, and earthquake actions with different structure orientations," *International Journal of Concrete Structures and Materials*, vol. 17, no. 1, p. 9, 2023.
[6] *Turkish Bridge Seismic Design Code*, Republic of Turkey Ministry of Transport and Infrastructure, Ankara, Turkey, 2020.
[7] (2019) AFAD Turkey Earthquake Risk Map Interactive Web Application. [Online]. Available:https://tdth.afad.gov.tr/
[8] *MIDAS Gen: Integrated Solution System for Building and General Structures*, MIDAS Information Technology Co., 2018.
[9] *PEER Ground* Motion Database. Pacific Earthquake Engineering Research Center (PEER), University of California, Berkeley, CA, USA. [Online]. Available: https://ngawest2.berkeley.edu
[10] SeismoMatch – A Computer Program for Spectrum Matching of Earthquake Records, Seismosoft, Pavia, Italy, 2022

ICENS 11TH INTERNATIONAL CONFERENCE ON ENGINEERING AND NATURAL SCIENCE October 22-26 2025 Sarajevo

Estimation of Optimum Insulation Thickness for the Buildings in Different Climate Zones of Turkiye

Atilla G. Devecioğlu[1], Vedat Oruç[1]*

Abstract

The application of insulation on outer walls of buildings is investigated in this study. The provinces of Istanbul, Ankara, Van and Erzurum are selected as 3rd, 4th, 5th and 6th zones, respectively in Turkiye for the investigation. The optimum insulation thickness (x_{opt}) values are computed using heating degree-day method. The extruded polystyrene (XPS) and glass wool are separately used as insulation materials in the analysis. According to the obtained results, x_{opt} of glass wool is higher compared to XPS material while the payback periods for glass wool are found to be shorter for all studied provinces. In addition, the amount of saved energy due to the application of x_{opt} increases as going from 3rd zone (Istanbul) to 6th zone (Erzurum). The saved energy is seen to be over 80% due to the presence of x_{opt}. The saved energy amount is also determined to be greater using glass wool than XPS for the presence of insulation material with optimum thickness in all studied cities. The glass wool can be suggested as a potential insulation material than XPS for these investigated provinces considering quicker payback period, higher energy savings and suitable value of overall heat transfer coefficient.

Keywords: building insulation, glass wool, HDD, optimum insulation thickness, XPS

1. INTRODUCTION

In line with the Paris Currency and the European Green Deal, building programming rules have been revised to increase technical, storage, and economic changes to support Turkiye's net-zero energy goal. According to the new building protocol introduced in Turkiye, heating energy needs will be calculated separately for cooling energy. The calculation method is based on the monthly method according to EN ISO 52016-1. This aims to reduce CO_2 by 600 million tons annually [1]. With the new regulation, the number of climate zones has been increased from 4 to 6, allowing for more sensitive insulation to regional conditions. The new regulation sets indoor design temperatures at 20°C (winter) and 26°C (summer). Hourly, monthly meteorological data, and solar radiation data have been updated according to climate zones. The new standard aims to reduce energy consumption from 120–150 kWh/m^2 to 70–90 kWh/ m^2. Furthermore, the total heat transfer coefficient of the wall (U) values of buildings have been improved, ranging from 0.25–0.45 W/m^{2}K for walls, 0.2–0.35 W/m^{2}K for roofs, and 0.25–0.40 W/m^{2}K for floors. The U-value of windows has been reduced to 1.8 W/m^{2}K, making the use of Low-E/solar glass mandatory [2].

Most of the energy is consumed in residences, public buildings and commercial buildings. Sector-based energy consumption of the last 20 years in Turkiye is shown in Figure 1. While approximately 34% of the energy consumed in Turkey in 2005 was developed in residences, public buildings and commercial buildings, this rate decreased to 32% in 2023 [3].

* Corresponding author: Department of Mechanical Engineering, Faculty of Engineering, Dicle University, Diyarbakır, Turkiye. atillad@dicle.edu.tr

[1] Department of Mechanical Engineering, Faculty of Engineering, Dicle University, Diyarbakır, Turkiye

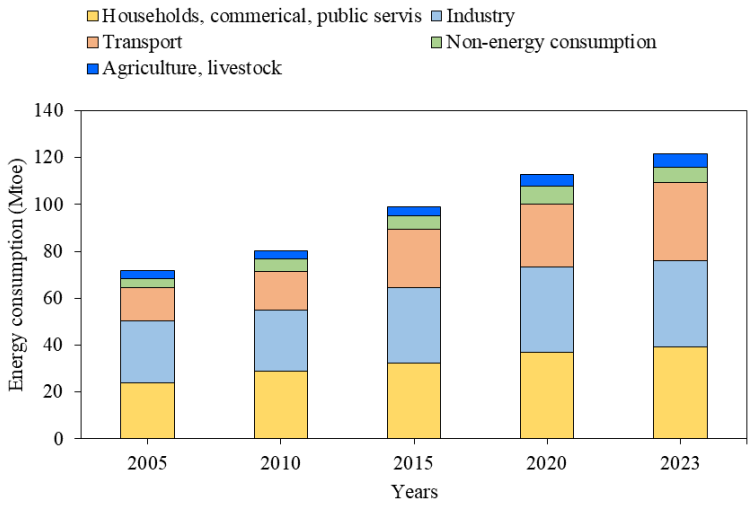

Figure 6. The energy consumption information for the last 20 years of Turkiye depending on application field

Insulation is a critical component in building design, aimed at reducing heat transfer through the building envelope including walls, roofs, floors, and windows. The insulation enhances energy efficiency, reduces heating and cooling energy requirement, and improves indoor thermal comfort by minimizing heat loss in winter and heat gain in summer. Furthermore, a suitable insulation contributes to environmental sustainability due to reduced energy consumption and associated greenhouse gas emissions. In residential and commercial buildings, the building envelope accounts for 50–60% of total heat loss or gain hence, insulation plays a major role in providing energy savings of up to 50%. In addition to energy efficiency, insulation leads to benefits such as fire resistance, sound control, and condensation control, which makes it essential for establishing sustainable and comfortable indoor mediums.

A critical aspect of insulation design is to determine the optimum insulation thickness (x_{opt}), which balances the initial insulation cost with the long-term energy savings. In fact, x_{opt} depends on factors such as climate, insulation material properties (e.g., thermal conductivity), fuel types, and economic parameters (e.g., insulation costs and energy prices). Generally, x_{opt} is calculated using life-cycle cost analysis (LCCA) which consider both economic and environmental impacts over the building's lifespan. The degree-days or degree-hours approach methods estimate annual heating and cooling loads, while advanced techniques account for dynamic thermal conditions. These computations demonstrate that x_{opt} maximizes energy savings without excessive material costs, with payback periods often ranging from 1 to 5 years, according to the variables such as region and insulation type.

There are related investigations in the available literature. For example, the degree-hours method is used to calculate x_{opt} for external walls in Turkiye's warmest zone, which emphasizes the greater impact of insulation on cooling loads [4]. The results indicated x_{opt} of 3.2–3.8 cm for cooling and 1.6–2.7 cm for heating, with energy savings of 8.47–12.19 \$/m^2 and payback periods of 3.39–5.47 years. In another study, LCCA is applied to optimize insulation thickness [5]. The results indicate economic savings of up to 21 \$/m^2 for rock wool and polystyrene in Palestine, with payback periods of 1–2.3 years. It highlights the economic feasibility of insulation in reducing energy costs. The impact of dynamic heat transfer and electricity tariffs on optimum insulation thickness, is investigated [6]. It is found that wall orientation has a minor effect on total cost and thickness, with optimal thicknesses ranging from 5.4–19.2 cm.

A dynamic thermal model is used to determine x_{opt} under varying structural materials [7]. It is determined that x_{opt} values are 5.4–19.2 cm and payback periods are 3.56–8.85 years, with substantial energy savings. A 100 m^2 residential house was modelled using Design Builder to determine x_{opt} for external walls in Kirkuk, Iraq (hot climate) and Konya, Turkey (cold climate) [8]. The analysis evaluated XPS, EPS, rock wool, and glass wool, with electricity and natural gas as energy sources for Kirkuk and Konya, respectively, finding XPS to be the most effective insulation material. The values of x_{opt} were 7 cm and 9 cm for Kirkuk, and 7 cm and 15 cm for Konya, achieving energy savings of 6.7% and 8.3% with XPS at 9 cm and 11 cm, respectively.

An analysis is performed across 16 cities from four climate zones using life-cycle cost analysis and heating degree-days [9]. Is determined that x_{opt} values range from 2 to 17 cm, with energy savings between 22% and 79%. Payback periods vary from 1.3 to 4.5 years depending on the city and fuel type used (coal, natural gas, fuel oil, LPG, or electricity). In a recent study, x_{opt} for expanded and extruded polystyrene is evaluated in diverse Indian climates [10]. The results are reporting x_{opt} values as 0.0428–0.891 m for cooling and 0.0063–0.1522 m for heating, and payback periods as 1.49–6.52 years. It also includes emission analysis, highlighting reductions in greenhouse gas emissions. The HDD method is applied across all Turkish

provinces to find x_{opt} for various materials (glass wool, rock wool, XPS, EPS) [11]. The energy savings, payback period, and CO_2 emissions reductions are also evaluated in the study. The results demonstrate x_{opt} varied between 0.07 m and 0.23 m, depending on HDD, with payback periods as short as 0.11–0.38 years for the best cases. The values of x_{opt} are calculated via heating degree day and cooling degree day methods and lifecycle cost analysis over 30 years [12]. The optimum insulation thickness values are reported as 10.5 cm–17.3 cm for walls, 6–9.8 cm for floors, and up to 26.8 cm for ceilings; energy savings in the range of 13–22% depending on region.

In the present investigation, four zones (Istanbul, Ankara, Van, and Erzurum) in Turkiye is selected to determine x_{opt} for the outer wall of buildings using HDD method. The studied insulation materials are XPS and glass wool (GW). The natural gas is considered as heating energy source in the analysis. The energy savings and payback periods corresponding to x_{opt} are computed. Finally, the results are compared and discussed to suggest the suitable insulation case for the studied provinces.

2. MATERIALS AND METHODS

The extruded polystyrene (XPS) and glass wool (GW) are used as insulation materials on outer walls of the buildings in Istanbul (3rd zone), Ankara (4th zone), Van (5th zone) and Erzurum (6th zone) which are the provinces of Turkiye. The natural gas is considered as heating energy source for the analysis. The heat losses (q) in W/m^2 through an exterior wall surface is given by

$$q = U.(T_i - T_0) \tag{1}$$

where U is the total heat transfer coefficient of the wall in W/m^2·K, T_i is the indoor air temperature and T_o is the outdoor air temperature. The value of U for external wall containing an insulation layer is calculated as

$$U = \frac{1}{R_i + R_w + R_{\text{ins}} + R_0} \tag{2}$$

where R_i and R_o represent the convection thermal resistance of the indoor and outdoor environments, which are 0.13 and 0.04 m^2·K/W, respectively, R_w is the thermal resistance of the uninsulated wall and R_{ins} is thermal resistance of the insulating material which is found as

$$R_{\text{ins}} = \frac{x}{k} \tag{3}$$

where x and k are the thickness and the thermal conductivity of the insulation element, respectively. Then, the total resistance of the uninsulated wall ($R_{w,t}$) can be obtained as

$$R_{w,t} = R_i + R_w + R_0 \tag{4}$$

The elements in the exterior wall are shown schematically in Figure 2. The specifications of the wall elements can be seen in Table 1, hence R_w is found to be 0.333 m^2·K/W while $R_{w,t}$ is obtained as 0.503 m^2·K/W. Some properties of investigated insulation materials are given in Table 2 where ρ is the density of material and C_i is the price of material per unit volume in \$/m^3.

Table 1. The specifications of wall components

Wall components	**Thickness, x (m)**	**Thermal conductivity, k (W/m·K)**	**Thermal resistance, R (m^2·K /W)**
Interior plaster	0.02	0.87	0.023
Brick	0.13	0.45	0.289
Exterior plaster	0.03	1.40	0.021

Table 2. Some information for the investigated insulation materials

Insulation	**k (W/m·K)**	**C_i (\$/m^3)**	**ρ (kg/m^3)**
XPS	0.031	115	28
GW	0.038	60	24

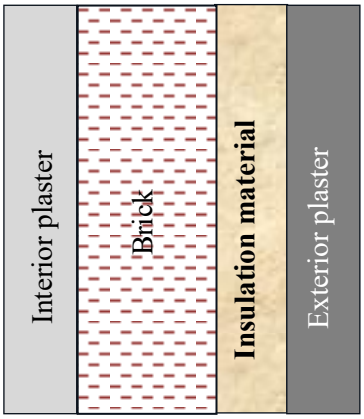

Figure 2. The schematic sketch for exterior wall elements

The optimum insulation thickness (x_{opt}) can be computed using heating degree-day (HDD) values as [5]

$$x_{\text{opt}} = 293.94\left(\frac{\text{HDD}\cdot C_F\cdot \text{PWF}\cdot k}{\text{LHV}\cdot C_i\cdot \eta}\right)^{\frac{1}{2}} - k\cdot R_{w,t} \tag{5}$$

where HDD values are 1786, 2599, 3465, and 4640 for İstanbul, Ankara Van, and Erzurum, respectively. C_F is the cost of natural gas taken as 0.3 \$/m^3 in the calculations while C_i and k are the values of insulation materials given in Table 2. Additionally, LHV is the lower heating value of natural gas (34485 kJ/m^3) and η is the efficiency of heating system accepted as 90% for the computations. PWF in Eq. (5) is the present worth factor that can be obtained as

$$\text{PWF} = \frac{(1+r)^N-1}{r\cdot(1+r)^N} \tag{6}$$

where N is the lifetime which is assumed as 15 years in the investigation and r is the real interest rate calculated as

$$r = \frac{i-g}{1+g} \tag{7}$$

where i is the annual interest rate (37%) and g is the inflation rate (35%) for Turkiye.

The annual energy saving, C_S in \$/(m^2.year) is the difference between the annual heating cost amounts for the uninsulated wall and insulated wall cases, respectively. Hence, the economic payback period of insulation cost (PP) is calculated in year as follows

$$\text{PP} = \frac{C_{\text{ins}}}{C_S} \tag{8}$$

where the cost of insulation (C_{ins}) is calculated in \$/m^2 as

$$C_{\text{ins}} = C_i x \tag{9}$$

where C_i is unit cost of the insulation material in \$/m^3 (Table 2) and x is the insulation thickness. The detailed information on the computation method of the investigated parameters can be found, for example in [5,13].

3. RESULTS AND DISCUSSION

The behavior of the energy cost, the insulation cost and the total cost (i.e., sum of energy cost and insulation cost) is determined depending on various insulation thickness values for the provinces of Istanbul (3rd zone), Ankara (4th zone), Van (5th zone), and Erzurum (6th zone). The results are demonstrated as samples cases in Figure 3 utilizing extruded polystyrene (XPS) for Istanbul and Van while glass wool (GW) for Ankara and Erzurum. The common behavior in these plots is that energy cost is reduced substantially with increasing insulation thickness. As expected, the insulation cost increases as insulation has greater thickness. However, the total cost decreases initially up to a certain insulation thickness but it starts to augment beyond that point. In fact, the insulation thickness at which total cost has the minimum amount is called as optimum insulation thickness, x_{opt}. Hence, the outer walls of the buildings should be insulated with suitable materials considering computed value of x_{opt}. The grater thickness than x_{opt} is not meaningful due to enhanced total cost.

Figure 3 shows clearly that energy cost without insulation (i.e., insulation thickness is zero) has the highest amount for all cases. Moreover, the cost of energy without insulation is lowest for Istanbul followed by Ankara, Van, and Erzurum with the

amounts of 39.62, 57.65, 76.86, and 102.92 \$/m^2, respectively. This behavior is due to selected zones as mentioned above such that the coldest region is 6th zone (Erzurum) while the warmest region is 3rd zone (Istanbul) in the present investigation.

As a sample illustration, the case of Istanbul using XPS can be focused. First of all, total cost reaches its minimum value of 15.06 \$/m^2 at insulation thickness of 5.8 cm which corresponds to x_{opt} (the cost of XPS insulation is 6.67 \$/m^2 for this situation). Obviously, the energy cost without insulation is 39.62 is \$/m^2, but it is significantly reduced to about 8.40 \$/m^2 at x_{opt}=5.8 cm. Hence, the cost of energy (i.e., amount of energy consumption) is lowered about by 78% as a result of application of XPS insulation having x_{opt}. Similar observation can be noted for other cases in Figure 3 with different numerical amounts as discussed.

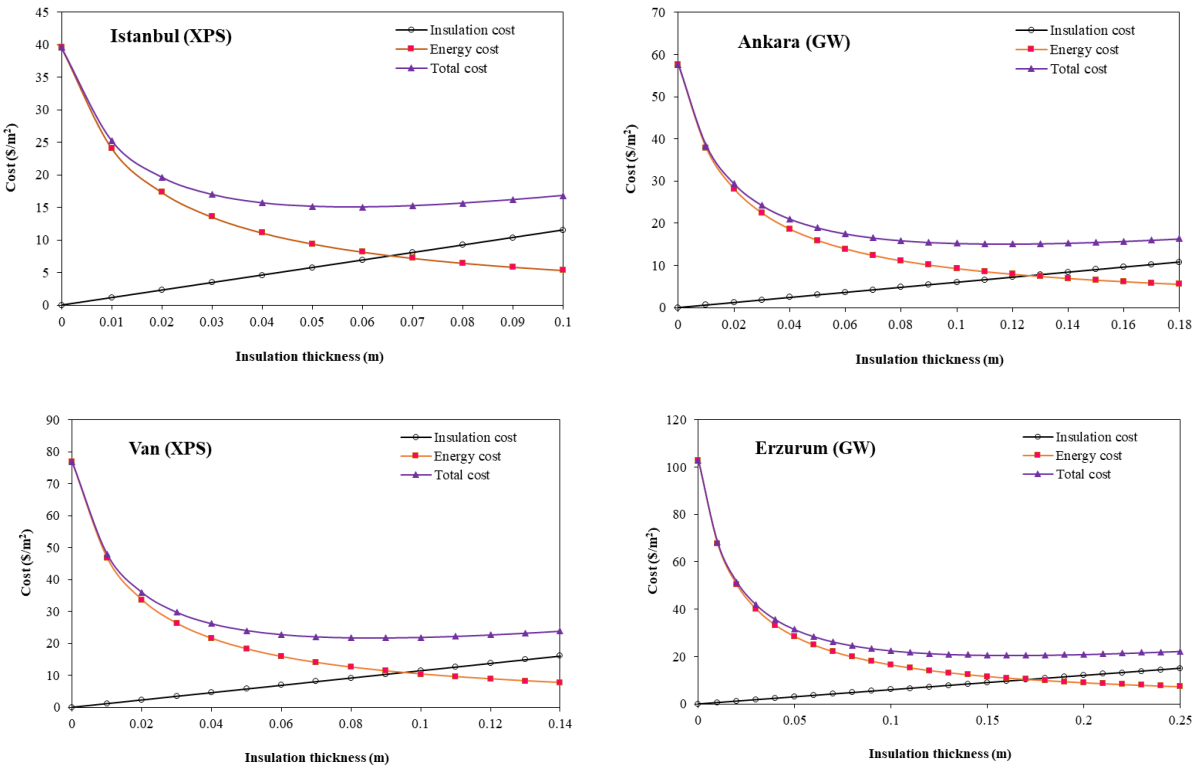

Figure 3. The behaviour of energy cost, insulation cost and total cost depending on insulation thickness for sample cases

The optimum insulation thickness (x_{opt}) values are detected considering both cases of XPS and GW as insulation material on the outside wall of the building in the considered provinces. The corresponding total heat transfer coefficient of the wall (U) as well as payback period (PP) values which are calculated with Eq. (2) and Eq. (8), respectively and the results are listed in Table 3. As a sample situation using GW in Istanbul, the following computations corresponding to optimum insulation thickness (x_{opt} = 9.3 cm) can be recalled as insulation cost, C_{ins} is 5.58 \$/m^2, annual cost without insulation is 2.97 \$/m^2·year, annual cost with insulation is 0.51 \$/m^2·year (i.e., annual saved cost, C_S occurs as 2.46 \$/m^2·year), and therefore PP is calculated as 2.27 years (Eq. 8). Table 3 denotes clearly that x_{opt} increases as HDD becomes greater for a given insulation material type. Moreover, x_{opt} of GW is thicker than that of XPS for all cities. The behaviours of both U and PP are similar such that they are reduced as HDD increases (i.e., as going from 3rd zone to 6th zone), in other words as x_{opt} becomes bigger whatever the type of insulation material. In addition, U and PP are smaller for a given province using GW than XPS. Although thicker values of x_{opt} in GW case, the quicker payback periods for all provinces are noticeable. Besides, the value of U should be below 0.25 W/m^2·K for 5th and 6th zones while the maximum values of U should be 0.45 and 0.4 W/m^2·K for 3rd and 4th zones, respectively according to the recent regulations [1, 2]. It is evidently seen in Table 3 that U values using XPS for Van and Erzurum violate the mentioned regulations since U >0.25 W/m^2·K while Istanbul and Ankara satisfy the requirement as U <0.45 W/m^2·K. On the other hand, when GW is utilized, all of the four provinces demonstrate suitable U values required by the new standard of heat insulation rules [1, 2]. Therefore, as well as considering its shorter payback periods, GW can be suggested to be applied as an insulation material on the outside wall of buildings in Turkiye due to the development of favorable U values.

Table 3. Some results with the application of optimum insulation thickness for the investigated cities

XPS					GW			
City	**HDD**	x_{opt} **(m)**	U **(W/m²·K)**	**PP (year)**	**City**	x_{opt} **(m)**	U **(W/m²·K)**	**PP (year)**
İstanbul	1786	0.058	0.423	2.84	İstanbul	0.093	0.338	2.27
Ankara	2599	0.073	0.351	2.36	Ankara	0.116	0.280	1.89
Van	3465	0.086	0.304	2.04	Van	0.137	0.243	1.63
Erzurum	4640	0.103	0.262	1.76	Erzurum	0.162	0.210	1.41

As it is seen from Table 3, x_{opt} is highly dependent on HDD as well as type of insulation material. Thus, the relationship between x_{opt} and HDD for both XPS and GW is depicted in Figure 4. Obviously, x_{opt} is higher as HDD linearly increases whatever the insulation material. On the other hand, x_{opt} of GW is thicker compared to XPS for a given HDD value. Then, data for GW in Figure 4 can be expressed with the following equation

$$x_{\text{opt}} = 2 \times 10^{-5}\text{HDD} + 0.052 \tag{10}$$

Similarly, the following expression can be fitted well to the variation of x_{opt} with HDD using XPS

$$x_{\text{opt}} = 2 \times 10^{-5}\text{HDD} + 0.031 \tag{11}$$

Eqs. (10, 11) could be useful to estimate x_{opt} for other provinces using GW or XPS since these expressions already include the effect of zone through HDD values.

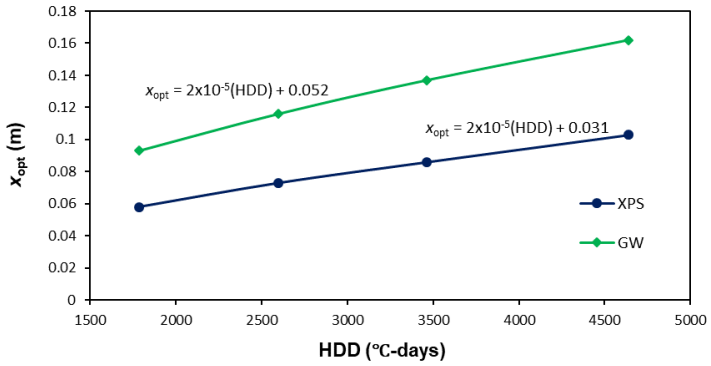

Figure 4. The dependence of x_{opt} on heating degree days for the studied insulation materials

The annual energy consumption without insulation (E_A) and the annual energy saving through the application of x_{opt} (E_S) on the exterior of building are also computed for covered cases of this investigation [9]. The obtained results are given in Table 4. Considering the case of Van, for example, E_A is 183.7 kWh/(m²·year) while the annual energy consumption dramatically drops to 28.2 kWh/(m²·year) when XPS with x_{opt}=8.6 cm is used, hence E_S develops as 155.5 kWh/(m².year). Obviously, E_A is augmented substantially as HDD increases, in other words, the coldest region of Erzurum in 6th zone causes the occurrence of the highest amount of E_A. The same behavior can be observed regarding the values of E_S. Table 4 also points out that the amount of E_S is greater about by 4% for GW compared to XPS for all provinces. Moreover, the ratio of E_S /E_A is found in Table 4 for all cases and the distribution of E_S/E_A depending on HDD is plotted in Figure 5. In comparison with the situation without insulation, energy savings can be developed as high as by 80% to 90% depending on the studied case when insulation with x_{opt} is present. Figure 5 demonstrates that E_S/E_A of GW higher than that of XPS. Additionally, E_S/E_A is enhanced exponentially as HDD has the bigger value for both insulation materials of XPS and GW. The remarkable diminishing of energy consumption via insulation of buildings not only provides economic saving but also contributes for environmental sustainability and protection due to the significantly reduced CO_2 emission.

Table 4. The annual energy consumption without insulation (E_A) and annual saved energy (E_S) for the application of x_{opt}

XPS				GW		
City	HDD	E_A kWh/(m².year)	E_S kWh/(m².year)	City	E_A kWh/(m².year)	E_S kWh/(m².year)
İstanbul	1786	94.69	74.62	İstanbul	94.69	78.54
Ankara	2599	137.79	113.54	Ankara	137.79	118.29
Van	3465	183.70	155.50	Van	183.70	161.21
Erzurum	4640	245.99	213.65	Erzurum	245.99	220.03

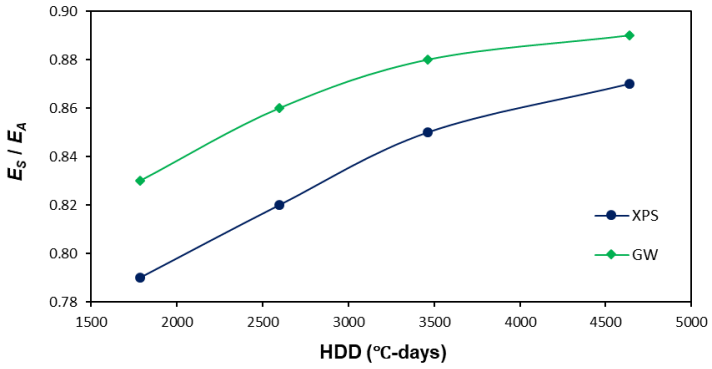

Figure 5. The variation of E_S/E_A with heating degree days for the application of optimum insulation thickness

4. CONCLUSIONS

This study investigated the optimum insulation thickness (x_{opt}) for the outer walls of buildings across four different climate zones (Istanbul, Ankara, Van, and Erzurum) in Turkiye using the Heating Degree-Day (HDD) method. Two insulation materials, extruded polystyrene (XPS) and glass wool (GW), were analyzed to assess their thermal and economic performance under varying climatic conditions.

The results show that x_{opt} increases linearly with HDD values, reflecting the enhanced requirement for insulation in colder regions. Compared to XPS, thicker insulation was consistently necessary for GW which also offered superior energy savings and shorter payback periods in all provinces. Moreover, GW achieved lower overall heat transfer coefficients (U values), complying with the latest national building insulation regulations across all studied zones, including the strict requirements for the 5th and 6th zones. In contrast, XPS did not meet the required standards in Van and Erzurum.

The study further revealed that applying x_{opt} leads to significant reductions in energy consumption, with savings reaching over 80% and approaching 90% in the coldest region. These results confirm that properly designed insulation systems can yield substantial economic and environmental benefits. Given its favorable performance in terms of energy savings, standard compliance of TS 825 [1], and financial advantage, glass wool emerges as a more suitable insulation material to use in diverse climatic zones of Turkiye.

REFERENCES

[1] Yapi Insaat Dergisi. (2024) TS 825:2024 Binalarda Isı Yalıtımı Kuralları Standardı ile İlgili Yenilikler. [Online]. Available: https://www.yapiinsaatdergisi.com/ts-8252024-binalarda-isi-yalitimi-kurallari-standardi-ile-ilgili-yenilikler
[2] İZODER. (2024) TS 825 Binalarda Isı Yalıtımı Kuralları Standardı. [Online]. Available: https://www.izoder.org.tr/sayfa/81/ts-825-2024-binalarda-isi-yalitimi-kurallari-standardi
[3] G. Devecioğlu, B. Bilici, and V. Oruç, "The evaluation and improvement for the energy performance of buildings: A case study," Next Energy, vol. 4, p. 100126, 2024.
[4] Bolatturk, "Optimum insulation thicknesses for building walls with respect to cooling and heating degree-hours in the warmest zone of Turkey," Building and Environment, vol. 43, no. 6, pp. 1055–1064, 2008.
[5] Hasan, "Optimizing insulation thickness for buildings using life cycle cost," Appl. Energy, vol. 63, no. 2, pp. 115–124, 1999.
[6] S. A. Al-Sanea and M. F. Zedan, "Effect of electricity tariff on the optimum insulation-thickness in building walls as determined by a dynamic heat-transfer model," Appl. Energy, vol. 82, no. 4, pp. 313–330, 2005.
[7] M. Ozel, "Thermal performance and optimum insulation thickness of building walls with different structure materials," Appl. Therm. Eng., vol. 31, no. 17–18, pp. 3854–3863, 2011.
[8] S. Kazancı and A. Samancı, "Investigation of optimum external wall insulation thickness of a house in two different climate regions," Int. J. Energy Studies, vol. 7, no. 1, pp. 49–65, 2022.

[9] Bolattürk, "Determination of optimum insulation thickness for building walls with respect to various fuels and climate zones in Turkey," Appl. Therm. Eng., vol. 26, no. 11–12, pp. 1301–1309, 2006.
[10] M.A. Kallioğlu, A. Yılmaz, A. Sharma, A. Mohamed, D. Dobrotă, T. Alam, R. Khargotra, and T. Singh, "Optimal insulation assessment, emission analysis, and correlation formulation for Indian region," *Buildings*, vol. 13, no. 1, p. 569, 2023.
[11] Aktemur, F. Bilgin, and S. Tunçkol, "Optimisation on the thermal insulation layer thickness in buildings with environmental analysis: An updated comprehensive study for Turkey's all provinces," J Ther Eng, vol. 7, no. 5, pp. 1239–1256, 2021.
[12] N. Aydin and A. Biyikoglu, "Determination of optimum insulation thickness by life cycle cost analysis for residential buildings in Turkey" Sci. Technol. Built Environ., vol. 27, no. 1, pp. 2–13, 2021.
[13] G. Devecioğlu, U. Yaman, and V. Oruç, **"**Determination of optimum insulation thickness and economic analysis for heat pump application in different degree day regions of Turkey," *Dicle Univ. J. Eng.*, vol. 15, no. 4, pp. 863–871, 2024.

ICENS 11TH INTERNATIONAL CONFERENCE ON ENGINEERING AND NATURAL SCIENCE October 22-26 2025 Sarajevo

Finite Wing Domain Size Sensitivity: Far-Field Boundary Location

Öztürk Özdemir Kanat[1], Umut Kaya[2], Yasin Özcan[3]*

Abstract

The paper is a systematic study of the impact of far-field boundary location on subsonic (M≤0.3) flow regime aerodynamic performance of a finite wing by simply changing the size of the solution domain. The given study is premised on the fact that when far-field boundaries are too close, errors may be generated as a result of artificial reflections and domain limitations on pressure recovery, wake transport, and tip vortex dynamics; making them too far away would lead to the computation cost being disproportionate without necessary physical accuracy. To eliminate this design instability, single-piece far-field boundaries were used. Layers of inflation having a fixed Number of Divisions and fixed first-layer thickness were placed at the wing edges to maintain the mesh in practice constant near the wing, wake, and tip vortex lines. Therefore, with the increase of the solution domain, the near-field mesh is not altered, and the cells in the far-field are increased, and the observed differences can be directly attributed to the distances of the boundaries. Pressure Far-Field boundary conditions, Symmetry in the root plane, and the k–ω SST turbulence model were chosen for the setup. Under the arrangement, it is possible to create data-intensive and reproducible far-field location suggestions by remediating the mesh variables. It makes sure that only validating results that represent the effects of solution domain scaling are gained.

The solution domain scaling was performed using four dimensionless distance parameters. These include K_u (L_E upstream), K_d (T_E downstream) K_v (top/bottom) and K_{tip} (tip-side gap). Varying these parameters resulted in design points. The comparison was performed based on Δ_{CL}, Δ_{CD}, Δ_{CM} (percentage), and differences in surface pressure distributions relative to the largest reference solution area.

The paper discusses the influences of the four distance parameters that are dimensionless (K_u, K_d, K_v, K_{tip}) on the solution in comparative analysis framework. Detailed evaluations of the effects of the Kd and K_{tip} parameters are planned. The research aims to accelerate the validation processes and reduce the computational load caused by unnecessarily large solution domains by presenting the solution domain sizing steps and direction-dependent design curves that must be followed to achieve the target accuracy level. Consequently, the minimum distances necessary to reach the target level of accuracy can be computed during the first iteration as a result of the proposed framework, which reduces the validation time and the overall cost of computation.

Keywords: Domain size sensitivity, far-field boundary location, CFD

1. INTRODUCTION

Computational Fluid Dynamics (CFD) has become one of the key solutions in modern aerodynamic design because it enables detailed flow simulation to be performed much more quickly and at lower cost compared to experimental methods [1–3]. CFD enables the high-accuracy analysis of complex flow phenomena such as pressure distribution, lift and drag forces, boundary layer development, and vortex interactions by numerically solving the Navier–Stokes equations [4]. The benefits have also resulted in the popularity of the technique in the fields of academic study and industrial design and validation. Nevertheless, the numerical modeling of external aerodynamic flows presents a big challenge.

The real flow field is physically unlimited but the solution domain applied in the numerical simulation is constrained. Thus, to capture the free-flow conditions correctly, far-field boundaries are to be put in the right position and defined. These boundaries have a direct influence on the accuracy of the results obtained. The manner in which the far-field boundaries are too near the body can result in some errors in the form of reflections on the pressure and the distortion of the vortex trails.

[1*] Corresponding author: Kastamonu University, School of Civil Aviation, Department of Aircraft Maintenance and Repair Kastamonu, Turkey. ozkanat@kastamonu.edu.tr

[2] Turkey, Graduate School of Science and Engineering, Hacettepe University, Ankara, Turkey

[3] Kastamonu University, Faculty of Engineering and Architecture, Department of Mechanical Engineering, Kastamonu, Turkey

Alternatively, too far away of the boundaries will also needlessly multiply the computational cells and solution time, thereby raising the cost. It is significant to determine the best solution domain size both in the area of computational efficiency and physical accuracy. Some general guidelines on the distance between the boundaries (usually in terms of chord length) have been suggested, in research on two-dimensional wing profiles. The recommendations might however be inadequate based on the complex flow structures that occur in three dimensional wings especially wing tip vortices, three dimensional separations and induced downwash effects. These flow characteristics may directly interfere with the location of the solution domain boundaries and boundary conditions and provide the erroneous calculation of the lift (C_L) and drag (C_D) coefficients. In the same way, systematic errors can also be introduced by the positioning of solution domain boundaries in the simulation of aerodynamic loads in CFDs [5]. A constant cell size in the vicinity of the wall and the boundary layer resolution is essential when varying the solution domain dimensions because of the consistency of the numerical comparison of external flow [6]. Otherwise, the inconsistencies in C_L and C_D might be numerical variations due to the difference in mesh arrangement and not solution domain variations [7].

Golmirzaee and Wood [8] studied the solution domain size and various boundary conditions on the lift and drag forces in flow around the NACA 0012 airfoil at high Reynolds number. When they analysed the solution domain with the use of OpenFOAM software, they discovered that there are important errors associated with the size of the solution domain, especially the pressure induced drag when under usual boundary conditions. They also demonstrated that incorrect boundary conditions generate undesired vortices in the domain that influence the correct computation of lift and drag forces. In their study, Patel and Ramani [9] used ANSYS CFX to conduct a 3D numerical analysis of the wind load on a cube-shaped structure and examined the size of the computational domain of maximum effectiveness. Their model incorporated 1.5 cm surface roughness, 5 percent inlet turbulence and k-eps turbulence model. Having decided on the best dimensions they compared their findings of the solution to the wind tunnel data that had been achieved before. Allahyari et al. [10] examined the performance of various computational grid generation methods (second-order scheme, fourth-order compact scheme, and Theodorsen transformation) on the numerical solution of the flow over NACA 0012 airfoil. They compared the accuracy, metrics and flow solution of the generated grids and discovered that the fourth-order compact scheme enhanced greatly the quality and orthogonality of the grid. They also observed that grid accuracy also has a direct impact on the solution of flows and that the higher the order of the flow solver, the more grid accuracy is needed.

This research paper is a systematic research work that aims to examine the influence of far-field boundary condition on the aerodynamic performance of a finite wing in subsonic flow ($M \leq 0.3$). Four dimensionless parameters (K_u, K_d, K_v, K_{tip}) which are normalized by the chord length are used to define the solution domain. One parameter was at a time varied and the remaining kept constant. This enabled the study of the effects only depending on the distance of the boundary to be studied in the various configurations obtained. Moreover, the mesh structure of the near-field and the number of the inflation layers as well as the $y+$ target were also held constant. In this way, it became possible to compare the effects of positions of boundaries in various directions (parallel, perpendicular and lateral to the flow) and to generate design suggestions that will provide an optimal solution between accuracy and cost of computations.

2. METHODOLOGY

2.1. Finite Wing Model

The model analyzed in the paper is a finite wing with a symmetrical NACA 0012 airfoil. The wing surface does not have a sweep, dihedral or twist angle. This is a simplistic geometry which was selected to decouple the action of boundary conditions as well as to remove interactions by geometric variables. Table 1 presents the basic flow and geometric parameters in the analyses.

Table 4. Flow and Geometric Parameters

Parameter	Symbol	Value	Unit
Mach Number	M	0.28	–
Angle of Attack	α	4	° (degree)
Density	ρ	1.14	kg/m³
Static Pressure	p	99 000	Pa
Reference Cord	c	0.25	m
Semi Span	b/2	0.95	m
Span	b	1.90	m
Reference Area	S_ref	0.475	m²
Flow Regime	–	subsonik	–

2.2. Boundary Conditions

Pressure far-field boundary condition has been specified on all external boundaries of the computational domain. Such a condition constitutes the free-flow conditions at the outer boundary as well and is applied to both the inlet and outlet surfaces, in which the flow would form naturally. The root of the wing forms a symmetry plane. Figure 1 illustrates schematically the general structure of these boundary conditions.

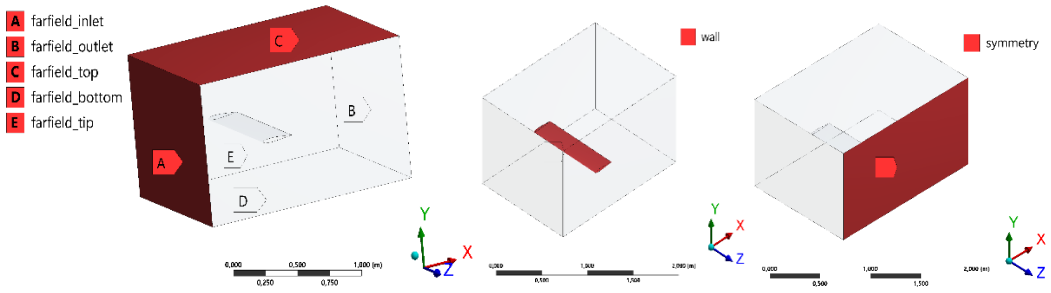

Figure 1. Appearance of the computational domain boundary conditions

2.3. Dimensionless Field Parameters

The dimensions of the solution area have been normalized according to the wing geometry and expressed using four dimensionless parameters:

- K_u: Distance from the leading edge to the inlet boundary
- K_d: Distance from the trailing edge to the outlet boundary
- K_v: Distance from the mid-plane to the top and bottom boundaries
- K_{tip}: Distance from the wing tip to the lateral boundary

The reference configuration was selected as $K_u = 7$, $K_d = 30$, $K_v = 5$, and $K_{tip} = 17$ based on previous literature and preliminary test results. All other variations were created by changing these parameters. This allows for separate sensitivity analysis for each aspect of the solution domain and determines in which direction the flow is more sensitive to boundary effects. The definitions of the dimensionless boundary parameters and their locations within the solution domain are shown in Figure 2.

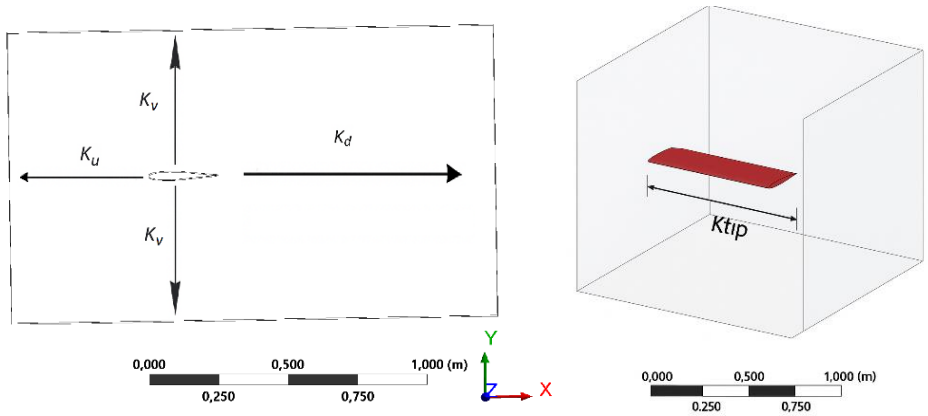

Figure 2. Dimensionless field parameters K_u, K_d, K_v, and their positions on the calculation area

Table 2 shows the dimensionless boundary distances used in five different domain configurations. It can be seen that the domain scales are systematically increased between configurations, and wider boundary distances are used particularly in C_4 and C_5 to prevent the flow field from being affected by boundary conditions.

Table 2. Dimensionless Domain Parameters

Configuration	K_u	K_d	K_v	K_{tip}
C_1	1c	2c	1c	4c
C_2	2c	5c	2c	5c
C_3	3c	10c	2c	10c
C_4	5c	30c	3.5c	15c
C_5	7c	30c	5c	17c

2.4. Calculation Model and Solution Settings

All analyses were performed using a pressure-based, steady-state solution approach. The solution method, turbulence model, and convergence criteria used are summarized in Table 3.

Table 3. Solution Settings and Model Parameters

Parameter	Description
Solver Type	Pressure-based steady-state
Separation Scheme	Second-order upwind
Turbulence Model	k–ω SST (Shear Stress Transport)
Desired y+	≈ 1.0
Convergence Criterion (Residuals)	$< 1\times10^{-4}$
CL/CD Stability Threshold	Δ(CL/CD) < 0.1%
Solution Termination Criteria	Aerodynamic coefficients reaching steady state

2.5. Mesh Strategy and Grid Consistency

The mesh structure used in this study has been designed to be both sufficiently detailed to resolve flow details around the wing and sufficiently efficient to reduce computational costs in the far-field. The near-field region has been modeled with high-resolution hybrid cells, while the mesh has been progressively refined in the far-field using a cell growth ratio. The near-field topology was kept constant in all configurations, with only the distance of the far-field boundaries being altered. This approach enabled the comparison of different solution domains in accordance with the principle of grid independence.

Table 4. Mesh and Grid Characteristics

Parameter	Description	Value
Cell Type	Hybrid mesh	–
Total Number of Cells (approx.)	Depends on the solution domain size	12–18 milyon
Growth Rate	Cell size increase ratio	1.15
First Layer Height	Constant near-wall first layer thickness	0.000025
Number of Inflation Layers	Boundary-layer mesh layers near the wall	19
Face Sizing	Applied on the wall surface	0.0015

The mesh structure used in the study is shown in Figure 3.

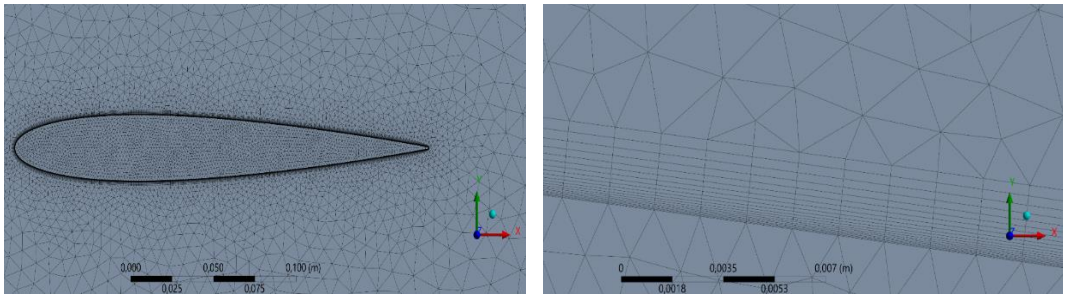

Figure 3. Mesh structure

3. RESULTS AND DISCUSSION

In this study, six different solution domain configurations (C_1–C_5) were created, each representing different far-field boundary locations. In all analyses, the mesh setup was kept constant, and only the total number of cells varied depending on the solution domain size. This allowed the differences obtained to be attributed entirely to the physical effects of the boundary locations. In the flow field, it was found out that the flow structure was very stable as the far-field boundaries were increased. In particular, it was observed that pressure fluctuations decreased in the wake region and flow lines became smoother. This situation shows that pressure reflections and artificial vortex shearing are more pronounced in small solution areas (e.g., C_1), and this effect decreases as the area expands. Figure 4 shows the pressure coefficient (C_p) distributions for the C_1 and C_5 configurations. In narrow solution areas, the wake dampens early and the pressure gradient is disrupted, while in wide areas, the wake extends and flow continuity is maintained. Accordingly, in the C_1 configuration, early pressure recovery and partial flow reflections are observed in the wake region; for C_5, extending the far-field boundaries results in wake extension and improved flow continuity.

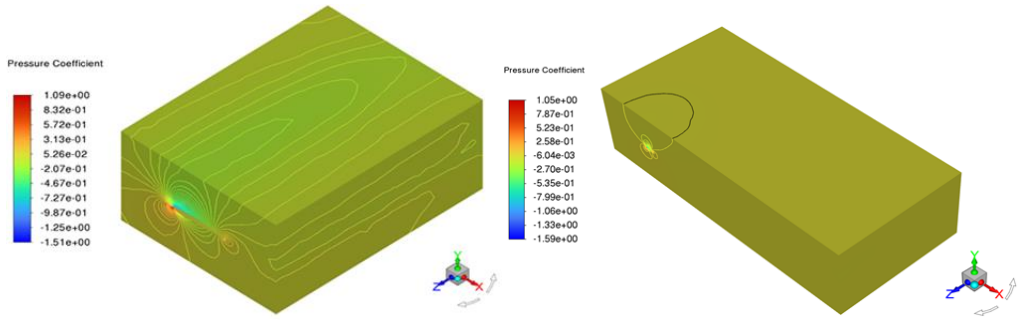

a. C_1 b. C_5

Figure 4. Pressure coefficient (C_p) distributions obtained in the C_1 and C_5 configurations

As shown in Figure 5, the net mass imbalance reaches its highest value in the C_2 configuration, indicating that the narrow domain structure negatively affects flow integrity. The rapid shift of values to negative from C_3 onwards indicates that mass imbalance decreases as the domain widens. The lowest imbalance was observed in C_5, suggesting that this configuration provides a more stable and balanced flow field.

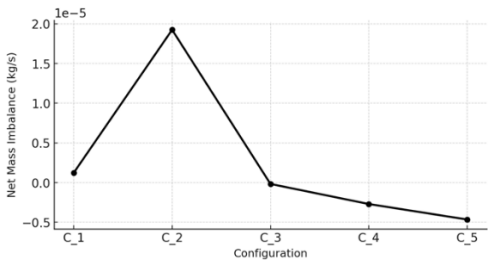

Figure 5. Net Mass flow imbalance and domain configuration

As shown in Figure 6, particularly in narrow domain configurations (C_1 and partially C_2), the far-field surfaces exhibit more pronounced deviations from the reference Mach number. As the domain expands, the Mach values on all surfaces approach the reference line and become almost completely stable in C_4–C_5. This indicates that wide domains do not disrupt the flow field and better preserve the physical consistency of the boundary conditions.

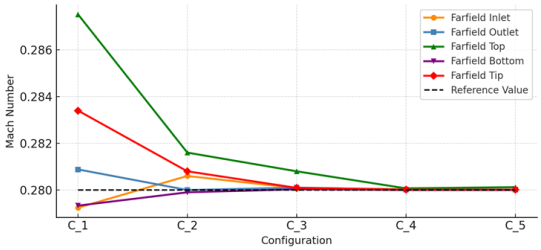

Figure 6. Far-field Mach Number Variation (All Boundaries)

As shown in Figure 7, although C_L values generally tend to decrease as the domain expands, a significant drop is observed particularly during the transition from C_1 to C_2, followed by a more gradual decrease. This indicates that C_L is sensitive to domain boundary effects and particularly influences the pressure distribution on the wing in narrow domains. C_D values, on the other hand, exhibit a much more regular and stable decrease compared to C_L, indicating that C_D responds more predictably to domain scaling. As a result, both C_L and C_D reach more physical and reliable values in wide domains. In analyzing the C_M values, it is noted that the moment coefficient approaches closer to a more negative value as the area of the solution increases. The effect of the artificial pressure distribution due to the proximity of the domain boundaries, especially C_1 and C_2, is markedly influential on C_M, whereas the influence grows less pronounced beyond C_3. This confirms that, the moment coefficient gives physically more consistent values in C_3-C_5 range, as with C_L and C_D.

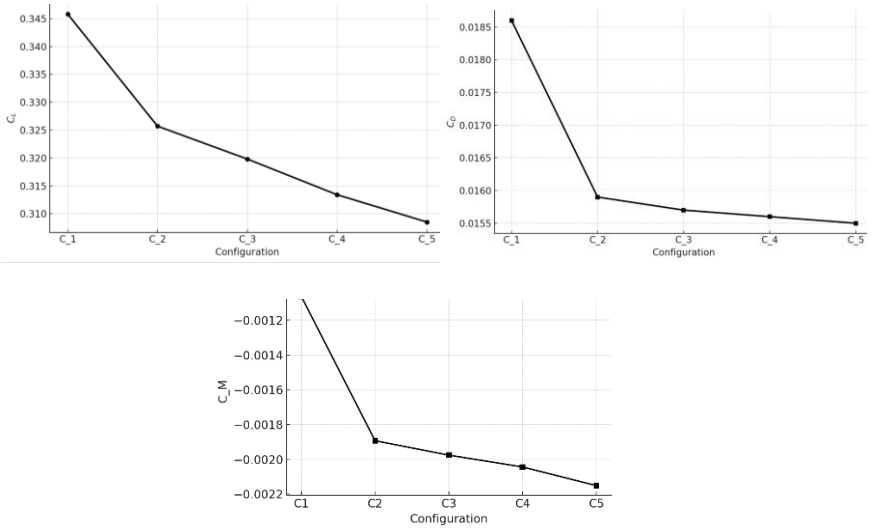

Figure 7. Change in C_L, C_D and C_M Values with Domain Scaling

4. CONCLUSIONS

This study provides a systematic framework for evaluating the effect of far-field boundary placement on aerodynamic results in finite-wing CFD analyses. The findings indicate that the downstream direction (Kd), the wing tip–side boundary distance (K_{tip}), and the upper–lower surface distances (K_v) significantly affect solution accuracy. It was found that as domain sizes increased, boundary effects on C_L, C_D, Mach number, and pressure field decreased, but beyond a certain scale, the increase in accuracy became limited. Furthermore, reliable comparisons between configurations were possible thanks to fixed near-field settings (inflation layer, y^+ control, and mesh structure). Overall, while larger domains produce more physically accurate solutions, the optimal domain was found to offer a balanced structure that minimizes boundary effects without creating unnecessary computational load.

As part of future studies, it is planned to re-evaluate the proposed methodology under different Mach numbers, Reynolds numbers, and turbulence models. Also, it will be possible to increase the generalizability of the framework when applied to different wing profiles, aspect ratios, and geometry adjustments. In the continuation of the study, the scope will be expanded

to include time-dependent (unsteady) analyses, high angles of attack, and potential separation regions, and the effects of far-field boundary placement in different flow regimes will be presented in greater detail.

ACKNOWLEDGMENT

The authors would like to thank Hacettepe University for permission to use Ansys Software in this study.

REFERENCES

[1] J. Blazek, Computational Fluid Dynamics: Principles and Applications, Elsevier, 2005..
[2] J.H. Ferziger, M. Perić, R.L. Street, Computational Methods for Fluid Dynamics, Springer International Publishing, Cham, 2020..
[3] J. Slotnick, A. Khodadoust, J. Alonso, D. Darmofal, CFD Vision 2030 Study: A Path to Revolutionary Computational Aerosciences, Nnasa/Cr-2014-218178 (2014).
[4] F.R. Menter, Two-equation eddy-viscosity turbulence models for engineering applications, AIAA J. 32 (1994) 1598–1605..
[5] Y. Abu-Zidan, P. Mendis, T. Gunawardena, Optimising the computational domain size in CFD simulations of tall buildings, Heliyon 7 (2021).
[6] A. Lozano-Durán, S.T. Bose, P. Moin, Performance of wall-modeled LES with boundary-layer-conforming grids for external aerodynamics, AIAA J. 60 (2021) 747–766.
[7] S. Lu, J. Liu, R. Hekkenberg, Mesh properties for rans simulations of airfoil-shaped profiles: A case study of rudder hydrodynamics, J. Mar. Sci. Eng. 9 (2021).
[8] N. Golmirzaee, D.H. Wood, Some effects of domain size and boundary conditions on the accuracy of airfoil simulations, Adv. Aerodyn. 6 (2024).
[9] R. Patel, S. Ramani, S. Murakami, A. Mochida, Y. Hayashi, S. Sakamoto, Determination of Optimum Domain Size for 3D Numerical Simulation in ANSYS CFX, Int. J. Innov. Res. Sci. Eng. Technol. 4 (2015) 4671–4679.
[10] M. Allahyari, V. Esfahanian, K. Yousefi, The effects of grid accuracy on flow simulations: A numerical assessment, Fluids 5 (2020) 1–21.

BIOGRAPHY

Öztürk Özdemir Kanat is an Assistant Professor in the Department of Aircraft Maintenance and Repair at Kastamonu University. His research focuses on innovative UAV projects, system integration, and computational fluid dynamics (CFD). He actively engages in research collaborations and has contributed to publications in reputable international journals. His work emphasizes advanced aerodynamic modeling and design optimization, supporting the development of high-performance VTOL and fixed-wing unmanned aerial platforms.

Yasin Özcan is an Assistant Professor in the Department of Mechanical Engineering at Kastamonu University. His research interests include renewable energy, energy optimization, machine learning, and computational fluid dynamics (CFD). He actively engages in both experimental and computational studies aimed at improving the efficiency and sustainability of systems.

Umut Kaya is a Research Assistant in the field of Mechanical Engineering, specializing in heat transfer, fluid mechanics, and deep learning applications in engineering systems. He is currently pursuing his PhD at Hacettepe University and serves as a Research Assistant at Kastamonu University. His academic and research interests lie in integrating computational methods and artificial intelligence with traditional thermal and fluid sciences to develop innovative and efficient engineering solutions. He continues to contribute to interdisciplinary research projects and aims to advance data-driven modeling approaches in thermal-fluid dynamics.

ICENS 11TH INTERNATIONAL CONFERENCE ON ENGINEERING AND NATURAL SCIENCE
October 22-26 2025 Sarajevo

Comparison of VTOL Concepts in Terms of Aerodynamics, Structural Characteristics, and Mission Suitability

Öztürk Özdemir Kanat[1], Yasin Özcan[2], Umut Kaya[3]*

Abstract

This paper provides a comparative analysis of vertical takeoff and landing (VTOL) aircraft taking design concepts as the only parameter, regardless of the energy source. The objective is to identify the best concept to be used in various mission profiles. There are five basic structural categories of VTOL platforms, including multicopter, tilt-rotor, tilt-wing, lift+cruise and tailsitter. It was established that multicopter systems have strengths in short range and low speed missions but cannot be used in level flight mode because of low level of aerodynamic efficiency. The contribution of fixed wings was found to ensure the high performance of the tilt-rotor and tilt-wing concepts in terms of high range and speed; nevertheless, they are also characterized by increased engineering requirements because of the complexity of the structure and control challenges. Lift+cruise systems are demonstrated to equalize energy consumption through separating vertical and horizontal flight engines as well as provide versatile solutions to both urban air transportation and cargo. The concept of tailsitter has been noted as coming up with low cost solution due to its small structures although it has problems with balance when making transitions.

The application scenarios have been discussed in three categories which are urban air transportation, cargo transportation, and defense applications. In urban air transportation, low noise, safety, and short range criteria were found to be important. In this context, multicopter and lift+cruise concepts were assessed as having the potential to stand out. When it comes to cargo transportation, load capacity, range, and energy efficiency can probably be the most important factors, and tilt-rotor and lift+cruise systems are believed to have an advantage in that aspect. Speed, multi-mode flight, and endurance will probably be of more importance in defense applications, and tilt-rotor and tailsitter systems will probably emerge into the limelight.

In general, rather than speaking of a single "ideal" VTOL concept, it can be stated that the choice of concept may vary depending on factors such as mission environment, control complexity, maintenance ease, and operational priorities. There are also assessments that hybrid structures and concept syntheses may become more important in the future.

Keywords: VTOL concepts, multicopter, tilt-rotor, tilt-wing, mission suitability

1. INTRODUCTION

Aircraft with vertical take-off and landing capabilities (VTOL – Vertical Take-Off and Landing) are a type of platform that is evaluated in many civil and military fields thanks to their ability to take off and land without the need for traditional runways. These systems have become a major focus of research and investment in recent years, particularly due to their ability to operate in confined spaces, their maneuverability, and their increasingly advanced propulsion systems[1,2].

VTOL vehicles are designed to meet different needs in different application areas. Figure 1 presents a bibliometric network analysis of the current research domains regarding the topic of one of the types of systems VTOL. Color clusters in the visualization describe the relationships between sub-themes which include flight dynamics, aerodynamic structure, control strategies, energy consumption performance, numerical simulation and distributed electric propulsion systems.

[1*] Corresponding author: Kastamonu University, School of Civil Aviation, Department of Aircraft Maintenance and Repair Kastamonu, Turkey. ozkanat@kastamonu.edu.tr

[2] Kastamonu University, Faculty of Engineering and Architecture, Department of Mechanical Engineering, Kastamonu, Turkey

[3] Graduate School of Science and Engineering, Hacettepe University, Ankara, Turkey

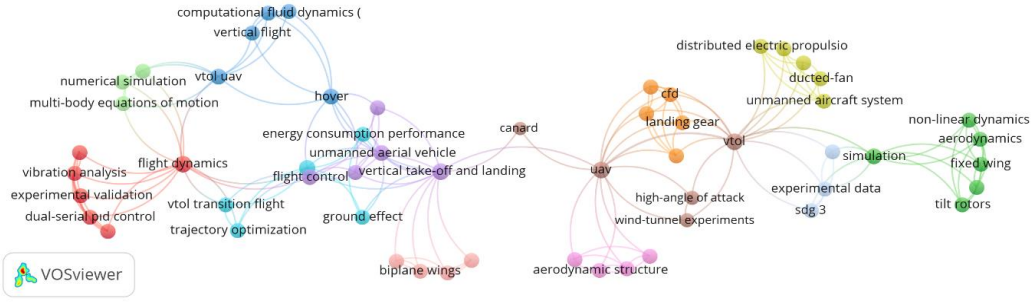

Figure 7. Bibliometric network map of research on VTOL systems

Urban air mobility (UAM), is one of the areas of application, and it is being created with a specific purpose of reducing the congested urban areas and providing time-saving transportation options. The electric VTOL (eVTOL) systems have been developed in the framework of UAM and are focused on carrying a small number of passengers. These are geared towards the saving of time, minimizing carbon emission to avoid air pollution and to minimize noise levels by the use of electric propulsion [3]. Among the remarkable points of UAM applications is not only the technological sufficiency, but also the fact that these systems are integrated into the current airspace management systems, ground infrastructure (e.g. vertiports) as well as the social acceptance extent [4,5].

VTOL systems are also under consideration in the cargo and logistics transport sector, especially in the last-mile delivery, and supply chain operations of inaccessible locations. VTOL platforms offer the flexibility to deploy their operations in geographical areas where it is difficult to use the traditional cargo aircraft or even motor vehicles due to the limited landing space. Depending on the necessity in this sphere, diverse models, based on unmanned aerial vehicles with a limited load on board, as well as platforms that can transport more significant quantities of cargo, are diversified [6]. Nevertheless, such technical complications like load capacity, battery efficiency, management of energy and resistance to the weather conditions are also among key issues which may restrict the prevalence of these systems [2].

VTOL systems have been used in military and tactical use basing on various needs. VTOL capability offers a major benefit of terrain operationalities that the traditional aircrafts are not able to get down or take off. Specifically, short response times, mobility, low radar signature, and platform versatility means that these systems can be used in reconnaissance, surveillance, air support, forward base, as well as emergency evacuation. Nevertheless, because platforms to be utilized in the defense sector need to be durable and multitasking high requirements on engineering are imposed on the aerodynamic structure, control system, and energy management [7].

Regardless of all these uses of VTOL systems, not one specific type of a system can be applied universally. Each of the various VTOL concepts that have been developed i.e. multicopters, tilt-rotors, tilt-wings, lift+cruise, tailsitters possesses distinct structural, aerodynamic and operational features. They have all been structured with emphasis placed on particular mission scenarios, instituted; hence, there is a variance in terms of aerodynamic efficiency, energy consumption, complexity of control systems, costs of production and maintenance [8]. Although multicopter systems have the benefit of basic structure and low speed stability, the range is limited because of low aerodynamic efficiency during advanced flight modes. Tilt-rotor systems, conversely, have a more extended range and speed benefits, whereas the problems of control systems and mechanism organization become more complicated [2].

The purpose of this paper is to comparatively analyze current concepts of VTOL with regards to their aerodynamic efficiency, structural complexity, and mission suitability in consideration of the above-discussed mission requirements. Therefore, it seeks to offer a systematic outlook of concept appropriateness in terms of environment of operation in design, production and implementation.

2. TECHNICAL AND OPERATIONAL CHARACTERISTICS OF VTOL CONCEPTS

The commercial VTOL systems are conceptualized as varied depending on the flight modes, structural design, and the priority of the mission. In this part, the comparative discussion focuses on five basic VTOL concepts which are common in terms of technical features.

The multicopter systems usually have four or more rotors that are fixed and lift is generated with the help of propellers. Such systems possess no wing surface; hence, all lift is obtained by engine propulsion. This aircraft design has a high angular efficiency during landings and takeoffs but the aerodynamic drag is very high in forward flight. The lack of wings to give lift makes all power to be produced by thrust. This is a huge power waste particularly in battery run platforms. These are rotor-only structures that possess smaller carrying capacity because the motors and the battery systems are located on the body. Regarding stability, multicopters are controlled with the help of the strict regulation of rotor speeds. Though it is a mechanically simple method, it demands very sensitive algorithms of control and real-time calculations [1,2].

Tilt-rotor engines place the propellers in a direction that exposes them upwards during a vertical takeoff and forward during the change of the propellers to forward flight. This enables the vertical take off and horizontal forward flight. The efficiency

in takeoff is managed in Angular since the rotation of the rotors is variable, but efficiency may be lost temporarily in case rotors limit the lift during the rotor shift. With a forward flight, there is a large decrease in aerodynamic drag during the engagement of fixed wings, thus the system can reach higher speed. Tilt-rotor systems have medium-to-high wing loading in terms of wing loading, the same way as fixed-wing planes. This however must be addressed regarding structural integrity and wing strength. It has one of the most complicated types of VTOL control systems; repositioning of propellers and thrust vectors are, in particular, tricky during vertical-horizontal flight transitions [9].

In the design of a tilt-wing, the propellers, but the whole wing structure, is tilted upwards during takeoff and horizontal during forward flight. Such a structure enhances the angular efficiency of the structure as it gives a larger percentage of surface area to create lift when taking off. Nonetheless, all wings are movable which makes the system weightier and more structurally complicated. The structure acting as a fixed wing during forward flight prevents much of the drag to develop but at the expense of certain aerodynamic losses, this is because of the engines that are situated at the ends of the wings. These systems have wing loading that takes care of the task of transporting as well as the engine weight. This adds the loads to the wing roots. Stability and control, as well as synchronized wings, propeller steering, and fuselage aerodynamics, should all be controlled simultaneously, particularly during transitional stages. This needs sophisticated control programs and synchronization [10].

Vertical takeoff and horizontal flight is done in Lift+Cruise systems with independent motor systems. Takeoff and landing are done by rotors located vertically, with the forward flight being powered by a fixed propeller or jet engine. This design has a high angular efficiency in the takeoff where only the vertical motors are active to produce lift. Most commonly, however, on transition to forward flight, the engines used during takeoff are turned off or stationary on fuselage. This generates extra drag. A study of aerodynamic analysis that was done on Lift+Cruise eVTOLs revealed that takeoff propellers were made retractable, and this cut down this drag by about 38%. This enhancement is capable of giving 21 percent greater speed at given range or 13 percent greater range at identical speed depending on how the system is being used. When the missions are endurance-oriented, the gains are of approximately 7% though these advantages may be constrained by the structural weight of the retraction mechanism. In others designed in modern times such as foldable engines or retractable engines, these losses are minimized. The lifting capacity has also been moved to forward flying wings in terms of wing loading, giving it performance that is comparable to that of standard fixed-wing aeroplanes. The two propulsion systems have to be synchronized in control systems. This complicates the software and also increases reliance on the automation system in cases of transition. Due to this fact, whereas the Lift+Cruise architecture provides an aerodynamically balanced design, the addition of a retractable propeller does provide a strong enhancement with forward flight performance of the system and can lead to an engineering trade-off where optimization between energy and mission range is required [11].

A tailsitter is a form of VTOL, in which during take-off the tailsitter maintains a vertical orientation and during conversion to a forward flight, the fuselage is tilted horizontally. During takeoff, thrust is directed entirely vertically; therefore, angular efficiency is high. However, maintaining balance during the fuselage rotation in the transition phase becomes complex. The greatest challenge for tail-sitters is control and the aerodynamic transition phase. During the transition from takeoff to horizontal flight, aerodynamic forces and moments change abruptly and non-linearly, complicating stability and control. Therefore, real-time trajectory planning and high-precision control algorithms are critical. The use of fixed wings in advanced flight reduces drag and increases energy efficiency. The wing loading is often low due to the design of these systems which are designed in most instances to be small in size. Nonetheless, reduced size entails accuracy in engineering pertaining to the balance of body and center of gravity. It is also difficult to be stable and be under control which happens mainly during landing and takeoff. When changing the position of ground approach, there might be sudden deviations between horizontal and vertical positions. This requires superior sensor design and accuracy of control software [12–14].

3. STRUCTURAL LOADING AND CENTER OF GRAVITY (CG) BALANCE

Structural loading is defined as the weight per wing area and directly affects wing design. This is expressed as:

$$\text{Wing Loading} = W \text{ (total weight)}/A \text{ (wing area)} \quad (1)$$

Table 1 summarizes the center of gravity (CG) behavior of different VTOL systems. This table quantitatively compares the wing loading and CG behavior of VTOL systems and shows the relationship between weight distribution and control stability in each structure type. In tilt-wing and tilt-rotor systems, placing the engines at the wing tips can cause the CG to shift toward the outer limits. This complicates the controllability of the system and requires special stabilizing systems (e.g., active CG management). Particularly in the tailsitter concept, failure to maintain the CG in the appropriate position during rotation creates a risk of instability during landing.

Table 5. Center of gravity (CG) behavior of different VTOL systems

System Type	CG Behavior	Description	Source
Tilt-rotor	CG generally shifts outward along the wing span due to the weight of the engines.	The location of the engines at the wing tips complicates roll moment control.	[15]
Tilt-wing	CG may vary around the wing rotation mechanism.	Moment imbalances may occur during wing rotation.	[16]
Lift+Cruise	CG tends to remain stable.	Thanks to separate lifting and propulsion engines, the load distribution is balanced.	[11]
Tailsitter	The CG is usually kept close to the center of the fuselage; however, there is a high risk of it shifting forward or backward during turns.	During the transition from vertical to horizontal flight, control surfaces are limited, making the CG position critically important.	[14]

Table 2 summarizes the general performance characteristics of different VTOL configurations. Multicopter systems offer advantages in short-range missions due to their high hover efficiency and simple structure, but their aerodynamic efficiency is low in forward flight. Tilt-rotor and tilt-wing systems are suitable for long-range and fast missions with high L/D ratios but are mechanically more complex. The Lift+Cruise concept offers both good hover and satisfactory cruise performance thanks to separate propulsion groups for vertical and horizontal flight and is suitable for urban air transportation and cargo applications. Tailsitter systems, on the other hand, are structurally simpler and offer moderate efficiency, making them particularly suitable for surveillance and reconnaissance missions [10].

Table 2. Hover Efficiency VTOL systems

Concept	Hover Efficiency	Forward Flight Efficiency (L/D)	Structural Complexity	Mission Suitability	Example VTOL Vehicle
Multicopter	High	(L/D ≈ 0) [17]	Simple	UAM, short-range transport	*EHang 216*
Tilt-Rotor	Medium	(L/D ≈ 20) [17]	High Complex	Cargo, defense, long range	*Bell V-280 Valor*
Tilt-Wing	Medium	(L/D ≈ 11) [18]	Medium	ISR, low-speed missions	*NASA GL-10 (Greased Lightning)*
Lift+Cruise	High	(L/D ≈ 9) [11]	Med	UAM, cargo transportation	*Lilium Jet*
Tailsitter	Medium	(L/D ≈ 4) [14]	Medium–Difficult	Surveillance, reconnaissance, patrol	*V-BAT*

Each concept has its own technical advantages and limitations. Multicopter systems are structurally simple but inefficient in advanced flight. Tilt-rotor and tilt-wing systems are complex but provide high speed and range. Lift+Cruise offers system flexibility by separating mission modes. Tailsitter produces low-cost solutions with its compact design but is limiting in terms of control. This assessment shows that mission type, maintenance ease, and structural integrity must be considered in concept selection, not just flight performance.

4. APPLICATION SCENARIOS

Aircraft capable of vertical takeoff and landing should be evaluated not only for their technical achievements but also for their suitability for operational needs. Different mission types have varying priorities in terms of parameters such as range, speed, carrying capacity, noise level, control flexibility, ease of maintenance, and safety. In this regard, the efficiency of VTOL concepts in various situations has been analyzed in three broad areas of application below.

4.1. Urban Air Mobility (UAM)

UAM systems will focus on offering transport solutions to passengers using small-scale transportation within metropolitan regions. These applications have the following criteria that are important:

- Noise level: Low noise production during urban activities is important to the acceptance of the people.
- Safety: As the take-offs and landings will take place in populated areas, the safety of control and resistance to the failure mode of the system are also significant.
- Short range: Its average mission profile is 10 to 50km and this offers a solution to operations with no high battery capacity needs.

Multicopters and lift+cruise systems are the ideas which fit these requirements most. The low speeds associated with the increased safety and accuracy of maneuvering of multicopters are enabled by the structural simplicity of the structural design; and also, some can have low-noise electric motors. They, however, can only be used in short range missions since they are low in advanced flight efficiency. Instead, lift+Cruise systems are also very effective in balancing energy consumption by efficiently separating take-off with cruise activities due to independent propulsion systems. More recent designs (e.g. Lilium Jet) will use channeled rotors or foldable motors to optimize the noise.

4.2. Cargo and Logistics Operations

Applications in cargo transportation normally demand longer distances and carrying capacities. The priorities in this place are:

- Cargo carrying capacity
- Energy efficiency and long range
- Advanced flight speeds
- Load balancing (CG optimization)

These applications are characterized by a large presence of tilt-rotor and lift+cruise concepts. Tilt-rotor systems result in fuel/battery efficiency in forward flight due to the forth wing flight having a high L/D ratio, and a rotor design enables the aircraft to land and unload without running a runway. Instead, Lift+Cruise systems can be considered an appropriate choice in terms of medium-scale cargo missions, as they are less complex in terms of structure. The foldable engines providing vertical takeoff on forward flight lowers the total drag and extends the range.

4.3. Defense and Tactical Operations

In military applications, mission environments are complex and risky. The following criteria are paramount:

- Multi-mode flight capability (hover + forward flight)
- High speed and long range
- Durability and adaptation to harsh environmental conditions
- Compactness and operational stealth

Tilt-rotor and tailsitter systems are the most appropriate in this regard. Tilt-rotor systems (i.e., Bell V-280 Valor) [2][19] offer high-speed and range performance with the benefit of short takeoff and landing like a helicopter. They can also carry internal cargo in the military logistics with their internal cargo carrying capacity. In turn, the tailsitter systems are very effective in reconnaissance missions, surveillance missions, and other short-term tactical assistance missions. They are capable of operating in tight spaces, provided by their small size, low radar signature and have few moving components. Nevertheless, they will need complex guidance algorithms because they face control issues upon changing the transitions between take-off and landing. Table 3 show that Hover Efficiency VTOL systems.

Table 3. Hover Efficiency VTOL systems

Application Area	Key Priorities	Suitable Concepts	Notes
UAM	Noise, Safety, Short Range	Multicopter, Lift+Cruise	Sound optimization is important
Cargo	Carrying Capacity, Range, CG Balance	Tilt-Rotor, Lift+Cruise	CG control and efficiency
Defense	Speed, Durability, Multi-Mode Flight	Tilt-Rotor, Tailsitter	Tactical flexibility is critical

5. DISCUSSION

The comparison created during the current paper was carried out without references to propulsion technologies (including energy source of the propulsion: electric, internal combustion engines, or hybrid system); rather it was built upon the design concepts as it was directly through system architecture. In this way, a similar operating system of principles is provided on finding the most relevant VTOL configuration to a specific mission profile although the type of engine might be different.

It is a technical solution to this question, which is: Which VTOL concept is more appropriate to this or that type of mission? As an example, although any concept could implement electric propulsion systems or even hybrids, that a system meets its mission effectiveness principles, such as angular efficiency, forward flight aerodynamics, structural balance, complexity of the control system, and payload capacity is much more important than its energy source.

In practice under actual working environments, the mission profiles of a large number of VTOL systems are limited by certain constraints:

- For urban air transportation applications, low speed, short range, and safety are paramount,
- High transport capacity and cruise efficiency are paramount in cargo transportation,
- In defense scenarios, multi-mode flight, endurance, speed, and maneuverability are critical.

These differing priorities require evaluating each concept's advantages and limitations within the mission context. For example:

- Multicopter systems are unique in UAM application applications with low speed, high maneuverability, low technical complexity advantages but cannot be applied to long distance missions because they lack high power flight efficiency.
- Tilt-rotor systems can be useful in missions that demand long range because they are fast and have high L/D ratio; but their complexity in terms of structure and control presents a load on the flexibility of operation.
- Lift+Cruise systems offer a balance for dual mission types such as UAM and cargo thanks to the separation of mission modes.
- Tailsitter systems offer compactness and low structural complexity advantages; however, they require precision in terms of transition stability and directional control.

It is a technical framework in addition to assessments realized on motor technologies. Even though motors are getting part of the system performance, as all types of motors can be combined with each idea of a VTOL, with such a design approach, the process of selecting the concept to work with can be more independent and methodical.

Moreover, operational factors at a higher level (scaling of system architectures, costs of maintenance, and air traffic integration) can also be evaluated through such analyses. As an example, a concept, although very efficient, can affect the mission cycle adversely because it has a high level of control or maintenance. Thus, the approach proposed will attempt to test the operational suitability of the VTOL systems through not just the technical aspect but also through the systems engineering.

6. CONCLUSION

In the framework of the current research, the VTOL vehicles were considered in the context of various architectural designs; they were compared technically and operationally, without relating to their source of energy, depending only on their flight and structural characteristics. The systems were thought of in such a way that they fulfilled different kinds of performance requirements based on the purpose they were to be used and were classified into five primary structural classes (multicopter, tilt-rotor, tilt-wing, lift+cruise, and tailsitter).

The results suggest that one can not find a single, best concept of VTOL; however, mission-based assessment should also be used when choosing a system. Both concepts are associated with some benefits and shortcomings. For example:

- Multicopters offer flexibility for low-speed and short-range missions but are limited in terms of energy efficiency.
- Tilt-rotor and tilt-wing systems offer benefits in terms of range and more advanced capability in flight; but are less structurally robust and more complex in terms of control systems.
- Lift+Cruise structures are adaptable to various scenarios thanks to the separation of mission modes, but drag-induced efficiency losses during advanced flight are a balancing factor.
- Tailsitter systems can be used in missions like reconnaissance and observation since they have a simple mechanical design although they need accurate control systems when performing maneuvers as transitions.

This discussion indicates that the concept selection needs to be made in a holistic manner regarding not just the aerodynamic parameter, but also the complexity of control, its maintenance, mission environment as well as its priority in operations.

In addition to that, the research states that hybrid structures and concept synthesis could become even more significant in the future. As an illustration, addition of fixed lift motors to tilt-wing systems to assist with lifting task can allow stability of the lift-off and transition phases and additionally, enhance aerodynamic performance. Likewise, hybrid energy systems (e.g., battery + generator systems) may enhance the performance of the system, especially on long-duration missions of high

energy density. Such structures are able to increase the flexibility of missions by alleviating constraints of a fixed architecture.

Therefore, during the design process of a VTOL system rather than a one-size-fits-all approach, mission-specific technical analyses, system engineering assessment, and operational requirements should be taken into account. These holistic assessments will deliver the creation of flexible, dependable and scalable air vehicle platforms especially in various areas including urban transport, logistics unmanned as well as military uses.

REFERENCES

[1] M.W. Mueller, S.J. Lee, R. D'Andrea, Design and Control of Drones, Annu. Rev. Control. Robot. Auton. Syst. 5 (2022) 161–177.
[2] M. Nosratollahi, H. Es-haghnia, VTOL Aircraft Architectures and Parametric Analysis, A Review, Res. Nosratollahi, H Es-Haghniaresearchgate.Net (2025) 1–72.
[3] K. Schweiger, L. Preis, Urban Air Mobility: Systematic Review of Scientific Publications and Regulations for Vertiport Design and Operations, Drones 6 (2022).
[4] N. Moradi, C. Wang, F. Mafakheri, Urban Air Mobility for Last-Mile Transportation: A Review, Vehicles 6 (2024) 1383–1414.
[5] M. Brunelli, C.C. Ditta, M.N. Postorino, New infrastructures for Urban Air Mobility systems: A systematic review on vertiport location and capacity, J. Air Transp. Manag. 112 (2023) 102460.
[6] H. Pak, L. et al, Can Urban Air Mobility become reality? Opportunities and challenges of UAM as innovative mode of transport and DLR contribution to ongoing research, Springer Vienna, 2025.
[7] A. Cohen, S. Shaheen, Urban Air Mobility: Opportunities and Obstacles, Int. Encycl. Transp. Vol. 1-7 5 (2021) 702–709.
[8] M. Osman, Y. Xia, M. Mahdi, A. Ahmed, Hybrid VTOL UAV technologies: Efficiency, customization, and sector-specific applications, Alexandria Eng. J. 120 (2025) 13–49.
[9] Z. Liu, Y. He, L. Yang, J. Han, Control techniques of tilt rotor unmanned aerial vehicle systems: A review, Chinese J. Aeronaut. 30 (2017) 135–148..
[10] Y. Zhou, H. Zhao, Y. Liu, An evaluative review of the VTOL technologies for unmanned and manned aerial vehicles, Comput. Commun. 149 (2020) 356–369.
[11] A. Bacchini, E. Cestino, B. Van Magill, D. Verstraete, Impact of lift propeller drag on the performance of eVTOL lift+cruise aircraft, Aerosp. Sci. Technol. 109 (2021) 106429.
[12] W. Zhou, S. Chen, C.W. Chang, C.Y. Wen, C.K. Chen, B. Li, System Identification and Control for a Tail-Sitter Unmanned Aerial Vehicle in the Cruise Flight, IEEE Access 8 (2020) 218348–218359..
[13] G. Lu, Y. Ren, F. Zhu, H. Li, R. Xue, Y. Cai, X. Lyu, F. Zhang, Autonomous Tail-Sitter Flights in Unknown Environments, IEEE Trans. Robot. 41 (2025) 1098–1117.
[14] X. Lyu, H. Gu, J. Zhou, Z. Li, S. Shen, F. Zhang, Simulation and flight experiments of a quadrotor tail-sitter vertical take-off and landing unmanned aerial vehicle with wide flight envelope, Int. J. Micro Air Veh. 10 (2018) 303–317..
[15] D. Felix Finger, C. Braun, C. Bil, A Review of Configuration Design for Distributed Propulsion Transitioning VTOL Aircraft, Asia-Pacific Int. Symp. Aerosp. Technol. (2017) 1–15.
[16] P. Hartmann, C. Meyer, D. Moormann, Unified velocity control and flight state transition of unmanned tilt-wing aircraft, J. Guid. Control. Dyn. 40 (2017) 1348–1359.
[17] W.J. Fredericks, M.D. Moore, R.C. Busan, Benefits of hybrid-electric propulsion to achieve 4x increase in cruise efficiency for a VTOL aircraft, 2013 Int. Powered Lift Conf. (2013) 1–21.
[18] B. Xiang, G. Tao, L. Jin, J. Zhang, J. Chen, CFD Aerodynamic Analysis of Tandem Tilt-Wing UAVs in Cruise Flight and Tilt Transition Flight, Drones 9 (2025).
[19] M.J.S. Lopez, C.S. Duffy, M.B. Tischler, P. Ruckel, Bell V-280 hover flight dynamics model validation and update with flight test data, 77th Annu. Vert. Flight Soc. Forum Technol. Display, FORUM 2021 Futur. Vert. Flight (2021).

BIOGRAPHY

Öztürk Özdemir Kanat is an Assistant Professor in the Department of Aircraft Maintenance and Repair at Kastamonu University. His research focuses on innovative UAV projects, system integration, and computational fluid dynamics (CFD). He actively engages in research collaborations and has contributed to publications in reputable international journals. His work emphasizes advanced aerodynamic modeling and design optimization, supporting the development of high-performance VTOL and fixed-wing unmanned aerial platforms.

Yasin Özcan is an Assistant Professor in the Department of Mechanical Engineering at Kastamonu University. His research interests include renewable energy, energy optimization, machine learning, and computational fluid dynamics (CFD). He actively engages in both experimental and computational studies aimed at improving the efficiency and sustainability of systems.

Umut Kaya is a Research Assistant in the field of Mechanical Engineering, specializing in heat transfer, fluid mechanics, and deep learning applications in engineering systems. He is currently pursuing his PhD at Hacettepe University and serves as a Research Assistant at Kastamonu University. His academic and research interests lie in integrating computational methods and artificial intelligence with traditional thermal and fluid sciences to develop innovative and efficient engineering solutions. He continues to contribute to interdisciplinary research projects and aims to advance data-driven modeling approaches in thermal-fluid dynamics.

ICENS 11TH INTERNATIONAL CONFERENCE ON ENGINEERING AND NATURAL SCIENCE October 22-26 2025 Sarajevo

Integrating Design Principles and Post_Occupancy Evaluation of Educational Buildings :A Shrjah Case Study

Dr. Mousa Al-Dghaimat[59], Dr. Alaa Abdou [60]

Abstract

This study applies a customized Post Occupancy Evaluation (POE) to a private school in the UAE, addressing the gap in region-specific evaluation frameworks for educational buildings. A two-part assessment—technical performance analysis and occupant perception surveys—was developed from a targeted literature review. Using base drawing analysis and structured walk-through observations, the study identified design strengths and areas for improvement directly affecting user experience. Outcomes aim to embed POE into facility management practices and provide actionable feedback for the design of future educational facilities in the UAE

Keywords: Post Occupancy Evaluation (POE), Functional Performance Specifications, Walk-through, Educational Buildings.

1. INTRODUCTION

Post-Occupancy Evaluation is a process of systematically evaluating the performance of buildings after they are built and occupied for some time. This evaluation differs from other types of buildings' performance evaluations because it focuses on the needs and requirements of building occupants including health, safety, security, and functionality [1].

The term Post Occupancy Evaluation is defined as a process, which involves evaluating a buildings performance after it has been occupied by its target users. It is concerned with several issues such as: health, safety, security, efficiency, comfort and many other requirements, and provides feedback about the current of the project and proposes solutions to the existing problems. In addition, it can provide guideline principles and design criteria to improve similar future projects. POE

POE has been seen as one of a number of practices aimed at understanding design criteria, predicting the effectiveness of emerging designs, reviewing completed designs, supporting building activation and facilities management, and linking user response to the performance of buildings [2]. BOE is recently evolving toward more process-oriented evaluations for planning, programming, and capital asset management, it generates overall beneficial changes and outcomes, including: Saving dollars and energy, improving the quality of facilities, involving stakeholders in the process of POE, and improving the satisfaction of building occupants [3].The paper starts with providing a background status on the benefits, uses, and methods and techniques of POE in general and for educational facility in particular. The paper then presents the proposed criteria for the POE and the implementation of its assessment, starting with Technical Part, which include: base plan analysis and walk through observations, then Occupant Perception which include: questionnaire development, design – based modifications. Finally, the paper ends with a conclusion and a plan for future work.

2. BENEFITS AND USES OF POES

During the development of any project, the value delivery is the key goal of all stakeholders. Austin [4] defined value as "the trade-off between what each stakeholder gets and what they have to give up". All participants in the building delivery process should have a clear understanding of what type and level of performance should be achieved in a facility [5]. After the delivery of the facility and its occupancy by the target users, facility managers can utilize the POE as a diagnostic tool to identify and evaluate the critical aspects of building performance systematically. By comparing the performance criteria with the actual measures on ground, the outcomes of POE can benefit facility managers to maintain and improve their facilities and can also be documented as lesson learned with direct input into the next building cycle. Figure 1 illustrates the performance concept in the building delivery process as well as the basic outcomes of post occupancy evaluations from short- medium and long-term perspectives.

1 Ajman University, UAE

* Corresponding author: Ajman University, UAE. mousadghaimat@gmail.com

Several benefits can be obtained from performing POE. Preiser [6] categorized the uses and benefits of POE into short, medium, and long term. While the short term refers to immediate action; medium term includes three to five-year time frame, which is necessary for the development of new construction projects; and the long- term time frame is ranging from 10 to 25 years, which is necessary for strategic planning, budgeting, and master planning of similar facilities. In more details, the short-term benefits include the following:

1) Identification of possible solutions to problems in the facilities, responding to building user needs and values.

2) Improving space utilization and obtaining feedback on the building performance.

3) Improving the attitudes of building occupants through

active involvement in the evaluation process.

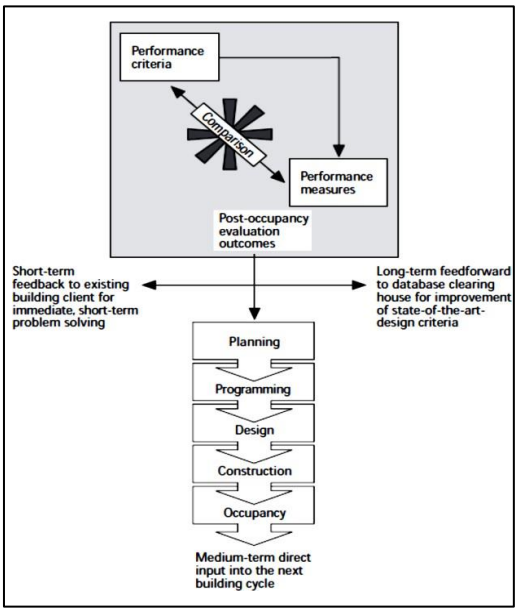

Figure 1. The performance concept in the building delivery process -Source: [5]

The medium-term benefits include:

1) Built-in capacity for facility adaptation to organizational change and growth over time, including recycling of facilities into new uses.
2) Significant cost savings in the building process and throughout the life cycle of a building.
3) Accountability for building performance by design professionals and owners.

While, the long-term benefits include:

4) Long-term improvements in building performance.
5) Improvement of design databases, standards, criteria, and guidance literature. Improved measurement of building performance through quantification via improvements in the programming and planning of buildings.
6) Preiser [6] and Other researchers [3, 7-10] recounted in their research work almost the same benefits that was discussed earlier, including: recommendations that are brought back to the client; re-modeling that is done to correct problems; lessons learned that influence design criteria for future buildings; and finally positive influence upon the delivery of humane and appropriate environments for people

3. TYPES, TECHNIQUES, AND METHODOLOGIES OF POST

3.1 Occupancy Evaluation

According to Hadjri and Crozier [9], there are numerous approaches to the concept of POE with a wide variety of methodologies that have been developed in order to address the specific conducting POE. When reviewing the different methodologies of POE, it is important to refer to the research work in [11]; where the authors discussed the common strategies and techniques of POE. They described realism as the original of all techniques and methods used in POE's research.

According to [5] and [2], POEs are traditionally conducted using questionnaire, interviews, site analysis, and observations of building users. Over time, more specific processes, levels of survey, and new technologies have been developed to better-fit stakeholder's objectives and budget. Currently, there are numerous methods and approaches to POE, depending on the contextual agenda and the required outcomes. In reviewing the research work of [3, 6, 7, 12], the POE can be analyzing and arrange into three levels of typical process, defined as:
Indicative Post Occupancy Evaluation: This provides an indication of the major strengths and weaknesses of a particular building's performance.
Diagnostic Post Occupancy Evaluation: where the evaluation criteria are either explicitly stated in the functional program of a facility or have to be compiled from guidelines, performance standards, and published literature on a given building type.
Investigative Post Occupancy Evaluation: in this level, it correlates physical environmental measures with subjective occupants' response measures, see Figure 2 for details.

3.2 The Pros and Cons of POE

One of the characteristics of POE activities is the discrepancy that exists between the reasons for doing POE and the difficulty of doing them. The possible benefits of doing POE are discussed in [13]. The author stated that POE is a useful tool for improving buildings, increasing occupants' comfort, and managing costs, while the barriers to widespread adoption of POE are cost, defending professional territory, time, and skills needed [13].

According to [12], one of the problems of the POE is the ownership. There are benefits to both the client and the designer, but who should pay for it? Customers/clients may view their payment for the building as including any testing that needs to be undertaken to ensure everything is working in order

In contrast, the project design team will not want to utilize all their profits by paying for an evaluation, as POE is not part of standard procurement procedures, there is little incentive for the designer to differ from the standard approach. Despite the increasing climate for POE to work, there is still a reluctance to engage in any form of systematic evaluation process of those involved in the design and construction industry. It is likely that many clients and designers have not heard of POE yet. As a result, the benefits of POE cannot be achieved and this will lead to future problems when using the facility [12].

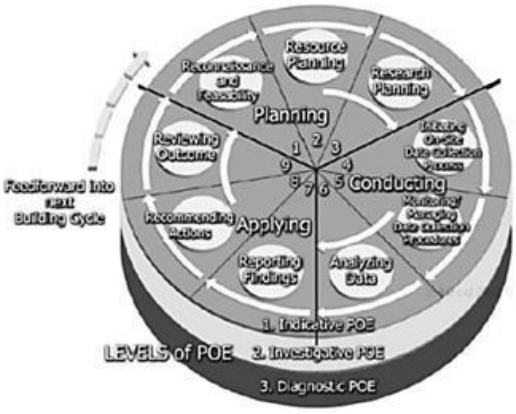

Figure 2. Post Occupancy Evaluation: evolving performance criteria. Source: [6]

Barriers to widespread adoption of POE were discussed in [2]. The first identified obstacle is the cost, as discussed earlier, while the second barrier is professional territory that is necessary for POE to be seen as useful for remote knowledge. Finally, skills, where there are no specific skills or technique or even tools with POE studies which can lead to other problems when evaluating the buildings performance.

3.4. The Use of POE for Educational Buildings

Reviewing literature, several research projects investigated POE in educational buildings, particularly in schools. Two case studies of educational buildings were reviewed and analyzed in details to discuss how they were implemented; understand the objectives of the POE process; describe the techniques and methods used; and finally, to illustrate the findings and lessons learned, the summary of those four cases is described in the coming paragraphs.
The First case study was conducted in the UK, by [14]. The aim of this study was to describe the development of evidence based for establishing the best conditions for optimal learning spaces. The study was implemented at five diversified primary schools in the UK. The POE methodologies used in this study consist of: first, a questionnaire survey which was used for gathering the information in regard to interviewees' views. The
goal of this survey was to gain an understanding of people's experience and perception of the schools. Secondly, interview sessions, with head teachers to explore in more depth, the complex feelings, beliefs and attitudes surrounding the questionnaire responses. Finally, workshops and site observations were conducted with team members involved in the process to communicate and refine the outputs of the study. This multi-POE work, with its comparative study between many

schools, provided opportunities for the principals and head teachers of schools and local authorities to understand the current performance of school spaces which resulted in routine feedback into the briefing, design, construction stages.
The second case study was implemented in Saudi Arabia [15]. Its POE method was developed in order to evaluate three primary schools. The toolkit used in this research aimed to position the children, teachers and parents who use the school. This method identified weaknesses in the three schools and differences in response from the three groups consulted. The POE was implemented in three stages, first stage commenced with a familiarization of the three schools, through guided tours, conducting interviews with teachers, and walk through observation. Second stage included the design checklists, to assess the presence and adequacy of different educational facility design features. Finally, the third stage, the POE questionnaire survey, which was conducted with teachers, students and parents. The analysis of responses revealed that the parents agreed with teachers that the building was aesthetically pleasing, age appropriate, spacious, and had good circulation, with clear and visible signage that was easy to follow. The parents also felt that the building was well landscaped, with (adequate) lighting and ventilation. However, students' results focused on the weaknesses of some facilities' spaces and how it hindered their ability to learn. They were dissatisfied with their cafe, rating this as being unattractive place to eat which was echoed in the POE results of the teachers as well, students were also dissatisfied with the restroom facilities

3.4 Criteria for Post Occupancy Evaluation of the School Facility

The aim of the presented research in this paper is to test whether the selected school and its spaces provide students, teachers and staff with spaces that fulfil their needs, and enable them to perform their work effectively during the different educational activities performed. The proposed POE criteria have two main parts: 1) Technical evaluation and 2) Occupants' perception. The first part, the technical evaluation, involves the analysis of existing base plans and available documentation's; and a Walk-through observational technique to investigate the possible POE problems/issues and take photos and measurements, if needed. In the second part, to obtain occupants' perception for facility performance; a semi structure interviews/group meeting, with teachers and staff, is proposed to investigate possible problem/issues.

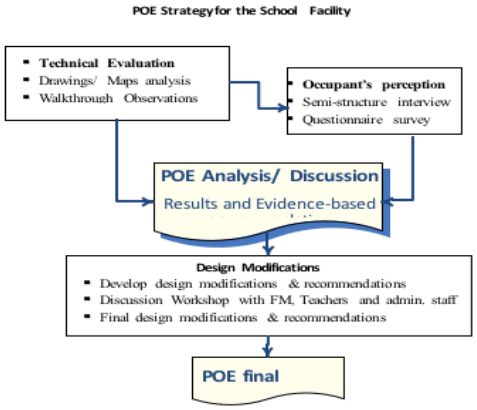

Figure 3 illustrates the proposed POE criteria

Based on the previous step, a questionnaire survey will be developed and conducted to quantitatively measure the perception of students and teachers in regard to observed problems and issues in previous steps.

Following that, a proposal for design modifications and recommendations to improve facility performance will be developed and discussed with school principal and the administration staff members. Final design modifications & recommendations will be then conducted. The implementation of the first part of the POE criteria, i.e. the technical evaluation is described in the following sections.

4. THE IMPLEMENTATION OF POST OCCUPANCY EVALUATION CRITERIA: THE TECHNICAL PART

4.1 *Base Plans Analysis*

The selected case study that was examined in this research project is a private school, located in the city of Sharjah, UAE, where it's inaugurated and occupancy began on September 2010. The school is owned and operated within the private sector. Its initial construction cost was approximately 20,000,000 AED. The ministry of education sub-divided the school grades in to 3 categories: primary, elementary, and the secondary levels.

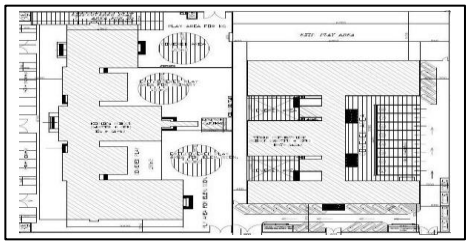

Figure 4. School layout

A primary level begins at grade one until grade six, while the elementary level incorporates grade seven to grade nine, and the secondary level commences from grade ten till grade twelve. The total student capacity is: 375 students at the primary level, 200 students at the elementary level, and 100 students at the Secondary level

The main aim of this research is to investigate the effectiveness of the school facilities. Furthermore, the research was intended to identify any gaps or inefficacies in the design and to make recommendations for future new schools' improvements. This evaluation covered the following area of the school building:

1) Spaces functionality, including Safety and security.
2) Physical environment (lighting, cooling, air quality, etc.
3) Occupants' control which aims to measure the degree of case with which the end users are able to control elements such as the AC's system, lighting system, and the spaces used in the school
4) Document analysis is the method used for POE implementation, which includes investigating and analyzing, archiving, drawings, maps, and specifications. Figure 4 illustrates the layout plan for the selected school. The analysis of the school site plan revealed the following issues:
5) The school has only one main entrance which creates a
6) gender conflict, and cause disorganization and congestion.
7) The buses parking area has time tabled for the use of the school buses and the same area is the students' congregation point.
8) The playing and open area in the north side looks small and insufficient for the700+ student body.
9) The analysis of the school ground and first floor plan, illustrated in figures 5 and 6, revealed the following issues:
10) Corridors of different school zones are directly connected,
11) without any doors, which result in congestion between the senior and junior students, who are younger and are more vulnerable children.
12) Inadequate number of toilet facilities for the students. In addition, the European WC type is missing, which is crucial for some students, especially those with special needs.
13) Figure 5. Ground floor plan
14) Music room is located between the classrooms, with low sound insulation treatment, which cause noise and create distraction.
15) Activity room is located in-between the classrooms causing problems by the noise of the performed activities. All labs are located in the first floor, which are a source of possible hazard and cause congestion in using corridors and stairs

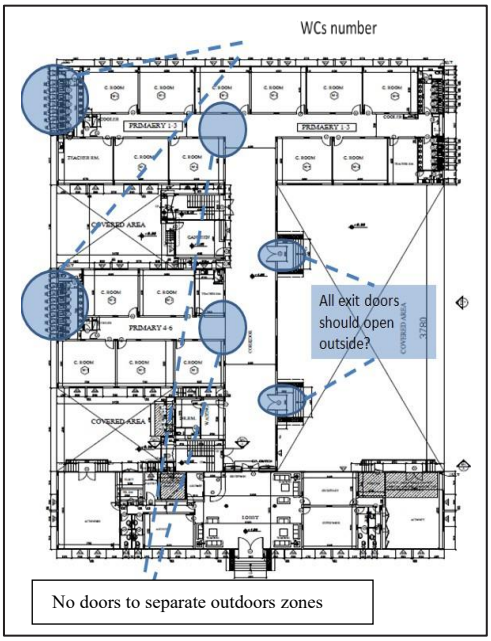

Figure 5. First floor plan

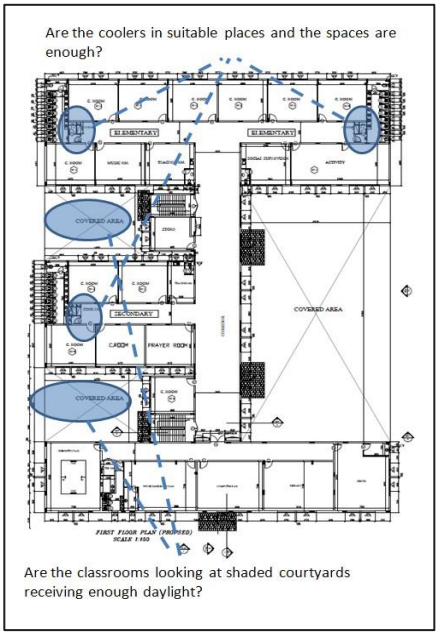

Figure 6. First floor plan

4.2 Walk Through Observations

Walk through observations were conducted for several days to investigate and evaluate a potential issues and shortcomings in the school buildings and its site layout. It was recorded using a note pad and a digital camera. Several photographs were taken during the walkthrough observations during the tour accompanied by the facility manager. Table 1 illustrates the anticipated problems that were observed during the walk through

	
The activity room was transferred into an office area, causing a lack of space for students' different activities	The old built-in water coolers were replaced, with temporary Ones
	
The passage to the lavatory area is narrow and the space within the maneuvering and movements of vehicles.	Only one gate is available for vehicles entrance and exit, another gate is needed to ease
	
Students' assembly area is used in the same time for buses parking.	A wooden step was built to help children to reach the wash basins

Table 1. The Walk Through Observations

5. THE IMPLEMENTATION OF THE QUESTIONNAIRE

To facilitate effective research methods, a questionnaire was compiled and distributed to various students' samples in the selected private School. The survey was part of a primary research exercise to understand more about the field opinions. Furthermore, the questionnaire was a key component of this project, as it provides the foundation for recommendations with respect to the views of the occupants in the private schools in Sharjah, Dubai and Northern Emirates. The aim of this questionnaire was to investigate the effectiveness of future school facilities and the impact of the school's enhancement on the learning objectives of private schools. Furthermore, the research was intended to identify any gaps or inefficacies in the design and to make recommendations for improvements for future school developments.

The first part of the questionnaire assesses the effectiveness of school building in light of different categories, i.e. functionality, learning environment comfort (lighting, cooling, noise, air quality, etc.)., and occupants' control which aimed to measure the degree of how easily the final occupants could control facility elements such as the AC's system, the lighting system, the spaces used within the school, and the safety within the school building.

The second part of questionnaire focuses on the availability of open areas and play yards, green areas access to school, movement, and approach to school.

The third part of the questionnaire focused on safety and security in the school. There were 8 statements assessing the safety measure in the school facilities, such as indoor and outdoor circulation, firefighting system, emergency exits, and the free flow of movement when transitioning between spaces.

The fourth part of the questionnaire focuses on the learning environment comfort. It assesses the day-light, air quality and sound isolation between classroom and other facilities.

The fifth part of the questionnaire discusses the interior quality. And evaluates the proper use of the interior furniture and finishing materials for the floors and walls, this part highlighted 7 positive statements.

And the following part of questionnaire assesses the access and approach to school, including ease movement inside and around the school, and the availability parking for cars and buses. Finally .The last section of questionnaire discusses and evaluates the aesthetic and architectural appearance in the school. It is focuses on the external view of the school, landscape, and the aesthetic appeal of the main entrances.

5.1 The Sample Characteristics:

The questionnaire was distributed to the respondents, as shown below in table (No-2) and figure (No-7). A total of 295 students and 50 employees were invited to join this research project.

To ensure that the questionnaire was well distributed and the respondents understood it, and the questions were properly answered, the researchers visited the school several times.

The questionnaire was distributed to the elementary and secondary students from grades 6-12. The statements were explained to each student. The researchers conducting the investigation had a meeting with the teachers in the teacher's room and met with the employees in the principal's meeting room. The purpose of the explanation was to make it easier for them to understand the details of the questionnaire to gather more accurate data.

The respondents included 277 students, 36 teachers, and the administration staff. The valid questionnaire used for statistical analysis amounted to 265 for students, which represented about 89% of total grades of students in the school, and 36 employees, representing about 72% of the total number of the employees in the school.

Table 2. The respondent's categories

Table OF Figures Entries Found	Total Sample	Received Sample	Valid Questionnaire	Percentage OF Valid Respondent
Grades 6,7,8,9,10,11,12	295	277	275	93,2%
Employees	50	36	36	72%
Total	345	313	311	90,1%

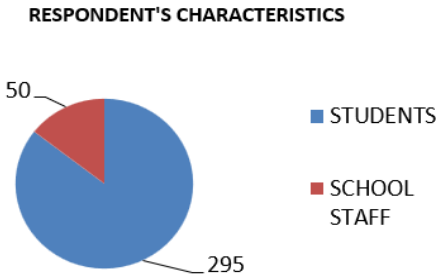

Figure 7. respondent's characteristics

5.2 Questionnaire Results and Analysis:

The questionnaire investigates 6 main categories as the following:

Functionality, safety and approach, security, learning environment comfort, interior quality, access and approach, finally aesthetic and architectural appearance. Table No-3, shows the overall average of respondent's opinions about all categories.

Category No	Category		Average		
		S	Employee	Students	All
1	Functionality	1.30	3.19	2.4	2.8
2	Safety and Security	1.36	3.17	3.03	3.1
3	Learning Environment Comfort	1.32	3.65	2.7	3.17
4	Interior Quality	1.23	3.77	2.44	2.81
5	Access and Approach	1.24	2.41	2.44	2.33
6	Aesthetic and Architectural Appearance	1.17	2.71	2.25	2.48
Total		1.27	3.15	2.54	2.78

Table 3 .Overall average of respondent's opinion for allcategories

Through analyzing the six categories of the questionnaire, it was conducted that the highest average opinion of employees which is (3.77) was for the quality of the interior. It showed their satisfaction regards the flooring and walls finishing materials used.

The second category related to the comfort of learning environment which scored an average of 3.65, indicating that the employees were satisfied with the amount of natural day light acoustics, lightings, and air quality.

The next two categories review the functionality, safety and security in the school and averaged 3.19 and 3.17 respectively.

The next category reviewed the aesthetic and architectural appearance with the respondents' average being 2.71, a little under the midpoint. It revealed a less than favorable response from employees, indicating that some modifications in the redesign process were required. This category showed an agreement between the questionnaire respondents and the interview respondents.

The final category was in regards to the ease of access and approach to the school. This category only got an average of 2.41, which was near to disagree on the scale provided on the questionnaire. It indicated that the teachers and staff were dissatisfied, and the access and approach to the school required major modifications in order to find a suitable solution to the problem of access to the school.

Through the analysis of the same six categories, it was found that the highest average opinion of student's sample was 3.03, regarding the safety and security. This scored a mid-point average indicating that further improvements for school design would be beneficial.

The next category concerned the learning environment and its general comfort with average score of 2.70. This was lower than the midpoint and showed less agreement over the day light, acoustics, lighting, and air-conditioning, requiring some minor improvements in this category.

The third, fourth, and fifth categories reviewed the interior quality, access and approach to the school, and its functionality, with averages of 2.44, 2.44, and 2.40 respectively. These three categories gave a less than neutral response, which indicates a consensus from the respondents to these three categories. It revealed that there is a need to make some modifications to the

design to improve the use of clinic and cafeteria spaces. The questionnaire results agreed with the respondents' opinions from the initial interview survey. In addition to this, there is a need to enhance and develop the accessibility to school redesigning the setting layout plan. This was also noted in the interviewers complains and was observed by the researcher during the walk-through survey of the school facilities.

The findings revealed that the highest average for all respondents in the school was 3.1, which related to the learning environment comfort. This is a slightly over the midpoint. It indicates that there is some consensus from all respondents regarding this category, proving it to be to some degree, satisfactory.

The safety and security category had the second largest average with a score of 3.10. This category gained approximately the same result as the first one, which is little over neutral.

The next two categories related to the interior quality and functionality of the building with total average of all respondents of 2.81 and 2.80 respectively. These results were close to neutral showing less consensus to the previous category, and therefore would require some minor modifications to be carried out to and improve the learning environment, which was also echoed in the interviewees complains documented at the beginning of this paper.

The aesthetic and architectural appearance category scored a very low average of 2.48, much less than midpoint, but still above unsatisfactory. It showed an agreement between all respondents. This category recommended further modifications in the redesign of the external facades.

The last and lowest average for all respondents was 2.33 in regards to the access and approach to the building, which is still above unsatisfactory, but much lower than midpoint. It revealed that there was a big consensus between all respondents indicating that this category needs significant modifications to the redesign of the setting layout plan in order to find suitable solutions for the issues of accessibility to school. This matched the observation made by the researchers during a walk-through survey, and was in agreement with the complaints raised by interviewees during the interview.

The final average for all six categories was 2.78. This is a little under neutral. It revealed a general consensus and was in agreement with the complaints that were made during the interview stage of this process.

6. DESIGN-BASED MODIFICATION

Based on the data collected from the interviews, walkthrough, questionnaire survey and the technical evaluation, positive aspects were clearly identified, as well as other elements of the school building that would benefit from improvement. The following suggestions were made to improve the spaces in the school so that activities in these spaces could be carried out as efficiently as possible.

Every aspect of the school was subject to investigation. Based on this investigation, the researchers concluded that there was an urgent need for modifications in the areas listed below:

1) The setting layout plan including parking, exits, and landscaped areas.
2) Segregation of all student categories; primary, elementary, and secondary.
3) A lift for special needs students.
4) Improved cafeteria and dining spaces for students and staff.
5) The addition of emergency stairs for labs spaces.
6) European Lavatories for Students.
7) Improvement made to the aesthetic and architectural facades.

6.1 The Setting Layout Plan İncluding Parking, Exists, And Landscaped Areas:

In response to the data collected during this research project, it was agreed that the school required at least one additional gate for vehicles to exit, and required more landscaping. It was proposed by the researchers that one more back exit gate be added to the building. See figure (No-8).

The installation of an additional exit gate would solve the issue of traffic congestion and facilitates the flow of cars and buses around the school. The researchers proposed a redesign of the setting layout plan, adding additional grassy areas and trees adding to the aesthetic appeal of the school.

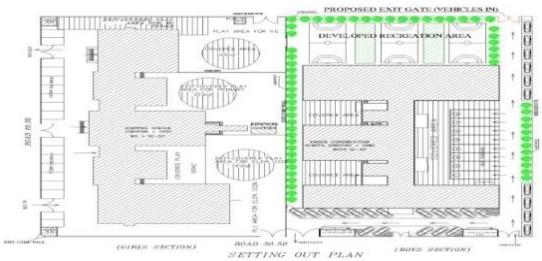

Figure 8. Proposed exit gates.

6.2 Zoning Between Students' Categories:

Based on the researcher's explanation of the zoning process separating the varying age levels of students during the walk through and interview process, the consensus of the teachers and staff who participated in the questionnaire, was that they all agreed that the zoning and partitioning between students divisions will result in greater privacy in each zone, and keep the noise levels at a minimum, and would keep the younger students safe and away from the older students.

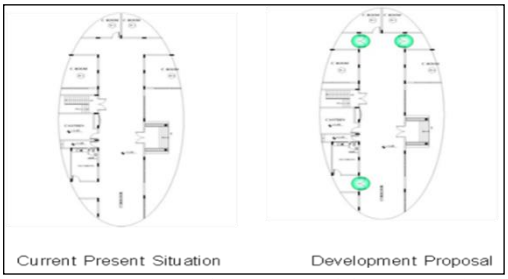

Figure 9. proposed partitions and doors (zoning)

The researchers proposed a partition wall and door be constructed in each zone on the ground floor for this purpose, as shown in figure (No-9).

6.3 Lift for Special Needs Students:

This problem was also flagged during the walk through of the school facilities. Most students agreed that the school needs at least one elevator to serve the special needs students and teachers. It would also help in the transportation of goods and materials to the first floor. Therefore, the researchers proposed the installation of an elevator near the students' entrance and administration area, which would serve both students and staff, in addition to any guests of the school. See figure (No-10).

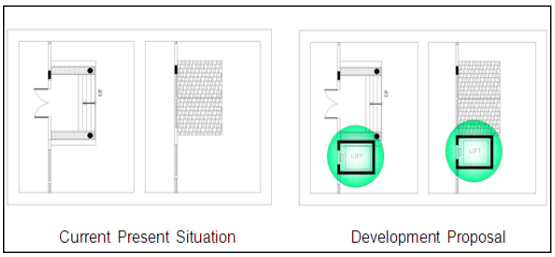

Figure 10.Additional lift to serve special needs students' ease and help transportation the goods.

6.4 Cafeteria and Dining Spaces for Students:

There was a general consensus from the questionnaires and interviews with the teachers and administration staff; they all agreed that the cafeteria space is too small and not suitable to serve the student body and staff. The researchers proposed to use an open shaded area behind the cafeteria as a dining and relaxing area, see figure (No-11).

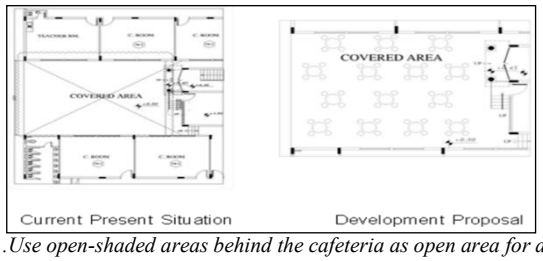

Figure 11 .Use open-shaded areas behind the cafeteria as open area for dining and resting.

6.5 Emergency Stairs for Labs Spaces:

Base on the data collected during the internal walk-through of the building, the information collected from the questionnaire and the inspection report from the civil defense inspector it was cleaned that the issues raised required urgent and immediate attention. After reviewing the blueprints of the school, it was recommended that 2 additional emergency steel stair well be added to each end of the laboratory corridor. In the event of a fire; this would ease the evacuation process. See figure (No-12).

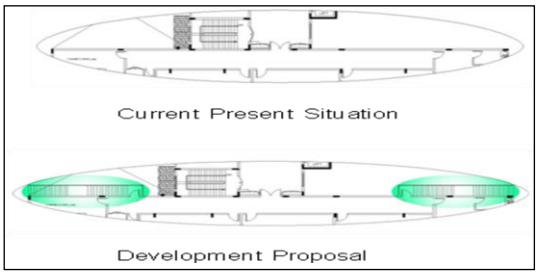

Figure 12 .Additional steel stairs for emergency exit

6.6 European Lavatories for Students:

The researchers encountered this problem during their observation walk inside the school. In the questionnaire, there was a consensus of opinion from the students concerning this as well as in issue, the teacher's responses during the interview process. The researcher's therefore proposed to make minor modifications to the existing lavatories which all are of Asian design. They proposed to change 25% percent of the lavatory units from the Asian model to a European model, which would satisfy students offering greater comfort when using lavatories.

6.7 Aesthetic and Architectural Facades:

In reference to the questionnaire results, it was found that most of the students' responses concerning this issue were same, a consensus from both students and staffs regarding this issue. Their opinions were supported by the results gained during the interview process with the employees, and the researcher's opinion gathered after a walk through survey. It shows that the school views were very traditional style.

The researchers proposed modification and the redesign the facades. The improved design for school facades was a modern style using the latest cladding material, (Aluminum composite panels), which would add to school modern, state of the art look. It would also fit more comfortably with the architectural appearance of the surrounding community. See figure (No-13). It shows the old and the new look of the school after modificatio

Figure 13 .Old and the new look of the school after modification

7. CONCLUSIONS AND RECOMMENDATIONS

The Post Occupancy Evaluation POE is an interesting process, which assesses the deferent uses of building after they have been occupied for a short period of time [2]. To conduct such an evaluation, the researchers should be fully qualified and experienced in both the architectural and construction fields.

The school selected to conduct this research project is located in the city of Sharjah. It is a private school, constructed and began its occupancy 3 years ago .These characteristics make this school a suitable building for research and re-evaluation, based on the knowledge and skills gained from the literature review, and lesson learned from the case studies.

The objectives of this research project were to evaluate performance of the future school facilities and to study the impact of the school's enhancement of the learning and education process in the private sector schools, highlight the inefficiencies in the school design, and to eliminate these shortfalls by recommending the requirement improvements for future schools.

Several tools were used in this case study to assess the performance of the school facilities such as; walk-through of the school facilities, semi-structured interviews with the administration staff, teachers, teachers' supervisors, and facility managers, and the qualitative techniques which led to the problems that were quantified in the questionnaire.

The questionnaire included examined six categories as follows:

Functionality, safety and security, comfort of the learning environment comfort, interior quality of the interior, access and approach, and aesthetic and architectural appearance.

The questionnaire sample consisted of 345 employee and student, 87% of the total sample responded to the questionnaire survey.

Analysis of the questionnaire results shows that both employees and students are satisfied with the interior

In addition, the survey revealed need to install a lift for special needs users. quality, and learning environment comfort within the school building. These two categories were generally directly linked to the safety, comfort and quality of the materials used, which were the main criteria and requirements for the completion of the building used for educational purposes.

These two categories were also explored, through the researcher's observations when conducting a walk- through in the school. During the semi-structured interviews it was indent that admin staff and teachers were satisfied with the safety, comfort and quality of the school building.

In the category for functionality employees were satisfied, evidenced in their responses during the semi-structured interview in the beginning of this study. Based on the qualitative techniques used in the questionnaire, and after analyzing the results, it was found that the respondents were generally satisfied, but did find some shortcomings in the design, such as the small cafeteria space, and the requirement to add another area to be used as dining space for the students and employees.

Most of the respondents in the semi-structured interview agreed that separated zones between the student's categories were vital, and must be acted upon to ensure the younger students safety.

The category concerning the access and approach to the school was unsatisfactory according to the data collected. According to the questionnaire results, it was found that most of the students didn't like the aesthetic and architectural appearance of the school, which also commented on unfavorably by the researchers. They found that the school facade was traditional and simple, and required minor modification.

In the modification of the design of the building, the researchers focused on the necessary modification of the school facilities. There were eight areas that were suggested under so minor changes in their design, which would offer as a solution to the main problems identified by the post occupancy evaluation used in this research. These changes will affect the accessibility and traffic in and outside of the school, the zoning between students' levels, lift installation, emergency stairs, acoustic isolation, and additional space for cafeteria.

7.1 Recommendations for the Existing School Building:

7.1.1 Short term recommendations:

1) Availability of at least one more exit gate for vehicles (especially buses) from rear of the school. This will facilitate the movement of traffic inside the compound wall of the school.
2) Installing zoning between student's levels (categories) by creating partitions with doors to separate each zone. This will keep younger students safe and avoid accidents and injuries.
3) It is vital to ensure that the cafeteria space is increased through use the open covered area adjacent to it, as a dining area with tables and chairs for all students and employees. This will achieve a more strangled environment for its users.
4) The availability of one elevator for the special needs students, and for transporting goods, books, and other

materials to the first floor would be advantageous.

5) Enhance the external appearance of the school by fixing modern aluminum composite paneled cladding to the front aspect of the building and students entrance. This will achieve the required architectural appearance to the school.

7.1.2 Long term recommendations:

1) The school requires a larger area which allows designers to present a unique and comprehensive design such as adequate recreational areas, a covered swimming pool a mosque, additional parking areas, and an adequate number of gates
2) School zoning is required, separating the students' categories; separate buildings to house 3) each age group would be preferable.
3) Each school should ensure that there is an amble car parking space for employees, visitors, and the service sector and buses.

7.2 Conclusion and Future Work

POE has a wide variety of methodologies that vary in nature, size, and level of interaction. Decisions regarding POE use need to take into account the purpose of the study or the organizational benefits that can be derived from the results of POE. By using the POE, several benefits can be gained such as: improved space utilization and feedback on the building performance; recommendations that are brought back to the client; lessons learned that influence design criteria for future buildings; and finally, positive influence upon the delivery of humane and appropriate environments for people.

The presented work in this paper is a part of an ongoing research work aiming at developing and implementing criteria for a POE for a private school facility in Sharjah city, UAE, to determine its performance based on its users' satisfaction and experiences. Proposed criteria for the POE are presented with two main parts: technical evaluation, and occupants' perceptions. The technical evaluation part is presented in this paper, and commenced with the analysis of existing base drawings and documentations; and a Walk-through observational technique

to provide a closer investigation and to reveal aspects of interior design that could be further examined and evaluated. In regards to the functionality of different facility spaces, it was observed by the walk through and drawings analysis that some inadequacies are there, such as the small cafeteria space, and the need to add another area to be used as dining space for the students and employees.

The future work will focus on obtaining occupants perceptions for the facility performance. A semi structure interviews/group meeting, with teachers and admin staff will be utilized to further investigate the identified issues and other possible problems/issues in using the facility. Based on that, a questionnaire survey will be developed and conducted to measure the perception of users for facility performance. Following that, a proposal for design modifications and recommendations to improve the performance of the school spaces will be developed and discussed.

ACKNOWLEDGMENT

The authors would like to thank Dubai and Northern Emirates Education Council, and the principal of the investigated school and all employees, including teachers and the facility manager for their cooperation during the date collection and implementation stages of this research project.

REFERENCES

[1] *C.F.F, Overview: A Summary of Finding, in Learning from Our Buildings : A State-of-the-Practice Summary* of Post-Occupancy Evaluation, C.F.F, Editor 2001, National Academies Press: Washington, DC, USA. p. 9-15.
[2] Council, F.F., Learning from Our Buildings : A State-of- the-Practice Summary of Post-Occupancy Evaluation2001, Washington, DC, USA: National Academies Press.
[3] Preiser, W.F.E., Continuous quality improvement through post-occupancy evaluation feedback Journal of Corporate Real Estate, 2002. 5(1): p. 42 - 56.
[4] Austin, S.A. Principales of Managing Value in Design. 2005 [cited 2011 10 October]; Available from: http://www.valueindesign.com/principles/principles.htm.
[5] Preiser, W.F.E., Post-occupancy evaluation: how to make buildings work better Facilities, 1995. 13(11): p. 19 - 28.
[6] Preiser, W.F.E., The Evolution of Post- Occupancy Evaluotion: TowardBuilding Performance and Universal Design Evaluation, in Learning from Our Buildings : A State-of-the- Practice Summary of Post-Occupancy Evaluation, C.F. F., Editor 2001, National Academies Press: Washington, DC, USA.
[7] Preiser, W.F.E., Building Performance Assessment—From POE to BPE, A Personal Perspective. Architectural Science Review, 2005. 48(3): p. 201-204.
[8] Whyte, J. and D.M. Gann, Closing the loop between design and use: post-occupancy evaluation. Building Research & Information, 2001. 29(6): p. 460-462.
[9] Hadjri, K. and C. Crozier, Post-occupancy evaluation: purpose, benefits and barriers Facilities, 2009. 27(1/2): p. 21 - 33.
[10] Zimring, C., Post-occupancy evaluation - issues and implementation, in Handbook of Environmental Psychology, R.B.B. Arza Churchman, Editor 2002, John Wiley & Sons: New York, USA. p. 306 - 319.
[11] Zimring, C.M., Wineman, J.D., & Carpman, J.R The new demand- driven post-occupancy evaluation. Journal of Architecture and Planning Research, 1988(5/4): p. 273-283.

[12] Brooks, S.T. and G. Viccars, The development of robust methods of post occupancy evaluation. Facilities, 2006. 24(5/6): p. 177 - 196.
[13] Vischer, J., Post-Occupancy Evaluation: A Multifaceted Tool for Building Improvement, in Learning from Our Buildings : A State-of- the-Practice Summary of Post-Occupancy Evaluation, C.F. F., Editor 2001, National Academies Press: Washington, DC, USA.
[14] Zhang, Y. and P. Barrett, Findings from a post-occupancy evaluation in the UK primary schools sector. Facilities, 2010. 28(13/14): p. 641-656.
[15] Omari, S. and A. Woodcock, Post occupancy evaluation of primary schools in Saudi Arabia. Work, 2012. 41: p. 881-887.
[16] Uline, C.L., et al., Improving the quality of school facilities through building performance assessment. Journal of Educational Administration, 2009. 47(3): p. 350-367.
[17] Leung, M.y. and I. Fung, Enhancement of classroom facilities of primary schools and its impact on learning behaviors of students. Facilities, 2005. 23(13/14): p. 585-594.

ICENS

11TH INTERNATIONAL CONFERENCE ON ENGINEERING AND NATURAL SCIENCES

CSUN · University of CINCINNATI · National University of Public Service · International University of Sarajevo IUS · EUROPE CONGRESS www.europecongress.org · CNR GROUP